# DESIGN, SYNTHESIS AND SELF-ASSEMBLY OF A FEW OLIGO(*p*-PHENYLENEVINYLENE) DERIVATIVES: CONTROL OF CHROMOPHORE ASSEMBLIES AND OPTICAL PROPERTIES OF π-ORGANOGELS



THESIS SUBMITTED TO
**THE UNIVERSITY OF KERALA**
FOR THE DEGREE OF
**DOCTOR OF PHILOSOPHY**
IN CHEMISTRY
UNDER THE FACULTY OF SCIENCE

***By***
**VIJAYAKUMAR C.**

PHOTOSCIENCES AND PHOTONICS GROUP
CHEMICAL SCIENCES AND TECHNOLOGY DIVISION
NATIONAL INSTITUTE FOR INTERDISCIPLINARY SCIENCE AND TECHNOLOGY
CSIR, TRIVANDRUM 695 019
KERALA, INDIA

*SEPTEMBER 2007*

# DESIGN, SYNTHESIS AND SELF-ASSEMBLY OF A FEW OLIGO(*p*-PHENYLENEVINYLENE) DERIVATIVES: CONTROL OF CHROMOPHORE ASSEMBLIES AND OPTICAL PROPERTIES OF π-ORGANOGELS

THESIS SUBMITTED TO
**THE UNIVERSITY OF KERALA**
FOR THE DEGREE OF
**DOCTOR OF PHILOSOPHY**
IN CHEMISTRY
UNDER THE FACULTY OF SCIENCE

*By*

**VIJAYAKUMAR C.**



PHOTOSCIENCES AND PHOTONICS GROUP
CHEMICAL SCIENCES AND TECHNOLOGY DIVISION
NATIONAL INSTITUTE FOR INTERDISCIPLINARY SCIENCE AND TECHNOLOGY
CSIR, TRIVANDRUM – 695 019
KERALA, INDIA

*SEPTEMBER 2007*

*Dedicated To My Beloved Parents...*

# *DECLARATION*

I hereby declare that the matter embodied in the thesis entitled: "**Design, Synthesis and Self-Assembly of a few Oligo(*p*-phenylenevinylene) Derivatives: Control of Chromophore Assemblies and Optical Properties of π-Organogels**" is the result of the investigations carried out by me at the Photosciences and Photonics Group of the National Institute for Interdisciplinary Science and Technology, CSIR, Trivandrum, under the supervision of Dr. A. Ajayaghosh and the same has not been submitted elsewhere for any other degree.

In keeping with the general practice of reporting scientific observations, due acknowledgement has been made wherever the work described is based on the findings of other investigators.

**Vijayakumar C.**

**National Institute for Interdisciplinary Science and Technology (NIST)**

*(Formerly Regional Research Laboratory)*

**Council of Scientific & Industrial Research (CSIR)**
Industrial Estate P.O., Trivandrum.- 695 019
Kerala, INDIA

ISO 9001 REGISTERED

Dr. A. Ajayaghosh, F. A. Sc.
Scientist
Photosciences and Photonics Group
Chemical Sciences and Technology Division

Tel: 91-471-2515 306
Fax: +91-471-2491 712
E-mail: aajayaghosh@rediffmail.com

17th September 2007

# *CERTIFICATE*

This is to certify that the work embodied in the thesis entitled: "**Design, Synthesis and Self-Assembly of a few Oligo(*p*-phenylenevinylene) Derivatives: Control of Chromophore Assemblies and Optical Properties of π-Organogels**" has been carried out by Mr. Vijayakumar C. under my supervision at the Photosciences and Photonics Group of the National Institute for Interdisciplinary Science and Technology, CSIR, Trivandrum and the same has not been submitted elsewhere for a degree.

**A. Ajayaghosh**
***(Thesis Supervisor)***

# ACKNOWLEDGEMENTS

*It is with great pleasure that I extend my deep sense of gratitude to Dr. A. Ajayaghosh, my thesis supervisor, for suggesting the research problem, for his constant guidance, support and encouragement, leading to the successful completion of this work.*

*I would like to express my gratitude to Prof. M. V. George for his constant encouragement, inspiration and useful discussions during my stay at NIST.*

*I thank Prof. T. K. Chandrashekar, Director, NIST, Trivandrum for providing me the necessary facilities and infrastructure of the laboratory for carrying out this work.*

*I take this opportunity to thank the former Directors (in charge) of NIST, Dr. B. C. Pai and Dr. G. D. Surendar for supporting my research activities at NIST.*

*My Sincere thanks are also due to:*

- *Dr. Suresh Das, Head, Chemical Sciences and Technology Division, Dr. K. R. Gopidas, Dr. D. Ramaiah, Dr. K. George Thomas, Dr. A. Sreenivasan and Dr. V. G. Anand, Scientists of the Photosciences and Photonics Group, for their help and valuable suggestions.*
- *Dr. E. Arunkumar, Dr. Subi J. George and Mrs. Priya Carol, the former members of the Photosciences and Photonics Group for their help and advice.*
- *Mr. V. K. Praveen, Mr. Reji Varghese, Ms. P. Chithra, Mr. S. Mahesh, Mr. S. Sreejith, Mr. S. Santhosh Babu, Mr. S. Srinivasan, Ms. K. P. Divya, Mr. S. Prasanth Kumar, Mr. Anesh Gopal and other members of Photosciences and Photonics Group for their help and cooperation.*
- *Mr. Robert Philip and Mrs. Sarada Nair of Photosciences and Photonics Group for general help.*
- *Mrs. Saumini Mathew for NMR spectra, Mrs. S. Viji for HRMS, Ms. Priya A. Nair for GC-MS and IR spectra, Mr. P. Prabhakar Rao and Mr. M. R. Chandran for SEM, Dr. U. Shyamaprasad and Mr. P. Guruswamy for XRD, Mr. S. G. K. Pillai for optical microscopy.*
- *Dr. T. R. Santhosh Kumar of RGCB for fluorescence microscopic studies and Mr. Saravanakumar of RGCB for MALDI-TOF mass spectra.*
- *Members of the Organic Chemistry Section for general help.*
- *All my friends at NIST for their support.*
- *All my teachers for their encouragement at different stages of my academic career.*
- *My parents, sister and brother for their support, love and prayers throughout my life.*
- *CSIR and DST for financial assistance.*

***Vijayakumar C.***

# *CONTENTS*

# *PREFACE*

Nature has the unique ability to control the self-organization of molecules for various biological functions. The control of energy and electron transfer processes in light harvesting assemblies and in photosynthetic reaction centers are classic examples. In artificial systems, control of chromophore arrangements in nanoscopic structural level has great significance from the viewpoint of optical, chiroptical and related electronic properties. In this context, self-assembly and gelation of linear π-conjugated systems, particularly oligo(*p*-phenylenevinylene)s (OPVs) and oligo(*p*-phenyleneethynylene)s (OPEs) have received considerable attention because of their unique optoelectronic properties and widespread usage as active supramolecular organic materials in various electronic devices such as solar cells, field effect transistors and light emitting diodes. Gelation allows the modulation of optical and morphological properties of these functional chromophores. However, a precise control over the packing of chromophores in such systems is extremely important for the realization of desired functional properties. The present thesis entitled "**Design, Synthesis and Self-Assembly of a few Oligo(*p*-phenylenevinylene) Derivatives: Control of Chromophore Assemblies and Optical Properties of π-Organogels**" describes the results of our attempt to control the chromophore packing in gel forming OPVs and their application as donor scaffolds for fluorescence resonance energy transfer (FRET).

The thesis is comprised of four chapters. In the first chapter, an overview of chromophore based functional supramolecular organogels is described. Attention has been paid to discuss various luminescent organogels with interesting optical and

electronic properties. Light harvesting and stimuli responsive organogels are also discussed in detail. At the end of the chapter, the aim and outline of the thesis are also presented.

The second chapter describes the design, synthesis and self-assembly of a few cholesterol tethered OPV derivatives.[1] The optical, chiroptical and morphological features of the mono- and bischolesterol appended OPVs, **MC-OPV** and **BC-OPV**, are significantly different from each other in the self-assembled gel state. These observations are rationalized on the basis of distinct chromophore packing for these molecules during the self-assembly. Monocholesterol OPV derivatives prefer to form pseudo J-aggregates with tilted chromophore packing which is evident from the red-shifted bands in the absorption and emission spectra. However, the corresponding bischolesterol OPV derivatives form pseudo H-aggregates with a twisted chromophore arrangement having blue-shifted absorption and relatively less shifted emission bands when compared to those of the monocholesterol OPVs. The circular dichroism (CD) spectra of the latter showed exciton coupled bisignate signals whereas those of the former were of non-bisignate in nature. As a consequence of the differences in chromophore packing, **MC-OPV**s form strong gels in hydrocarbon solvents while **BC-OPV**s are weak gelators. The morphological features of the hierarchical assemblies formed from the pseudo J-aggregates of **MC-OPV**s resulted in flat, sidewise aligned and coiled structures with irregular helical pitch and uniform height whereas the pseudo H-aggregates of **BC-OPV**s evolved into twisted helical structures with zigzag pitch and variable height profiles as revealed by AFM studies.

The third chapter deals with the detailed study of the effect of chromophore packing on the efficiency of fluorescence resonance energy transfer (FRET) in cholesterol-OPV gelators in the self-assembled state. FRET studies were carried out

using mono- and bischolesterol OPVs as the energy donors and a π-conjugated oligomer, pyrrolylenevinylene-co-phenylenevinylene (**PYPV**), as the acceptor. This donor-acceptor system was selected in view of their suitable coassembly and photophysical properties. Time resolved emission spectroscopic (TRES) studies revealed that excitation energy migration is highly efficient in the self-assembly of **MC-OPVs**, whereas, it is found to be slow in **BC-OPVs**. Efficient energy migration within the donor scaffold of the former results in an efficient energy transfer to the encapsulated acceptor (2 mol%) with 90% quenching of the donor fluorescence to give bright red emission in the gel state at room temperature. Less efficient energy migration in **BC-OPVs** results in a partial transfer of its excitation energy to the acceptor with 63% quenching of the donor emission under similar conditions giving rise to an intense white-light emission with CIE coordinates of (0.31,0.35). This is the first example of an organogel showing white-light emission.

The fourth chapter illustrates the self-assembly of donor-acceptor type organogelators with color tunable FRET emission.[2] TRES studies of a few OPV derivatives in the gel state showed that energy migration is less efficient in OPV gelators with bulky end groups (**OPV1-2**) when compared to that of the gelators with small end groups (**OPV3-4**). FRET studies were carried out using **OPV1** and **OPV3** as the donors and **OPV6** as the acceptor. Less efficient energy migration results slow quenching of **OPV1** fluorescence at 509 nm on addition of the acceptor (0-2 mol%) with the formation of the monomer emission of the latter at 555 nm. Upon further addition of **OPV6** (2-20 mol%), the emission was continuously red-shifted to 610 nm which corresponds to the aggregate emission of **OPV6**. Consequently, 98% quenching of the donor emission was observed at 509 nm. Fluorescence microscopic studies provided visual evidence for the tunable FRET emission. Thus

efficient trapping of excitons by "isolated" or "aggregated" acceptors through a subtle control of the self-assembly and the photophysical properties of the donor-acceptor building blocks allowed a continuous shift of the emission color from green to red ($\lambda_{max}$ = 509-610 nm). However, **OPV3** showed maximum quenching (82%) even in the presence of 3.1 mol% of the acceptor (**OPV6**) due to fast energy migration. Less stable gel of **OPV3** disrupted on further addition of the acceptor and hence monomer emission of the former was observed. Emission tuning was not possible in this system because of these two effects. Thus remarkable control on the FRET emission could be achieved in a supramolecular light harvesting system by controlling the self-assembly of the donor-acceptor molecules.

In summary, proper functionalization of OPVs with cholesterol moieties allowed control of chromophore packing to give distinct optical, chiroptical and morphological properties in the self-assembled state. The difference in chromophore packing affects the energy migration properties of the resulting self-assemblies which could be exploited for the control of FRET resulting in red emitting and white emitting organogels. Self-location of a gel forming acceptor within the donor self-assembly as "isolated" or "aggregated" species result in color tunable FRET emission ranging from green to red.

**References:**


1. A. Ajayaghosh, C. Vijayakumar, R. Varghese, S. J. George, *Angew. Chem. Int. Ed.* **2006**, 45, 456.
2. A. Ajayaghosh, C. Vijayakumar, V. K. Praveen, S. S. Babu, R. Varghese, J. *Am. Chem. Soc.* **2006**, *128*, 7174.

*Chapter 1*

# Chromophore Based Supramolecular Organogels: An Overview

## 1.1. Abstract

*The development of functional organic materials for electronic and photonic application is one of the most exciting areas of advanced materials research. The "bottom up" approach towards the construction of supramolecular architectures of chromophores and π-systems using noncovalent interactions is of great importance in the field of nanoelectronics. A class of soft materials that has received significant attention is organogels derived from π-conjugated molecules due to their favorable optoelectronic properties. In many cases, gelation helps alignment of chromophores which is vital for facilitating electron and energy transport properties. Therefore, many of the chromophore derived organogels are used as scaffolds for energy transfer and light harvesting processes. Gels that respond to external stimuli such as temperature, light, pH and metal ions find applications in sensing and actuating. In this chapter, an overview of chromophore based functional supramolecular organogels is given. Finally, the aim and outline of the thesis are presented.*

## 1.2. Introduction

Gels are viscoelastic solid-like materials comprised of an elastic, cross-linked network and a solvent in which the latter is the major component. Gels have been used in everyday life in a variety of forms such as cosmetics, food, medicines etc. Most of these gels are composed of covalently crosslinked polymers having high molecular weights.[1] More recently there has been an enormous increase of interest in the design of low molecular weight gelators, which immobilize various organic fluids or water as a result of three-dimensional supramolecular network formation.[2] Gels derived from low molecular mass compounds are also known as "supramolecular gels". This novel class of supramolecular materials exhibit striking properties with respect to self-assembly phenomena leading to diverse architectures. The diversity of nanostructures provided by supramolecular gels makes them promising candidates for several potential applications ranging from medicines to material sciences and catalysis to optoelectronics and related areas.

In contrast to the macromolecular gels, low molecular weight organogel network is held together solely by noncovalent interactions such as hydrogen bonding, $\pi$-stacking, solvophobic, electrostatic and donor-acceptor interactions rendering the gelation process thermally or mechanically reversible. The directional nature of intermolecular interactions allows gelator molecules to self-organize in one-dimensional arrays producing elongated fibrous nanostructures. Entanglement of these fibers subsequently produces three-dimensional networks

capable of trapping solvent molecules thereby yielding a gel (Figure 1.1). Usually, low molecular weight organogels are formed by dissolving a small amount of the gelator in hot solvents and the subsequent cooling below gel transition temperature ($T_{gel}$). The gelation of organic molecules can be visualized by the formation of a thick non-flowing mass, even when turned upside down. Organogels are usually characterized by a variety of analytical methods, particularly spectroscopic and microscopic techniques. At the microscopic level, the structures and morphologies of supramolecular gels have been investigated by techniques such as scanning electron microscopy (SEM), transmission electron microscopy (TEM) and atomic force microscopy (AFM), while thermal and mechanical studies are used to understand the interactions between these structures. However, at the nanoscale, X-ray diffraction, small angle neutron scattering and X-ray scattering (SANS, SAXS) are required to elucidate the structures of supramolecular gels.

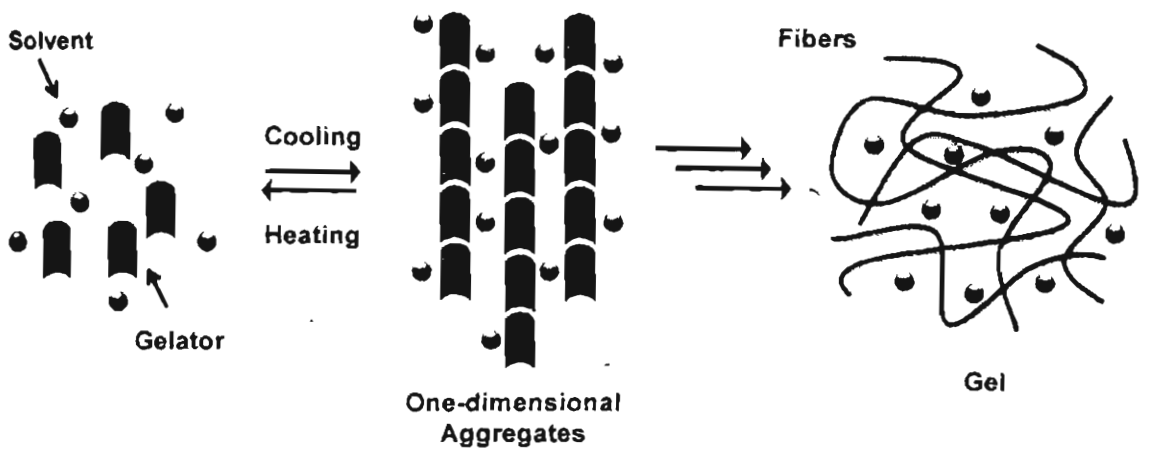


**Figure. 1.1.** Schematic representation of the self-assembly of low molecular weight organogelators into one-dimensional aggregates and the subsequent formation of an entangled network.

A large variety of low molecular weight organogelators are known in the literature which includes molecules from the simplest alkanes to the complex porphyrins and phthalocyanines. Incidentally, most of the early discovery of organogelators has been found by accident, in many cases during the workup procedures of a synthetic experiment. However, the knowledge gained on the aggregation of gelator molecules during the past decade, has helped to 'design' gelators through the incorporation of structural features that are known to promote aggregation. The following features are considered to be of importance in the design of organogelators: (i) formation of one-dimensional aggregates via anisotropic growth process, (ii) intertwining of these one-dimensional aggregates to form three-dimensional network and (iii) the prevention of crystallization or precipitation of the self-assembled aggregates through a balance between order and disorder. Therefore, the design of new gelling agents needs to account for all these aspects and hence continues to be a challenging task.

## 1.3. Chromophore Based Functional Organogels

Highly organized arrays of chromophores are of great interest as mimics of natural photosynthetic systems. Several organized chromophore assemblies with functional properties are known in the literature, which are mainly based on polymers, dendrimers, liquid crystals and gels. Supramolecular organogels based on chromophores are suitable for various applications such as optoelectronic, light

harvesting, sensing etc. In addition, the gel phase, which is different from either the solid phase or the liquid phase, is so unique as a medium that is expected to provide a novel environment to arrange functional molecules indispensable to a natural photosynthetic system. Functional organogels based on various chromophores and their potential application is discussed in the following sections.

### 1.3.1. Luminescent Organogels

There has been considerable interest in the development of organic based luminescent materials because of their potential applications in optoelectronic devices.[3] The optical and electronic properties of these materials are dependent not only the structure but also the intermolecular interactions. Self-assembly and gelation of π-conjugated molecules induces considerable modulation of the absorption and emission properties. Many fluorescent molecules such as anthracene, pyrene, triphenylene, oligo(*p*-phenylenevinylene) etc. that are functionalized with alkyl side chains, cholesterol moieties and various hydrogen bonding groups have been reported to form gels.

For example, molecular self-assembly of [n]acenes such as anthracene, tetracene and pentacene has attracted much attention, because of their significant charge mobility, photochromism, intense absorption and emission, which have potential applications in the fields of organic electronics and photovoltaic

devices.[4] Chart 1.1 shows some of the representative examples of this class of organogelators based on polyaromatics.

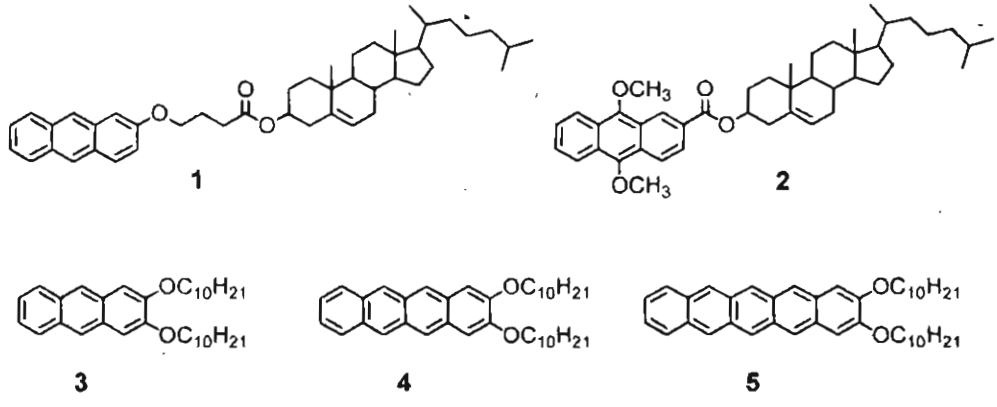


**Chart 1.1**

The serendipitous observation of the gel formation of 3-β-cholesteryl-4-(2-anthryloxy)butanoate (**1**) in a variety of organic liquids has led to a novel class of steroid based gelators.[5] They consist of an aromatic group (A), connected to a steroidal moiety (S) via a linking group (L) and hence are called ALS gelators. Desvergne and coworkers have reported that alkoxy substituted anthracene (**3**) tetracene (**4**) and pentacene (**5**) can form fluorescent gels in various alkanes, alcohols, aliphatic amines and nitriles, through dipole-dipole interactions, van der Waals forces and π-π stacking.[6] Gel formation is accompanied by significant changes in the absorption and emission properties of the anthracene chromophores.

Pyrene, due to its strong fluorescence and excimer formation is a useful probe for photophysical and photobiological studies. Pyrene can also be used as a

probe to study the self-assembly properties of organic molecules. In this context, the two component system consisting of bile acid based molecular tweezers (**6** and **7**, Chart 1.2) and 2,4,7-trinitrofluorenone (TNF, **8**) acceptor molecules are shown to form organogels in a variety of hydroxyl and hydrocarbon solvents through charge transfer interactions.[7]

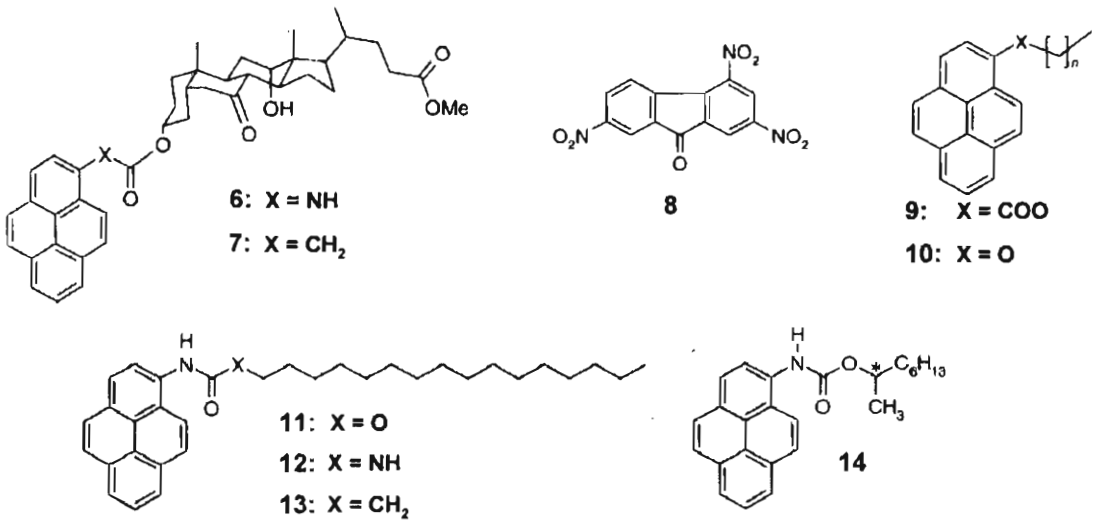


**Chart 1.2**

Later, a new class of pyrene derived organogelators in which the bile acid part is replaced by alkyl chains through different linkers has been reported.[8] Compounds with ester (**9**) or ether (**10**) linkages are shown to form gels only in the presence of TNF. However, the compounds with urethane (**11**), urea (**12**) and amide (**13**) linkers can self-assemble into one-dimensional gels through H-bond and π-stack interactions.[8,9] The chiral pyrene organogelator (**14**), substituted with a (*R*)-2-octyl urethane group self-assemble into *P*-helical aggregates.

Fluorescent gelators containing pyrene moieties and dendritic oligopeptides (**15-17**) have been developed by Kato and coworkers.[10] These molecules self-assemble into 1D helical columnar structures that lead to the formation of 3D fibrous random networks to form a gel (Figure 1.2). This gel material exhibited monomer emission of pyrene because of the hydrogen-bonded arrays of the oligopeptide moieties which greatly suppress the formation of pyrene excimers. In contrast, in the sol state, green excimer emission of the pyrene is observed as a result of the dissociation of intermolecular hydrogen bonds. This is the first example of the reverse-mode color switching of fluorescence for supramolecular pyrene assemblies.

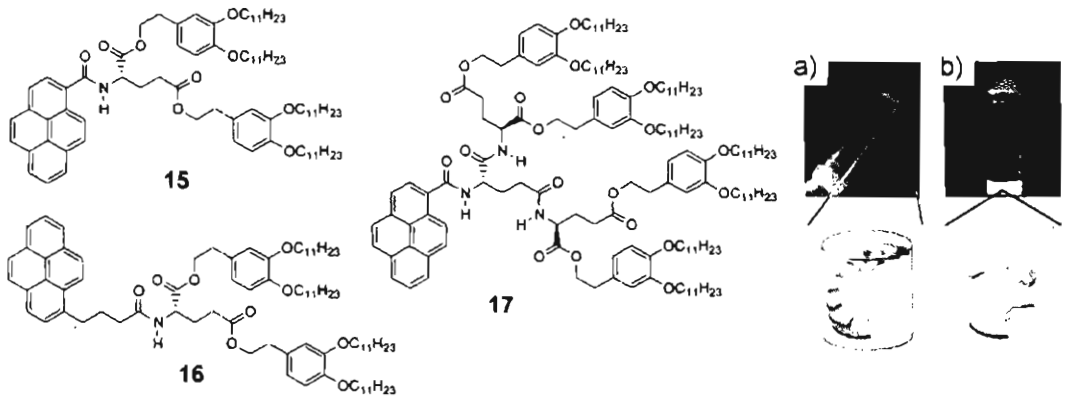


**Figure 1.2.** Photograph of fluorescent a) gel and b) solution of **15** in cyclohexane. Corresponding schematic illustration of the molecular arrangement is shown below. (adapted from ref. 10)

The triphenylene derivatives (**18** and **19**) substituted with six amide groups and six hydrocarbon side chains are found to form organogels with unusual emission properties in nonpolar solvents as a result of highly directional columnar self-assemblies through a cooperative effect of π-π, hydrogen bonding and van der

Waals interactions.[11] Detailed fluorescence measurements have shown that the triphenylene cores of **18** in the gel state are arranged in a staggered manner, whereas, it is arranged in an eclipsed manner in **19** leading to an unusual observation of excimer emission, at 525 nm (Figure 1.3). Furthermore, XRD analysis of the xerogels revealed a lateral rectangular and hexagonal columnar arrangement for **18** and **19** respectively, indicating the crucial role of alkyl chains in controlling the packing mode.

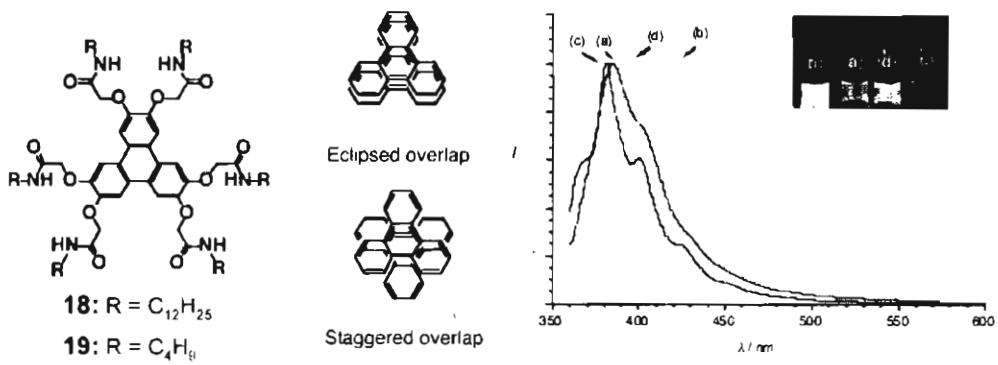


**Figure 1.3.** Fluorescence spectra of a) chloroform solution of **18**, b) cyclohexane gel of **18**, c) chloroform solution of **19** and d) cyclohexane gel of **19**. (adapted from ref. 11)

3,4,5-Tris(*n*-dodecyloxy)benzoyl-amide appended 8-quinolinol/copper(II)-, palladium(II)- and platinum(II)-chelates (**20-22**) are efficient gelators for various organic solvents.[12] The gelation ability of these molecules is attributed to the cooperative effect of π-π interactions of the chelate moieties as well as the hydrogen bond interactions among the amide groups. As confirmed by the field-emission measurements, the electronic properties of the three kinds of gel fibers obtained are evidently different depending on the metal centers. In the case of Pt

chelate (**22**), the π-π interaction results in thermo- and solvatochromism. Color change in the phosphorescence emission is observed in response to the sol–gel phase transition (Figure 1.4). Furthermore, it was shown that dioxygen quenching of the excited triplet state is efficiently inhibited in the gel phase. These findings indicate that introduction of metal chelates into the low molecular weight gel system is one of the most effective strategies to obtain a wide variety of photo- and electro active nanomaterials.

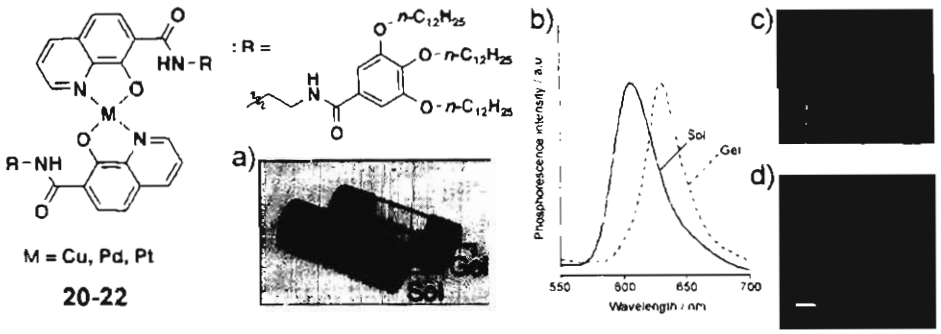


**Figure 1.4.** a) Photograph of *p*-xylene gel of **22** and the heated solution, b) Phosphorescence spectra of *p*-xylene gel and tetrachloroethane solution of **22**, c) photograph of **22** gel and solution under UV light (365 nm) and d) CLSM image of the *p*-xylene gel of **22**. (adapted from ref. 12)

Platinum-terpyridine complexes have attracted widespread interest as functional materials because of their intense phosphorescence in the visible region. Zeissel *et al.* have reported the gelation of luminescent platinum-terpyridine complex (**23**) containing long-chain alkoxydiacylamidotoluene platform in nonpolar solvents (Chart 1.3).[13] Dodecane gel of **23** showed intense phosphorescence with an emission maximum at 850 nm. Self-assembly and gelation of fluorescent borondipyrromethane (Bodipy) derivatives (**24**, **25**)

containing the same alkoxydiacylamidotoluene platform forms organogels with intense absorption in the visible region, high fluorescence quantum yields, and narrow emission bandwidths with high peak intensities.[14]

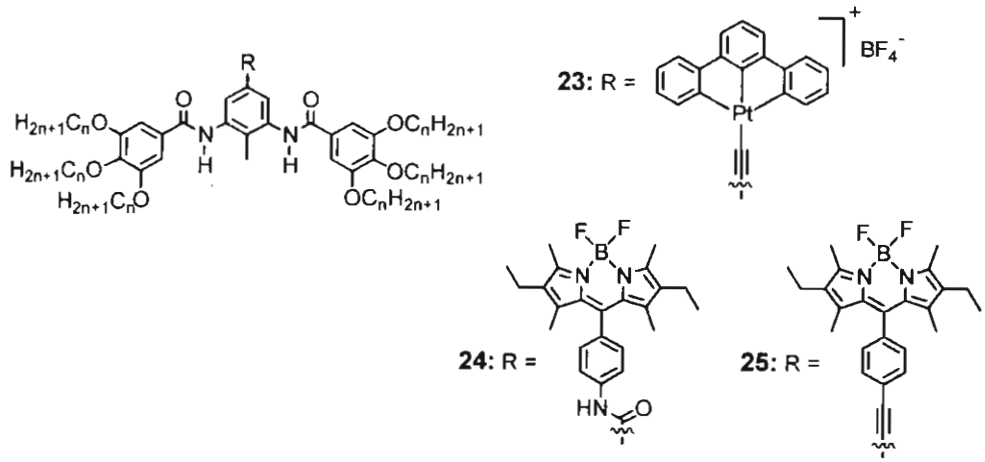


**Chart 1.3**

A number of molecules which are less emissive or non-emissive in solution show strong emission in the gel state due to aggregation-induced enhanced emission phenomenon. For example, a highly fluorescent organogel was reported to be formed by the intermolecular hydrogen bonding interactions between the non-emissive oxadiazole based benzene-1,3,5-tricarboxamide molecule (**26**).[15] Studies have shown that the intermolecular face-to-face H-bonding interactions in the columnar gel aggregates play a key role in the enhancement of fluorescence upon gelation, by providing significant singlet-triplet splitting to reduce the rate of inter system crossing. Enhancement in fluorescence intensity on gelation has been reported for a trifluoromethyl-based cyanostilbene derivative (**27**) (Figure 1.5).[16]

The gelation of **27** is attributed to the cooperative effect of the π-π stacking interactions of the rigid rod-like aromatic segments and the supplementary intermolecular interactions induced by the four $CF_3$ units.

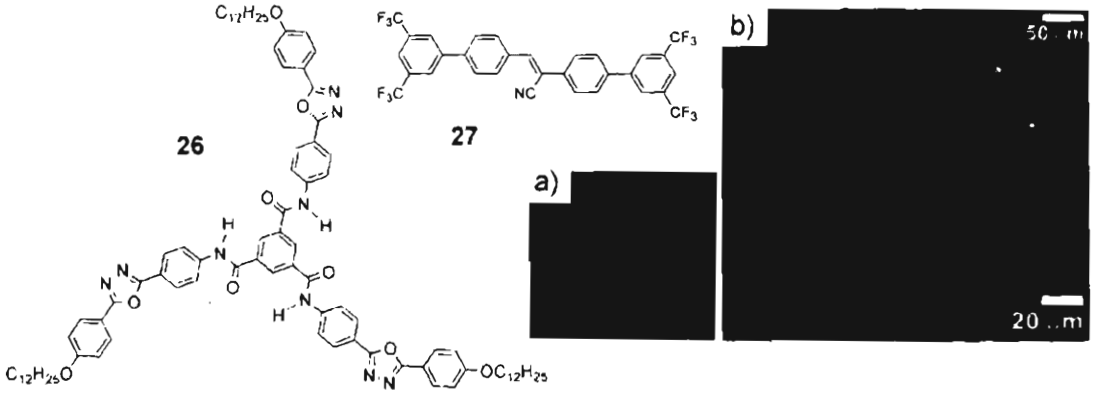


**Figure 1.5.** a) Fluorescence emission of **27** in the solution (left vial) and gel phase (right vial) in 1,2-dichloroethane under UV light (365 nm). b) Fluorescence microscopy images of an organogel of **27**. (adapted from ref. 16)

Aida and co-workers have reported a phosphorescent organogel which shows reversible RGB color switching through metallophilic interactions.[17] The gelator consists of a trinuclear Au(I) pyrazolate complex bearing long alkyl chains (**28**) which self-assembles in hexane via Au(I)-Au(I) metallophilic interaction, to form a red-luminescent organogel (Figure 1.6). This gel on doping with a small amount of $Ag^+$ results in a blue luminescence without disruption of the gel, while removal of doped $Ag^+$ with cetyltrimethylammonium chloride results in complete recovery of the original red-luminescent gel. Upon heating, these organogels undergo gel-to-sol transition due to the destabilization of the metallophilic interactions, where the red luminescence of the non-doped system becomes hardly

visible, while the blue luminescence of the $Ag^{+}$ doped system turns green. On cooling, these solutions undergo gelation and simultaneously recover the original luminescence. The observed RGB (red-green-blue) luminescences are all long-lived (3-6 $\mu$s) and assigned to electronic transitions from triplet-excited states.

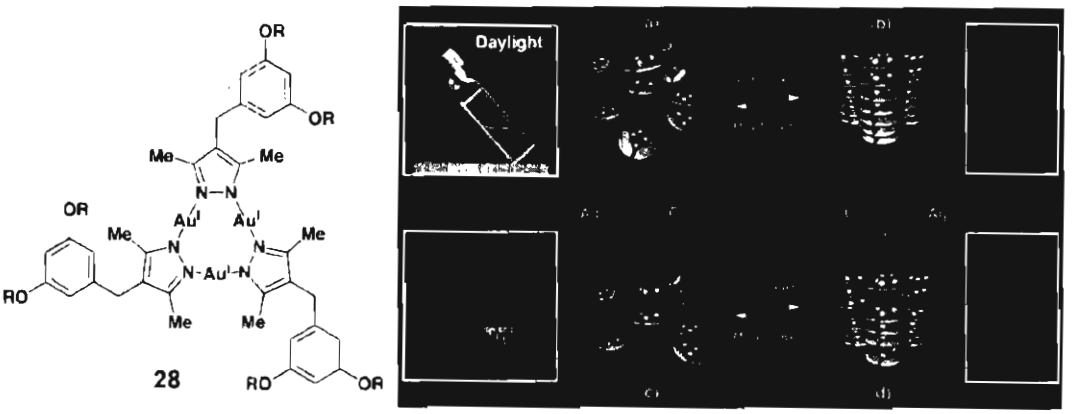


**Figure 1.6.** Luminescence profiles of Au(I) pyrazolate complex **28** in hexane. Pictures and schematic self-assembling structures: a) sol, b) gel, c) sol containing AgOTf, and d) gel containing AgOTf. (adapted from ref. 17)

Linear π-conjugated molecules, due to the presence of delocalized π-electrons, show interesting optical and electronic properties in the monomer as well as in the self-assembled states. These properties make them useful to the development of various organic electronic devices. Control of the optical and electronic properties of conjugated systems is necessary for their applications in electronic devices. A viable approach towards this end is the design of conjugated building blocks that form organogels in appropriate solvents through noncovalent interactions leading to entangled fibrous assemblies. Recent examples include the thermoreversible gelation of fluorescent oligo(*p*-phenylenevinylene) (OPV)

derivatives (Chart 1.4) and the control of their photophysical as well as morphological properties by structural modifications and noncovalent interactions.[2j,18] For example, OPVs functionalized with C12-C16 alkyl chains and hydroxymethyl end groups are supergelators of nonpolar hydrocarbon solvents.

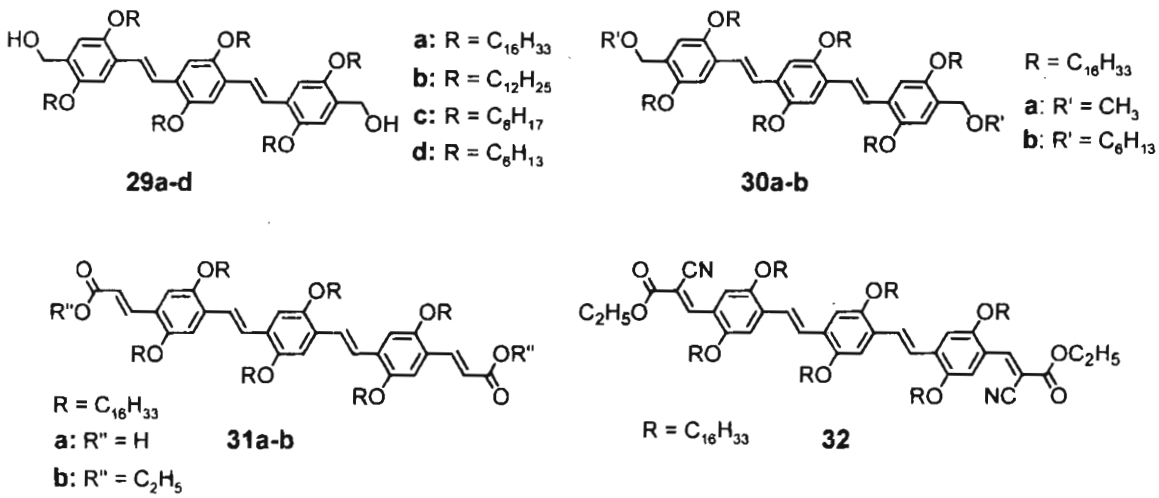


**Chart 1.4**

The most striking feature of the gelation of OPVs is the remarkable shift in the emission towards the long wavelength region. For example, the absorption and emission properties of OPV derivative **29a** in chloroform showed characteristic features of molecularly dissolved species. However, in dodecane at 20 °C, the absorption spectrum showed a reduction in the intensity with the formation of a red shifted shoulder (Figure 1.7). Similarly, the emission intensity is significantly reduced and red shifted. Temperature induced reversible optical changes of **29a** revealed the co-existence of different self-assembled species in dodecane at room temperature.

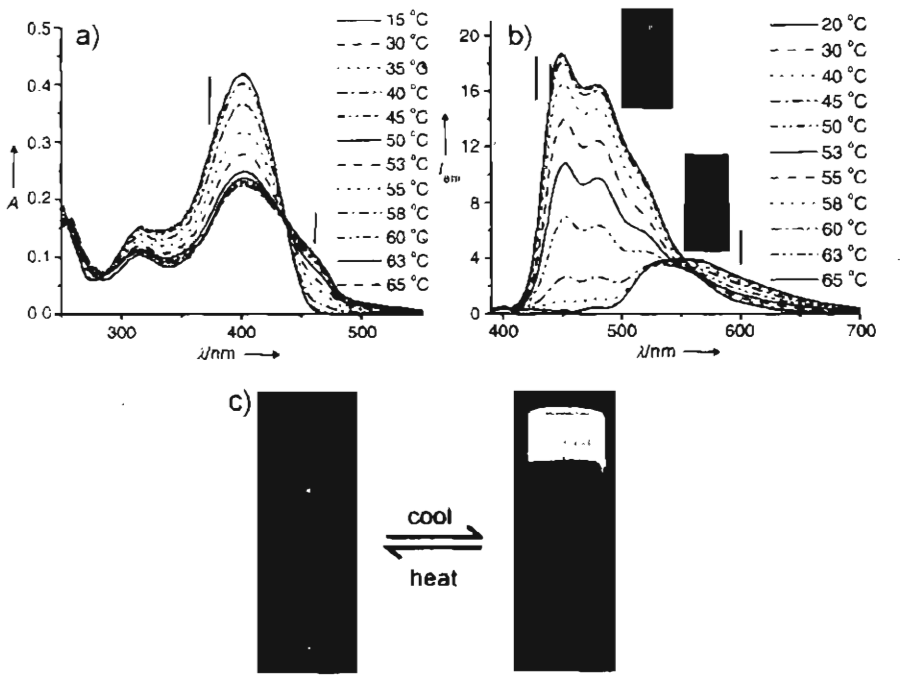


**Figure 1.7.** Temperature-dependent a) absorption and b) fluorescence spectra ($\lambda_{ex}$ = 380 nm) of **29a** in dodecane (1 × $10^{-5}$ M). Inset shows the emission colors of the molecularly dissolved (blue) and the self-assembled (green) species of **29a** in dodecane. c) Photograph of **29a** in decane (CGC = 0.9 mM) under illumination at 365 nm before and after gelation. (adapted from ref. 18c)

Stupp and coworkers have reported the self-assembly of a series of linear π-conjugated molecules with dendron rod-coil architecture that contain conjugated segments of oligo(thiophene), oligo(phenylenevinylene) and oligo(phenylene) (**33-38**) (Figure 1.8).[19] Electron and atomic force microscopy reveal that these molecules self-assemble into high aspect ratio ribbon-like nanostructures which induce gelation in nonpolar solvents. Self-assembly of these molecules induce a blue-shift in the absorption spectra and a red-shift in the fluorescence spectra with significant quenching indicating aggregation of the conjugated segments within the ribbon-like structures. Moreover, self-assembly leads to three orders of

magnitude increase in the conductivity of iodine-doped films of thiophene derivatives. Electric field alignment of these assemblies creates arrays of self-assembled nanowires on suitable substrates which is useful for the fabrication of electronic devices.

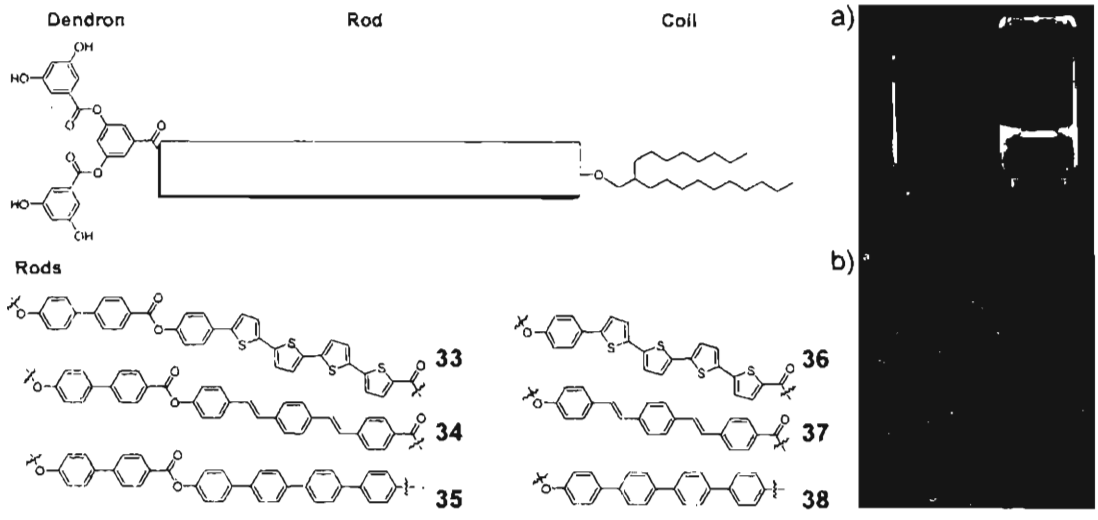


**Figure 1.8.** a) Photographs of **33** in toluene (left) and THF (right) under illumination with 365 nm light and b) AFM texture of **34**. (adapted from ref. 19b)

In contrast to the self-assembly of oligo(*p*-phenylenevinylene) to nanotapes, an analogous oligo(*p*-phenyleneethynylene) (**39**) in decane resulted in the formation of nanoparticles, microspheres, bundled fibers and eventually to blue-emitting organogels (Figure 1.9).[20] At a concentration of $1 \times 10^{-6}$ M, nanoparticles with average size of 100 nm were formed whereas up to a concentration of $1 \times 10^{-4}$ M, microspheres of 5-10 $\mu$m with intense blue fluorescence were obtained. However, at higher concentrations elongated giant structures of micrometer size were formed as evident from the SEM analysis.

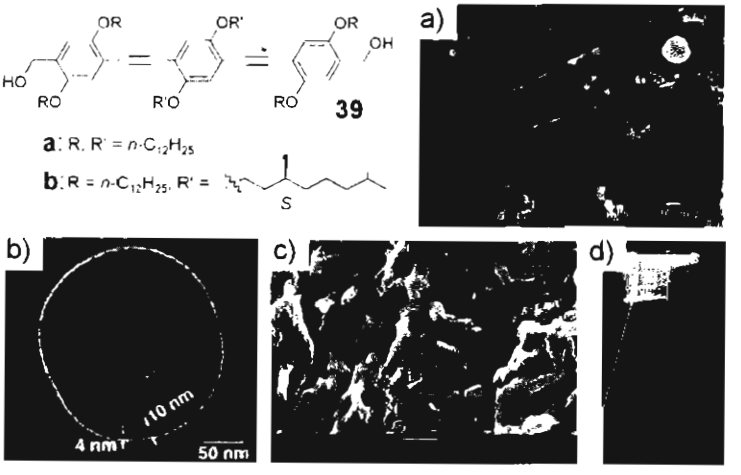


**Figure 1.9.** a) Optical microscopic picture under illumination with UV light (365 nm), b) HR-TEM image of a sphere, c) SEM image of the gel and d) photograph of the gel of **39** in decane. (adapted from ref. 20a)

## 1.3.2. Light Harvesting Organogels

Light harvesting is one of the most important natural processes by which photosynthetic organisms absorb sunlight and transfer to the reaction center where photoinduced redox processes are initiated to convert the energy harvested from sunlight into increasingly more stable forms of energy.[21] Pigments (chlorophylls and carotenoids) are responsible for converting the energy of an absorbed photon into an electronic excitation. The mesoscale organization of these pigment molecules in the photosynthetic membrane allows the unidirectional excitation energy transfer towards the reaction center (RC), which is the final destination of the collected energy. Inspired by natural light harvesting systems, scientists have been attempting to mimic such process with the help of synthetic molecular architectures. These include dendrimers,[22] polymers,[23] molecular complexes,[24]

hydrogen bonded supramolecular assemblies,[25] self-assembled monolayers[26] and self-assembled fibers (gels).[18h,27-34] The light harvesting process involves photonic excitation of the donor, followed by the transfer of the absorbed energy to a nearby energy acceptor. Organized arrays of chromophores are important for directional and efficient energy transfer process. Gelation in many cases is known to facilitate the preferential alignment of donor-acceptor chromophores which can be used as scaffolds for efficient energy transfer and light harvesting. Described below are the various examples of light harvesting organogels reported in literature so far.

An early example of energy transfer process in an organogel medium is reported by Sagawa *et al.* They have prepared fibrous gel assemblies of porphyrin **40** and pyrene **41** substituted by L-glutamic acid (Figure 1.10).[28] By amide hydrogen bonding, both chromophores self-assemble co-facially into chiral fibers

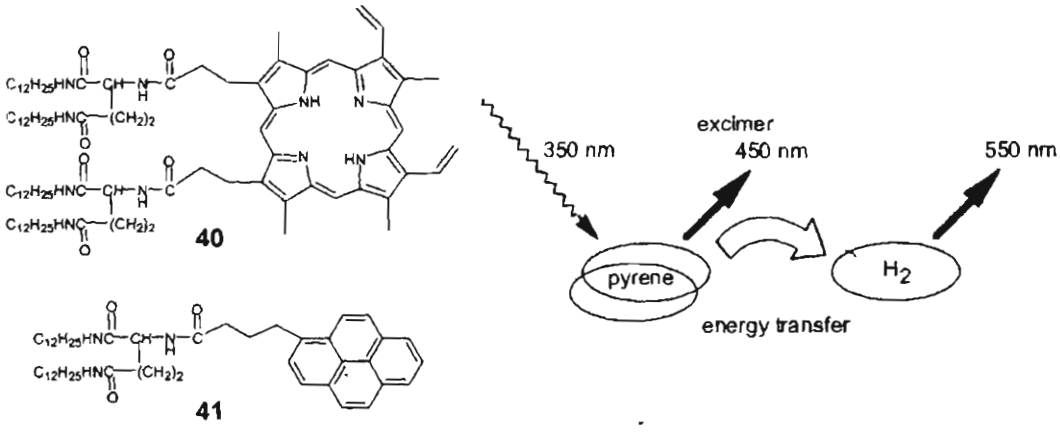


**Figure 1.10.** Didodecyl L-glutamic acid substituted porphyrin (**40**) and pyrene (**41**) form mixed assemblies in benzene, the energy transfer process in these assemblies is schematically depicted. (adapted from ref. 28)

of several micrometers in length which can be controlled by temperature. The porphyrin **40** forms a physical gel whereas the pyrene **41** does not form gel at room temperature. When the two molecules were allowed to form a co-assembly, energy transfer occurs from pyrene excimers to the porphyrin traps.

Shinkai and coworkers have designed a proton sensitive, fluorescent 1,10-phenanthroline-appended cholesterol based gelator (**42**), which is an efficient energy transfer system (Figure 1.11).[29] In the presence of two equivalents of TFA, the purple emission (360 nm) of the gel phase is quenched completely, with the appearance of an yellow emission (530 nm) corresponding to the protonated form of **42**, due to efficient energy transfer from the neutral to the protonated form of **42**. However, when the gel was converted into the solution phase at 90 °C in the presence of TFA, a blue emission with bimodal emission maxima was obtained indicating the absence of energy transfer.

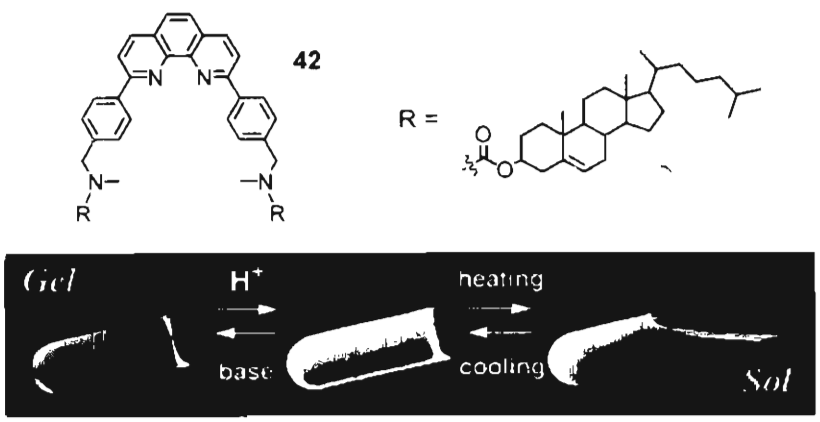


**Figure 1.11.** Emission color changes in phenanthroline based gelator **42** upon protonation and sol-gel transition. (adapted from ref. 29)

Co-assembled organogels of cholesterol functionalized perylene bisimide derivatives (**43a-d**) exhibit cascade energy transfer.[30] The absorption maxima of these derivatives could be tuned across the visible spectrum by attaching different substituents at the bay positions of the perylene moiety. Various binary, ternary and quaternary perylene gels were prepared and subjected to energy transfer studies. Selective excitation of **43a** at 457 nm resulted in the quenching of its emission at 544 nm with efficiencies of 68% for **43b**, 53% for **43c** and 34% for **43d**, consistent with decreasing donor-acceptor spectral overlap (Figure 1.12). The perylene derivative **43d** acts as an energy sink because of its low emissive nature which arises from the twisted intramolecular charge transfer (TICT) state. It is interesting to note that the gel state guarantees the success of this cascade transfer process, whereas in solution the mentioned effects are not observed.

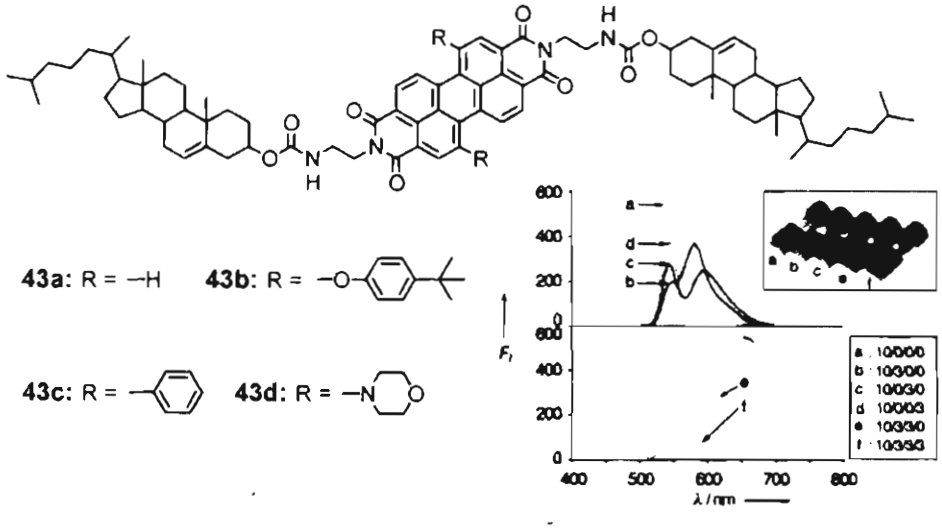


**Figure 1.12.** Fluorescence spectra of mixed perylene gels. The numbers in the inset denote the molar ratios for **43a/43b/43c/43d**. The corresponding photographs of the mixed gels are also shown in the inset. (adapted from ref. 30)

Recently, Del Guerzo *et al.* have demonstrated the versatility of anthracene based organogel as a medium to study energy transfer process.[31] They have used 2,3-*n*-didecyloxyanthracene (**3**) as the excitation energy donor and 2,3-*n*-didecyloxytetracene derivative (**4**) as the acceptor which are known to form organogels (see section 1.3.1). DMSO gel of **3** on doping with **4** facilitates energy transfer from excited anthracenes to the tetracene derivatives (Figure 1.13). The energy transfer process was found to be highly efficient, as the acceptor is required in very small quantities. Detailed energy transfer studies revealed that the efficiency of the process is highly influenced by the structural and chemical similarity between donor and acceptor as well as the involvement of exciton migration in the donor gel scaffold.

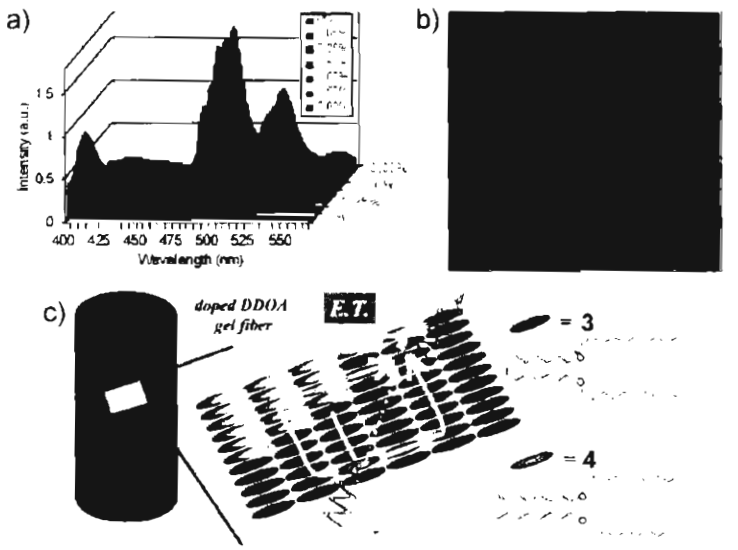


**Figure 1.13.** a) Emission spectra of the DMSO gel of **3** ($\lambda_{exc}$ = 384 nm) doped with increasing proportions of **4**, b) Fluorescence confocal microscopy image of the DMSO gel of **3** at 298 K with 2 mol % of **4** ($\lambda_{exc}$ = 405 nm) and c) Simplified representation of a doped gel fiber of **3** as well as energy transfer pathways. (adapted from ref. 31a)

The metallo-supramolecular gelator **44** forms stimuli responsive gels upon addition of a lanthanoid (III) nitrate (3 mol%) followed by transition metal ion perchlorate (97 mol%) in $CHCl_3/CH_3CN$.[32] Different binding modes of the tridentate ligand 2,6-bis(1′-methylbenzimidazolyl)-4-hydroxypyridine (**44**) with transition metal ions (2:1 complex) and lanthanide ions (3:1 complex) are responsible for the formation of supramolecular gel (Figure. 1.14a). Excitation ($\lambda_{ex}$ = 340 nm) of **44**:Zn/Eu system results in intense emission from Eu(III) ions (Figure. 1.14b). The emission is due to efficient ligand to metal energy transfer process. While **44**:Zn/La displayed emission from metal-bound ligand ($\lambda_{ex}$ = 397 nm), **44**:Co/Eu did not emit at all, probably due to the presence of low energy

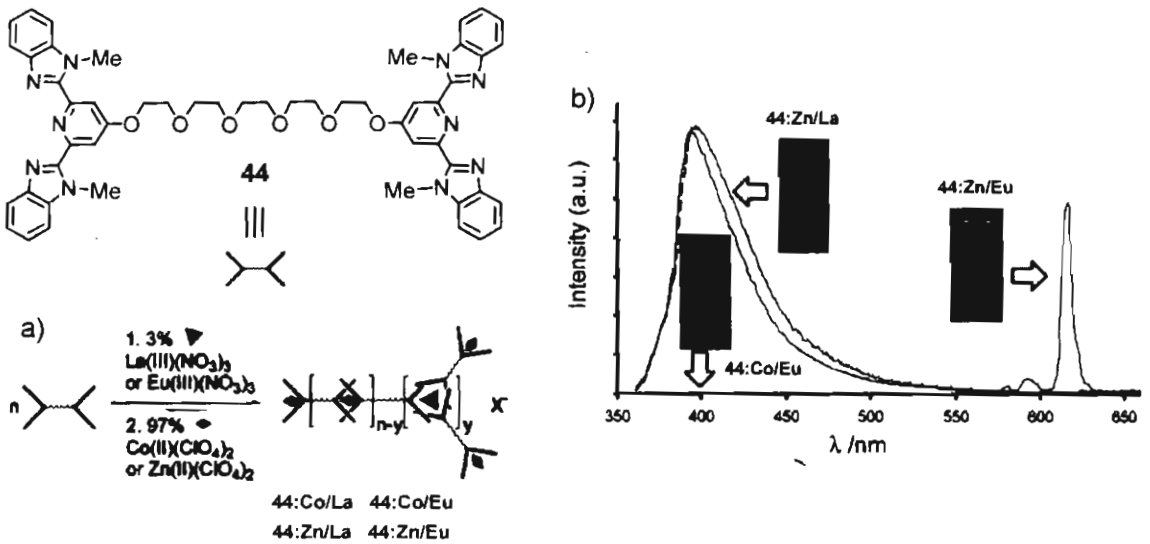


**Figure 1.14.** a) Schematic representation of the formation of a metallo-supramolecular gel using a combination of lanthanoid and transition metal ions mixed with the monomer **44**. b) Photoluminescence spectra of metallo-supramolecular gels prepared in acetonitrile ($\lambda_{ex}$ = 340 nm). **44**:Co/Eu shows no photoluminescence and lies essentially along the baseline. The insets show the gels under UV light (365 nm). (adapted from ref. 32)

metal centered levels which will facilitate radiationless decay process. Addition of small amount of formic acid to the luminescent gel of **44**:Zn/Eu results in the disruption of the gel and a strong quenching of Eu(III) emission. This could be due to the displacement of the ligands by formate ions, which eventually 'switch off' the antenna effect. This process could be reversed by the evaporation of the solvent followed by reswelling of the material with $CH_3CN$, which restore the Eu(III) emission.

OPV derived π-gels are excellent energy donor scaffolds to encapsulated acceptors. This could be due to efficient exciton migration within the aggregates of different HOMO-LUMO levels. Therefore, emission occurs mainly from aggregates of lower energy resulting in a red-shift in the wavelength. In the presence of an acceptor, energy transfer occurs resulting in emission from the latter. This has been demonstrated by entrapping rhodamine B dye within OPV gels as shown in Figure 1.15.[33]

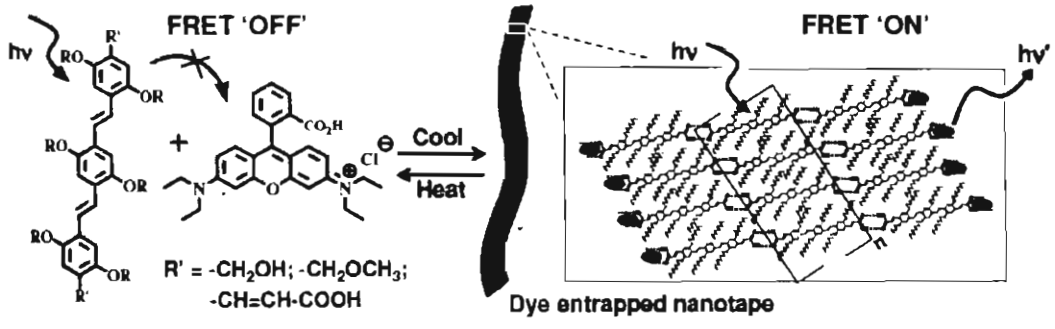


**Figure 1.15.** Schematic representation of the energy transfer process in Rhodamine B dye encapsulated OPV gel fibers. (adapted from ref 33b)

The main drawback of the above system is the incompatibility of the polar dyes with the OPV self-assembly in nonpolar medium. In order to design an efficient light harvesting system which can funnel excitation energy to a few acceptor molecules, it is necessary to have an acceptor which is compatible with the donor self-assembly. Recently this issue was addressed with the help of OPVs (**45-48**) having different HOMO-LUMO energy levels as donor and acceptor.[18h] The rational choice of OPVs with dipolar end functional groups allowed the tuning of the emission in the molecular level and in the supramolecular level (Figure 1.16a). Detailed studies revealed that the optical properties of the gel-forming

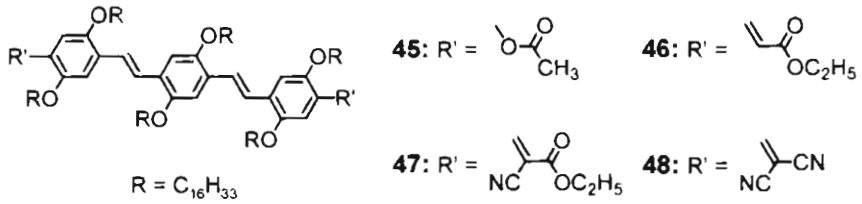


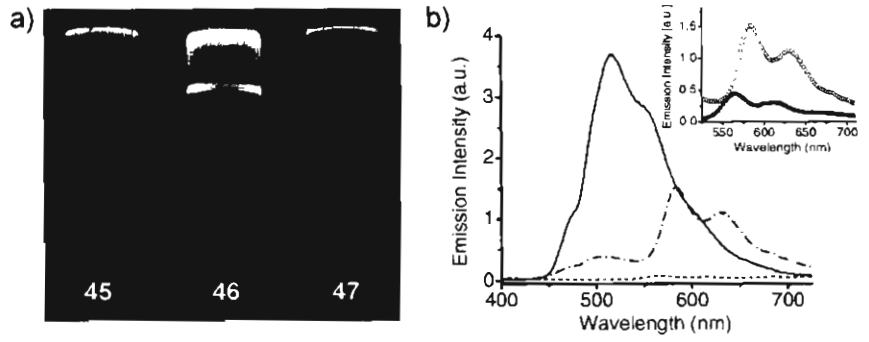


**Figure 1.16.** a) Photographs of the hexane gels under illumination at 365 nm. b) Energy transfer between **45** and **48** in the gel state. Emission spectra of **45** in the absence (——) and in the presence (– · – ·) of **48** (2.62 mol%) in *n*-decane, emission of acceptor in the absence of donor (----). The inset shows the emission of the acceptor on indirect excitation at 380 nm (○) and direct excitation at 495 nm (●). (adapted from ref. 18h)

molecule **45** (donor) and the nongelling molecule **48** (acceptor) are ideal for energy transfer. Addition of 2.62 mol% of **48** to the *n*-decane gel of **45** showed 90% quenching of the emission of donor and the simultaneous emission from the acceptor (Figure. 1.16b). A three fold increase in the luminescence of **48** after energy transfer ($\lambda_{ex}$ = 380 nm) when compared to that of direct excitation ($\lambda_{ex}$ = 495 nm) indicates efficient energy transfer in this system (Figure. 1.16b inset).

Development of inorganic-organic hybrid materials consisting of gold nanoparticles and OPV gels has recently been reported which exhibit energy transfer properties.[34] The OPV derivative **29b** which forms a gel in toluene was selected as a template. Another OPV derivative **49** which contains a disulfide moiety at one end was used to bind gold nanoparticles. Mixing of **29b**/**49**-Au in toluene at different ratios followed by heating and cooling of the solution resulted in a coassembled gel. The formation of **29b**/**49**-Au hybrid supramolecular tapes is visualized by TEM that showed arrays of Au particles on both sides of the tape, indicating the formation of supramolecular hybrid tapes of **29b**/**49**-Au (Figure 1.17a). Fluorescence studies revealed that incorporation of **49**-Au into the tapes of **29b** results in the quenching of the OPV luminescence (Figure 1.17b). In the case of the 100:1 **29b**/**49**-Au mixture, the intensity was reduced by a factor of 33 in comparison with the emission intensity of **29b** alone. Time resolved photoluminescence studies revealed shortening of the lifetime of **29b** upon addition of **49** attached nanoparticles, when compared to that of **29b** alone. This

observation indicates that at least part of quenching is due to a dynamic process that takes place in nanosecond time scale and involves exciton energy migration towards docked gold nanoparticles. Further confirmation to this speculation is obtained from photoinduced absorption (PIA) studies, which showed a clear difference in the population of the excited state of **29b** and **29b**/**49**-Au hybrid gels, mainly in the nanosecond time scale. A very short lifetime observed for **49**/Au system in PIA studies points towards a rapid energy transfer from **49** to the gold core. Result of these studies demonstrate that the close proximity of gold nanoparticles to the OPV nanotapes facilitates strong electronic communication which makes them attractive candidates for the fabrication of electron and energy transport based nanodevices.

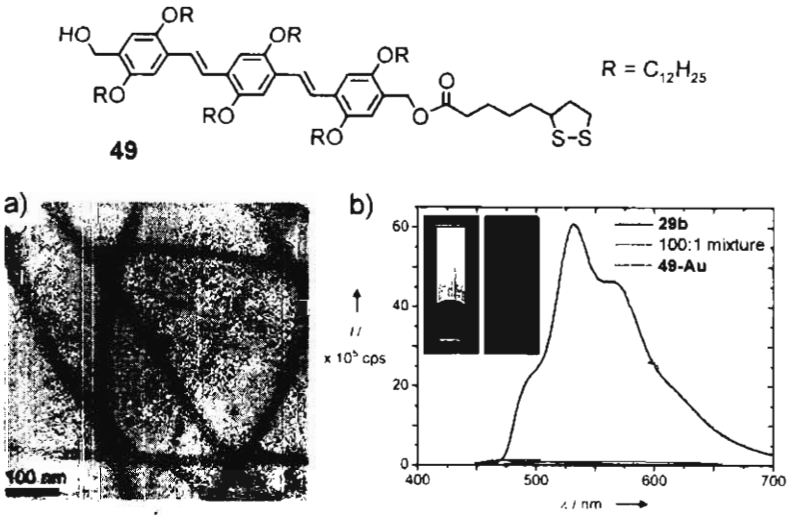


**Figure 1.17.** a) TEM image of **29b**/**49**–Au (100:1) tapes deposited from toluene. b) Fluorescence spectrum of a 100:1 mixed gel of **29b** and **49**–Au and of the separate compounds in toluene. Inset: photographs of the luminescent **29b** gel (left) and of the 100:1 **29b**/**49**–Au mixed gel (right). (adapted from ref. 34)

### 1.3.3. Organogels for Conducting Nanowires

The preparation of conducting nanofibers based on the self-assembly of functional π-conjugated molecules is very important since they may find applications in molecular electronic devices. Even though supramolecular wires offer many advantages, controlling the self-assembly process is a challenging task. In particular, deposition of nanostructures on surfaces is difficult to control, and in many cases different morphologies and size distributions are common. Gelation of molecules offers an interesting way to form fibers in a homogeneous medium, which can then be physically deposited on any surface. Many supramolecular gels based on functional chromophores are reported to form conducting nanowires.

Tetrathiafulvalene (TTF)[35] is known as an organic conducting material whose high electron conductivity is originated from their π-stacked columnar structures. They form fibrous aggregates as a result of hydrophobic and π-stacking interactions. The first attempt to design self-assembling molecular wires using TTF was done by Jorgensen and Bechgaard, in which TTF molecules were attached to bis-arborol, to provide the compound **50** (Chart 1.5), which was found to be an efficient organogelator.[36] TTF core attached to 3,4,5-tridodecyloxy benzene (**51**) through a flexible linker containing two amide groups form aggregates and gels in *n*-hexane.[37] This on $I_2$ doping, showed a characteristic near-infrared (NIR) absorption band at room temperature assignable to a mixed-valence state, which is known to be indispensable for constructing conductive nanowires.

An amphiphilic bis-TTF annulated macrocycle derivative (**52**) reported by Nakamura *et al.* form redox active organogels as well as electrically active nanostructures.[38] TTF incorporated phthalocyanine derivatives (**53a-b**) showed conductance when doped with 7,7,8,8-tetra-cyanoquinodimethane (TCNQ) in DMSO.[39] A new absorption band was observed in the UV-vis spectrum at 750 nm which corresponds to a mixed-valence state. Doping of **53b** in $CH_2Cl_2$ with $I_2$ produced a similar effect in the UV-vis spectrum as in the case of doping with TCNQ in DMSO.

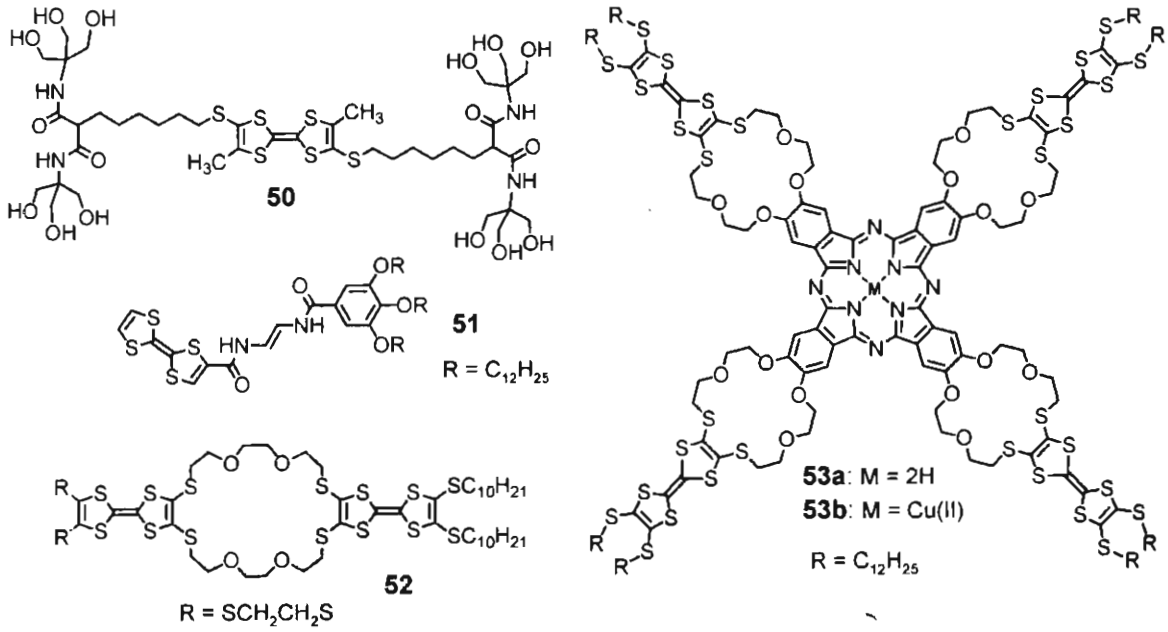


**Chart 1.5**

The amide-functionalized TTF (**54**) forms stable gels in decane or hexane.[40] Nanofibers formed by this gelator was transformed into conducting or metallic nanowires by doping (with iodine) and annealing, leading to a bulk material which

conducts electricity. This procedure allows the formation of stable TTF-based nanowires on different substrates and generation of a thin film which is electrically conducting (Figure 1.18). The hydrogen-bonding amide unit plays the key to generate the conducting nanowires. The ease of the processing method makes it very appealing for applications in molecular electronics.

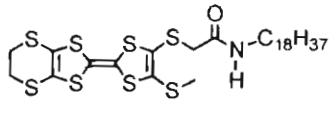


**54**

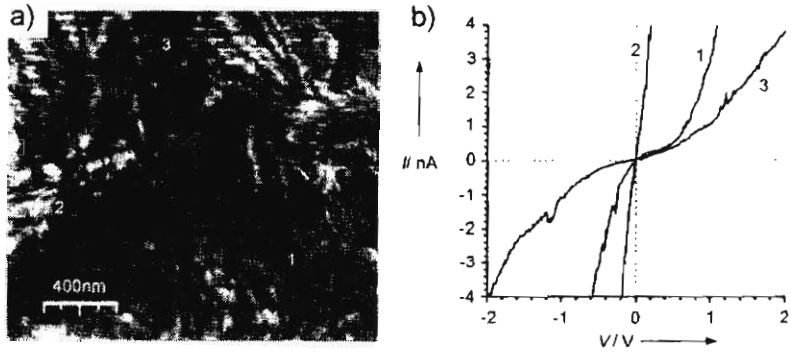


**Figure 1.18.** a) Current-sensing AFM image showing the current response of a doped annealed xerogel of **54** on graphite. b) Representative spectroscopic curves of different areas of the material which correspond to the numbered areas in image a. (adapted from ref. 40)

The bisurea-appended oligo(thiophene)s (**55a-b**) have been reported to self-assemble into elongated fibers resulting in the formation of organogels in solvents such as tetralin and 1,2-dichloroethane.[41] Electron microscopy and X-ray diffraction studies revealed that the fibers have a lamellar structure, in which the molecules are arranged as one-dimensional ribbons with their long molecular axis parallel to each other (Figure 1.19). Moreover, it was shown by pulse-radiolysis time resolved microwave conductivity experiments that the good electronic

overlap between the thiophene rings due to the H-bond assisted π-stacking of adjacent oligomers results in high charge carrier mobility of 0.001 $cm^2/Vs$ for **55a** and 0.005 $cm^2/Vs$ for **55b**. These values are relatively high when compared to that of simple thiophene oligomers.

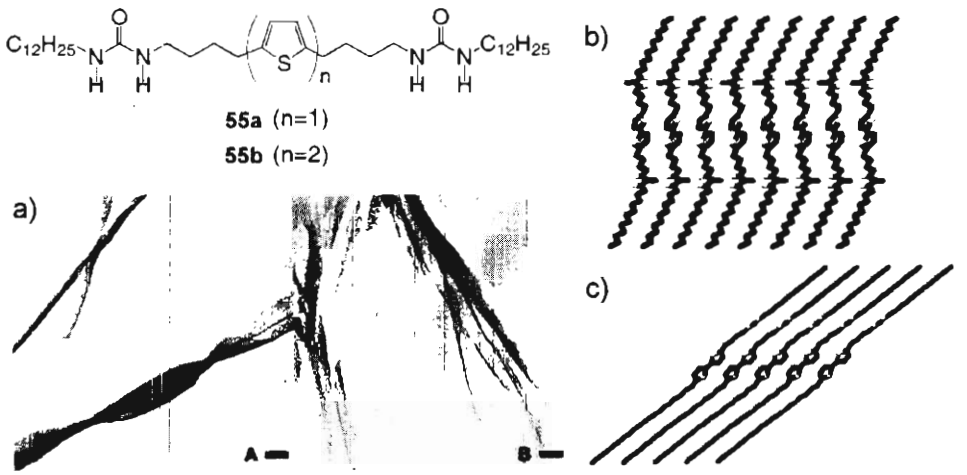


**Figure 1.19.** a) Electron micrographs of the lamellar fibers of **55a** (A) and **55b** (B). Possible arrangement of **55a** in the lamella: b) view of a H-bonded ribbon, and c) a tilted stack of ribbons that form lamella. (adapted from ref. 41)

In recent years, there has been considerable interest in the self-assembly of diacetylene derivatives as they allow the covalent fixation of supramolecular assemblies through photopolymerization reactions to give polydiacetylenes (Figure 1.20), which are attractive candidates as conducting nanowires.[42] Ge forming diacetylenes are particularly interesting because the gel network which i stabilized by the noncovalent interactions can be permanently supported by stron covalent bonds under photolytic conditions, thereby retaining the morphologica characteristics with increased thermal stability.

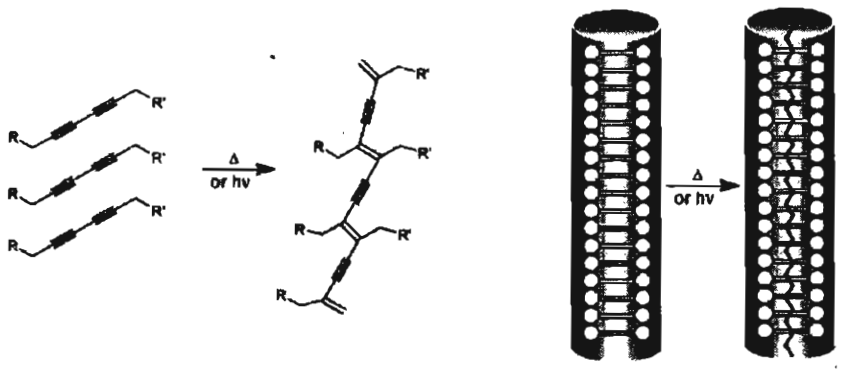


**Figure 1.20.** Photopolymerization of diacetylenes to polydiacetylenes and the schematic representation of the concept of covalent fixation of diacetylenes derived self-assemblies.

Masuda *et al.* have reported diacetylene-1-glucosamide bolaamphiphiles (**56a-b**), which self-assemble to form nanofibers leading to the gelation of organic solvents (Chart 1.6).[43] Diacetylene dicholesteryl ester derivative (**57**) having urethane linkages have been polymerized in the organogel state to form nanowires.[44] A series of 10,12-pentacosadiynoic acid derived organogelator with conjugated diyene units (**58**) and their photopolymerization was reported by Weiss and coworkers.[45] 1,2-Aminocyclohexyl derivative have also been polymerized in the gel network, by incorporating diacetylene linkages to the alkyl side chains (**59**).[46] Recently, Shinkai and coworkers reported a series of polydiacetylene based conducting nanofibers from low molecular weight gelators.[47] The gelator consists of two trialkoxybenzoic acid connected to a diacetylene group on both ends (**60**) through a flexible alkyl chain containing two amide groups. These molecules may find applications as conductive materials for nanowires and nanodevices.

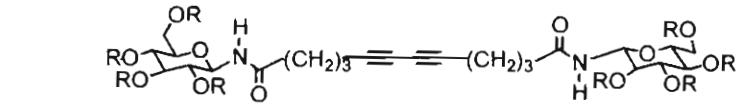


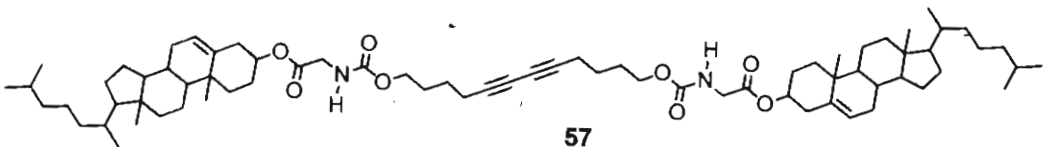

57

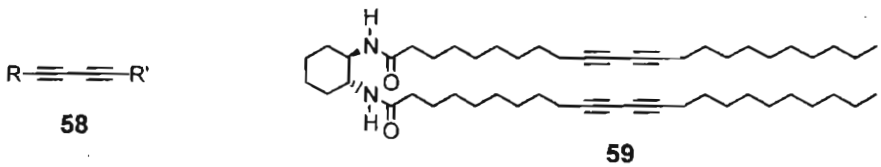

58 59

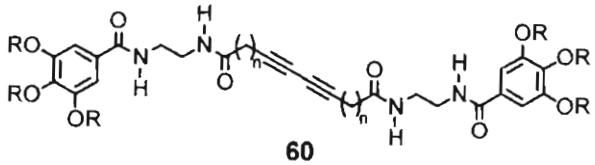


60

**Chart 1.6**

Polycyclic aromatic hydrocarbons (PAHs) are considered as one of the promising components for molecular electronics because of their strong tendency to form one-dimensional columnar structures via π-stacking interactions. Unidirectionally assembled PAHs have been shown to exhibit anisotropic charge- and energy transport activities. A representative example of PAHs includes hexa-*peri*-hexabenzocoronene (HBC), which consists of thirteen fused benzene rings.

Self-assembly and gelation of HBCs result in highly ordered nanostructures with one-dimensional charge transport properties. First report of the gelation of HBC derivatives (**61-62**) was from Müllen's group (Chart 1.7).[48] Later Aida and coworkers demonstrated that graphitic nanotubes and gels composed of achiral

and chiral hexa-*peri*-hexabenzocoronene amphiphile (**63-64**) can be readily obtained by self-assembly,[49] where majority of the nanotubes are aligned unidirectionally along the fiber axis. The fiber upon doping with $I_2$ displays an anisotropic conduction.

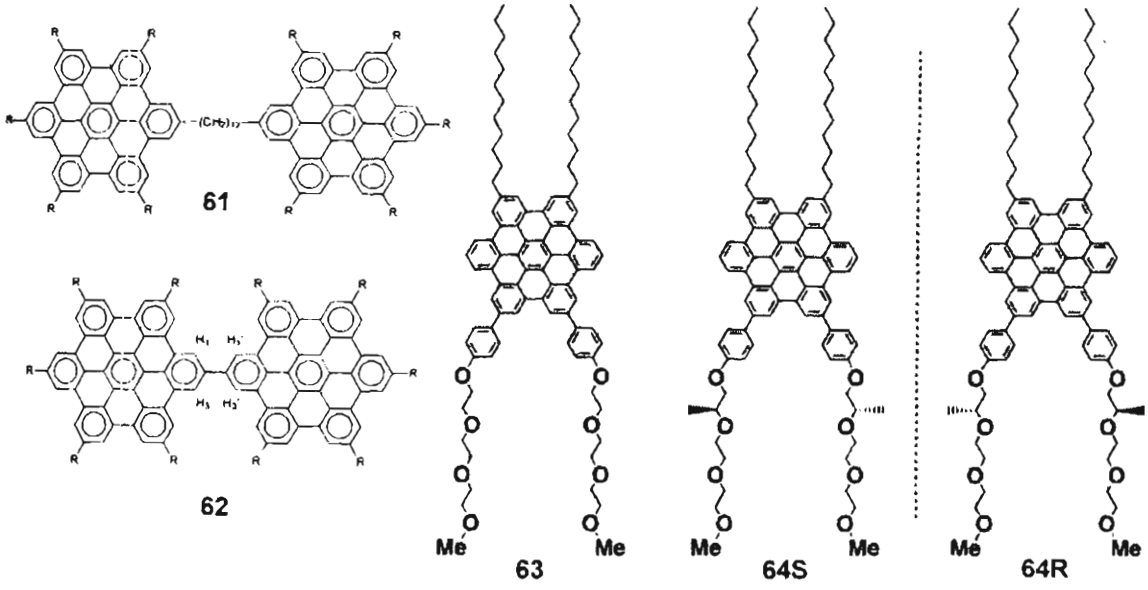


Chart 1.7

## 1.3.4. Stimuli Responsive Organogels

Stimuli-responsive supramolecular materials in general and gels in particular are becoming increasingly important because of their implications in controlled-release systems and sensing devices. Introduction of functional groups that can reversibly change the structure of organogels by stimuli other than heat has been of much interest as a method to design multiresponsive materials.

Self-assembled materials containing photoresponsive chromophores show light-induced photoswitchable properties. Azobenzene, stilbene, dithienylethene

and butadiene based stimuli responsive gels are reported in the literature. Gelators containing substituted azobenzenes as the aromatic part have been studied extensively by Shinkai and coworkers. In their first report, two types of azobenzene gelators containing cholesterol units with either a natural (S)-configuration (**65**-S) or the inverted (R)-configuration (**65**-R) at the C-3 position have been reported.[50] These molecules specifically undergo gelation either in nonpolar solvents (S derivatives) or in polar solvents (R derivatives) and show circular dichroism (CD) in the gel state. In this case, the sol-gel transition could be controlled by the *cis*-to-*trans* isomerization of azobenzene, leading to photoresponsive organogels (Figure 1.21)

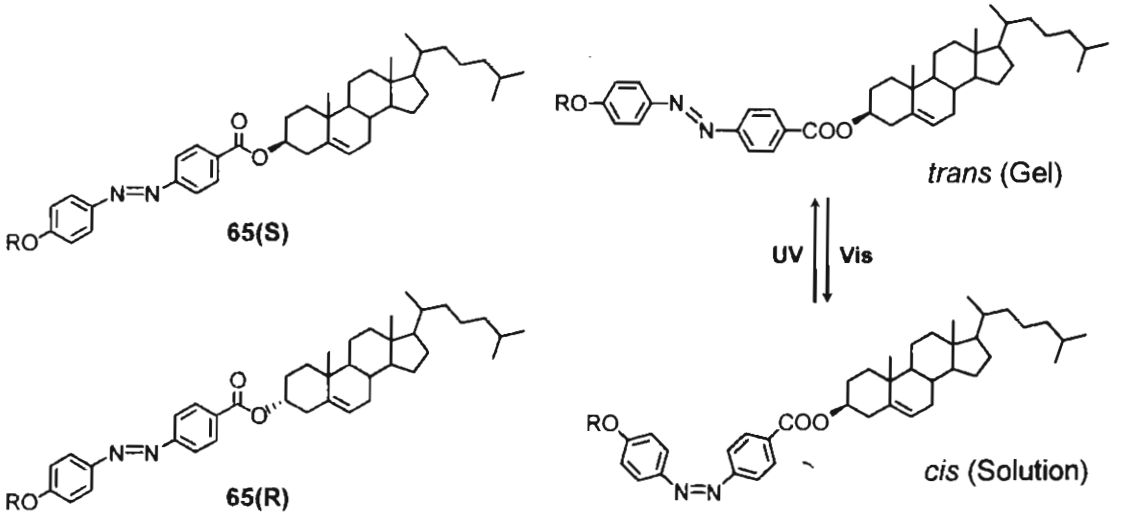


**Figure 1.21.** The *trans*-to-*cis* isomerization of **65**(S). (adapted from ref. 50)

Tamaoki *et al.* have reported a photoresponsive azobenzene gelator containing cholesterol end caps (**66**) connected through a flexible linker (Chart 1.8).[51] The sol-gel properties and morphology of the self-assemblies are

significantly influenced by the isomerization of the photochromic moiety. Huang and coworkers reported a two-component organogel system with tunable morphology and photoresponsive properties.[52] The $C_3$-symmetrical photoresponsive trisurea compounds connected with three azobenzene moieties through flexible alkyl spacers (**67**) when mixed with another trisamide gelator (**68**) formed a stable gel in 1,4-dioxane. Morphology of the self-assembled structure varies with varying the composition between the two components. Since the azobenzene moiety is present at the rim of the packing, the **67/68** gel exhibits reversible photoisomerization from *trans* to *cis* without the breakage of the gel state which is a rare observation.

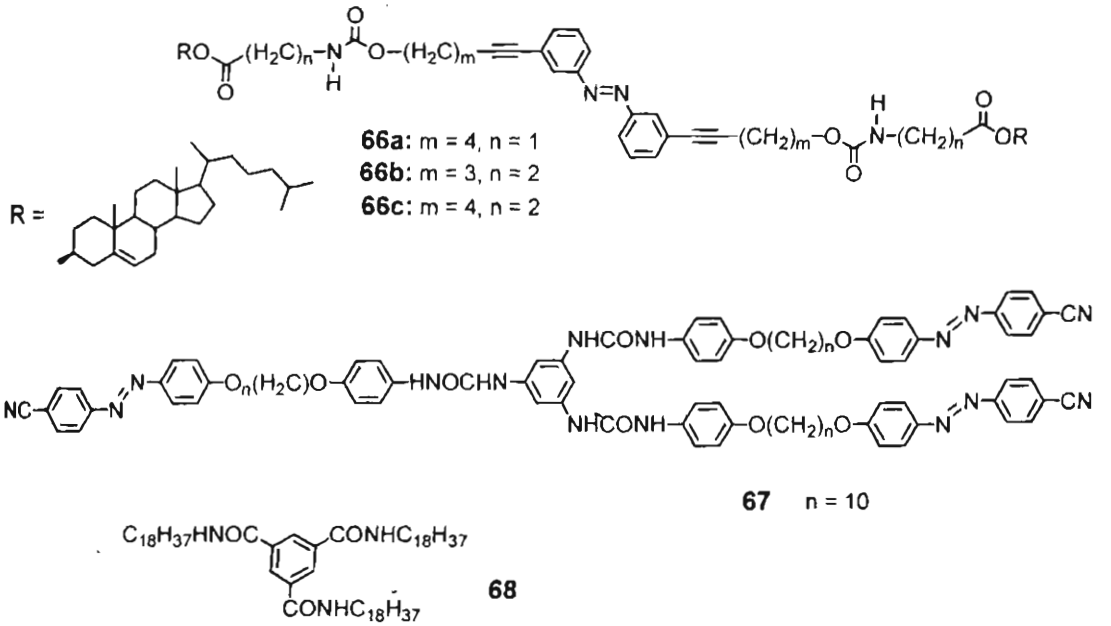


**Chart 1.8**

Yagai and coworkers have reported a photoresponsive organogel based on hydrogen-bonded rosettes composed of azobenzene-appended melamine (**69**) and

barbiturate (**70**) or cyanurate (**71**) derivatives.[53] In aliphatic solvents, rosette possessing the sterically bulky tridodecyloxyphenyl substituent in the barbiturate component does not hierarchically organize into higher-order columnar aggregates. However, sterically nondemanding *N*-dodecylcyanurate results hierarchically organized elongated columnar fibrous aggregates in cyclohexane, which eventually leads to the formation of an organogel (Figure 1.22). Dynamic light scattering and UV-vis studies revealed that the dissociation and the reformation of columnar aggregates can be controlled by the *trans-cis* isomerization of the azobenzene moiety. Molecular modeling indicates that the rosette possessing *cis*-azobenzene side chains loses its planarity on irradiation resulting in the disruption of the aggregates and hence the dissociation of the organogel.

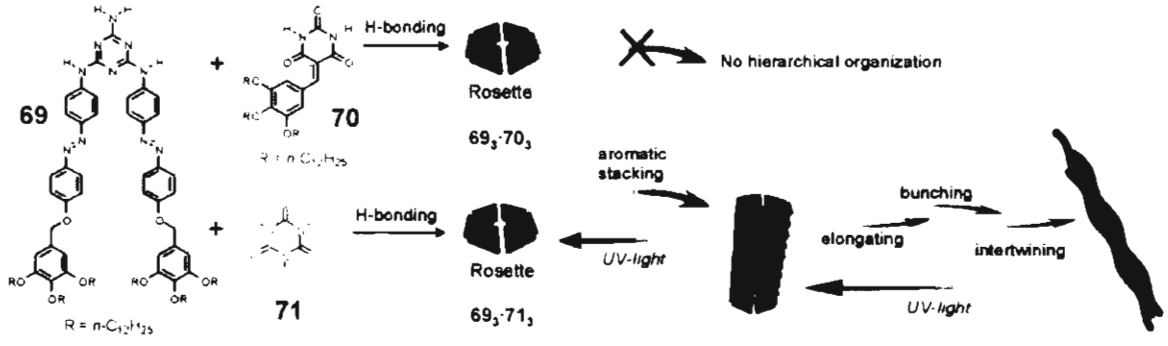


**Figure 1.22.** Agregation of **69** with **70**/**71** in cyclohexane. Red arrows indicate the hierarchical organization of rosettes into intertwined fibers. Blue arrows show the dissociation of higher order aggregates into rosettes on irradiation with light. (adapted from ref. 53)

The azobenzene-functionalized diaminopyrimidinone derivative (**72**) can hierarchically organize into lamellar superstructures to form organogels in

nonpolar media, which undergoes photoinduced disruption and reformation as demonstrated by photochemically reversible sol–gel transition.[54] Irradiation with UV light (350 nm) slowly dissolve macroscopic aggregates, resulting in the collapse of the gel into soluble supramolecular tapes (Figure 1.23).

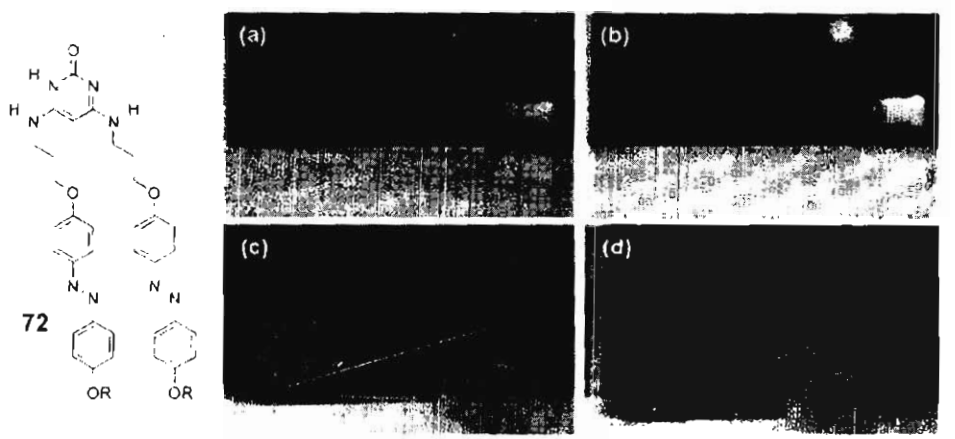


**Figure 1.23.** Photoinduced collapse of the heptane gel of **72** ($c = 1 \times 10^{-2}$ M) in a 1 mm cuvette (a→b, 1 h) and in a 1 cm cuvette (c→d, 4 h) upon irradiation with UV light (350 nm). (adapted from ref. 54)

Among various types of photochromic compounds, bisthienylethene (BTE) derivatives are the most promising because of their excellent fatigue resistance and thermal stability in isomeric forms, picosecond switching rate, and high photochemical quantum yields. In an interesting work, switching of the chirality of the supramolecular aggregates of a gel derived from a BTE derivative (**73**) has been realized through interconversion between cyclic and acyclic forms with the aid of light.[55] The gelator **73** exists in the acyclic form as *P*- and *M*-helical conformers and undergoes reversible photocyclization to yield a diastereomeric pair of cyclic forms. Both forms could gelate toluene. When an isotropic solution

of the acyclic form of **73** in toluene was cooled, a stable gel of *P*-helicity was obtained. Irradiating this gel at 313 nm resulted in a metastable gel (*P*-helicity) of the cyclic form with a diastereoselectivity of 96%. The high diastereoselectivity obtained is attributed to the existence of only one of the acyclic conformers (*P*-helical or *M*-helical) in the fibers due to stereoselective aggregation. When this metastable gel was heated to obtain an isotropic solution followed by cooling gave a thermodynamically stable gel of the cyclic form with *M*-helicity. Furthermore, irradiating this gel with visible light gave a metastable gel of the acyclic form with *M*-helicity, which upon a heating and cooling cycle returned to the original gel (acyclic form with *P*-helicity) (Figure 1.24). Thus, the supramolecular chirality was preserved during both photochemical reactions (ring-opening and ring-closing steps), yielding thermodynamically less favored aggregate structures. These structures could easily be converted to the thermodynamically favored aggregates via a heating and cooling cycle.

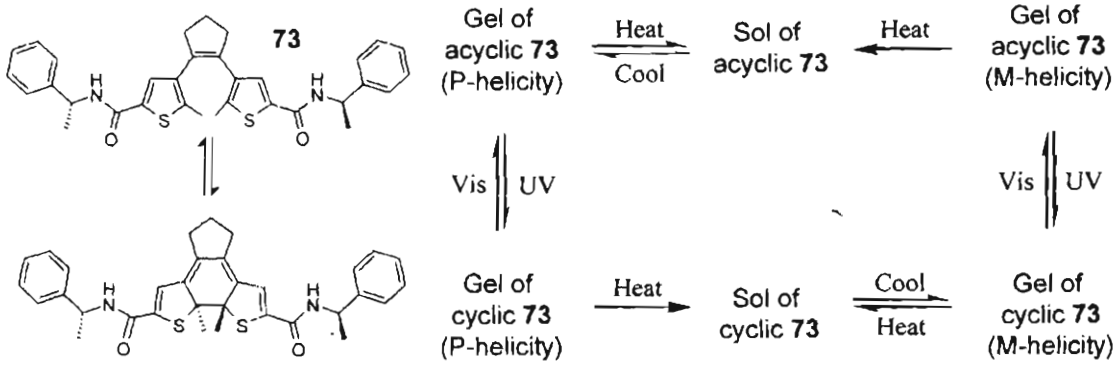


**Figure 1.24.** Four different chiral aggregate states and the switching processes of the chiroptical supramolecular switch consisting of the open and closed forms of **73**. (adapted from ref. 55)

Tian and coworkers have reported a multiple switching organogel based on bisthienylethene bridged naphthalimides (**74**) which respond to light, temperature, fluoride ion and proton.[56] Both open and closed forms of **74** are found to be excellent gelators. Upon irradiation with 365 nm UV light and visible light ($\lambda >$ 510 nm), the yellow colored open form of **74** can be interconverted through a red colored closed-ring form in the gel or in solution. Irradiation of **74** with UV light at 365 nm led to the appearance of a new absorption band around 540 nm and a large enhancement in fluorescence. The interconversion between the gel phase and solution could be easily achieved by thermal stimulus. In addition, the solutions of **74**, both in the open form and in the closed-ring form were sensitive to fluoride ion. Upon addition of $F^-$, the band around 330 nm progressively increases along with a new peak at 495 nm and the solution become orange red in color (Figure 1.25). This could be due to the deprotonation of the amino moiety by $F^-$, which would result in a negative charge density on the amide nitrogen, with associated enhancement in the push–pull effect of the ICT transition. Significant emission at 570 nm was also observed in presence of $F^-$ ions possibly due to the change in electron density of the amide moiety upon fluoride addition which influences the charge transfer between the amide group and the acceptor.

Bisurea-functionalized naphthalene derivatives (**75a-c**) are examples of stimuli responsive organogelators. The gel-sol transition of these systems, as well as the fluorescent emission are reversibly controlled by the change of temperature

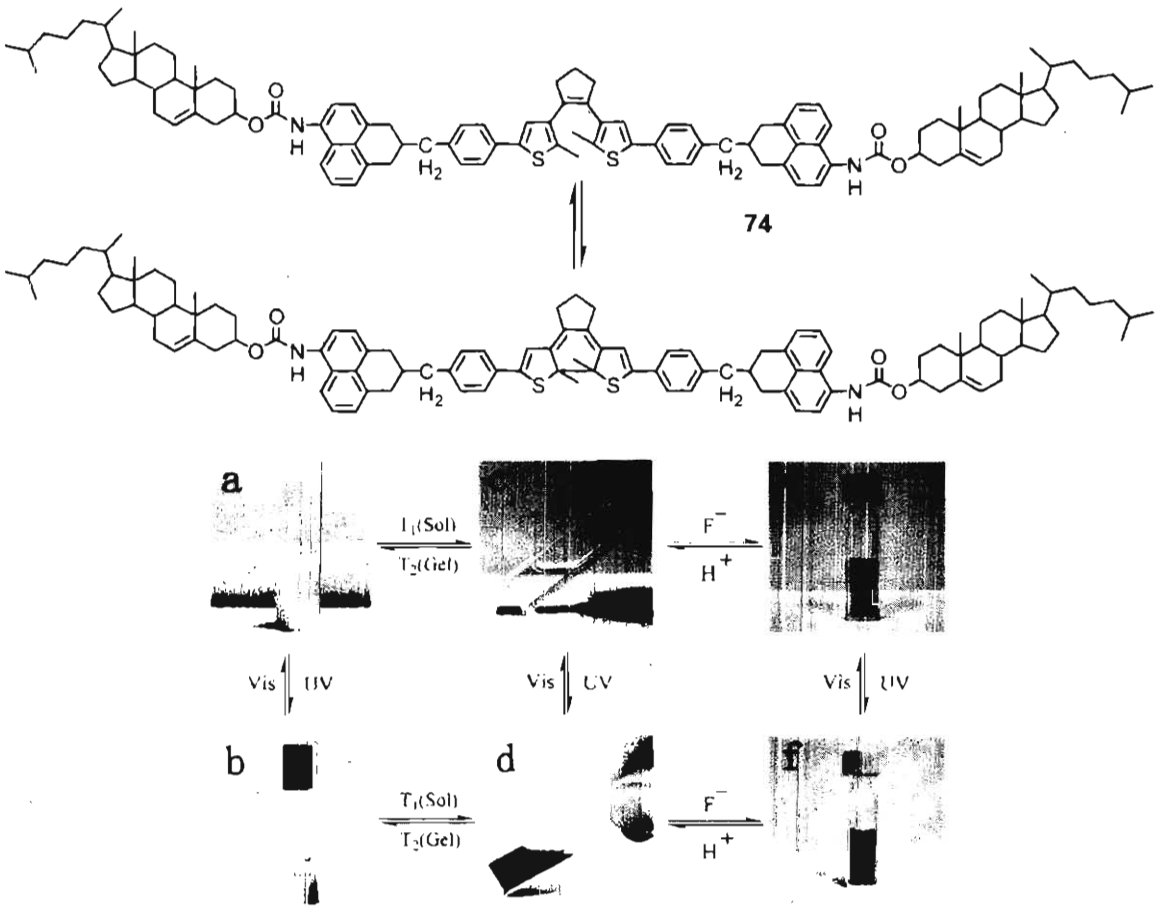


**Figure 1.25.** Multiple switching images of **74** under the cooperative effects of light, thermal, fluoride anions and protons. a) Gel (open); b) Gel (closed); c) Sol (open); d) Sol (closed); e) Sol (open) + $F^-$; f) Sol (closed) + $F^-$. (adapted from ref. 56)

or upon alternative addition of fluoride anions or protons.[57] Organogels of 2H-chromene derivative (**76**) were shown to be both light and pH sensitive.[58] The neutral carboxylic acid forms are readily soluble in DMF and DMSO and form gels upon the addition of NaOH. Furthermore, on irradiation at 366 nm, an yellow color was rapidly developed and the gel started to flow upon inversion. In dark, a colorless viscous solution was formed, which on heating followed by cooling

regenerated the original gel. These transitions were caused by the photoinduced ring opening of the colorless cyclic form to the colored acyclic form, which partially disrupts the gel structure due to its incompatibility with the network. The acyclic form is, however, thermally unstable and returns to the cyclic form upon heating and cooling resulting in the formation of a gel (Chart 1.9).

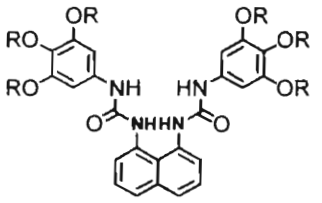

**75a:** R = $C_6H_{13}$
**75b:** R = $C_{12}H_{25}$
**75c:** R = $C_{16}H_{33}$

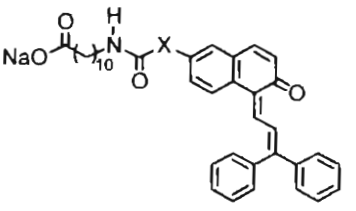

**76a:** X = None
**76b:** X = $CH_2O$

**Chart 1.9**

A two component system consisting of an acid derivative of anthracene (**77**) and an amine derivative (**78**) with C10 alkyl chain shows good gelation ability in cyclohexane.[59] It showed both thermal and photochemical responses. Upon irradiation with mercury lamp, the gel in cyclohexane at 15 °C transformed into a sol via photo-induced dimerization of the anthracene units leading to a non-gelator. However, warming this sol to 30 °C in the dark, thermally dissociates the anthracene dimer and the gelator is regenerated leading to precipitate. The initially formed precipitate may be heated to form a sol and subsequent cooling produces the gel (Figure 1.26).

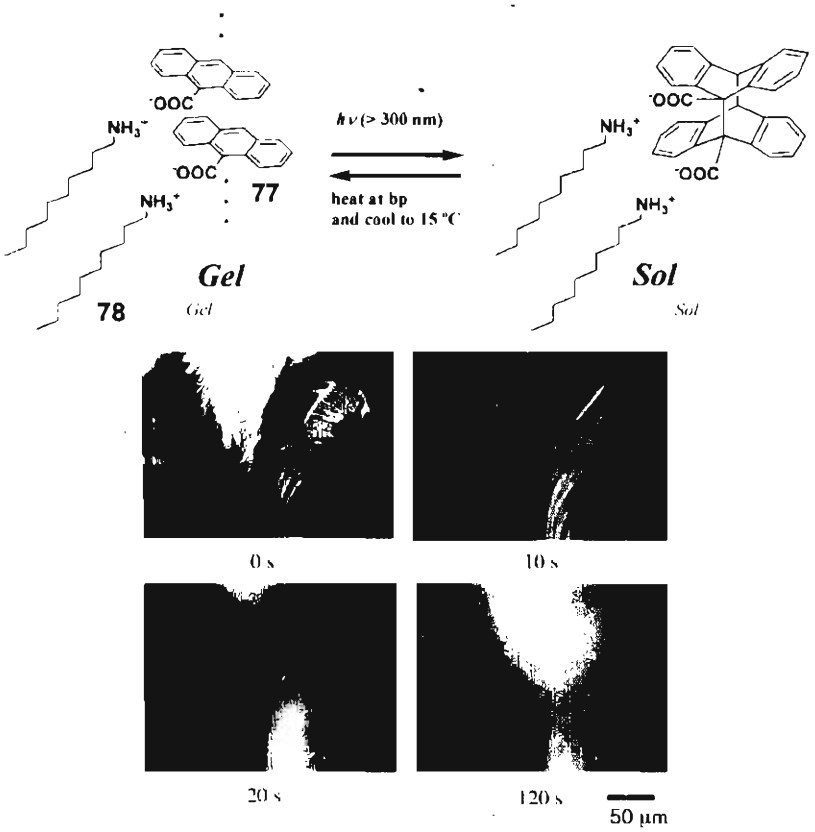


**Figure 1.26.** a) Photo- and thermo-responsive phase changes in **77**, b) Morphological change in the cyclohexane gel of **77** monitored by dark-field optical microscopy with the photoirradiation time. (adapted from ref. 59)

Several other photoresponsive chromophores are also used for the development of stimuli responsive gels (Chart 1.10). Polycatenar-type organogelators comprising a cyanochalcone unit and a half disk-like phenyl group with two or three long alkoxy chains (**79-80**) form photoresponsive organogels in *n*-alkanes, cyclohexane, and alcohols.[60] Upon photoirradiation, the [2 + 2] addition reaction of the chalcone units occurred, which induced a gel-to-sol transition. The oxalyl amide derivatives bearing 4-dodecyloxy-stilbene (**81**) formed stable gels in the *trans* form, whereas the corresponding *cis* derivative showed a poor gelation

ability or none at all.[61] Recently Das *et al.* reported a novel class of donor-acceptor substituted amphiphilic butadienes (**82**) capable of undergoing spontaneous concentration dependent hierarchical self-assembly from vesicles to gels.[62] The self-assembly process was associated with unique changes in the fluorescence of the system. Moreover, the presence of a photoisomerizable chromophore makes these materials photoresponsive.

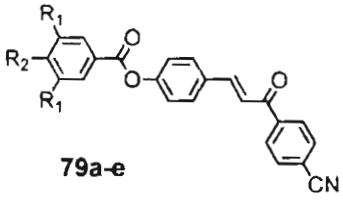

**79a-e**

**a**: $R_1$, $R_2 = OC_8H_{17}$
**b**: $R_1$, $R_2 = OC_{10}H_{21}$
**c**: $R_1$, $R_2 = OC_{12}H_{25}$
**d**: $R_1$, $R_2 = OC_{14}H_{29}$
**e**: $R_1 = OC_{10}H_{21}$, $R_2 = H$

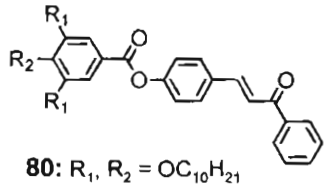

**80**: $R_1$, $R_2 = OC_{10}H_{21}$

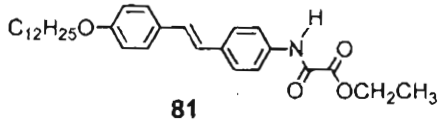

**81**

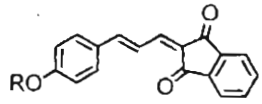

**82a-d**

**a**: $R = C_8H_{17}$
**b**: $R = C_{12}H_{25}$
**c**: $R = C_{16}H_{33}$
**d**: $R = OC_{18}H_{37}$

**Chart 1.10**

Shinkai *et al.* have reported a new class of stimuli responsive gels which can be used for the colorimetric detection of various naphthalene derivatives (Figure 1.27).[63] Cyclohexane gel of **83a** can differentiate different classes of electron-rich naphthalene compounds such as dihydroxynaphthalenes from alkoxy- and hydroxynaphthalenes (**84a-g**). Naked-eye differentiation of several positional isomers of dihydroxynaphthalene becomes possible as a result of hydrogen bonding-driven recognition that significantly amplifies the binding in the gel state.

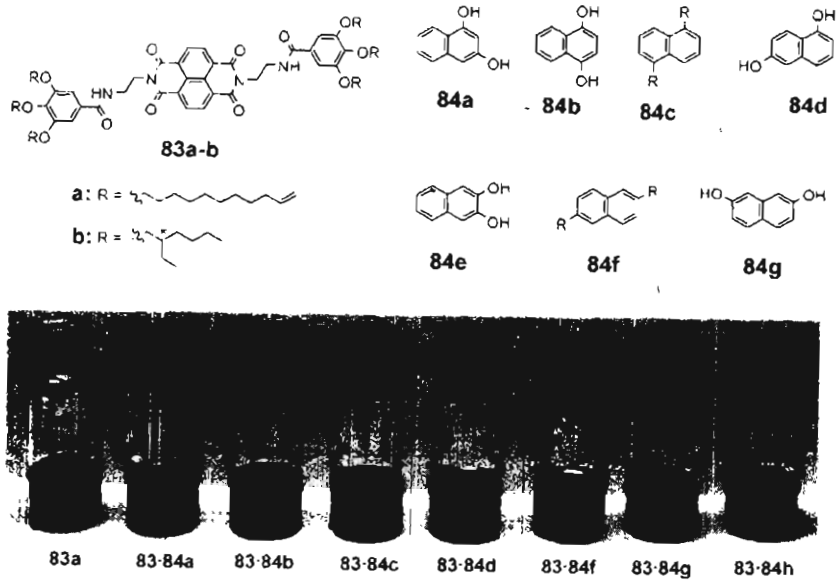


**Figure 1.27.** The photographs showing the spontaneous color changes of organogel **83a** upon addition of positional isomers of dihydroxynaphthalene (**84a–g**). (adapted from ref. 63)

Redox active gels are important for the construction of electromechanically active soft materials, such as artificial muscles and electro-rheological fluids. Gelators that contain metal ions (metallo-gelators) in several cases, form stimuli sensitive gels that undergo sol–gel phase transition when the redox state or the coordination number of the metal center changes. For example, a reversible color change was observed during the sol–gel transition of a gel derived from the Cu(I) complex of a 2,2′-bipyridyl derivative **85** of cholesterol in 1-butyronitrile.[64] The reddish brown sol of **85** turned into a greenish blue gel upon cooling. It is believed that a distortion of the tetrahedral Cu(I) complex in the confined environment of the gel fiber is responsible for this color change. The gelation ability of this complex depends upon the oxidation state of copper and hence could be tuned by a

redox process. Accordingly, heating the Cu(II) complex with ascorbic acid – to reduce Cu(II) to Cu(I) – followed by cooling produced a greenish-blue gel. Heating this gel with the oxidant $NOBF_4$ and cooling produced a sol with a small amount of blue precipitate (Figure 1.28).

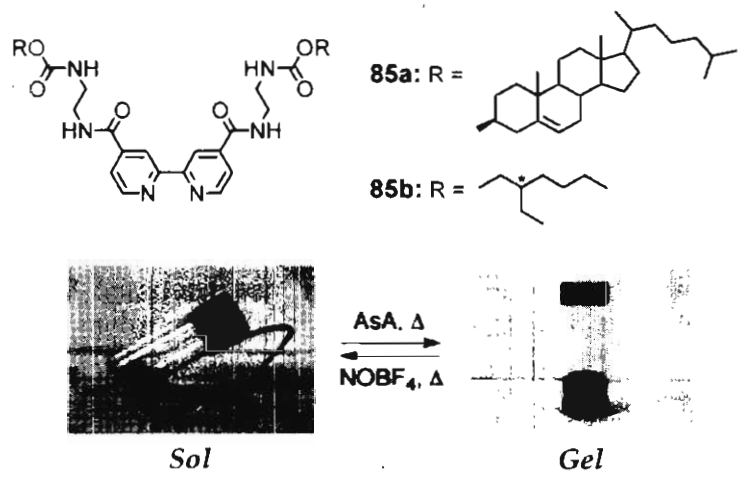


**Figure 1.28.** Reversible sol-gel transition and color changes of the Cu(II) complex of **85a** on addition of ascorbic acid (AsA) and $NOBF_4$. (adapted from ref. 64)

Recently, Shinkai *et al.* have reported a redox responsive organogel based on oligothiophene bearing cholesteryl groups at both ends (**86a-c**).[65] These molecules showed unique thermochromic properties during sol-gel transition in nonpolar solvents. When an oxidizing reagent such as $FeCl_3$ was added to the tetrachloroethane (TCE) gel of **86c** followed by vigorous stirring of the mixture for two minutes, the red gel turned into dark-brown solution. Addition of reducing agents such as ascorbic acid (AsA) to this solution regenerated the red gel after keeping for 1 h (Figure 1.29).

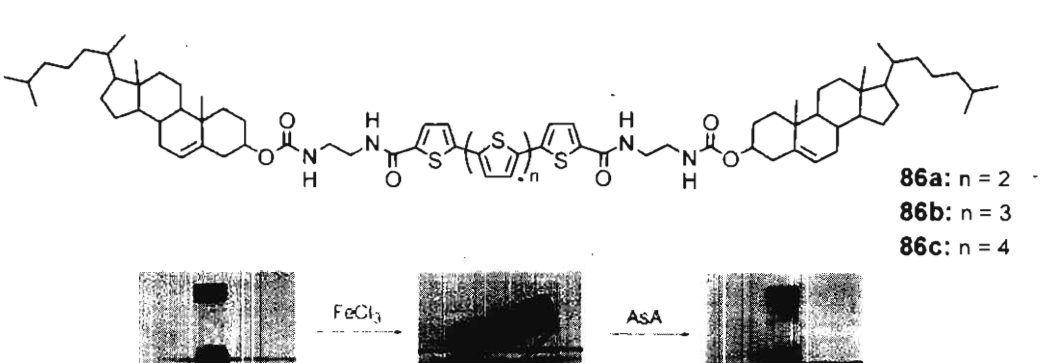


**Figure 1.29.** Sol–gel phase transition and color changes of the **86c** gel in TCE triggered by chemical oxidation and reduction. (adapted from ref. 65)

An analysis of the various reports as discussed above reiterate the importance of functional organogels in the field of advanced materials. A large number of chromophores and π-conjugated molecules have been exploited to the design of organogels that show intriguing optical and electronic properties. The insights gained over the years from these studies have helped chemists to design newer systems with improved properties.

## 1.4. Origin, Objectives and Approach to the Thesis

Self-assembly of electronically and photonically active molecules to supramolecular architectures of different size and shapes are important to the design of optoelectronic devices. Electronic properties of such molecules are strongly dependent upon the way in which the chromophores are organized. This is particularly true in the case of linearly π-conjugated molecules which are extensively used in the fabrication of organic electronic devices and light

harvesting systems. Therefore, rational approaches to the synthesis of molecular systems which are functionalized with proper self-assembly directing groups are extremely crucial. In this context, self-assembly and gelation of linear π-conjugated molecules such as OPVs and OPEs have been receiving much attention in recent years.[18,20] However, control on the organization of these molecules to supramolecular structures of a definite size and shape is a challenging task. The present work is a systematic investigation on the design, synthesis and properties of OPVs having different functional groups, their ability to form controlled supramolecular architectures and their use in excitation energy transfer processes.

We have decided to explore the end functionalization approach for controlling the organization of OPVs through different packing modes, leading to the control of the nanoscopic properties of resultant hierarchical self-assembly. For this purpose, we have prepared mono- and bischolesterol functionalized OPVs. Detailed investigation on the optical, chiroptical and morphological properties has been planned. The use of these self-assemblies as donor scaffolds for energy transfer processes in presence of suitable acceptors was another objective of the present investigation. In another strategy we have utilized bulky end functional groups in controlling the self-assembly of OPVs and their application to the design of supramolecular energy transfer systems with tunable emission colors. Detailed morphological investigations and photophysical properties of these OPV self-assemblies are presented.

## 1.5. References

1. a) J.-M. Guenet, *Thermoreversible Gelation of Polymers and Biopolymers*, Academic Press, London, **1992**; b) A. Saiani, J.-M. Guenet, *Macromolecules* **1997**, *30*, 967; c) A. Matsumoto, T. Kurata, D. Shiino, K. Kataoka, *Macromolecules* **2004**, *37*, 1502; d) T. Suzuki, S. Shinkai, K. Sada, *Adv. Mater.* **2006**, *18*, 1043.

2. Reviews on low molecular weight organogels: a) P. Terech, R. G. Weiss, *Chem. Rev.* **1997**, *97*, 3133; b) J. H. van Esch, B. L. Feringa, *Angew. Chem. Int. Ed.* **2000**, *39*, 2263; c) D. J. Abdallah, R. G. Weiss, *Adv. Mater.* **2000**, *12*, 1237; d) V. A. Mallia, N. Tamaoki, *Chem. Soc. Rev.* **2004**, *33*, 76; e) T. Shimizu, M. Masuda, M. Minamikawa, *Chem. Rev.* **2005**, *105*, 1401; f) N. M. Sangeetha, U. Maitra, *Chem. Soc. Rev.* **2005**, *34*, 821; g) M. George, R. G. Weiss, *Acc. Chem. Res.* **2006**, *39*, 489; h) F. Fages, *Angew. Chem. Int. Ed.* **2006**, *45*, 1680; i) D. K. Smith, *Chem. Commun.* **2006**, 34; j) A. Ajayaghosh, V. K. Praveen, *Acc. Chem. Res.* **2007**, *40*, 644; k) S. Rieth, C. Baddeley, J. D. Badjić, *Soft Matter* **2007**, *3*, 137.

3. a) F. Garnier, *Acc. Chem. Res.* **1999**, *32*, 209; b) C.-Y. Liu, A. J. Bard, *Acc. Chem. Res.* **1999**, *32*, 235; c) A. C. Grimsdale, K. Müllen, *Angew. Chem. Int. Ed.* **2005**, *44*, 5592; d) J. Hanna, *Opto-Electron. Rev.* **2005**, *13*, 259; e) R. U. A. Khan, O. P. Kwon, A. Tapponnier, A. N. Rashid, P. Günter, *Adv. Funct. Mater.* **2006**, *16*, 180; f) M. Muccini, *Nat. Mater.* **2006**, *5*, 605; g) P. L. Burn, S.-C. Lo, I. D. W. Samuel, *Adv. Mater.* **2007**, *19*, 1675; h) C.-Q. Ma, E. Mena-Osteritz, T. Debaerdemaeker, M. M. Wienk, R. A. J. Janssen, P. Bäuerle, *Angew. Chem. Int. Ed.* **2007**, *46*, 1679.

4. P. T. Herwig, K. Müllen, *Adv. Mater.* **1999**, *11*, 480.

5. Y.-C. Lin, R. G. Weiss, *Macromolecules* **1987**, *20*, 414.

6. T. Brotin, R. Utermöhlen, F. Fages, H. Bouas-Laurent, J.-P. Desvergne, *J. Chem. Soc., Chem. Commun.* **1991**, 416.

7. U. Maitra, P. V. Kumar, N. Chandra, L. J. D'Souza, M. D. Prasanna, A. R. Raju, *Chem. Commun.* **1999**, 595.

8. P. Babu, N. M. Sangeetha, P. Vijaykumar, U. Maitra, K. Rissanen, A. R. Raju, *Chem. Eur. J.* **2003**, *9*, 1922.

9. U. Maitra, V. K. Potluri, N. M. Sangeetha, P. Babu, A. R. Raju, *Tetrahedron: Asymmetry*, **2001**, *12*, 477.

10. Y. Kamikawa, T. Kato, *Langmuir* **2007**, *23*, 274.

11. M. Ikeda, M. Takeuchi, S. Shinkai, *Chem. Commun.* **2003**, 1354.

12. M. Shirakawa, N. Fujita, T. Tani, K. Kaneko, M. Ojima, A. Fujii, M. Ozaki, S. Shinkai, *Chem. Eur. J.* **2007**, *12*, 3287.

13. F. Camerel, R. Ziessel, B. Donnio, C. Bourgogne, D. Guillon, M. Schmutz, C. Iacovita, J.-P. Bucher, *Angew. Chem. Int. Ed.* **2007**, *46*, 2659.

14. a) F. Camerel, L. Bonardi, M. Schmutz, R. Ziessel, *J. Am. Chem. Soc.* **2006**, *128*, 4548; b) F. Camerel, L. Bonardi, G. Ulrich, L. Charbonnière, B. Donnio, C. Bourgogne, D. Guillon, P. Retailleau, R. Ziessel, *Chem. Mater.* **2006**, *18*, 5009.

15. S. Y. Ryu, S. Kim, J. Seo, Y.-W. Kim, O.-H. Kwon, D.-J. Jang, S. Y. Park, *Chem. Commun.* **2004**, 70.

16. B.-K. An, D.-S. Lee, J.-S. Lee, Y.-S. Park, H.-S. Song, S. Y. Park, *J. Am. Chem. Soc.* **2004**, *126*, 10232.

17. A. Kishimura, T. Yamashita, T. Aida, *J. Am. Chem. Soc.* **2005**, *127*, 179.

18. a) A. Ajayaghosh, S. J. George, *J. Am. Chem. Soc.* **2001**, *123*, 5148; b) S. J. George, A. Ajayaghosh, P. Jonkheijm, A. P. H. J. Schenning, E. W. Meijer, *Angew. Chem. Int. Ed.* **2004**, *43*, 3422; c) S. J. George, A. Ajayaghosh, *Chem. Eur. J.* **2005**, *11*, 3217; d) R. Varghese, S. J. George, A. Ajayaghosh, *Chem. Commun.* **2005**, 593; e) A. Ajayaghosh, R. Varghese, S. J. George, C. Vijayakumar, *Angew. Chem. Int. Ed.*

**2006**, *45*, 1141; f) M. Durkut, M. Mas-Torrent, P. Hadley, P. Jonkheijm, A. P. H. J. Schenning, E. W. Meijer, S. J. Goerge, A. Ajayaghosh, *J. Chem. Phys.* **2006**, *124*, 154704; g) V. K. Praveen, S. J. George, A. Ajayaghosh, *Macromol. Symp.* **2006**, *241*, 1; h) A. Ajayaghosh, V. K. Praveen, S. Srinivasan, R. Varghese, *Adv. Mater.* **2007**, *19*, 411; i) A. Ajayaghosh, V. K. Praveen, *Acc. Chem. Res.* **2007**, *40*, 644.

19. a) E. R. Zubarev, M. U. Pralle, E. D. Sone, S. I. Stupp, *J. Am. Chem. Soc.* **2001**, *123*, 4105; b) B. W. Messmore, J. F. Hulvat, E. D. Sone, S. I. Stupp, *J. Am. Chem. Soc.* **2004**, *126*, 14452.

20. a) A. Ajayaghosh, R. Varghese, V. K. Praveen, S. Mahesh, *Angew. Chem. Int. Ed.* **2006**, *45*, 3261; b) A. Ajayaghosh, R. Varghese, S. Mahesh, V. K. Praveen, *Angew. Chem. Int. Ed.* **2006**, *45*, 7729.

21. a) *Energy Harvesting Materials* (Ed.: D. L. Andrews) World Scientific, Singapore, **2005**; b) X. Hu, A. Damjanović, T. Ritz, K. Schulten, *Proc. Natl. Acad. Sci. U. S. A.* **1998**, *95*, 5935; c) A. M. van Oijen, M. Ketelaars, J. Köhler, T. J. Aartsma, J. Schmidt, *Science* **1999**, *285*, 400.

22. a) C. Devadoss, P. Bharathi, J. S. Moore, *J. Am. Chem. Soc.* **1996**, *118*, 9635; b) A. Adronov, J. M. J. Fréchet, *Chem. Commun.* **2000**, 1701; c) S. Hecht, J. M. J. Fréchet, *Angew. Chem. Int. Ed.* **2001**, *40*, 74; d) M.-S. Choi, T. Yamazaki, I. Yamazaki, T. Aida, *Angew. Chem. Int. Ed.* **2004**, *43*, 150.

23. a) S. E. Webber, *Chem. Rev.* **1990**, *90*, 1469; b) X. Schultze, J. Serin, A. Adronov, J. M. J. Fréchet, *Chem. Commun.* **2001**, 1160.

24. a) K. Sasaki, H. Nakagawa, X. Zhang, S. Sakurai, K. Kano, Y. Kuroda, *Chem. Commun.* **2004**, 408; b) J. M. Haider, Z. Pikramenou, *Chem. Soc. Rev.* **2005**, *34*, 120; c) C. Minkowski, R. Pansu, M. Takano, G. Calzaferri, *Adv. Funct. Mater.* **2006**, *16*, 273.

25. a) M. D. Ward, *Chem. Soc. Rev.* **1997**, *26*, 365; b) E. H. A. Beckers, P. A. van Hal, A. P. H. J. Schenning, A. El-ghayoury, E. Peeters, M. T. Rispens, J. C. Hummelen, E. W. Meijer, R. A. J. Janssen, *J. Mater. Chem.* **2002**, *12*, 2054; c) J. Zhang, F. J. M. Hoeben, M. J. Pouderoijen, A. P. H. J. Schenning, E. W. Meijer, F. C. De Schryver, S. De Feyter, *Chem. Eur. J.* **2006**, *12*, 9046; d) F. J. M. Hoeben, M. Wolffs, J. Zhang, S. De Feyter, P. Leclère, A. P. H. J. Schenning, E. W. Meijer, *J. Am. Chem. Soc.* **2007**, *129*, 9819.

26. L. A. J. Chrisstoffels, A. Adronov, J. M. J. Fréchet, *Angew. Chem. Int. Ed.* **2000**, *39*, 2163.

27. a) T. Nakashima, N. Kimizuka, *Adv. Mater.* **2002**, *14*, 1113; b) J. H. Ryu, M. Lee, *J. Am. Chem. Soc.* **2005**, *127*, 14170; c) S. Yamaguchi, I. Yoshimura, T. Kohira, S.-i. Tamaru, I. Hamachi, *J. Am. Chem. Soc.* **2005**, *127*, 11835. d) M. Montalti, L. S. Dolci, L. Prodi, N. Zaccheroni, M. C. A. Stuart, K. J. C. van Bommel, A. Friggeri, *Langmuir* **2006**, *22*, 2299.

28. T. Sagawa, S. Fukugawa, T. Yamada, H. Ihara, *Langmuir* **2002**, *18*, 7223.

29. K. Sugiyasu, N. Fujita, M. Takeuchi, S. Yamada, S. Shinkai, *Org. Biomol. Chem.* **2003**, *1*, 895.

30. K. Sugiyasu, N. Fujita, S. Shinkai, *Angew. Chem. Int. Ed.* **2004**, *43*, 1229.

31. a) A. D. Guerzo, A. G. L. Olive, J. Reichwagen, H. Hopf, J.-P.Desvergne, *J. Am. Chem. Soc.* **2005**, *127*, 17984; b) J.-P. Desvergne, A. G. L. Olive, N. M. Sangeetha, J. Reichwagen, H. Hopf, A. D. Guerzo, *Pure. Appl. Chem.* **2006**, *78*, 2333.

32. J. B. Beck, S. J. Rowan, *J. Am. Chem. Soc.* **2003**, *125*, 13922.

33. a) A. Ajayaghosh, S. J. George, V. K. Praveen, *Angew. Chem. Int. Ed.* **2003**, *42*, 332; b) V. K. Praveen, S. J. George, R. Varghese, C. Vijayakumar, A. Ajayaghosh, *J. Am. Chem. Soc.* **2006**, *128*, 7542.

34. J. van Herrikhuyzen, S. J. George, M. R. J. Vos, N. A. J. M. Sommerdijk, A. Ajayaghosh, S. C. J. Meskers, A. P. H. J. Schenning, *Angew. Chem. Int. Ed.* **2007**, *46*, 1825.

35. a) C. Rovira, *Chem. Rev.* **2004**, *104*, 5289; b) M. FourMigué, P. Batail, *Chem. Rev.* **2004**, *104*, 5379 ; c) N. Martín, L. Sánchez, M. A. Herranz, B. Illescas, D. M. Guldi, *Acc. Chem. Res.* **2007**, (10.1021/ar700026t).

36. M. Jorgensen, K. Bechgaard, *J. Org. Chem.* **1994**, *59*, 5877.

37. T. Kitahara, M. Shirakawa, S.-i. Kawano, U. Beginn, N. Fujita, S. Shinkai, *J. Am. Chem. Soc.* **2005**, *127*, 14980.

38. T. Akutagawa, K. Kakiuchi, T. Hasegawa, S.-i. Noro, T. Nakamura, H. Hasegawa, S. Mashiko, J. Becher, *Angew. Chem. Int. Ed.* **2005**, *44*, 7283.

39. J. Sly, P. Kasák, E. Gomar-Nadal, C. Rovira, L. Górriz, P. Thordarson, D. B. Amabilino, A. E. Rowan, R. J. M. Nolte, *Chem. Commun.* **2005**, 1255.

40. J. Puigmart-Luis, V. Laukhin, A. P. del Pino, J. Vidal-Gancedo, C. Rovira, E. Laukhina, D. B. Amabilino, *Angew. Chem. Int. Ed.* **2007**, *46*, 238.

41. F. S. Schoonbeek, J. H. van Esch, B. Wegewijs, D. B. A. Rep, M. P. de Haas, T. M. Klapwijk, R. M. Kellogg, B. L. Feringa, *Angew. Chem. Int. Ed.* **1999**, *38*, 1393.

42. a) J. M. Warman, M. P. de Haas, G. Dicker, F. C. Grozema, J. Piris, M. G. Debije, *Chem. Mater.* **2004**, *16*, 4600; b) K. Takami, J. Mizuno, M. Akai-kasaya, A. Saito, M. Aono, Y. Kuwahara, *J. Phys. Chem. B*, **2004**, *108*, 16353.

43. M. Masuda, T. Hanada, Y. Okada, K. Yase, T. Shimizu, *Macromolecules* **2000**, *331*, 9233.

44. N. Tamaoki, S. Shimada, Y. Okada, K. Belaissaoui, G. Kruk, K. Yase, H. Matsuda, *Langmuir* **2000**, *16*, 7545.

45. M. George, R. G. Weiss, *Chem. Mater.* **2003**, *15*, 2879.

46. M. De Loos, J. van Esch, I. Stokroos, R. M. Kellogg, B. L. Feringa, *J. Am. Chem. Soc.* **1997**, *119*, 12675.

47. N. Fujita, Y. Sakamoto, M. Shirakawa, M. Ojima, A. Fujii, M. Ozaki, S. Shinkai, *J. Am. Chem. Soc.* **2007**, *129*, 4134.

48. S. Ito, P. T. Herwig, T. Bolhme, J. P. Rabe, W. Rettig, K. Müllen, *J. Am. Chem. Soc.* **2000**, *122*, 7698.

49. a) J. P. Hill, W. Jin, A. Kosaka, T. Fukushima, H. Ichihara, T. Shimomura, K. Ito, T. Hashizume, N. Ishii, T. Aida, *Science* **2004**, *304*, 1481; b) Y. Yamamoto, T. Fukushima, W. Jin, A. Kosaka, T. Hara, T. Nakamura, A. Saeki, S. Seki, S. Tagawa, T. Aida, *Adv. Mater.* **2006**, *18*, 1297.

50. K. Murata, M. Aoki, T. Suzuki, T. Harada, H. Kawabata, T. Komori, F. Ohseto, K. Ueda, S. Shinkai, *J. Am. Chem. Soc.* **1994**, *116*, 6664.

51. N. Koumura, M. Kudo, N. Tamaoki, *Langmuir* **2004**, *20*, 9897.

52. Y. Zhou, M. Xu, T. Yi, S. Xiao, Z. Zhou, F. Li, C. Huang, *Langmuir* **2007**, *23*, 202.

53. S. Yagai, T. Nakajima, K. Kishikawa, S. Kohmoto, T. Karatsu, A. Kitamura, *J. Am. Chem. Soc.* **2005**, *127*, 11134.

54. S. Yagai, T. Iwashima, K. Kishikawa, S. Nakahara, T. Karatsu, A. Kitamura, *Chem. Eur. J.* **2006**, *12*, 3984.

55. J. J. D. de Jong, L. N. Lucas, R. M. Kellog, J. H. van Esch, B. L. Feringa, *Science* **2004**, *304*, 278.

56. S. Wang, W. Shen, Y. Feng, H. Tian, *Chem. Commun.* **2006**, 1497.

57. H. Yang, T. Yi, Z. Zhou, Y. Zhou, J. Wu, M. Xu, F. Li, C. Huang, *Langmuir* **2007**, *23*, 8224.

58. S. A. Ahmed, X. Sallenave, F. Fages, G. Mieden-Gundert, W. M. Müller, U. Müller, F. Vögtle, J.-L. Pozzo, *Langmuir* **2002**, *18*, 7096.

59. M. Ayabe, T. Kishida, N. Fujita, K. Sada, S. Shinkai, *Org. Biomol. Chem.* **2003**, *1*, 2744.

60. G. S. Lim, B. M. Jung, S. J. Lee, H. H. Song, C. Kim, J. Y. Chang, *Chem. Mater.* **2007**, *19*, 460.

61. S. Miljanić, L. Frkanec, Z. Meić, M. Žinić, *Langmuir* **2005,** *21,* 2754.

62. N. S. S. Kumar, S. Varghese, G. Narayan, S. Das, *Angew. Chem. Int. Ed.* **2006**, *45*, 6317.

63. P. Mukhopadhyay, Y. Iwashita, M. Shirakawa, S.-i. Kawano, N. Fujita, S. Shinkai *Angew. Chem. Int. Ed.* **2006**, *45*, 1592.

64. S.-i. Kawano, N. Fujita and S. Shinkai, *J. Am. Chem. Soc.* **2004**, *126*, 8592.

65. S.-i. Kawano, N. Fujita, S. Shinkai, *Chem. Eur. J.* **2005**, *11*, 4735.

*Chapter 2*

# Synthesis and Self-Assembly of Cholesterol Tethered Oligo(*p*-phenylenevinylene) Derivatives: Controlled Chromophore Packing in π-Organogels

## 2.1. Abstract

*Precise control of chromophore self-assembly leading to long-range supramolecular architectures of nanometer dimension is a challenging task. Through a rational approach we have exploited cholesterol moieties in directing chromophore assemblies in controlled pathways leading to helical assemblies with distinct optical, chiroptical and morphological features. The monocholesterol attached oligo(p-phenylenevinylene)s (**MC-OPV1-3**) prefer to form pseudo J-aggregates with tilted chromophore packing which showed red-shifted bands in the absorption and emission spectra. However, the corresponding bischolesterol derivatives, (**BC-OPV1-3**) form pseudo H-aggregates with a twisted chromophore arrangement having blue-shifted absorption and relatively less shift in the emission bands. The circular dichroism (CD) spectra of **BC-OPV**s showed bisignate signals whereas those of **MC-OPV**s were of non-bisignate in nature. Due to the differences in chromophore packing **MC-OPV**s form strong gels in hydrocarbon solvents while the **BC-OPV**s resulted in weak gels. The morphological features of the hierarchical assemblies generated*

*from the pseudo J-aggregates of **MC-OPVs** resulted in coiled helical structures whereas the pseudo H-aggregates of **BC-OPVs** evolved into twisted helical structures as revealed by AFM studies.*

## 2.2. Introduction

Controlled self-assembly of chromophores in nano- to micrometer length scale using the principles of supramolecular chemistry is a topic of considerable importance.[1] The cooperative effect of weak noncovalent interactions are the driving force behind the self-assembly of molecules, leading to a variety of novel supramolecular architectures with reversible functional properties. In the domain of functional molecular assemblies and nanoarchitectures, supramolecular control of chromophore-linked molecular systems is a challenging task, particularly in the fabrication of nanoscale devices since chromophore orientation has tremendous influence on the optoelectronic properties.[2] This is particularly important in the emerging area of supramolecular electronics.[3] Therefore controlled self-assembly of polyaromatic and linear π-conjugated molecules to construct supramolecular wires of nanometer range using the 'bottom-up" self-assembly approach is gaining importance.

Müllen *et al.* have reported the uniaxially aligned thin films of hexabenzocoronene (HBC) **1** by a simple solution zone-casting method.[4] The aromatic interaction and the out of plane orientation of the peripheral phenyl rings in **1** induce a helical orientation of the HBC cores giving a helical crystalline phase

with a higher persistence length. Spin-casted films of **1** revealed arrays of uniform parallel nanoribbons with lengths of 300 nm as studied by AFM (Figure 2.1). Slow evaporation of the solvent resulted in long, isolated regular ribbons of 3.8 nm in height and 21 nm in width representing parallel single columns with the columnar axis oriented parallel to the substrate. XRD of the bulk samples shows that at room temperature, the disks are tilted by approximately 45° with respect to the columnar axes and this tilt alternates within adjacent columns (herringbone-like).

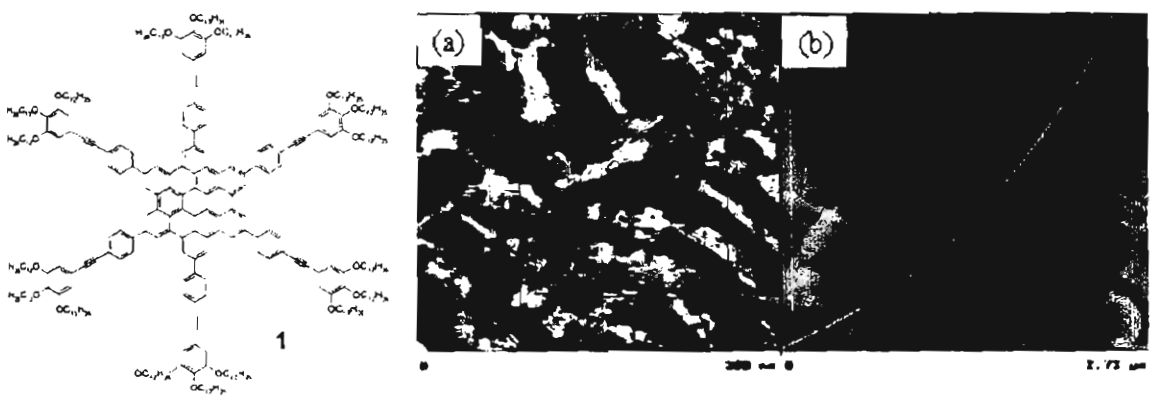


**Figure 2.1.** AFM images showing nanoribbons of **1** having 21 nm width and 3.8 nm height, obtained from a) spin-cast and b) drop-cast solutions. (adapted from ref. 4b)

Self-assembly of various donor and acceptor dendrons into supramolecular columns has been shown to be useful for the design of organic electronic materials (Figure 2.2).[5] This is a simple and versatile strategy for producing conductive π-stacks of aromatic molecules. The building blocks are composed of semifluorinated dendrons bearing electroactive carbazole, naphthalene, and pyrene as donors and trinitrofluorenone as acceptor. Moreover, co-assembly of donor and

acceptor dendrons leads to columns incorporating a central donor-acceptor complex. The columns further self-organize between electrodes into highly ordered homeotropic liquid crystals of various symmetries. The advantages of the ordering of π-conjugated moieties on material properties was reflected in the electron and hole mobilities, which are 2-5 orders of magnitude higher than those of the corresponding amorphous polymers.

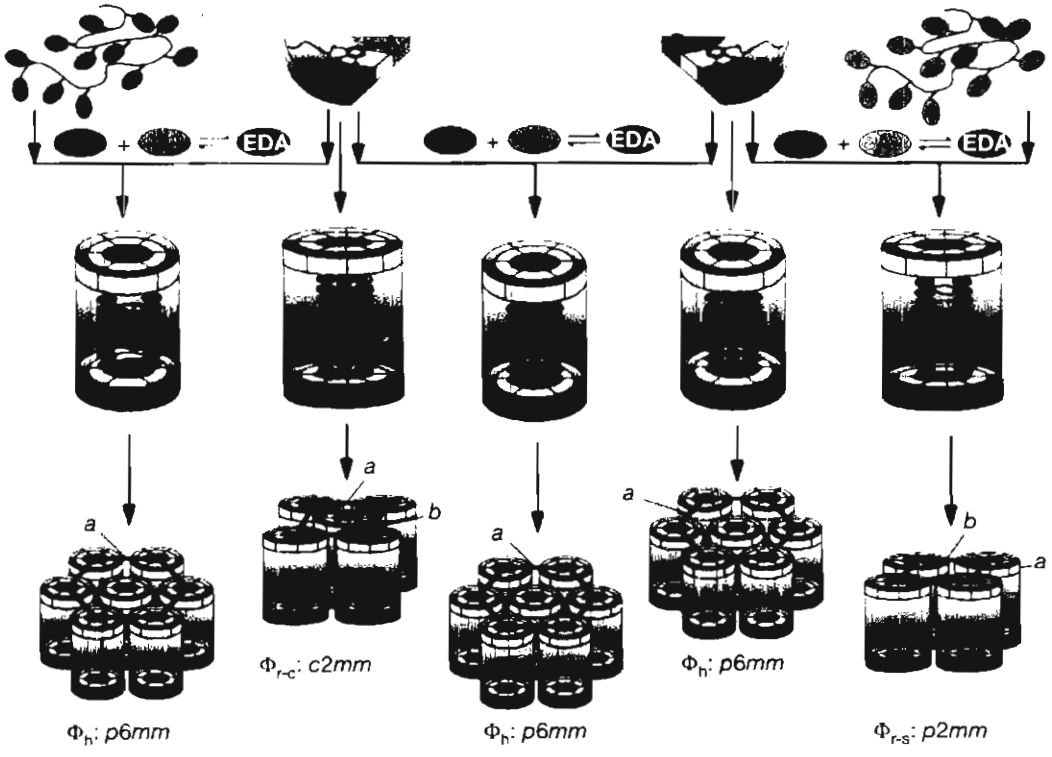


**Figure 2.2.** Schematic representation of the self-assembly of various donors and acceptors into highly ordered, complex structures. (adapted from ref. 5)

Long-range supramolecular ordering has been extensively studied in many other chromophoric assemblies.[6,7] However, precise control of such hierarchical assemblies to functionally and morphologically different nanoscopic architectures

through a preferred packing of the individual chromophore is a difficult task. This is particularly true with linear π-conjugated systems which play crucial role in organic electronic devices.[8-10]

Among various π-conjugated systems, phenylenevinylenes are one of the well studied class of molecules due to their importance in various electrooptical devices such as LEDs,[11] photovoltaic cells[12], FETs[13] etc. Control of the emission properties of phenylenevinylenes by donor-acceptor interaction and by varying the conjugation length of oligomers provide materials with well-defined functional properties.[14] Extensive studies have been reported in the literature, pertaining to the optical and electronic properties of oligo(*p*-phenylenevinylene)s (OPVs).[15-18] Meijer and co-workers have made significant contributions towards the supramolecular organization of oligo(*p*-phenylenevinylene) based linear π-conjugated molecules. Recently, we have shown the self-assembly induced gelation of oligo(*p*-phenylenevinylene) and oligo(*p*-phenyleneethynylene) (OPE) based systems in organic solvents to form supramolecular architectures of different size and shape.[19]

Among various non-hydrogen bonded gelators, cholesterol based gelators are the most extensively studied molecules.[20] In cholesterol based gelators, the C-3 hydroxyl group of the steroid unit is appropriately functionalized with a variety of aromatic moieties through different linkers. In most of the cases, the driving force for the gelation of such molecules is the aggregation of the cholesterol skeleton, as

a result of dipole-dipole and van der Waals forces, which is assisted by the π-π interactions between the aromatic moieties. In the aggregated state, cholesterol will interact in an asymmetric manner and induce its chirality to the attached chromophores. A schematic representation of the cholesterol based gel assemblies are shown in Figure 2.3, in which the cholesterol groups are stacked in a helical manner to form the central core thereby directing the aromatic groups outwards to form a spiral staircase assembly. A large number of functional aromatic groups such as anthracene, azobenzene, stilbene, squaraine, thiophene, perylene and porphyrin have been appended to the cholesterol for designing new gelator molecules.[20]

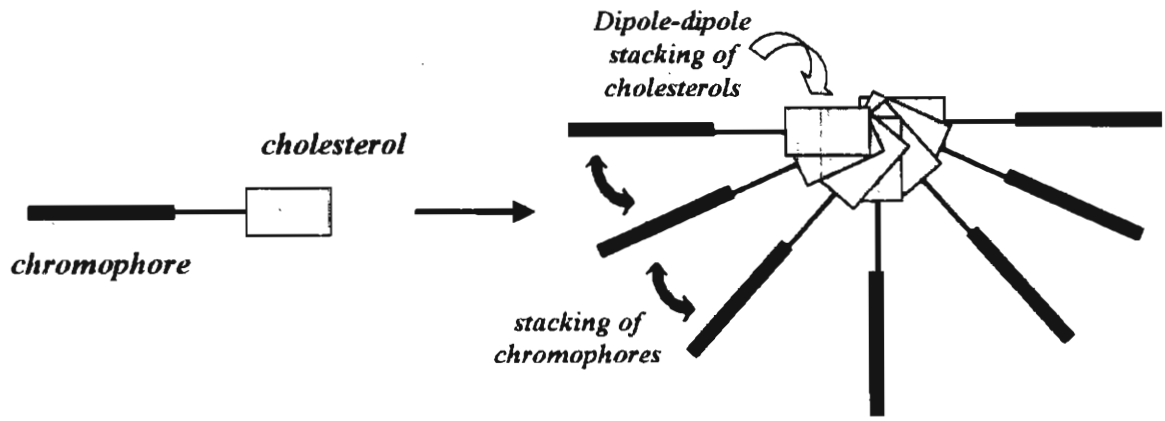


**Figure 2.3.** Schematic representation of the self-assembly of cholesterol derived organogelators.

Weiss and coworkers have carried out detailed investigation on low molecular weight organogelators containing cholesterol moiety.[20i] Shinkai *et al.* have reported an interesting case of sol-gel transition through photoisomerization in a cholesterol based organogelator containing azo group.[20a] They have studied

the application of these gels as a proton sensor[20e] and used as templates for the preparation of various inorganic nanostructures.[21] In the present study, we have investigated the gelation, morphology and optical properties of cholesterol appended OPV self-assemblies and demonstrate distinct helical packing of mono- and bischolesterol linked OPVs.

## 2.3. Results and Discussion

### 2.3.1. The Design Strategy

Since gelation is a delicate balance between crystallization, precipitation and solubility of noncovalently interacting molecules in a suitable solvent, we set to design π-conjugated molecules in such a way that they satisfy most of the conditions necessary for the formation of an extended self-assembly required for gelation. Thus, a variety of tailor-made OPV-cholesterol derivatives were synthesized. In this design, an appropriate linear π-conjugated system (OPV) is equipped with one or two cholesterol units and sufficient number of long hydrocarbon side chains resulting in the OPV derivatives **MC-OPV1-3** and **BC-OPV1-3** (Chart 2.1). The presence of long hydrocarbon side chains provides sufficient solubility to the molecules in various nonpolar solvents. It can also facilitate the packing of the chromophores through weak van der Waals interactions. The end part of the OPV backbone is connected to the C-3 chiral center of the cholesterol moiety. In the monocholesterol derivatives, the presence

of the free hydroxyl group allows H-bonding interactions that reinforce π-stacking of the rigid aromatic OPV backbone. A cooperative interaction of all these forces will eventually lead the molecules to form ordered assembly, resulting in the formation of entangled nanoscopic structures which are able to hold large amount of appropriate solvent molecules within the self-assembly, thereby forming a stable gel at room temperature. The monocholesterol-OPV derivative without hydroxyl groups (**MC-OPV4**) was prepared to study the role of hydrogen bonding groups in the self-assembly process of **MC-OPV1-3**.

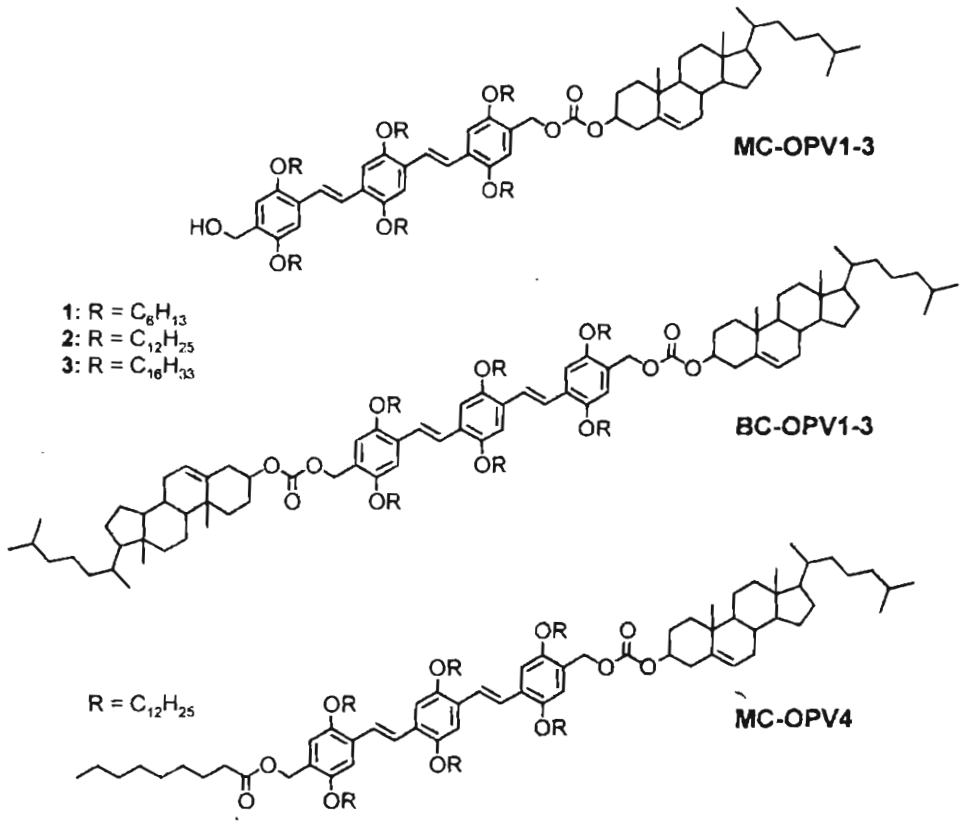


**Chart 2.1.** Structure of monocholesterol-OPV (**MC-OPV1-4**) and bischolesterol-OPV (**BC-OPV1-3**) derivatives.

## 2.3.2. Synthesis of Cholesterol-OPV Derivatives

The cholesterol appended OPVs were synthesized from the corresponding OPV alcohols **10a-c** and **11**, which are prepared according to a known procedure as shown in Scheme 2.1.[22] The 1,4-hydroquinone (**2**) on reaction with 1-bromoalkane in DMF in the presence of NaOH readily afforded the dialkoxy benzene derivative **3** in 75% yield. Subsequent bromomethylation of **3**, using paraformaldehyde and HBr in acetic acid provided the bisbromomethyl derivative **4** with 90% yield. Compound **4** on acetylation with potassium acetate (**5**, 88% yield) followed by hydrolysis with KOH, gave the bisalcohol **6** in 90% yield. Oxidation of the bisalcohol with PCC gave the corresponding bisaldehyde **7** in 92% yield. The bisphosphonium salt **8** was prepared *in situ* by the reaction of the corresponding bisbromo derivate **4** with $PPh_3$ in benzene under refluxing. Wittig reaction of 7 with **8** in $CH_2Cl_2$ in presence of LiOEt as catalyst yielded a mixture f *trans*- and *cis*-vinylene isomers of the conjugated bisaldehyde **9**. These isomeric ixtures were converted to the all-*trans* derivative by treating with iodine in ichloromethane at room temperature, in 71% yield. This on reduction using $NaBH_4$ in $CH_2Cl_2$ and $CH_3OH$ (5:1) results in the bisalcohol derivatives (**10a-c**) with 92-96% yield. Controlled esterification reaction between the bisalcohol (**9**) nd the octanoic acid in presence of DCC and DMAP in dichloromethane afforded e OPV monoalcohol **11** in 41% yield.

The cholesterol-OPV derivatives **MC-OPV1-4** and **BC-OPV1-3** were prepared by refluxing the corresponding OPV alcohols (**10a-c**, **11**) with cholesteryl chloroformate in benzene in presence of pyridine as catalyst (Scheme 2.2). These compounds were characterized by IR, $^{1}H$ NMR, $^{13}C$ NMR, and MALDI-TOF mass spectrometry.

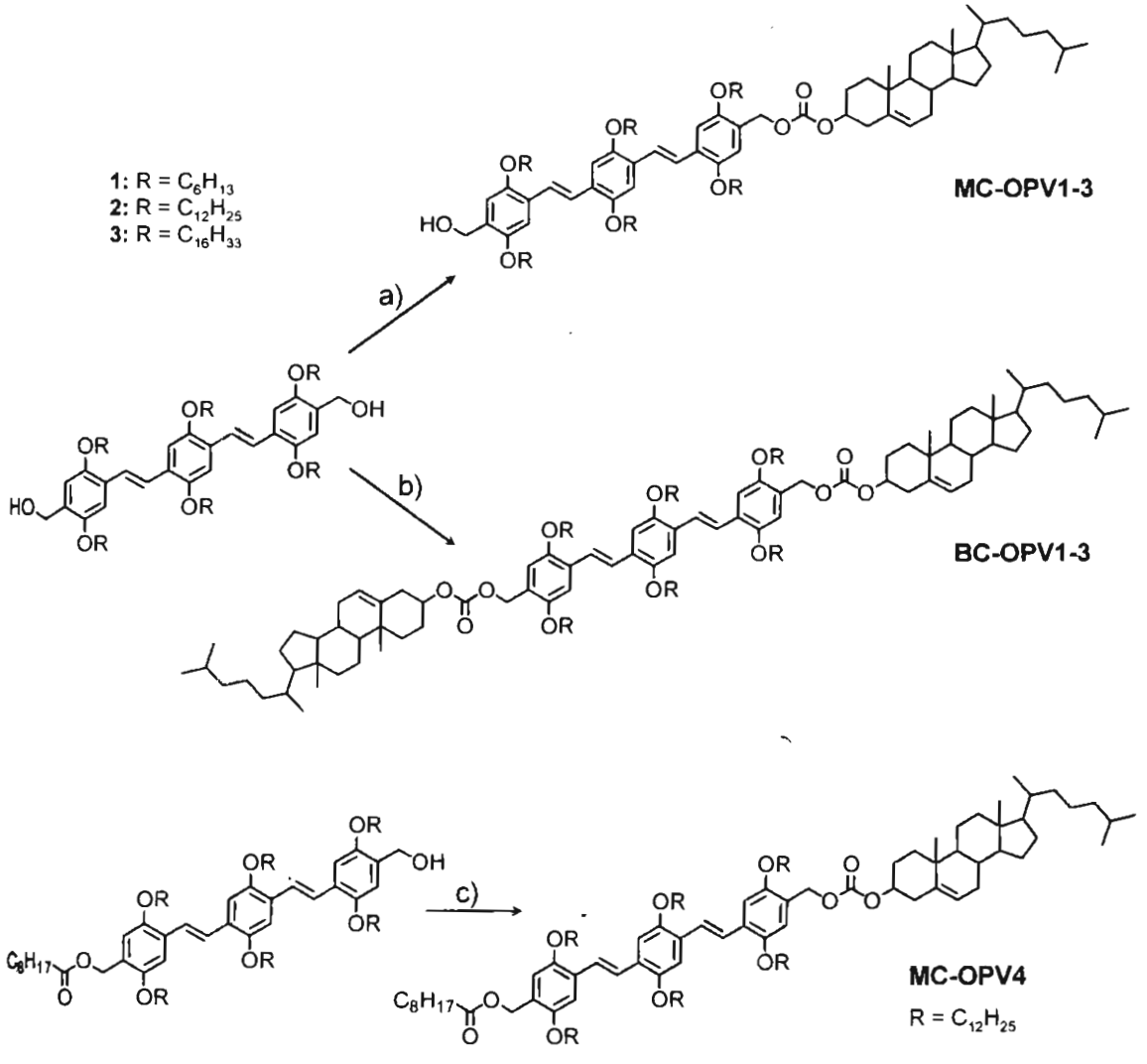


**Scheme 2.2**. Synthesis of **MC-OPV1-4** and **BC-OPV1-3**. Reagents and conditions: a) and c) cholesteryl chloroformate (1.2 equiv.), pyridine (dry), benzene (dry), reflux, 8 h; b) cholesteryl chloroformate (2.2 equiv.), pyridine (dry), benzene (dry), reflux, 12 h.

## 2.3.3. Absorption and Emission Studies

**Table 2.1.** Photophysical Properties of Cholesterol-OPV Derivatives in Different Solvents

| Compound | Solvent | Absorption | | Emission | | | |
|---|---|---|---|---|---|---|---|
| | | $\lambda_{max}$ (nm) | $\varepsilon \times 10^4$ ($M^{-1}cm^{-1}$) | $\lambda_{max}$ (nm) | $\Phi_f$ [a] | $\Phi_f$ [b] | $\tau$ (ns) |
| **MC-OPV1** | Chloroform | 409 | 4.55 | 467, 495 | 0.74 | - | 1.74 |
| | Decane | 402 | 4.24 | 456, 483 | 0.71 | - | 1.83 |
| **MC-OPV2** | Chloroform | 408 | 4.63 | 466, 494 | 0.76 | - | 1.75 |
| | Decane | 402, 470 | 3.17 | 555 | - | 0.32 | 3.93 |
| **MC-OPV3** | Chloroform | 407 | 4.75 | 465, 493 | 0.78 | - | 1.74 |
| | Decane | 400, 470 | 3.02 | 556 | - | 0.28 | 3.91 |
| **BC-OPV1** | Chloroform | 409 | 4.54 | 468, 495 | 0.76 | - | 1.73 |
| | Decane | 402 | 4.29 | 457, 484 | 0.72 | - | 1.87 |
| **BC-OPV2** | Chloroform | 408 | 4.63 | 466, 494 | 0.77 | - | 1.77 |
| | Decane | 397, 414, 444 | 3.54 | 494, 528 | - | 0.55 | 2.81 |
| **BC-OPV3** | Chloroform | 407 | 4.77 | 465, 492 | 0.79 | - | 1.73 |
| | Decane | 396, 413, 442 | 3.31 | 493, 526 | - | 0.50 | 2.69 |
| **MC-OPV4** | Chloroform | 407 | 4.65 | 465, 493 | 0.75 | - | 1.74 |
| | Decane | 399, 414, 443 | 3.74 | 494, 529 | - | 0.58 | 2.74 |

[a] Fluorescence quantum yields of the monomeric species (in chloroform) was determined using quinine sulphate as the standard ($\Phi_f$ = 0.546 in 0.1 N $H_2SO_4$) on excitation at 380 nm. [b] Fluorescence quantum yields of the self-assembled molecules (in decane) was determined using Rhodamine 6G ($\Phi_f$ = 0.9 in ethanol) on selective excitation at 470 nm, error limit ± 5%. [c] Minor contribution from the self-assembled species cannot be ruled out.

The photophysical properties of the cholesterol-OPV derivatives under investigation are presented in Table 2.1. All of them exhibited absorption corresponding to the $\pi$-$\pi^*$ transition and intense emission with high quantum

yields in various solvents. In chloroform ($3 \times 10^{-4}$ M) **MC-OPV1-3** and **BC-OPV1-3** showed identical absorption and emission properties. As a representative case, absorption and emission spectra of **MC-OPV2** and **BC-OPV2** in chloroform are shown in Figure 2.4. They exhibit absorption maximum at 408 nm ($\pi$-$\pi^*$ transition, $\varepsilon = 4.63 \times 10^4\ M^{-1}cm^{-1}$) and emission maxima at 466 nm and 494 nm ($\Phi_f = 0.76$ for **MC-OPV2** and 0.77 for **BC-OPV2**).

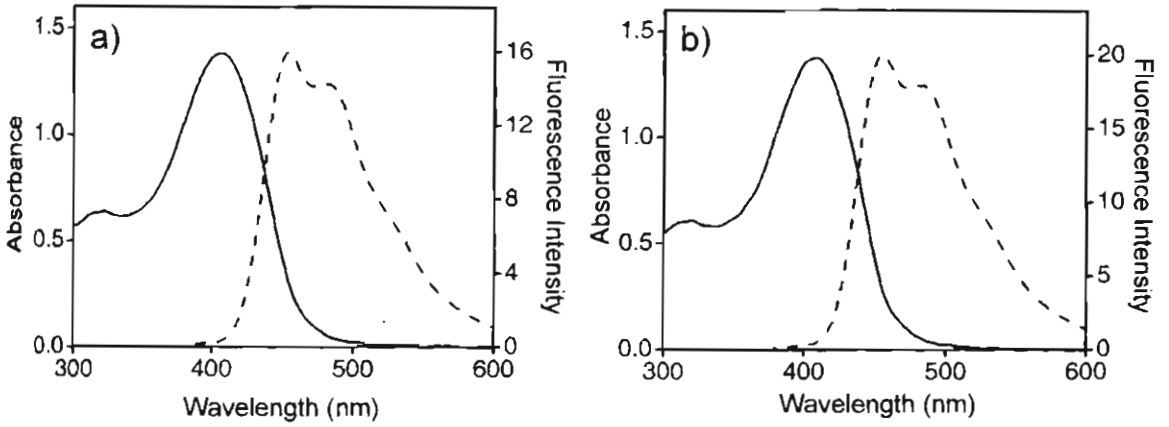


**Figure 2.4.** Absorption (——) and emission (– –) spectrum of a) **MC-OPV2**, b) **BC-OPV2** in chloroform. ($c = 3 \times 10^{-4}$ M, $l = 1$ mm, $\lambda_{ex} = 380$ nm).

The absorption and emission spectra of **MC-OPV1-3** and **BC-OPV1-3** in decane at elevated temperatures showed identical features as in chloroform. However, the UV-vis spectrum of **MC-OPV2-3** in decane at 20 °C exhibited a broad absorption with a red-shifted shoulder around 470 nm. On the contrary, **BC-OPV2-3** showed structured absorptions with a blue-shifted maximum and a new red-shifted shoulder under similar conditions. For example, the absorption spectra of **MC-OPV2** and **BC-OPV2** at two different temperatures are shown in Figure

2.5. **MC-OPV2** showed an absorption maximum at 402 nm with a shoulder band at 470 nm ($\varepsilon = 3.17 \times 10^4\ M^{-1}cm^{-1}$). This is a general feature of OPV derivatives forming J-type aggregates in nonpolar hydrocarbon solvents.[10a,23] However, **BC-OPV2** exhibited a slightly blue shifted emission maximum at 397 nm with a shoulder band at 444 nm ($\varepsilon = 3.54 \times 10^4\ M^{-1}cm^{-1}$). Noticeably, the new band of **BC-OPV2** at 444 nm is nearly 26 nm blue-shifted when compared to the shoulder band of **MC-OPV2** and appeared more structured. Similar blue-shifted spectra were reported for some OPV derivatives by other groups which are ascribed to the formation of H-aggregates.[24]

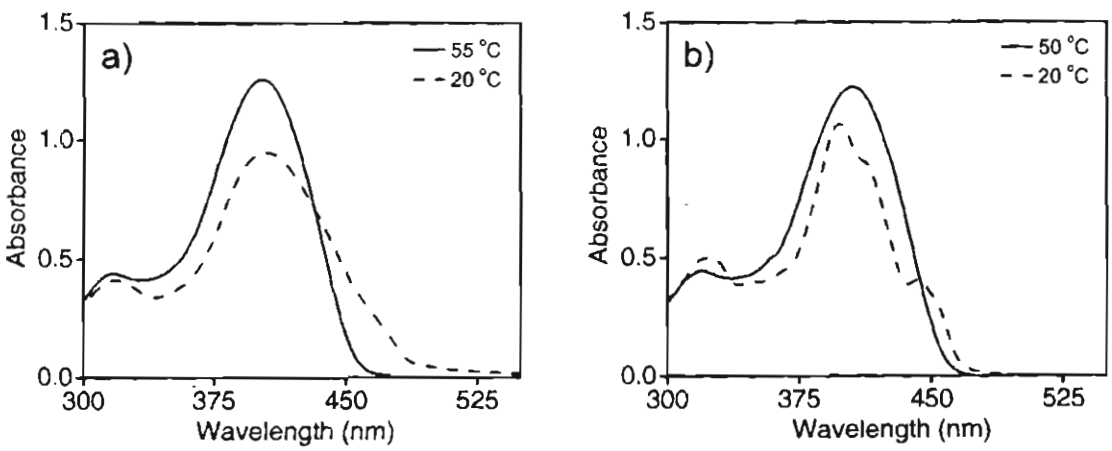


**Figure 2.5**. Absorption spectra of a) **MC-OPV2** and b) **BC-OPV2** in decane at two different temperatures. ($c = 3 \times 10^{-4}$ M, $l = 1$ mm).

The emission spectra of **MC-OPV2** and **BC-OPV2** in decane above 50 °C showed identical features with two maxima (456 nm and 484 nm for **MC-OPV2**; 457 nm and 485 nm for **BC-OPV2**). However, in decane at 20 °C, **MC-OPV2** showed a broad structureless emission between 500-700 nm ($\Phi_f = 0.32$) with a

maximum around 560 nm (Figure 2.6a) whereas, **BC-OPV2** had a structured emission ($\Phi_f$ = 0.55) with two emission maxima at 494 nm and 528 nm (Figure 2.6b). Nature of the absorption and emission spectra with solvents and temperature reveals that these molecules form aggregates in decane at ambient temperatures, the electronic properties of which are different from each other.

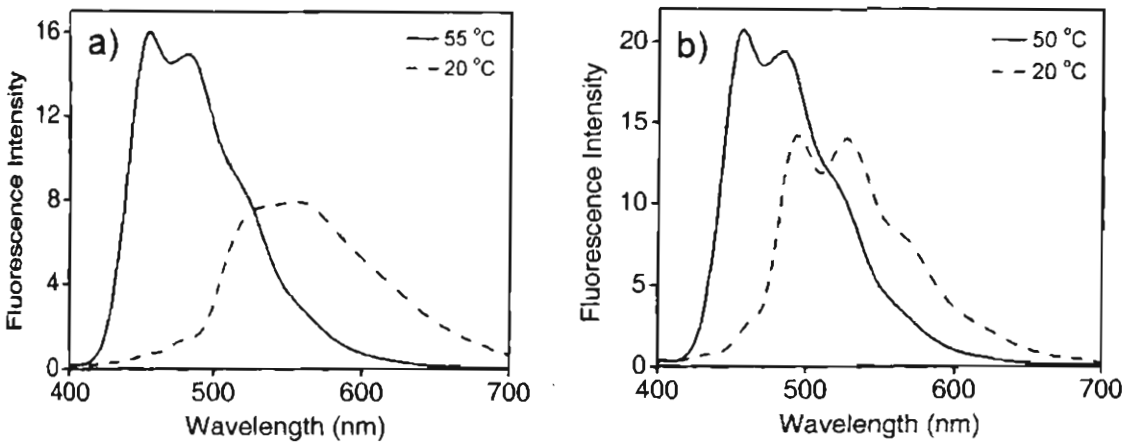


**Figure 2.6.** Fluorescence emission spectra of a) **MC-OPV2** and b) **BC-OPV2** in decane at two different temperatures. ($c$ = 3 x $10^{-4}$ M, $l$ = 1 mm, $\lambda_{ex}$ = 370 nm).

Though these observations can be rationalized invoking J-type and H-type aggregation in analogy to previous reports, the optical properties of these species indicate that they are different from the conventional H- and J-aggregates of functional dyes. For example, the red- and blue-shift of the aggregates of **MC-OPV2** and **BC-OPV2** with respect to the corresponding monomers are not very predominant. Further, the emission spectrum of **BC-OPV2** was more intense than that of **MC-OPV2**. By normal practice, if the blue-shifted absorption spectrum of **BC-OPV2** is assigned to H-aggregates, it should be less emissive compared to the

J-aggregates of **MC-OPV2**. Therefore, these aggregates may preferably be represented as 'pseudo-J' and 'pseudo-H' with 'tilted' and 'twisted' chromophore stacks for **MC-OPV2** and **BC-OPV2**, respectively. In such cases, the difference in the excited state dipole moment orientation of the two aggregates results in distinct optical and chiroptical features. Our studies on the chiroptical properties and AFM morphological analysis provided strong support for the difference in the chromophore packing as stated above.

The mono- and bischolesterol derivatives with C16 alkyl chains, **MC-OPV3** and **BC-OPV3**, showed similar properties as that of the corresponding C12 derivatives (**MC-OPV2** and **BC-OPV2** respectively). However, the mono- and bischolesterol derivatives with C6 alkyl chains (**MC-OPV1** and **BC-OPV1**) were found to be highly soluble in decane and other nonpolar and polar solvents even at low temperatures and high concentrations. Because of the absence of aggregation, no changes in the absorption and emission spectra were observed for these molecules in hydrocarbon solvents.

The aggregate stability and the cooperative nature of the self-assembly process of mono- and bischolesterol derivatives in decane were studied by the temperature dependent UV-vis absorption and fluorescence spectra. Both **MC-OPV2** and **BC-OPV2** showed an increase in intensity at the absorption maximum with a concomitant decrease in the intensity of the red-shifted shoulder band on increasing temperature (Figure 2.7a,c). Similarly, the red-shifted emission

corresponding to the aggregate fluorescence decreases with an increase in the blue-shifted monomer emission (Figure 2.7b,d). These absorption and emission changes in decane are due to the disruption of the self-assembled species to the molecularly dissolved species with increase in temperature.

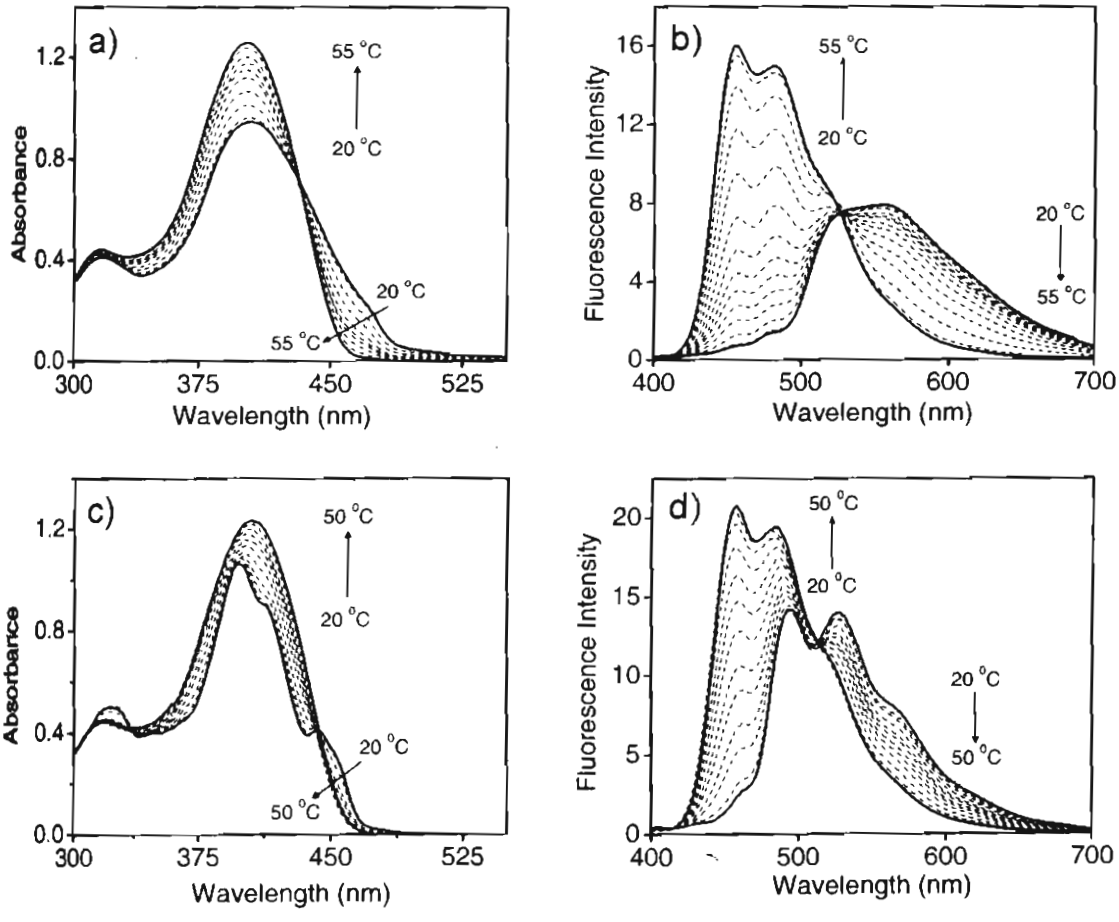


**Figure 2.7.** Temperature dependent a) absorption and b) emission spectra of **MC-OPV2**; c) absorption and d) emission spectra of **BC-OPV2** in decane. ($c$ = 3 x $10^{-4}$ M, $l$ = 1 mm, $\lambda_{ex}$ = 380 nm).

Plots of the fraction of aggregated species[25] ($\alpha$) versus the temperature was drawn from the data obtained from the temperature dependent UV-vis absorption

(Figure 2.8a) and fluorescence (Figure 2.8b) experiments. In both cases, a good correlation was obtained for the melting temperatures of the self-assembled species. The sigmoidal nature of the plots reveal the cooperative noncovalent interactions during the self-assembly and disassembly processes in these derivatives. Moreover, these plots indicate better aggregate stability for monocholesterol derivatives (**MC-OPV2-3**) than that of the bischolesterol derivatives (**BC-OPV2-3**). The effect of the alkyl side chains on the stability of the resulting self-assemblies is also established from the temperature transition plots. These plots reveal that the stability is more for derivatives with hexadecyl side chains (**MC-OPV3** and **BC-OPV3**) than that of the corresponding derivatives with dodecyl chains (**MC-OPV2** and **BC-OPV2**).

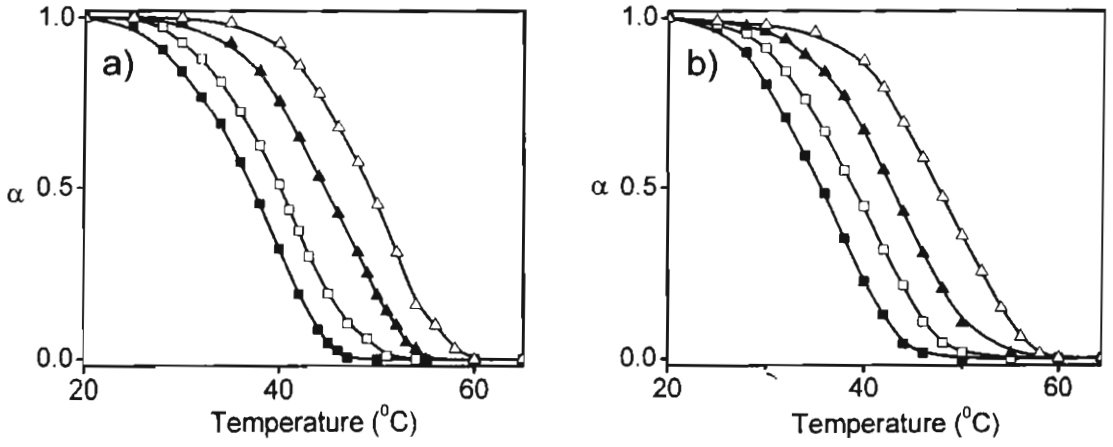


**Figure 2.8.** Plots of the fraction of aggregate (α) versus temperature of **BC-OPV2** (■), **BC-OPV3** (□), **MC-OPV2** (▲) and **MC-OPV3** (△). The data points were acquired by monitoring a) absorption and b) emission spectral changes with temperature in decane.

## 2.3.4. Circular Dichroism Studies

As discussed earlier, cholesterol can induce chirality to the attached chromophores in the aggregated state. Circular dichroism (CD) spectroscopy is a useful tool for the detection of chiral induction and the helical organization of chromophores in the aggregated state. Mono- and bischolesterol derivatives in chloroform were CD inactive (Figure 2.9) indicating that they do not aggregate in chloroform. However, the CD spectrum of **BC-OPV2** in decane ($3 \times 10^{-4}$ M) showed an exciton coupled bisignate signal with negative ($\lambda_{max}$ = 418 nm) and positive ($\lambda_{max}$ = 385 nm) Cotton effects which changes the sign exactly through the $\pi$-$\pi^*$ absorption maximum at 398 nm (Figure 2.9a). This is characteristic of a left-handed helical bias of the supramolecular chirality.[26] However, in the case of **MC-OPV2**, the CD spectrum in decane showed a strange behavior with a first

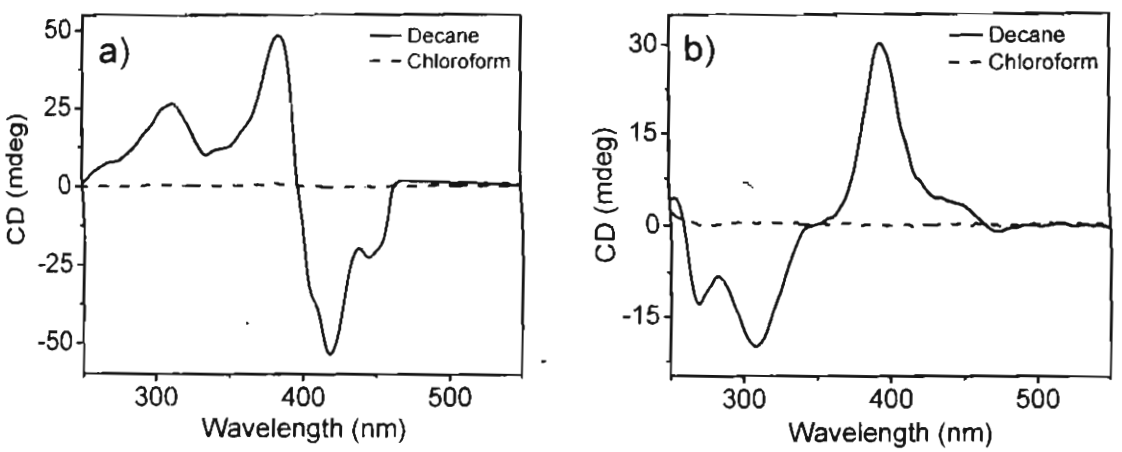


**Figure 2.9.** CD spectra of a) **BC-OPV2** and b) **MC-OPV2** in chloroform and in decane at room temperature. *(c = 3 x 10$^{-4}$ M, l = 1 mm).*

positive ($\lambda_{max}$ = 393 nm) followed by two negative ($\lambda_{max}$ = 308 and 269 nm) Cotton effects (Figure 2.9b). The nonbisignate exciton couplet with opposite signals indicates the possibility of different chiral dispositions. Furthermore, the measure of chirality 'g' of **MC-OPV2** is low ($g_{393nm} = 5.2 \times 10^{-4}$) when compared to that of **BC-OPV2** ($g_{385nm} = 9.3 \times 10^{-4}$) indicating a weak excitonic coupling in the former. These differences in the CD spectra reiterate the differences between the aggregates of **MC-OPV2** and **BC-OPV2** which agree with the absorption and emission properties.

Temperature dependent CD spectra of the mono- and the bischolesterol derivatives (**MC-OPV2** and **BC-OPV2**) showed decrease in the CD intensity with increase in temperature (Figure 2.10). CD signals of both derivatives were completely disappeared above 55 °C. This is due to the dissociation of the helical self-assemblies into individual molecules with increase in temperature. CD spectral changes with temperature showed good correlation with the corresponding UV-vis and fluorescence changes.

Interestingly, the monocholesterol derivative **MC-OPV4** in which the hydroxyl group is protected with a C8 ester group showed similar properties as that of the bischolesterol derivatives revealing that H-bonding play a crucial role on deciding the properties of the monocholesterol-OPV derivatives. **MC-OPV4** exhibited a structured absorption with a blue shifted maximum ($\lambda_{max}$ = 399 nm, $\varepsilon$ = $3.74 \times 10^4$ $M^{-1}cm^{-1}$) and a red-shifted shoulder band at 443 nm in the gel state in

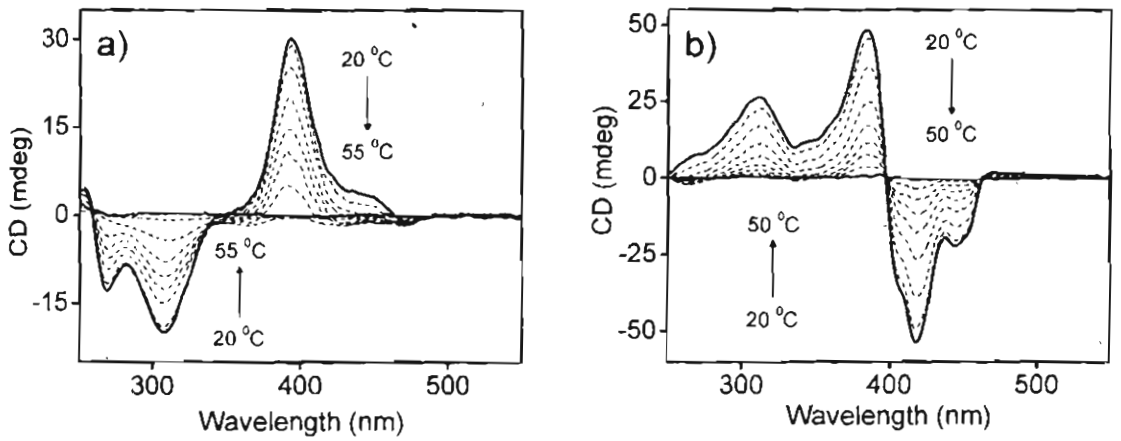


**Figure 2.10.** Temperature dependent CD spectral changes of a) **MC-OPV2** and b) **BC-OPV2** in decane. ($c$ = 3 x $10^{-4}$ M, $l$ = 1 mm).

decane at room temperature (Figure 2.11a). Similarly, the emission spectrum is structured with two emission maxima ($\lambda_{em}$ = 494 nm and 529 nm, $\Phi_f$ = 0.58) which is relatively less red-shifted. As in the other cases, the absorption and emission corresponding to the aggregate species decreases with a concomitant increase in the absorption and emission corresponding to the monomer species (Figure 2.11).

CD properties of **MC-OPV4** resemble that of bischolesterol OPV derivatives. In this case, a bisignate CD signal with a first negative Cotton effect ($\lambda_{max}$ = 417 nm) followed by two positive Cotton effects ($\lambda_{max}$ = 382 and 312 nm) with a zero crossing through the absorption maximum at 399 nm (Figure 2.12) is observed. This observation indicates an anticlockwise arrangement of the OPV chromophores in the aggregated state of **MC-OPV4**.

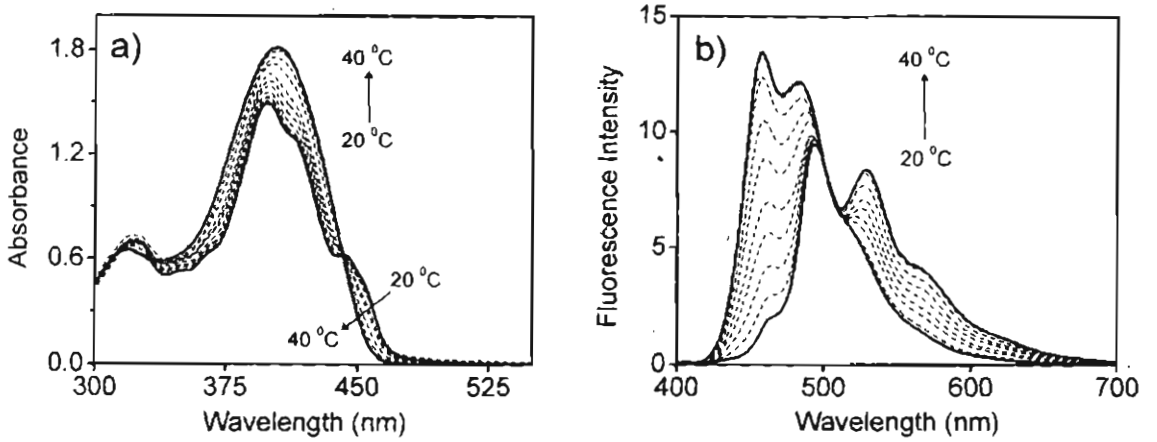


**Figure 2.11.** Temperature dependent a) absorption and b) emission spectra of **MC-OPV4** in decane. ($c$ = 3 x $10^{-4}$ M, $l$ = 1 mm, $\lambda_{ex}$ = 380 nm).

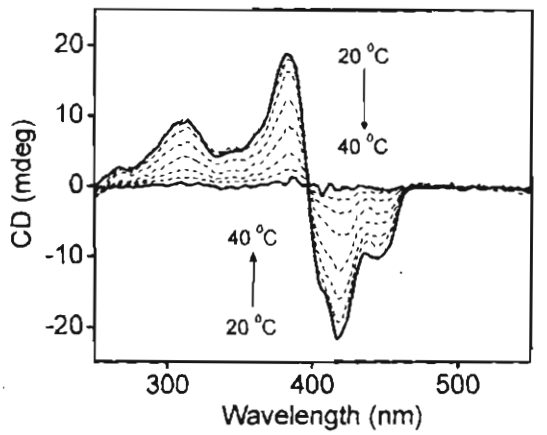


**Figure 2.12.** Temperature dependent CD spectra of **MC-OPV4** in decane. ($c$ = 3 x $10^{-4}$ M, $l$ = 1 mm).

## 2.3.5. Gelation Studies

Gelation behavior of the newly synthesized cholesterol-OPV derivatives was examined in a range of organic nonpolar solvents by dissolving different amounts in a specific volume (1 mL) of the solvent under heating and cooling. It has been observed that either gelation, precipitation or a clear solution could be obtained depending upon the solvent and structure of the compound. Gel

formation could be detected readily by the failure of the resultant mass to flow when the vial was tilted upside down and also from the soft and transparent appearance. A striking consequence of the different chromophore arrangements in **MC-OPV** and **BC-OPV** is the disparity in the gelation behavior between the two. For example, the **MC-OPV** gels had a weak yellow emission whereas the **BC-OPV** showed a relatively strong green emission (Figure 2.13). Moreover, the gelation ability of **BC-OPV**s is relatively weaker than that of **MC-OPV**s. For example, the critical gelator concentration (CGC, the minimum amount of the gelator required to form a stable gel in 1 mL solvent at room temperature) of **BC-OPV2** in decane is 7.0 mg/mL whereas that of **MC-OPV2** is only 3.4 mg/mL which is nearly two fold less compared to that of the former, showing a better gelation ability of the latter.

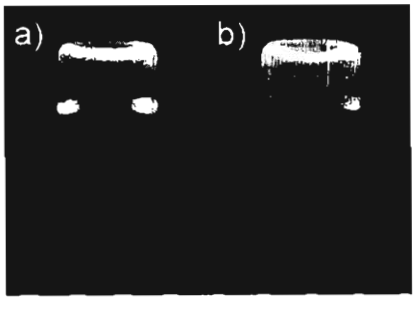


**Figure 2.13.** Photographs of the decane gels of a) **MC-OPV2** and b) **BC-OPV2** on illumination with UV light (365 nm)

The results of the gelation experiments are summarized in Table 2.2. Both mono- and bischolesterol derivatives with C6 alkyl side chains (**MC-OPV1** and **BC-OPV1**) failed to form gels in any of the tested solvents because of their high

solubility, whereas, all other derivatives are excellent gelators of nonpolar solvents such as hexane, methyl cyclohexane, cyclohexane, decane, *p*-xylene and toluene. However, they form homogeneous solutions in more polar solvents such as chloroform, dichloromethane and tetrahydrofuran, indicating that polar solvents do not facilitate gelation. Mono- and bischolesterol derivatives with C16 alkyl chains (**MC-OPV3** and **BC-OPV3**) were found to be better gelators than that of the corresponding C12 derivatives. Gelation ability of **MC-OPV4** was found to be less compared to that of the corresponding mono- and bischolesterol derivatives with C12 alkyl chains (**MC-OPV2** and **BC-OPV2**).

**Table 2.2.** Critical gelator concentration (mM) of **MC-OPVs** and **BC-OPVs** in various solvents.

| Solvent | **MC-OPV2** mg/mL (mM) | **MC-OPV3** mg/mL (mM) | **BC-OPV2** mg/mL (mM) | **BC-OPV3** mg/mL (mM) | **MC-OPV4** mg/mL (mM) |
|---|---|---|---|---|---|
| *n*-Hexane | 0.6 (0.32) | 0.5 (0.22) | 2.4 (1.06) | 1.5 (0.57) | 2.8 (1.40) |
| Methyl Cyclohexane | 0.8 (0.43) | 0.7 (0.31) | 2.8 (1.24) | 2.4 (0.92) | 3.1 (1.55) |
| Cyclohexane | 2.2 (1.18) | 1.6 (0.73) | 6.2 (2.74) | 4.0 (1.5) | 6.8 (3.40) |
| *n*-Decane | 3.4 (1.83) | 2.4 (1.1) | 7.0 (3.09) | 5.0 (1.9) | 7.5 (3.75) |
| *p*-Xylene | 6.2 (3.33) | 4.0 (1.8) | 10.1 (4.46) | 7.0 (2.7) | 14.9 (7.45) |
| Toluene | 12.0 (6.45) | 9.0 (4.1) | 30.0 (13.3) | 20.0 (9.1) | S |

### 2.3.6. Gel Melting Studies

Thermotropic behavior of the cholesterol-OPV gels was investigated by the dropping ball method[27] to understand the impact of the structure of cholesterol-OPV derivatives and the length of alkyl side chains on the gel stability. All the derivatives under study showed a regular increase in the gel melting temperature ($T_{gel}$) with increasing concentration of the gelator molecules. Phase diagrams of these gels in decane were obtained by plotting the $T_{gel}$ at different concentrations (Figure 2.14). The phase above each curve is a solution, whereas the phase below is a gel. Gel melting studies in decane have proved that **MC-OPV** gels are more stable than **BC-OPV** gels and hence they show high $T_{gel}$ values. Also cholesterol derivatives with hexadecyl alkyl chains (**MC-OPV3** and **BC-OPV3**) form stable gels than that of the corresponding derivatives with dodecyl chains (**MC-OPV2** and **BC-OPV2**). This could be due to the solvation assisted intermolecular packing of the long alkyl chains, which enhances the gelation ability of the molecules. Figure 2.14 shows the plot of the gel melting temperatures ($T_{gel}$) of the decane gels of **MC-OPV2-3** and **BC-OPV2-3** at different concentrations. Gel melting temperatures of **MC-OPV4** in decane at different concentration is also measured under similar conditions. It showed least gel stability compared to the other derivatives.

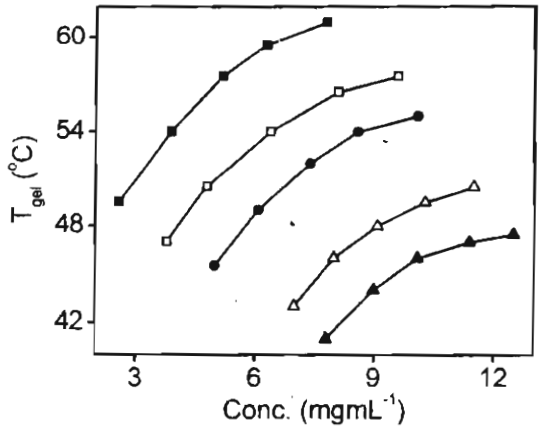


**Figure 2.14.** Plot of $T_{gel}$ versus temperature of a) **MC-OPV3** (■), **MC-OPV2** (□), **BC-OPV3** (●), **BC-OPV2** (△) and **MC-OPV4** (▲) in decane.

## 2.3.7. Optical Polarizing Microscopic Studies

The mesoscopic properties of the cholesterol-OPV gelators were studied by using optical polarizing microscopy (OPM). OPM texture of **MC-OPV2** gel in decane showed four-arm brush textures (Figure 2.15a) similar to other cholesterol based gelators[28a] and chiral OPV gelators.[28b] On the other hand, **BC-OPV2** gel in decane showed streak-like texture with strong birefringence (Figure 2.15b), as observed for many chiral lyotropic phases and thermally reversible organogels containing cholesterol.[28c] This observation reveals the differences in the supramolecular anisotropy leading to different mesoscopic structures. High birefringence of the **BC-OPV2** texture indicates well-defined organization of chromophores in its gel strands. Similar textures were obtained for the C16 derivatives (**MC-OPV3** and **BC-OPV3**) as that of the corresponding C12 derivatives (**MC-OPV2** and **BC-OPV2**).

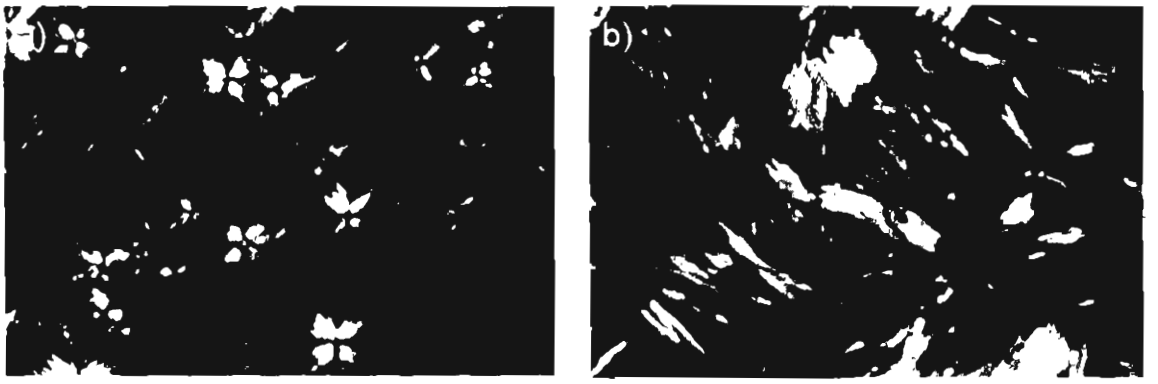


**Figure 2.15.** Optical polarizing microscopic pictures of the decane gels of a) **MC-OPV2** ($3.5 \times 10^{-3}$ M) and b) **BC-OPV2** ($7.2 \times 10^{-3}$ M) (magnification is 400x).

## 2.3.8. Atomic Force Microscopic Studies

The atomic force microscopic (AFM) textures of **MC-OPV2** and **BC-OPV2** self-assemblies drop-cast from decane solutions on freshly cleaved mica surface showed significant differences although both have right-handed (*P*) helical sense in most of the fibers. The helicity of **MC-OPV2** is in agreement with the CD spectrum, whereas that of **BC-OPV2** is not in agreement with the bisignate CD signal. Such contradiction of observed CD and morphological features are already known in the literature.[9c,29] In many cases, the initially formed 1D aggregates with left-handed twist may wind in the opposite direction during the hierarchical assembly formation resulting in an ultimate right-handed twist as can be seen in some of the large fibers of **BC-OPV2**.

AFM analysis reveals ribbon-like structures for **MC-OPV2** self-assemblies which are flat and aligned sideways to form coiled superstructures (Figure 2.16a and 2.17a). Width of the individual ribbons varies from 30-70 nm with an average

height of 4-8 nm. The height of 8 nm corresponds to two individual tapes lying one over the other. Interestingly, **BC-OPV2** showed the morphology of entangled helical fibers of different sizes (Figure 2.16b and 2.17b). The width of the smallest fiber is 40 nm with a height of 4 nm which is several micrometers in length. The height profiles of large areas of the samples showed a uniform height for **MC-OPV2** whereas a height variation of 4-50 nm is observed for **BC-OPV2**.

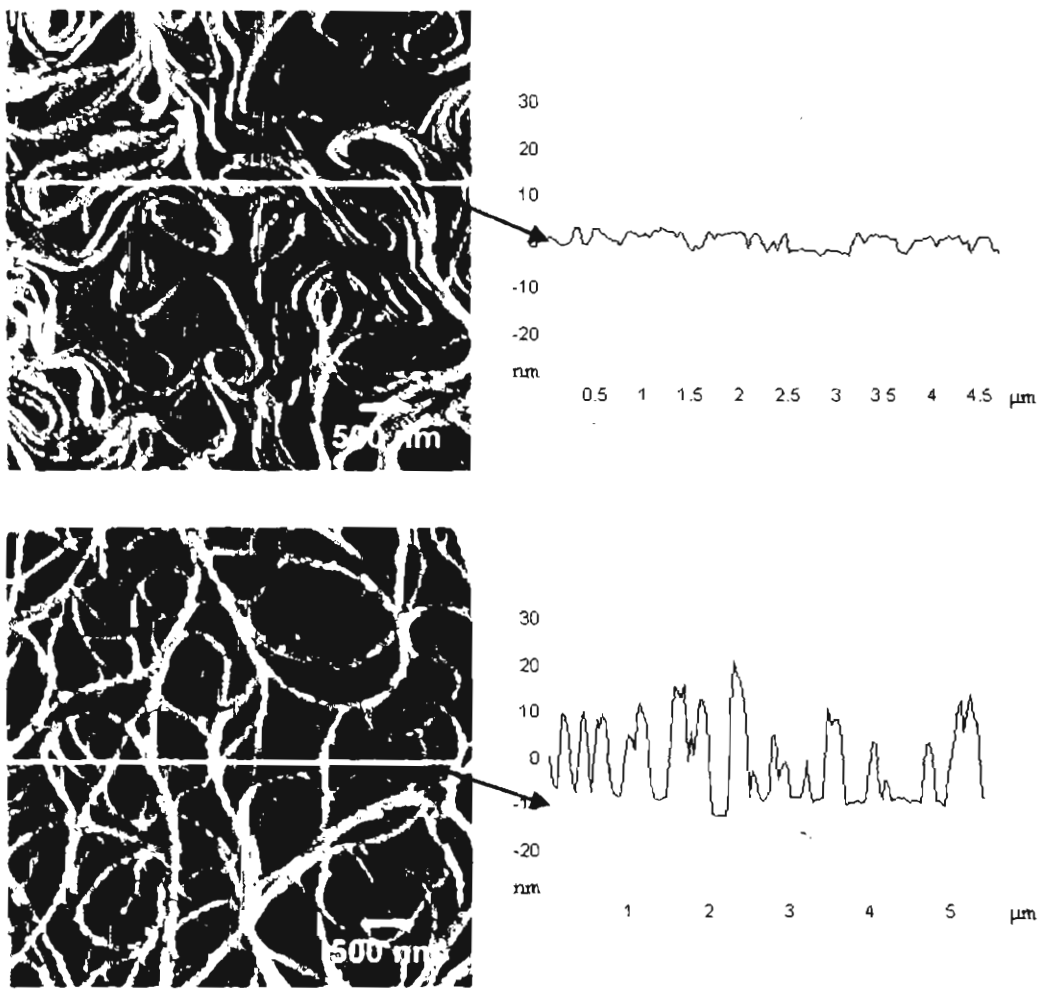


**Figure 2.16.** AFM height images of **MC-OPV2** (top) and b) **BC-OPV2** (bottom) with the corresponding height profiles. Samples were prepared from decane solution ($c$ = 1 x $10^{-5}$ M) and transferred to freshly cleaved mica sheet by drop casting.

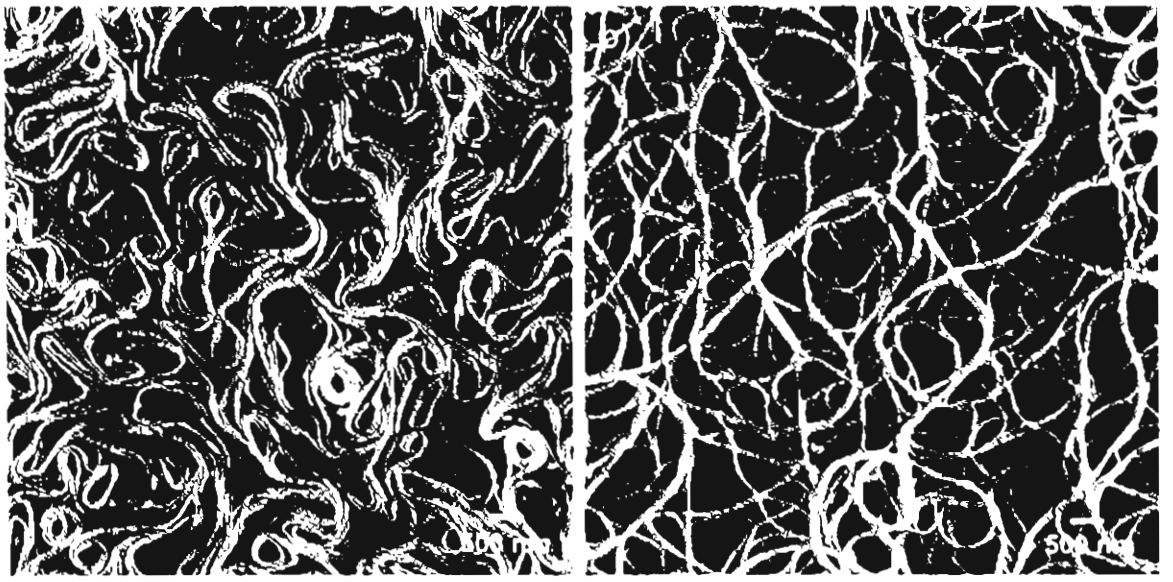

**Figure 2.17.** Large area AFM height images of a) **MC-OPV2** and b) **BC-OPV2** self-assembly.

Furthermore, section analysis along the axis (Figure 2.18) revealed that **MC-OPV2** self-assemblies have irregular helical pitch of 40-80 nm whereas that of **BC-OPV2** is almost uniform with zigzag patterns having pitch length of 46 nm. Irregular movements of the AFM tip through the long axis of the self-assembly with variable pitch length and uniform height profiles are characteristic of a flexible and flattened coiled tape-like morphology of **MC-OPV2**. Contrastingly, the uniform zigzag patterns along the axis and variable height profiles of **BC-OPV2** are characteristic of twisted helical fibrillar assemblies of different size which are intertwined.

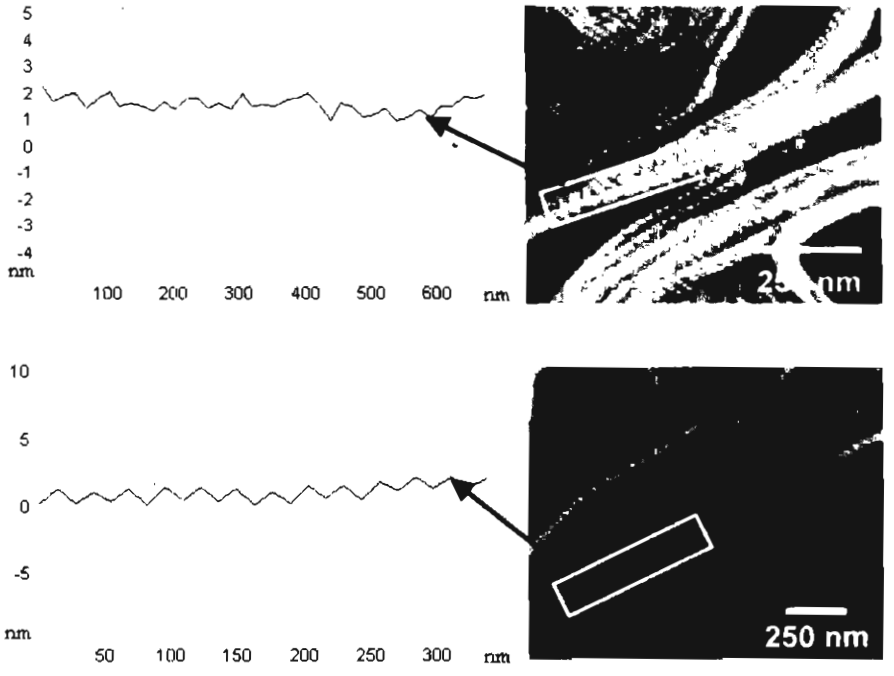


**Figure 2.18.** Zoomed region of **MC-OPV2** (top) and isolated fibers of **BC-OPV2** (bottom) self-assembly with the corresponding section analysis. Samples were prepared from decane solution ($c$ = 1 x $10^{-5}$ M) and transferred to freshly cleaved mica sheet by drop casting.

Based on the differences in the optical, chiroptical, gelation and morphological properties, it is clear that the molecular packing in the self-assemblies of **MC-OPV2-3** and **BC-OPV2-3** are remarkably different. Nature of the absorption, emission and CD spectra strongly support a tilted extended packing of the H-bonded chromophores in **MC-OPV**s, whereas, a well organized twisted helical arrangement of the chromophores is favored for **BC-OPV**s. The extended supramolecular assembly of the tilted packing (pseudo J-aggregates) may result in a coiled helical assembly, whereas, twisted packing (pseudo H-aggregates) leads to a twisted helical assembly the as shown in Figure 2.19.

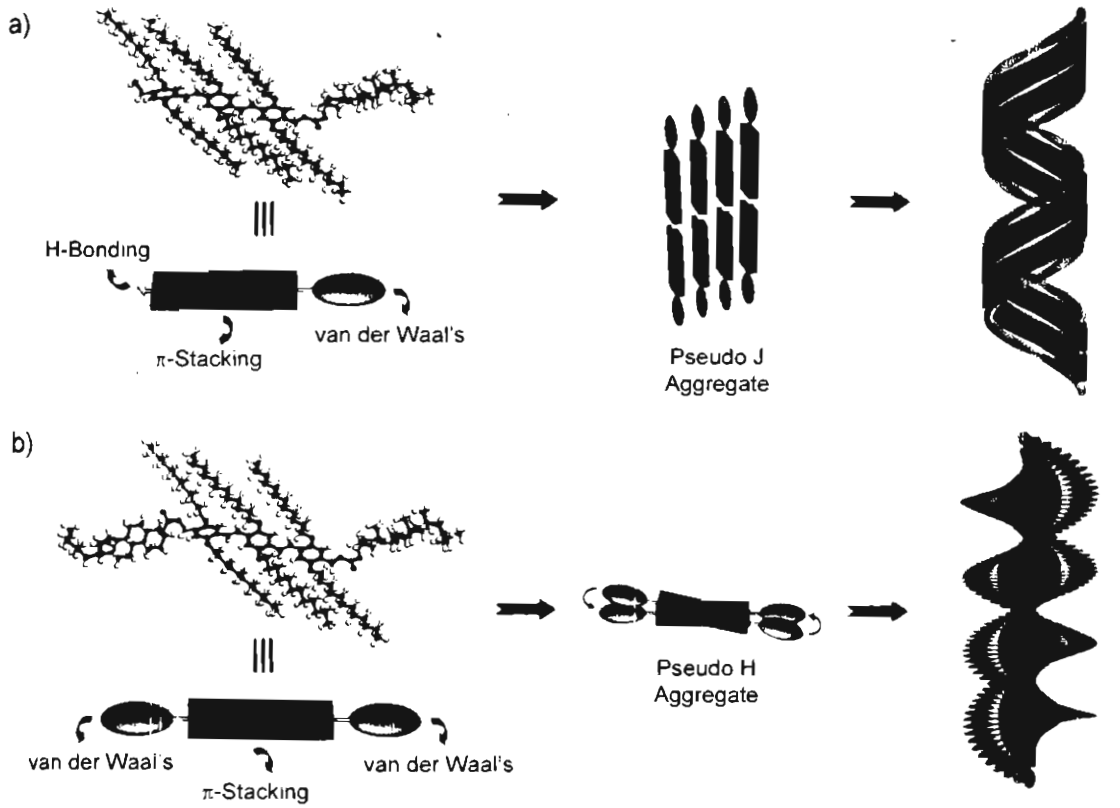


**Figure 2.19.** Schematic illustration of the probable self-assemblies of a) **MC-OPV2-3** and b) **BC-OPV2-3** in decane.

## 2.4. Conclusions

We have shown that symmetrical and unsymmetrical functionalization of OPVs with cholesterol moieties allow controlled supramolecular organization resulting in helical nanoscopic architectures with remarkable optical, chiroptical and morphological differences as illustrated with two different classes of molecules, mono- and bischolesterol OPV derivatives. Detailed studies revealed that the monocholesterol attached oligo(*p*-phenylenevinylene)s prefer to form pseudo J-aggregates with tilted chromophore packing, whereas, the corresponding

bischolesterol derivatives, form pseudo H-aggregates with a twisted chromophore packing. Monocholesterol derivative without the hydrogen bonding hydroxyl groups showed similar properties of bischolesterol derivatives indicating the role of H-bonding on the chromophore packing. The approach described here can be used as a general strategy to control the chromophore ordering which may be useful to the design of nanoscopic functional assemblies for optoelectronic applications.

## 2.5. Experimental Section

### 2.5.1. Synthesis and Characterization

Unless otherwise stated, all starting materials and reagents were purchased from commercial suppliers and used without further purification. The solvents and the reagents were purified and dried by usual methods prior to use. Alkyl bromides, $LiAlH_4$, triphenyl phosphine, $NaBH_4$, were purchased from Sigma-Aldrich. Hydroquinone, NaOH, paraformaldehyde, HBr in acetic acid, potassium acetate, TBAB, and PCC were used as received from commercial suppliers. All melting points were determined with a Mel-Temp-II melting point apparatus and are uncorrected. $^{1}H$ and $^{13}C$ NMR spectra were recorded on a 300 MHz Bruker Avance DPX Spectrometer. FT-IR spectra were recorded on a Shimadzu IRPrestige-21 Fourier Transform Infrared Spectrophotometer. MALDI-TOF mass spectrometry was conducted on a Perspective Biosystems Voyager DE PRO

MALDI-TOF mass spectrometer using α-Cyano-4-hydroxy cinnamic acid as the matrix.

**General Procedure for the Syntheses of Cholesterol-OPV Derivatives:** The appropriate precursor bisalcohols (**10a-c**, 1 mmol) or monoalcohol (**11**, 1 mmol) were dissolved in dry benzene (15 mL) by stirring. To this solution, cholesteryl chloroformate (1.2 mmol) and catalytic amount of pyridine (0.1 mmol) were added and refluxed for 8 h under argon atmosphere. The solvent was evaporated and the residue was dissolved in chloroform followed by precipitation by adding methanol. The crude mixture was filtered and the product was then purified by eluting through a silica column using chloroform-hexane (1:2) mixture. After purification, the monocholesterol derivatives were obtained as the major products (64-70%). The yields of the bischolesterol derivatives were around 10-20%, which could be improved by using 2.2 mmol of cholesteryl chloroformate followed by refluxing for 12 h under similar reaction conditions (83-92% yield). Yield, melting point and spectral details of each product are given below.

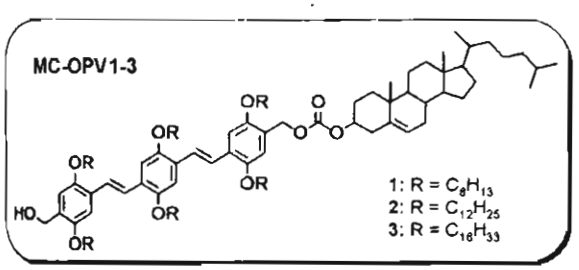


**MC-OPV1:** Yield 65%. mp 141-143 °C. $^1$H NMR (300 MHz, $CDCl_3$, TMS): δ 0.70 (s, 3H), 0.89 (m, 18H), 0.94-2.45 (m, 88H), 4.04-4.06 (m, 12H), 4.49-4.52 (m, 1H), 4.70 (s, 2H), 5.22 (s, 2H), 5.42 (S, 1H), 6.87-6.94 (d,

2H), 7.12-7.15 (d, 4H), 7.46 (s, 4H) ppm. $^{13}C$ NMR (75 MHz, $CDCl_3$): δ 12.12, 13.86, 19.06, 19.63, 21.52, 22.63, 22.92, 24.28, 24.59, 25.76, 27.72, 28.32, 28.55, 29.13, 31.53, 32.13, 32,21, 36.15, 36.73, 37.06, 37.56, 37.93, 39.94, 40.12, 42.53, 49.72, 56.66, 56.98, 60.61, 63.70, 68.61, 69.92, 76.44, 108.43, 108.64, 114.25, 115.88, 116.03, 123.42, 126.64, 126.92, 128.13, 128.48, 128,54, 135.29, 139.95, 142.24, 142.53, 151.44, 152.84, 154.89, 155.08 ppm. FT-IR (KBr): $\nu_{max}$ 694, 722, 806, 853, 965, 1012, 1073, 1208, 1255, 1345, 1388, 1423, 1458, 1466, 1508, 1740, 2850, 2921, 3327 $cm^{-1}$. MALDI-TOF MS (MW = 1355.03): m/z = 1355.02 $[M]^+$.

**MC-OPV2:** Yield 70%. mp 98-100 °C. $^1H$ NMR (300 MHz, $CDCl_3$, TMS): δ 0.68 (s, 3H), 0.87 (m, 18H), 0.93-2.43 (m, 160H), 4.02-4.04 (m, 12H), 4.49-4.51 (m, 1H), 4.68 (s, 2H), 5.20 (s, 2H), 5.40 (S, 1H), 6.84-6.89 (dd, 2H), 7.09-7.11 (d, 4H), 7.42-7.45 (d, 4H) ppm. $^{13}C$ NMR (75 MHz, $CDCl_3$): δ 12.14, 14.06, 19.00, 19.63, 21.55, 22.62, 22.95, 24.33, 24.64, 25.59, 27.72, 28.35, 28.55, 28.73, 28.92, 29.43, 29.56, 29.63, 29.62, 29.84, 31.73, 32.23, 36.15, 36.73, 37.00, 37.54, 37.92, 39.89, 40.12, 42.58, 49.70, 56.66, 56.92, 60.72, 63.70, 68.21, 69.52, 76.44, 108.50, 108.73, 114.32, 115.88, 116.08, 123.42, 126.84, 127.02, 128.21, 128.48, 128,65, 135.23, 139.92, 142.42, 142.73, 151.64, 152.84, 155.08, 155.32 ppm. FT-IR (KBr): $\nu_{max}$ 694, 722, 806, 853, 965, 1012, 1073, 1208, 1255, 1345, 1388, 1423, 1458, 1466, 1508, 1740, 2850, 2921, 3327 $cm^{-1}$. MALDI-TOF MS (MW = 1859.59): m/z = 1859.60 $[M]^+$.

**MC-OPV3:** Yield 64%. mp 94-96 °C. $^{1}$H NMR (300 MHz, $CDCl_3$, TMS): δ 0.69 (s, 3H), 0.88 (m, 18H), 0.93-2.44 (m, 208H), 4.02-4.06 (m, 12H); 4.48-4.51 (m, 1H), 4.67 (s, 2H), 5.21 (s, 2H), 5.43 (S, 1H), 6.85-6.90 (dd, 2H), 7.11-7.15 (d, 4H), 7.46 (d, 4H) ppm. $^{13}$C NMR (75 MHz, $CDCl_3$): δ 12.09, 13.12, 19.06, 19.63, 21.52, 21.72, 22.93, 24.35, 24.64, 25.65, 27.73, 28.32, 28.56, 28.73, 28.95, 29.34, 29.52, 29.53, 29.54, 29.60, 29.62, 29.63, 29.68, 30.54, 30.52, 32.12, 31.67, 32.25, 36.09, 36.71, 37.06, 37.52, 37.88, 39.91, 40.16, 42.56, 49.71, 56.56, 56.95, 60.67, 63.69, 68.22, 69.52, 76.50, 108.52, 108.75, 114.33, 115.89, 116.10, 123.44, 126.85, 127.06, 128.25, 128.54, 128,66, 135.25, 139.94, 142.43, 142.75, 151.66, 152.82, 155.10, 155.33 ppm. FT-IR (KBr): $\nu_{max}$ 694, 723, 805, 854, 967, 1011, 1073, 1209, 1255, 1343, 1389, 1425, 1459, 1466, 1508, 1741, 2851, 2920, 3328 $cm^{-1}$. MALDI-TOF MS (MW = 2195.97): m/z = 2195.93 $[M]^+$.

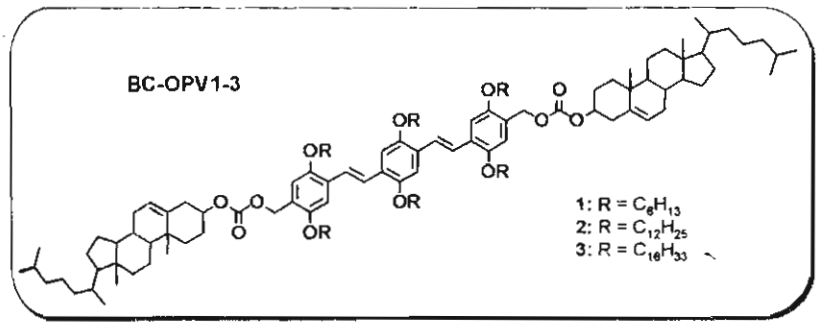


**BC-OPV1:** Yield 92%. mp 144–146 °C. $^{1}$H NMR (300 MHz, $CDCl_3$, TMS): δ 0.67 (s, 6H), 0.91 (m, 18H), 0.94-2.42 (m, 128H), 3.98-4.07 (m, 12H), 4.50-4.55 (m, 2H), 5.20 (s, 4H), 5.42 (s, 2H), 6.92 (s, 2H), 7.12-7.15 (d, 4H), 7.44 (s, 4H) ppm. $^{13}$C NMR (75 MHz, $CDCl_3$): δ 12.11, 13.93, 18.99, 19.67, 21.52, 22.63, 22.88, 24.31, 24.62, 25.74, 27.67, 28.31, 28.52, 29.13, 31.52, 32.09, 32.20, 36.12, 36.72, 37.00, 37.49, 37.89, 39.88, 40.06, 42.61, 49.72, 56.65, 56.82, 63.68, 68.66,

69.80, 76.41, 108.62, 114.23, 116.08, 123.46, 126.82, 127.04, 128.12, 135.20, 135.89, 142.54, 151.43, 152.85, 155.1 ppm. FT-IR (KBr): $\nu_{max}$ 696, 724, 793, 855, 947, 967, 1010, 1031, 1070, 1208, 1265, 1347, 1383, 1426, 1465, 1510, 1739, 2850, 2926 $cm^{-1}$. MALDI-TOF MS (MW = 1767.36): m/z = 1767.38 $[M]^+$.

**BC-OPV2:** Yield 90%. mp 110-112 °C. $^1H$ NMR (300 MHz, $CDCl_3$, TMS): δ 0.68 (s, 6H), 0.90 (m, 18H), 0.92-2.43 (m, 200H), 3.98-4.05 (m, 12H), 4.49-4.53 (m, 2H), 5.21 (s, 4H), 5.41 (s, 2H), 6.88-6.92 (dd, 2H), 7.11-7.14 (d, 4H), 7.43-7.46 (d, 4H) ppm. $^{13}C$ NMR (75 MHz, $CDCl_3$): δ 12.11, 14.01, 19.00, 19.63, 21.55, 22.64, 22.93, 24.30, 24.63, 25.59, 27.72, 28.28, 28.51, 28.75, 28.92, 29.34, 29.52, 29.61, 29.62, 29.82, 31.71, 32.08, 32.21, 36.09, 36.72, 37.01, 37.52, 37.93, 39.92, 40.14, 42.62, 49.71, 56.63, 56.93, 63.72, 68.22, 69.53, 76.42, 108.72, 114.35, 116.14, 123.40, 126.81, 127.06, 128.22, 135.21, 139.93, 142.73, 151.63, 152.84, 155.35 ppm. FT-IR (KBr): $\nu_{max}$ 695, 723, 793, 856, 947, 968, 1007, 1030, 1071, 1206, 1267, 1349, 1384, 1426, 1465, 1508, 1740, 2851, 2924 $cm^{-1}$. MALDI-TOF MS (MW = 2271.93): m/z = 2271.92 $[M]^+$.

**BC-OPV3:** Yield 83%. mp 98-100 °C. $^1H$ NMR (300 MHz, $CDCl_3$, TMS): δ 0.68 (s, 6H), 0.89 (m, 18H), 0.91-2.45 (m, 248H), 3.97-4.05 (m, 12H), 4.48-4.55 (m, 2H), 5.22 (s, 4H), 5.41 (s, 2H), 6.92 (s, 2H), 7.10-7.15 (d, 4H), 7.44 (s, 4H) ppm. $^{13}C$ NMR (75 MHz, $CDCl_3$): δ 12.16, 13.11, 19.05, 19.62, 21.54, 21.72, 22.93, 24.29, 24.61, 25.58, 27.72, 28.27, 28.51, 28.74, 29.35, 29.52, 29.55, 29.59, 29.60, 29.62, 29.63, 29.70, 30.49, 32.07, 32.17, 36.09, 36.72, 37.01, 37.52, 37.91, 39.92,

40.12, 42.58, 49.70, 56.63, 56.93, 63.67, 68.22, 69.47, 76.42, 109.02, 114.35, 116.14, 123.40, 126.81, 127.04, 128.27, 135.21, 139.93, 142.73, 151.58, 152.76, 155.35 ppm. FT-IR (KBr): $\nu_{max}$ 804, 854, 963, 1032, 1087, 1209, 1265, 1344, 1390, 1417, 1424, 1518, 1746, 2863, 2953 $cm^{-1}$. MALDI-TOF MS (MW = 2608.30): m/z = 2608.31 $[M]^+$.

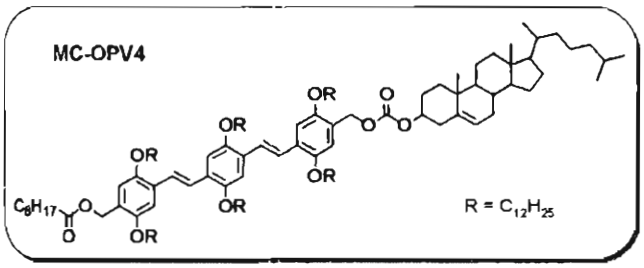


**MC-OPV4:** Yield 95 %. mp 87-89 °C. $^1H$ NMR (300 MHz, $CDCl_3$, TMS): δ 0.70 (s, 3H), 0.86 (m, 21H), 0.95-2.44 (m, 174H), 3.8 (t, 2H), 4.01-4.03 (m, 12H), 4.50-4.52 (m, 1H), 4.92 (s, 2H), 5.20 (s, 2H), 5.40 (s, 1H), 6.84-6.90 (dd, 2H), 7.10-7.12 (d, 4H), 7.42-7.46 (d, 4H) ppm. $^{13}C$ NMR (75 MHz, $CDCl_3$): δ 12.13, 14.06, 19.02, 19.64, 21.55, 22.62, 22.98, 24.33, 24.65, 25.60, 27.72, 28.34, 28.56, 28.72, 28.93, 29.44, 29.56, 29.63, 29.73, 29.24, 31.73, 32.23, 36.16, 36.74, 37.01, 37.54, 37.92, 39.90, 40.13, 42.58, 49.71, 56.66, 56.92, 60.73, 63.72, 68.23, 69.53, 76.45, 108.50, 108.72, 114.31, 115.88, 116.08, 123.42, 126.85, 127.03, 128.21, 128.49, 128,65, 135.24, 139.93, 142.42, 142.73, 151.64, 152.85, 155.09, 155.33 ppm. FT-IR (KBr): $\nu_{max}$ 696, 722, 805, 854, 966, 1013, 1074, 1208, 1256, 1344, 1389, 1423, 1458, 1467, 1508, 1741, 2852, 2922 $cm^{-1}$. MALDI-TOF MS (MW = 1999.71): m/z = 1999.86 $[M]^+$.

### 2.5.2. General Procedure for Gelation Studies

The gelation studies were carried out as per reported procedures.[23b] A typical procedure is as follows: A weighed amount of the compound in an appropriate solvent (1 mL) was placed in the vial (1 cm diameter), which was sealed and heated until the compound was dissolved. The solution was allowed to cool. The gel formation was confirmed by the failure of the content to flow by inverting the glass vial. Repeated heating and cooling confirmed the thermal reversibility of gelation. The critical gelator concentration (CGC) is determined from the minimum amount of gelator required for the formation of a stable gel in 1 mL solvent at room temperature.

### 2.5.2. Description of Instrumental Techniques

#### 2.5.2.1. Optical Measurements

Electronic absorption spectra were recorded on a Shimadzu UV-3101 PC NIR scanning spectrophotometer and the emission spectra were recorded on a SPEX-Fluorolog F112X spectrofluorimeter using the front face geometry. Optical studies were carried out in a quartz cuvette with 1 mm path length. Temperature dependent studies were carried out using a thermistor directly attached to the wall of the cuvette holder.

### 2.5.2.2. Quantum Yield Measurements

Fluorescence quantum yields of molecularly dissolved OPV molecules upon excitation at 380 nm are reported relative to quinine sulfate ($\Phi_f$ = 0.546), whereas the quantum yields of the self-assembled molecules are reported relative to Rhodamine 6G ($\Phi_f$ = 0.9). The experiments were done using optically matching solutions and the quantum yield is calculated using equation 1.1.[30]

$$\Phi_f = \Phi_r (A_r F_s / A_s F_r) (\eta_s^2 / \eta_r^2) \qquad 1.1$$

where, $A_s$ and $A_r$ are the absorbance of the sample and reference solutions, respectively at the same excitation wavelength (380 nm), $F_s$ and $F_r$ are the corresponding relative integrated fluorescence intensities and $\eta$ is the refractive index of the solvent.

### 2.5.2.3. Fluorescence Lifetime Experiments

Fluorescence lifetimes were measured using IBH (FluoroCube) time-correlated picosecond single photon counting (TCSPC) system. Solutions were excited with a pulsed diode laser (<100 ps pulse duration) at a wavelength of 375 nm (NanoLED-11) with a repetition rate of 1 MHz. The detection system consists of a microchannel plate photomultiplier (5000U-09B, Hamamatsu) with a 38.6 ps response time coupled to a monochromator (5000M) and TCSPC electronics (DataStation Hub including Hub-NL, NanoLED controller and preinstalled Fluorescence Measurement and Analysis Studio (FMAS) software). The

fluorescence lifetime values were determined by deconvoluting the instrument response function with biexponential decay using DAS6 decay analysis software. The quality of the fit has been judged by the fitting parameters such as $\chi^2$ (<1.2) as well as the visual inspection of the residuals. All measurements were carried out in a 1mm cuvette using the front face sample holder (5000U-04).

### 2.5.2.4. Optical Polarizing Microscopic Studies

The gel texture was observed on a polarizing light microscope (Nikon HFX 35 A Optiphot equipped with a Linkan THMS 600 heating and freezing stage connected to Linkan TP 92 temperature programmer).

### 2.5.2.5. Atomic Force Microscopic Studies

Atomic Force Microscopic images were recorded under ambient conditions using a Digital Instrument Multimode Nanoscope IV operating in the tapping mode regime. Micro-fabricated silicon cantilever tips (MPP-11100-10) with a resonance frequency of 299 kHz and a spring constant of 20-80 $Nm^{-1}$ were used. The scan rate varied from 0.5 to 1.5 Hz. AFM section analysis was done offline. Samples for the imaging were prepared by drop casting the decane solution at the required compositions on freshly cleaved mica. Concentration of the solution was kept at $1 \times 10^{-5}$ M. Blank experiments with neat solvents on mica sheet were carried out to eliminate the possibility of any artifacts, prior to the measurements of the samples.

## 2.6. References


1. a) J.-M. Lehn, *Supramolecular Chemistry, Concepts and Perspectives*, VCH, Winheim, **1995**; b) H.-J. Schneider, A. Yatsimirsky, *Principles and Methods in Supramolecular Chemistry*, Wiley, Chichester, **2000**; c) J. W. Steed, J. L. Atwood, *Supramolecular Chemistry*, Wiley, Chichester, **2000**; d) D. N. Reinhoudt, M. Crego-Calama, *Science* **2002**, *295*, 2403; e) G. M. Whitesides, B. Grzybowski, *Science* **2002**, *295*, 2418; f) J. A. A. W. Elemans, R. van Hameren, R. J. M. Nolte, A. E. Rowan, *Adv. Mater.* **2006**, *18*, 1251.

2. a) J. L. Sessler, B. Wang, A. Harriman, *J. Am. Chem. Soc.* **1995**, *117*, 704; b) S. I. Stupp, V. Le Bonheur, K. Walker, L. S. Li, K. Huggins, M. Keser, A. Amstutz, *Science* **1997**, *276*, 384; c) A. E. Rowan, R. J. M. Nolte, *Angew. Chem. Int. Ed.* **1998**, *37*, 63; d) A. K. Burrell, D. L. Officer, P. G. Plieger, D. C. W. Reid, *Chem. Rev.* **2001**, *101*, 2751; e) J. J. L. M. Cornelissen, A. E. Rowan, R. J. M. Nolte, N. A. J. M. Sommerdijk, *Chem. Rev.* **2001**, *101*, 4039; f) T. Yamaguchi, N. Ishii, K. Tashiro, T. Aida, *J. Am. Chem. Soc.* **2003**, *125*, 13934; g) F. Radotondradany, M. Whitehead, A. Lebuis, H. Slieman, *Chem. Eur. J.* **2003**, *9*, 4771; h) J. F. Hulvat, M. Sofofs, K. Tajima, S. I. Stupp, *J. Am. Chem. Soc.* **2005**, *127*, 366; i) P. Jonkheijm, N. Stutzmann, Z. Chen, D. M. de Leeuw, E. W. Meijer, A. P. H. J. Schenning, F. Würthner, *J. Am. Chem. Soc.* **2006**, *128*, 9535; j) Y. Wang, N. Ma, Z. Wang, X. Zhang, *Angew. Chem. Int. Ed.* **2007**, *46*, 2823.

3. a) E. W. Meijer, A. P. H. J. Schenning, *Nature* **2002**, *419*, 353; b) M. V. D. Auweraer, F. C. D. Schryver, *Nat. Mater.* **2004**, *3*, 507; c) H. John, R. Bauer, P. Espindola, P. Sonar, J. Heinze, K. MDllen, *Angew. Chem. Int. Ed.* **2005**, *44*, 2447; d) A. P. H. J. Schenning, E. W. Meijer, *Chem. Commun.* **2005**, 3245; e) L. Sardone,

V. Palermo, E. Devaux, D. Credgington, M. de Loos, G. Marletta, F. Cacialli, J. van Esch, P. Samori, *Adv. Mater.* **2006**, *18*, 1276.

4. a) A. Tracz, J. K. Jeszka, M. D. Watson, W. Pisula, K. Müllen, T. Pakula, *J. Am. Chem. Soc.* **2003**, *125*, 1682; b) J. Wu, M. D. Watson, L. Zhang, Z. Wang, K. Müllen, *J. Am. Chem. Soc.* **2004**, *126*, 177.

5. V. Percec, M. Glodde, T. K. Bera, Y. Miura, I. Shiyanovskaya, K. D. Singer, V. S. K. Balagurusamy, P. A. Heiney, I. Schnell, A. Rapp, H. W. Spiess, S. D. Hudson, H. Duan, *Nature* **2002**, *419*, 384.

6. For selected chromophore assemblies: a) H. Engelkamp, S. Middelbeek, R. J. M. Nolte, *Science* **1999**, *284*, 785; b) F. Würthner, C. Thalacker, A. Sautter, W. Schärtl, W. Ibach, O. Hollricher, *Chem. Eur. J.* **2000**, *6*, 3871; c) T. Yamaguchi, N. Ishii, K. Tashiro, T. Aida, *J. Am. Chem. Soc.* **2003**, *125*, 13934; d) F. Würthner, S. Yao, U. Beginn, *Angew. Chem. Int. Ed.* **2003**, *42*, 3247; e) M. Kimura, T. Kuroda, K. Ohta, K. Hanabusa, H. Shirai, N. Kobayashi, *Langmuir* **2003**, *19*, 4825; f) A. Ajayaghosh, S. J. George, A. P. H. J. Schenning, *Top. Curr. Chem.* **2005**, *258*, 83; g) V. Huber, M. Lysetska, F. Würthner, *Small* **2007**, *3*, 1007; h) T. Murase, S. Sato, M. Fujita, *Angew. Chem. Int. Ed.* **2007**, *46*, 5133.

7. a) P. Leclère, A. Calderone, D. Marsitzky, V. Francke, Y. Geerts, K. Müllen, J. L. Brédas, R. Lazzaroni, *Adv. Mater.* **2000**, *12*, 1042; b) A. C. Grimsdale, K. Müllen, *Angew. Chem. Int. Ed.* **2005**, *44*, 5592; c) D. Wasserfallen, I. Fischbach, N. Chebotareva, M. Kastler, W. Pisula, F. Jäckel, M. D. Watson, I. Schnell, J. P. Rabe, H. W. Spiess, K. Müllen, *Adv. Funct. Mater.* **2005**, *15*, 1585; d) S. Yagai, *J. Photochem. Photobiol., C* **2006**, *7*, 164; e) R. A. Miller, A. D. Presley, M. B. Francis, *J. Am. Chem. Soc.* **2007**, *129*, 3104.

8. For reviews on π-conjugated systems: a) F. J. M. Hoeben, P. Jonkheijm, E. W. Meijer, A. P. H. J. Schenning, *Chem. Rev.* **2005**, *105*, 1491; b) A. P. H. J. Schenning, E. W. Meijer, *Chem. Commun.* **2005**, 3245.

9. a) F. S. Schoonbeek, J. H. van Esch, B. Wegewijs, D. B. A. Rep, M. P. de Haas, T. M. Klapwijk, R. M. Kellogg, B. L. Feringa, *Angew. Chem. Int. Ed.* **1999**, *38*, 1393; b) B. W. Messmore, J. F. Hulvat, E. D. Sone, S. I. Stupp, *J. Am. Chem. Soc.* **2004**, *126*, 14452; c) J. Bae, J.-H. Choi, Y.-S. Yoo, N.-K. Oh, B.-S. Kim, M. Lee, *J. Am. Chem. Soc.* **2005**, *127*, 9668.

10. a) A. P. H. J. Schenning, P. Jonkheijm, E. Peeters, E. W. Meijer, *J. Am. Chem. Soc.* **2001**, *123*, 409; b) P. Jonkheijm, A. Miura, M. Zdanowska, F. J. M. Hoeben, S. De Feyter, A. P. H. J. Schenning, F. C. De Schryver, E. W. Meijer, *Angew. Chem. Int. Ed.* **2004**, *43*, 74; c) P. G. A. Janssen, J. Vandenbergh, J. L. J. van Dongen, E. W. Meijer, A. P. H. J. Schenning, *J. Am. Chem. Soc.* **2007**, *129*, 6078.

11. a) J. H. Burroughes, D. D. C. Bradley, A. R. Brown, R. N. Marks, K. MacKay, R. H. Friend, P. L. Burns, A. B. Holmes, *Nature* **1990**, *347*, 539; b) A. Kraft, A. C. Grimsdale, A. B. Holmes, *Angew. Chem. Int. Ed.* **1998**, *37*, 402.

12. a) G. Yu, J. Gao, J. C. Hummelen, F. Wudl, A. J. Heeger, *Science* **1995**, *270*, 1789. b) J. J. M. Halls, C. A. Walsh, N. C. Greenham, E. A. Marseglia, R. H. Friend, S. C. Moratti, A. B. Holmes, *Nature* **1995**, *376*, 498; c) A. El-ghayoury, A. P. H. J. Schenning, P. A. van Hal, J. K. J. van Duren, R. A. J. Janssen, E. W. Meijer, *Angew. Chem. Int. Ed.* **2001**, *40*, 3660; d) A. M. Ramos, M. T. Rispens, J. K. J. van Duren, J. C. Hummelen, R. A. J. Janssen, *J. Am. Chem. Soc.* **2001**, *123*, 6714; e) O. Hagemann, M. Jørgensen, F. C. Krebs, *J. Org. Chem.* **2006**, *71*, 5546.

13. a) G. Horowitz, *Adv. Mater.* **1998**, *10*, 365; b) H. Sirringhaus, P. J. Brown, R. H. Friend, M. M. Nielsen, K. Bechgaard, B. M. W. Langeveld-Voss, A. J. H. Spiering,

R. A. J. Janssen, E. W. Meijer, P. Herwig, D. M. de Leeuw, *Nature* **1999**, *401*, 685; c) J. Cornil, D. Beljonne, J.-P. Calbert, J.-L. Bréads, *Adv. Mater.* **2001**, *13*, 1053.

14. a) K. Müllen, G. Wegner, *Electronic Materials: The Oligomer Approach*, VCH, Weinheim, Germany, **1998**; b) J. M. Tour, *Chem. Rev.* **1996**, *96*, 537; c) R. E. Martin, F. Diederich, *Angew. Chem. Int. Ed.* **1999**, *38*, 1350.

15. a) R. Schenk, H. Gregorius, K. Meerholz, J. Heinze, K. Müllen, *J. Am. Chem. Soc.* **1991**, *113*, 2634; b) J. Cornil, D. Beljonne, Z. Shuai, T. W. Hagler, I. Campbell, D. D. C. Bradley, J. L. Brèdas, C. W. Spangler, K. Müllen, *Chem. Phys. Lett.* **1995**, *247*, 425; d) J. Zhang, F. J. M. Hoeben, M. J. Pouderoijen, A. P. H. J. Schenning, E. W. Meijer, F. C. D. Schryver, S. D. Feyter, *Chem. Eur. J.* **2006**, *12*, 9046.

16. a) V. Gebhardt, A. Bacher, M. Thelakkat, U. Stalmach, H. Meier, H.-W. Schmidt, D. Haarer, *Adv. Mater.* **1999**, *11*, 119; b) H. Meier, J. Gerold, H. Kolshorn, W. Baumann, M. Bletz, *Angew. Chem. Int. Ed.* **2002**, *41*, 292; c) Y. Oseki, M. Fujitsuka, M. Hara, X. Cai, A. Sugimoto, T. Majima, *J. Phys. Chem. B* **2004**, *108*, 16727; d) A. Cirpan, H. P. Rathnayake, P. M. Lahti, F. E. Karasz, *J. Mater. Chem.* **2007**, *17*, 3030.

17. a) B. S. Gaylord, S. Wang, A. J. Heeger, G. C. Bazan, *J. Am. Chem. Soc.* **2001**, *123*, 6417; b) M. R. Robinson, S. Wang, A. J. Heeger, G. C. Bazan, *Adv. Funct. Mater.* **2001**, *11*, 413; c) B. Liu, B. S. Gaylord, S. Wang, G. C. Bazan, *J. Am. Chem. Soc.* **2003**, *125*, 6705.

18. a) E. Peeters, A. M. Ramos, S. C. J. Meskers, R. A. J. Janssen, *J. Chem. Phys.* **2000**, *112*, 9445; b) E. Peeters, P. A. van Hal, J. Knol, C. J. Brabec, N. S. Sacriciftci, J. C. Hummelen, R. A. J. Janssen, *J. Phys. Chem. B* **2000**, *104*, 10174.

19. See the references 18 and 20 cited in Chapter 1 of the thesis.

20. a) K. Murata, M. Aoki, T. Suzuki, T. Harada, H. Kawabata, T. Komori, F. Ohseto, K. Ueda, S. Shinkai, *J. Am. Chem. Soc.* **1994**, *116*, 6664; b) R. Wang, C. Geiger, L. Chen, B. Swanson, D. G. Whitten, *J. Am. Chem. Soc.* **2000**, *122*, 2399; c) M. Stanescu, H. Samha, J. Perlstein, D. G. Whitten, *Langmuir* **2000**, *16*, 275; d) T. Ishi-i, R. Iguchi, E. Snip, M. Ikeda, S. Shinkai, *Langmuir* **2001**, *17*, 5825; e) K. Sugiyasu, N. Fujita, M. Takeuchi, S. Yamada, S. Shinkai, *Org. Biomol. Chem.* **2003**, *1*, 895; f) K. Sugiyasu, N. Fujita, S. Shinkai, *Angew. Chem. Int. Ed.* **2004**, *43*, 1229; g) P. Xue, R. Lu, D. Li, M. Jin, C. Tan, C. Bao, Z. Wang, Y. Zao, *Langmuir* **2004**, *20*, 11234; h) S.-i. Kawano, N. Fujita, S. Shinkai, *Chem. Eur. J.* **2005**, *11*, 4735; i) M. George, R. G. Weiss, *Acc. Chem. Res.* **2006**, *39*, 489;

21. K. J. C. van Bommel, A. Friggeri, S. Shinkai, *Angew. Chem. Int. Ed.* **2003**, *42*, 980.

22. a) B. Wang, M. R. Wasielewski, *J. Am. Chem. Soc.* **1997**, *119*, 12; b) A. W. van der Made, R. H. van der Made, *J. Org. Chem.* **1993**, *58*, 1262.

23. a) A. Ajayaghosh, S. J. George, *J. Am. Chem. Soc.* **2001**, *123*, 5148; b) S. J. George, A. Ajayaghosh, *Chem. Eur. J.* **2005**, *11*, 3217;

24. a) P. A. van Hal, M. M. Weink, J. M. Kroon, R. A. J. Janssen, *J. Mater. Chem.* **2003**, *13*, 1054; b) T. Mori, T. Watanabe, K. Minagawa, M. Tanaka, *J. Polym. Sci. Part A: Polym. Chem.* **2005**, *43*, 1569.

25. The fraction of the aggregated species ($\alpha$) at each temperature was calculated on the assumption that in nonpolar solvents such as decane, all the OPV molecules are in the self-assembled phase at temperatures less than 20 °C and in the molecularly dissolved phase at temperatures greater than 55 °C.

26. N. Berova, K. Nakanishi in *Circular Dichroism: Principles and Applications* (Eds.: N. Berova, K. Nakanishi, R. W. Woody), 4$^{th}$ ed., Wiley-VCH, Weinheim, **2000**, p337.

27. In dropping ball method, a steel ball (150 mg) was placed on the top of a 1 mL volume gel in a sealed glass vial. Then the gel was slowly heated, while the position of the ball on the top of gel is continuously observed, until the gel no longer bears the ball. The temperature at which the ball reaches the bottom of the vial is taken as the sol-gel phase transition (gel melting) temperature ($T_{gel}$).

28. a) X. Huang, P. Terech, S. R. Raghavan, R. G. Weiss, *J. Am. Chem. Soc.* **2005**, *127*, 4336; b) S. J. George, A. Ajayaghosh, P. Jonkheijm, A. P. H. J. Schenning, E. W. Meijer, *Angew. Chem. Int. Ed.* **2004**, *43*, 3422; c) L. Lu, R. G. Weiss, *Chem. Commun.* **1996**, 2029.

29. A. Lohr, M. Lysetska, F. Würthner, *Angew. Chem. Int. Ed.* **2005**, *44*, 5071.

30. J. R. Lakowicz, *Principles of Fluorescence Spectroscopy* (2nd ed.), Kluwer Academic/Plenum Publishers, New York, **1999**.

# *Chapter 3*

# Effect of Chromophore Packing on Fluorescence Resonance Energy Transfer: Design of Red and White Light Emitting Organogels

## 3.1. Abstract

*The effect of chromophore packing on the efficiency of fluorescence resonance energy transfer (FRET) in π-organogels is described. Mono- and bischolesterol oligo(p-phenylenevinylene) derivatives (**MC-OPV2-3** and **BC-OPV2-3** respectively) were used as the donors. A π-conjugated oligomer, phenylenevinylene-co-pyrrolylenevinylene (**PYPV**) was found to be a good acceptor for the excitation energy from **MC-OPV**s and **BC-OPV**s. Time resolved emission studies revealed that excitation energy migration is highly efficient in **MC-OPV** gels, whereas, it is found to be less efficient in **BC-OPV** gels. Efficient energy migration in **MC-OPV2** gels leads to an efficient energy transfer to the encapsulated acceptor (2 mol%) with 90% quenching of the donor fluorescence resulting in bright red emission in the gel state. Under similar conditions, partial energy transfer with 63% quenching of donor fluorescence was observed for **BC-OPV2** to give an intense white light emission. These observations are rationalized based on the difference in the packing of the OPV molecules in the mono- and bischolesterol derivatives in the gel state.*

## 3.2. Introduction

The understanding of natural light harvesting process[1] has brought significant importance to the energy transfer processes in self-assembled multichromophoric arrays. Several strategies have been employed for the realization of higher order multichromophoric assemblies such as the use of hydrogen bonded supramolecular complexes,[2] dendrimers,[3] chromophore-linked polymers,[4] Langmuir-Blodgett films[5] and self-assembled monolayers.[6] In this context, higher order multichromophoric assemblies derived from linear π-conjugated systems, particularly oligo(*p*-phenylenevinylene)s (OPVs) have attracted attention because of their interesting optoelectronic properties and wide spread use in device fabrication.[7] Since OPVs are known to be efficient energy donors to suitable acceptors, self-assembled OPVs are excellent supramolecular scaffolds for energy transfer processes. Therefore, energy transfer (ET) properties of OPVs have been extensively studied by several groups.[8-11]

The transfer of excited-state energy from an initially excited molecule to another which is in the ground state is often referred to as excitation energy transfer. In an energy transfer process, the molecule which donates energy is called donor, whereas, the molecule which accepts energy is called acceptor. The energy transfer mechanisms can be of two types, viz., radiative (trivial) and non-radiative.[12] Trivial mechanism of energy transfer can be considered as a simple emission re-absorption process in which the emission of the excited donor is

absorbed by the ground state acceptor resulting in the excitation of the latter. Interactions of the donor-acceptor molecules are not needed in this mechanism.

On the other hand, electronic interactions of the donor-acceptor molecules are necessary for non-radiative energy transfer. In addition, they must satisfy the following requirements: (i) the energy of the donor excited state should be higher than that of the acceptor excited state and (ii) the rate of energy transfer should be more rapid than the decay rate of the donor excited state. Non-radiative energy transfer can occur either by through-bond (Dexter) or through space (Förster) mechanisms (Figure 3.1). In the former case, excitation of the donor results in electron exchange from the excited state of the donor to the excited state of the acceptor, with a simultaneous exchange of a ground state electron from the acceptor to the donor ground state. This electron exchange requires strong donor-acceptor orbital overlap and is therefore a short range (<10 Å) interaction that diminishes exponentially with distance. In contrast, the Förster mechanism does not require electron exchange and is rather a through-space dipole–dipole interaction. This energy transfer mechanism is termed "Förster resonance energy transfer", named after the German scientist Theodor Förster. When both molecules are fluorescent, the term "fluorescence resonance energy transfer" (FRET) is often used, although the energy is not actually transferred by fluorescence. In this case, donor-acceptor orbital overlap is not necessary, allowing the chromophores to be separated by a relatively large distance (10 – 100 Å). The FRET efficiency of a

donor-acceptor system mainly depends on the distance between the donor and the acceptor molecules, the spectral overlap of the donor emission and the acceptor absorption and the relative orientation of the donor-acceptor chromophores.

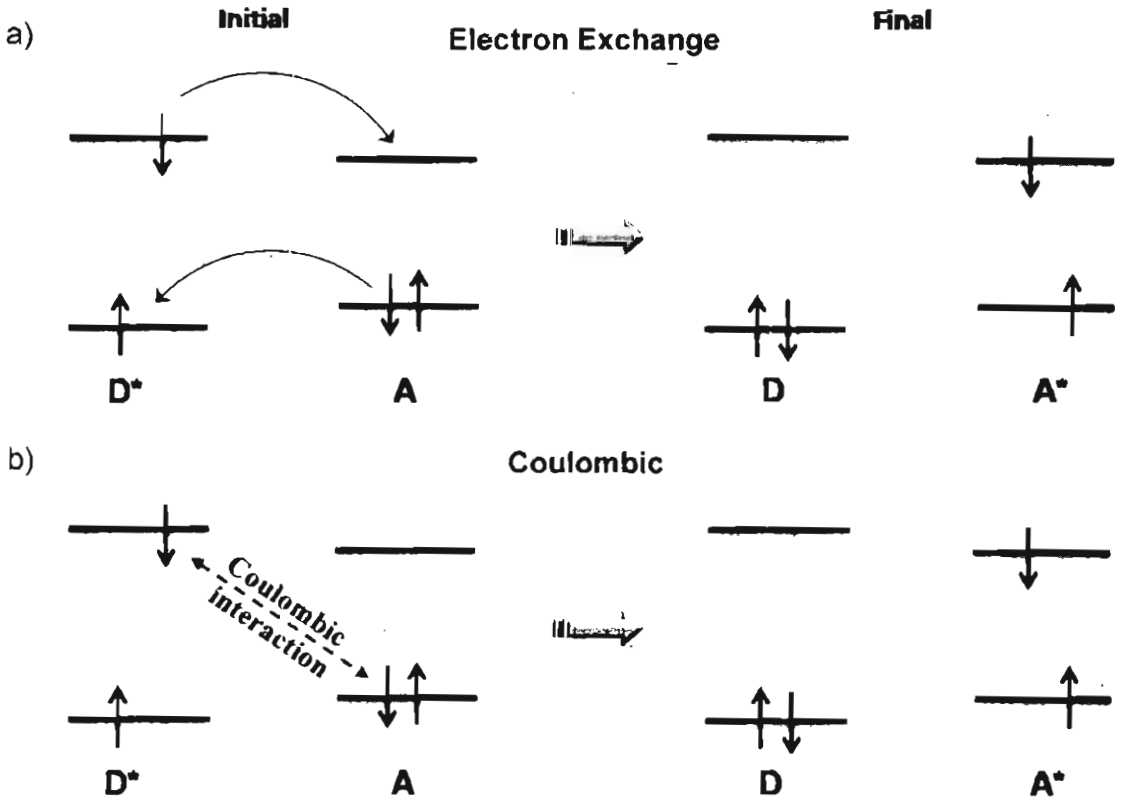


**Figure 3.1.** Schematic representation of excitation energy transfer processes. a) Electron exchange (Dexter) mechanism and b) coulombic (Förster) mechanism. 'D' is the energy donor, 'A' is the energy acceptor and * denotes an excited state.

The original theory of Förster resonance energy transfer,[13] which was developed more than 50 years ago, considered the transfer of electronic excitation energy from a single chromophoric donor to a single chromophoric acceptor. Recent studies on the energy transfer properties of multichromophoric assemblies shows that these systems show considerable deviation from the Förster theory.

Studies have shown that temperature and order of the chromophore arrangements play a crucial role on the energy transfer efficiency in multichromophoric systems, which are not considered in the original Förster mechanism. In a recent work, Silbey *et al.* have generalized the Förster theory by stressing the importance of order-disorder and temperature on energy transfer properties of multichromophoric systems.[14]

Meijer and coworkers experimentally proved the importance of structural order of chromophore assemblies on the efficiency of energy transfer using hydrogen bonded helical co-assembly of OPVs (**1-3**, Chart 3.1).[10a] The OPV derivative **1** and its bifunctional analogue **2** bearing quadruple hydrogen bonding ureido-*s*-triazine motif acts as the donors, whereas, **3** of higher conjugation length containing the same hydrogen bonding motif was used as the acceptor. The molecule **1** self-assemble to ordered helical structures, whereas, **2** forms disordered polymeric aggregates owing to the presence of a connecting hexyl spacer between the hydrogen bonding motifs (Figure 3.2). Fast and efficient energy transfer was observed from **1** to **3** on increasing the concentration of the acceptor molecules as evident from the decrease in the fluorescence intensity of the donor. Under identical conditions, the quenching efficiency for the disordered aggregates of **2** was found to be much lower than that of the well-ordered stacks of **1**. Detailed time resolved fluorescence studies indicates that for ordered helical assembly of **1**, a fast initial fluorescence depolarization and excitation transfer to

dopant occurs, which is in agreement with semi-coherent exciton diffusion along the chiral stacks of **1**. For disordered polymeric assemblies of **2**, both depolarization and energy transfer dynamics take place on a much longer time scale which is attributed to weak electronic coupling of chromophoric units that result in slow incoherent motion of excitations along the stacks of **2**.[15]

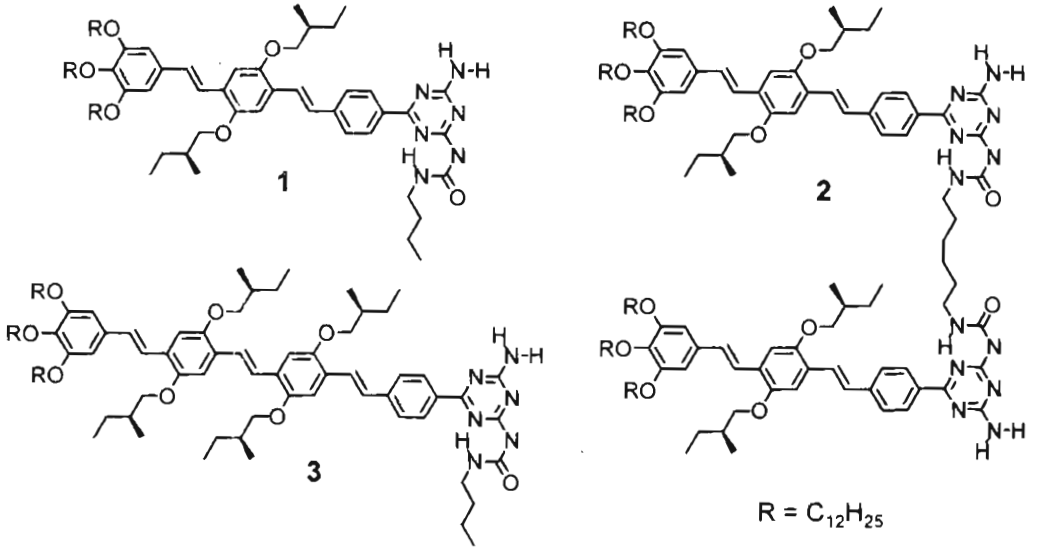


**Chart 3.1.** Molecular structures of ureido-*s*-triazine functionalized OPVs.

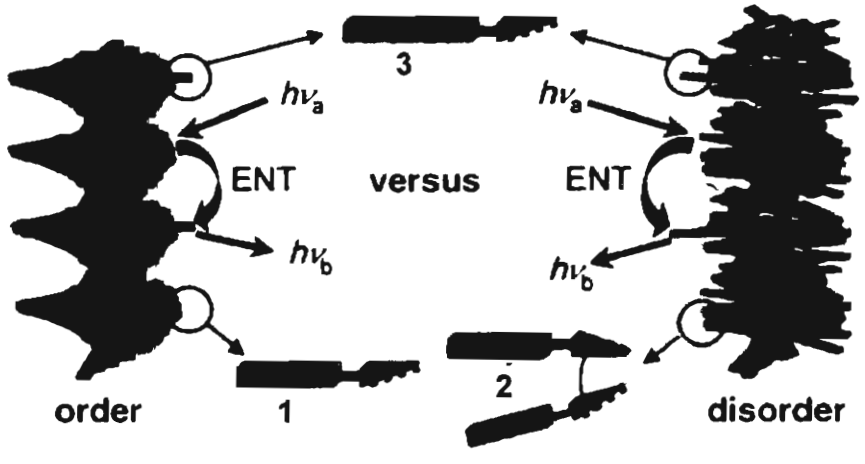


**Figure 3.2.** Schematic representation of the energy transfer process in helically ordered and disordered assemblies of **1** and **2**, respectively. (adapted from ref. 25a)

In addition to the order-disorder and temperature, chromophore packing may also affect the energy migration and FRET efficiency in multichromophoric supramolecular assemblies. With the help of various spectroscopic and microscopic techniques, we have established the different chromophore packing in the mono- and bischolesterol OPV derivatives (see Chapter 2). Monocholesterol derivatives (**MC-OPV2-3**) prefers to form 'pseudo J-aggregates' with tilted chromophore packing to give coiled helical structures, whereas, bischolesterol derivatives (**BC-OPV2-3**) form 'pseudo H-aggregates' with twisted chromophore packing to give twisted helical structures in the self-assembled gel state. In the present chapter, the details of the FRET properties of the mono- and bischolesterol OPV derivatives in the gel state are described.

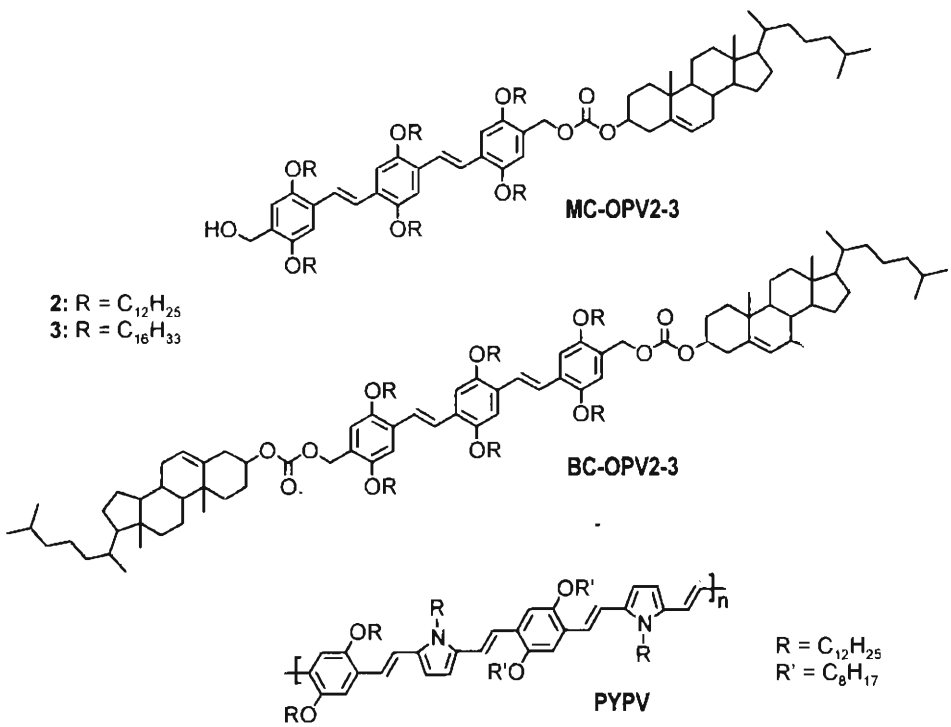


**Chart 3.2**. Structure of the donor and acceptor molecules under study.

## 3.3. Results and Discussion

### 3.3.1. Synthesis of PYPV

Synthesis and characterization of the mono- and bischolesterol OPV derivatives were described in Chapter 2. The starting compound for the preparation of phenylenevinylene-*co*-pyrrolylenevinylene (**PYPV**) oligomer was the bispyrrole derivative **11** which was prepared by the Wittig-Horner-Emmons reaction of the bisphosphonate **10a** and the *N*-dodecylpyrrole-2-carbaldehyde (**6**) using NaH in 64% yield (Scheme 3.1).[16] The required *N*-dodecylpyrrole-2-carbaldehyde (**6**) was prepared by the Vilsmeier formylation of the *N*-dodecylpyrrole (**5**) in 78% yield using a reported procedure (Scheme 3.1).[16] The

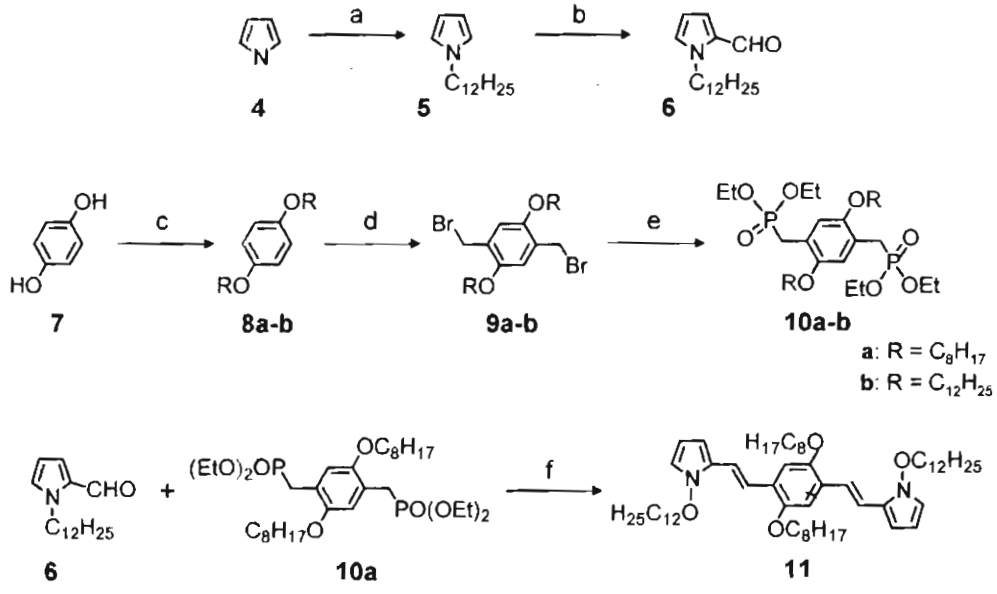


**Scheme 3.1.** Reagents and conditions: a) 1-Bromododecane, potassium *t*-butoxide, THF, 27 °C, 21 h (88%); b) DMF, $POCl_3$, 5-10 °C, 45 min (78%); c) alkyl bromide, NaOH, DMF, 100 °C, 24 h (70%); d) Paraformaldehyde, 33% HBr in $CH_3COOH$, glacial $CH_3COOH$, sonication, 4 h (90%); e) $P(OEt)_3$, 100 °C, 12 h (90-92%); f) NaH, THF, 70 °C, 10 h (64 %).

bisphosphonate derivatives (**10a-b**), were prepared starting from the hydroquinone 7 as reported earlier.[16] The dialkoxyhydroquinone **8a-b** were bromomethylated with 33% HBr in acetic acid under sonication to get the bisbromomethyl derivatives (**9a-b**) in 90-92% yields, which on reaction with triethyl phosphite gave the corresponding bisphosphonate derivatives (**10a-b**) (Scheme 3.1).

The oligomer **PYPV** was prepared by the Wittig-Horner olefination procedure (Scheme 3.2) as reported previously.[17] For this purpose, the bispyrrole **11** was converted to the corresponding bisaldehyde **12** by Vilsmeier formylation (62% yield).[16c] After column chromatographic purification, the product **12** was characterized by spectral analysis. Reaction of **12** with the bisphosphonate **10b** in THF using NaH as base turned the initial green fluorescence of the reaction mixture to red on progress of the reaction indicating the formation of the conjugated oligomer **13** (**PYPV**). The deep red solution obtained was concentrated

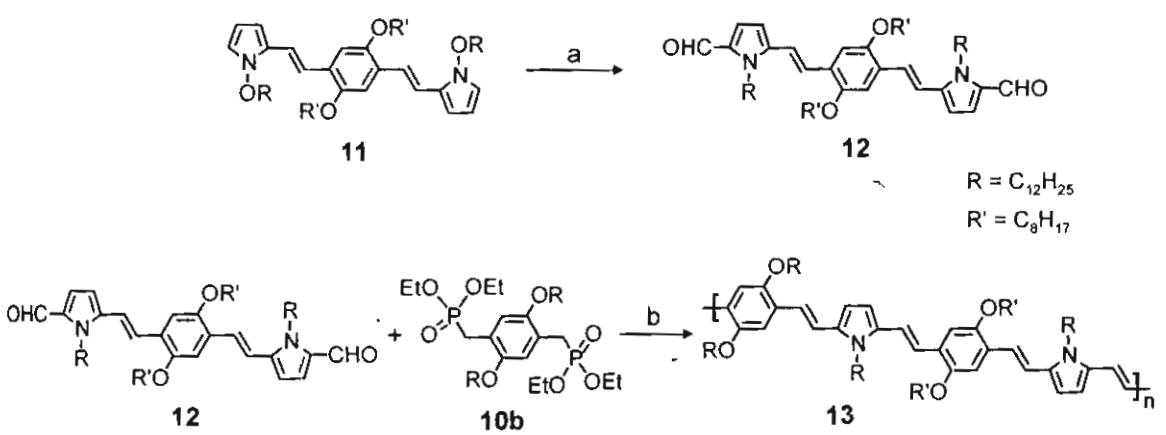


**Scheme 3.2.** Reagents and conditions: a) DMF, $POCl_3$, 1,2-dichlorobenzene, 0 °C, 3 h (62%); b) NaH, THF, 70 °C, 26 h (53 %).

and the oligomer was purified by repeated precipitation by adding methanol into a dichloromethane solution. The product (**PYPV**) was obtained as a dark red solid in 53% yield.

The molecular weight of **PYPV** was determined by gel permeation chromatography (GPC) after calibration with standard polystyrene. Number average molecular weight ($M_n$) was found to be 4358 with a polydispersity index of 1.12. $^1$H NMR spectrum of **PYPV** showed the required resonance peaks of the aromatic and vinylic protons (δ 6.60-7.40 ppm), $-NCH_2-$ and $-OCH_2-$ protons at δ 4.04 and 4.47 ppm, respectively and the aliphatic protons (δ 0.85-1.90 ppm). In addition, $^1$H NMR spectrum of **PYPV** showed weak resonance peaks at δ 9.46, corresponding to the terminal –CHO group. The all *trans* conformation of **PYPV** is established from the FT-IR spectral analysis. The absorption corresponding to the C–H out-of-plane vibration mode of the *trans*-vinylic group at 964 $cm^{-1}$ is very strong when compared to the C–H out-of-plane mode of the *cis*-vinylic group at 863 $cm^{-1}$.[18]

### 3.3.2. Excitation Energy Migration

Excitation energy migration (exciton migration or exciton hopping) could be defined as the movement of electronic excitation energy from one molecular entity to another of the same species, or from one part of a molecular entity to another of the same kind. Energy migration within the self-assembled

chromophoric aggregates plays a crucial role in natural light harvesting complexes of purple bacteria, algae, plants etc. Energy migration process in organized polymers has been extensively studied in recent years.[19]

Molecules with a weaker overlap of the π-electrons, exhibit a larger difference in energy between the highest occupied molecular orbital (HOMO) and the lowest unoccupied molecular orbital (LUMO), and therefore can transfer energy to molecules with a lower HOMO–LUMO spacing. Thus, energy migration can occur in similar types of species due to small local variations of the overlap of the π-electrons and hence the HOMO–LUMO spacing.[20] As a result of energy migration, the energy transfer process in polymers includes at least two steps: (1) diffusion within the host polymer and (2) transfer from the host polymer to the guest (Figure 3.3).[21] The former process plays a major role in systems in which efficient energy transfer is taking place in presence of low concentrations of the acceptor molecules.[22] The migration process of singlet excitons can be explained by a Coulomb or exchange interaction (Förster or Dexter)[23] depending on the distance of the molecules.

Energy migration may be possible in self-assembled aggregates and organogels due to the difference in the energy levels of the self-assembled species. In the gel state, the gelator molecules are self-assembled to form a continuous network in which the chromophores are close to each other (~ 3.8 nm). This continuum of energy levels allows fast and efficient energy migration from the

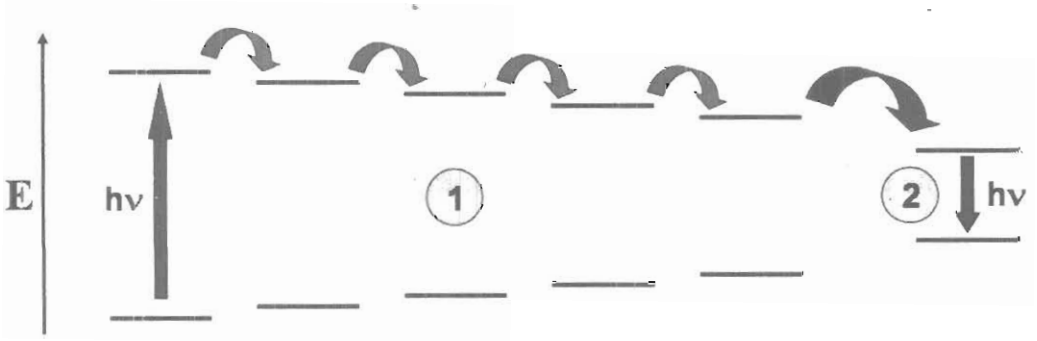


**Figure 3.3**. Schematic representation showing the energy migration process within the donor assembly (blue arrows) followed by energy transfer to the acceptor (red arrow).

lower order (large HOMO-LUMO gap) aggregates to higher order (small HOMO-LUMO) aggregates within the self-assembled scaffolds of the gelators. Since the distance between the interacting chromophores are ~ 3.8 nm, Förster type energy transfer will be the feasible mechanism in such systems.

Energy migration, which is initiated upon photoexcitation of the donor, proceeds to the lower energy sites present within the donor molecules. During this process, energy transfer occurs when the exciton meet an energy trap (acceptor). Since the energy migration proceeds toward lower energy sites, a time-dependent red-shift in the donor emission could be observed.[12a] Therefore, time resolved *emission spectroscopy* (TRES) is an appropriate tool for the study of excitation energy migration.

Time resolved emission spectra of **MC-OPV2** and **BC-OPV2** ($3 \times 10^{-4}$ M) in the gel state in decane at different time settings at room temperature are shown in Figure 3.4. In both cases, a red-shift was observed in the emission spectrum

with time. The dynamic red-shift of the emission maximum with time is due to the population build up of the excited states of the higher order aggregates with lesser HOMO-LUMO energy gap through excitation energy migration. It should be noted that under identical conditions, **MC-OPV2** and **BC-OPV2** exhibit remarkable differences in the time resolved emission spectrum. In the case of **MC-OPV2**, with increase in time after excitation, the emission spectrum becomes broad with a red-shift in the emission maximum. The spectrum obtained after 672 ps was almost identical with the steady state emission of **MC-OPV2** gel in decane (Figure 3.4a). Initially the emission maximum was at 485 nm and finally it reached around 560 nm. In the case of **BC-OPV2**, the red-shift of the emission maximum (494 nm) was marginal but the shoulder at 528 nm was intensified with time (Figure 3.4b). More over, 1.46 ns was needed to get the emission similar to steady state. These observations reveal slower or less efficient excitation energy migration in **BC-OPV2** when compared to that of **MC-OPV2** in the gel state. This difference in the efficiency of excitation energy migration could be due to the difference in the packing of chromophores in the self-assembled state.

Wavelength dependence of the emission decay of **MC-OPV2** and **BC-OPV2** in the gel state in decane is shown in Figure 3.5, which provides further evidence for energy migration. The lifetime profile collected at 430 nm is biexponential and decays faster when compared to the lifetime profile collected at higher wavelengths (lower energy), which has slow decay with multiexponential

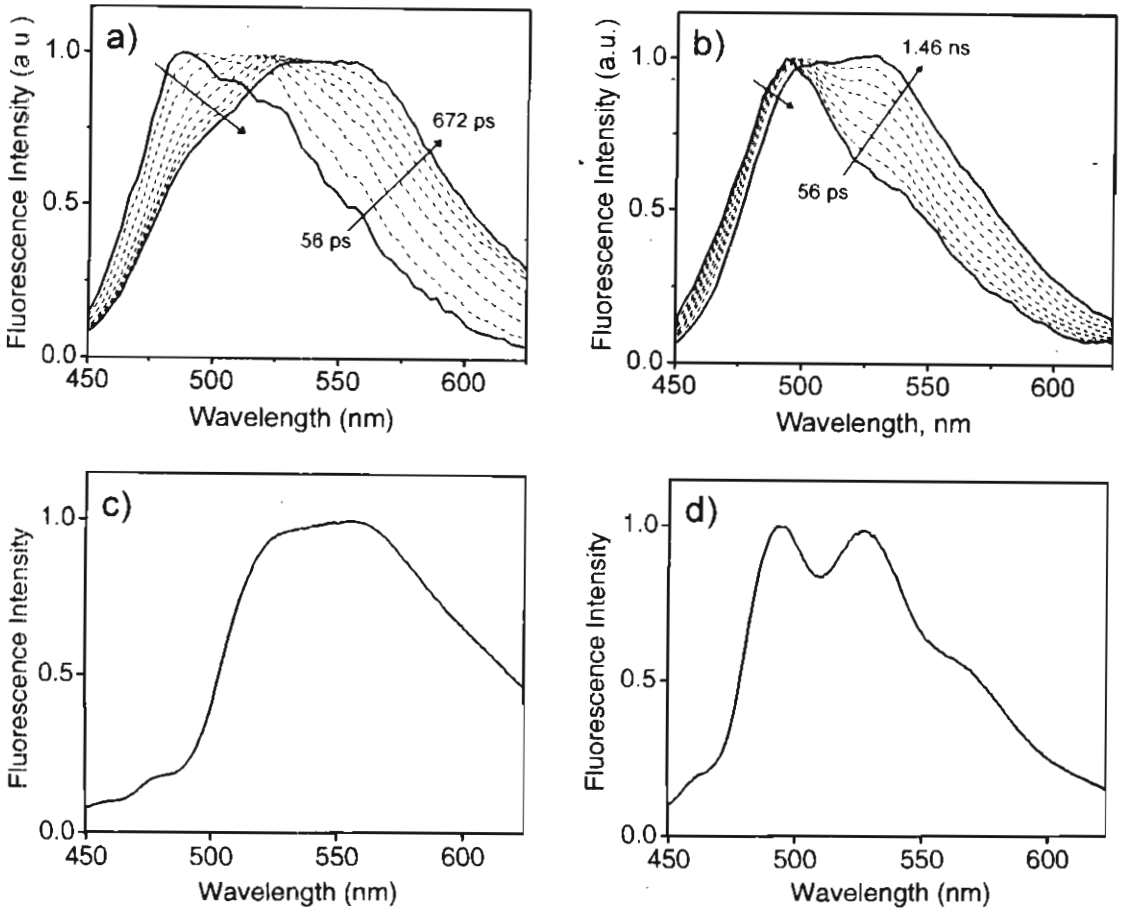


**Figure 3.4.** Time-resolved emission spectra of the decane gels of a) **MC-OPV2** and b) **BC-OPV2** at room temperature. ($c$ = 3 x $10^{-4}$ M, $l$ = 1 mm, $\lambda_{ex}$ = 375 nm). The corresponding steady state emission spectrum of c) **MC-OPV2** and d) **BC-OPV2** under similar conditions for comparison.

fit. This effect is more predominant in the case of **MC-OPV2**. It is known that the radiative lifetime of the aggregates with smaller HOMO-LUMO energy gap (higher order) is higher than that of the aggregates with the larger HOMO-LUMO energy gap (lower order).[24] The lifetime profiles of both derivatives showed a growth component at the initial time scales when collected at higher wavelengths (Figure 3.5c,d). Such delayed growth in the initial time scales indicate fast

migration of exctions from higher to lower energy sites and the population of the excited states of the latter.[25] The growth component of **MC-OPV2** and **BC-OPV2** corresponds to 332 ps and 764 ps, respectively indicating that energy migration is slow in the latter when compared to that of the former.

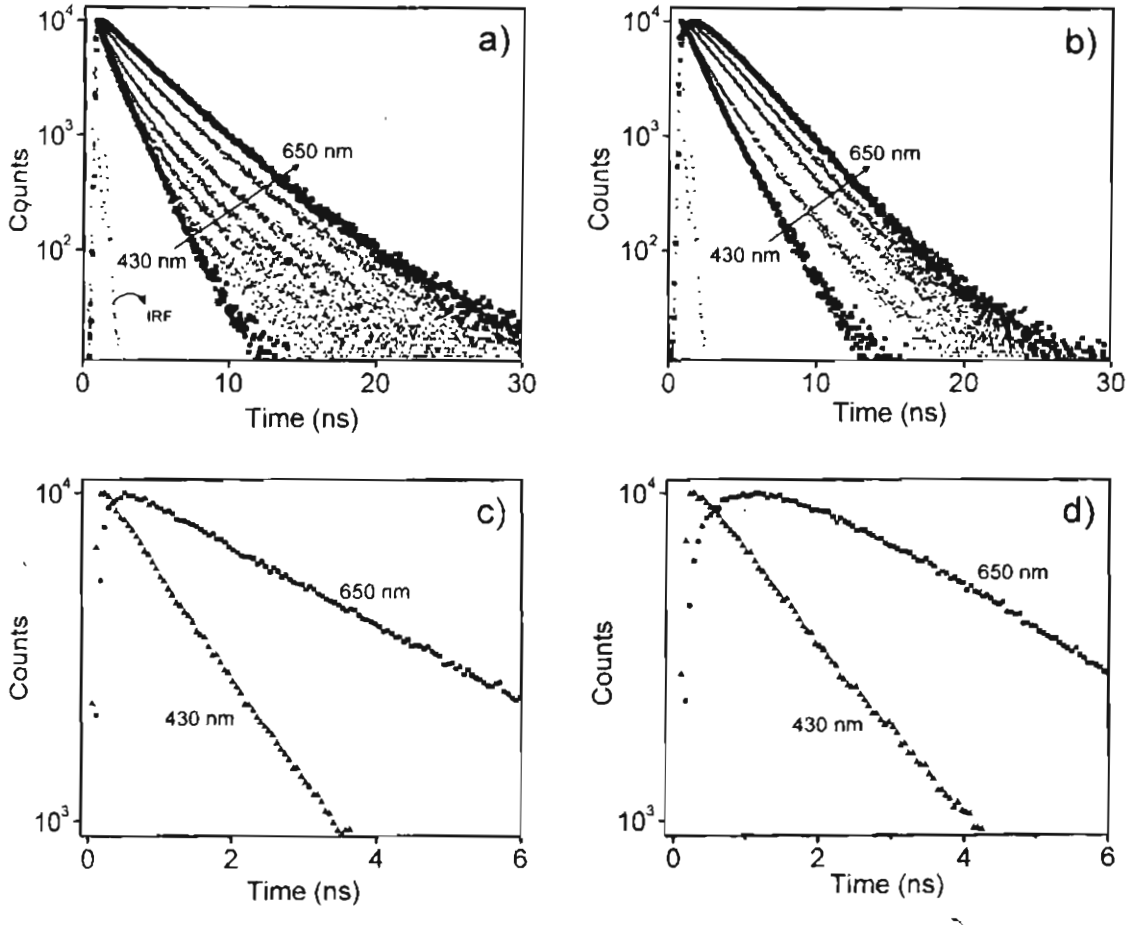


**Figure 3.5.** Wavelength dependent lifetime decay profiles of a) **MC-OPV2** and b) **BC-OPV2** in decane in the gel state at room temperature. ($c$ = 3 x $10^{-4}$ M, $l$ = 1 mm, $\lambda_{ex}$ = 375 nm). Zoomed initial time scale of the decay profile of c) **MC-OPV2** and d) **BC-OPV2** monitored at two different wavelengths.

Another evidence for the energy migration was obtained by fluorescence depolarization measurements. This is based on the principle that the emission from

molecules, which are excited by polarized light, is partially polarized.[26] Emission depolarization is caused by dipole orientation displacements of chromophores. A well-known factor leading to emission depolarization is the rotational diffusion of chromophores in solution.[27] Energy migration between like chromophores can also cause emission depolarization.[28] In this case, the polarized emission of the chromophore has two contributions: one from the original molecule which is excited by the polarized light and the other from the molecule to which the energy has been transferred. In rigid disordered systems, fluorescence depolarization via energy migration is caused by the different dipole orientations of the "donor" and "acceptor" chromophores. The more steps over which the energy is transferred, the greater the degree of depolarization.

Time-resolved fluorescence anisotropy measurement is a useful technique to measure the time-dependent emission polarization loss. Unlike fluorescence intensity decay, anisotropy decay is very sensitive to the change of the dipole orientation.[29] Fluorescence anisotropy is defined by eq 3.1 in terms of the ratio of the fluorescence intensity of the emitted light which is polarized either parallel ($I_{||}$) or perpendicular ($I_{\perp}$) to that of the excitation source.[12a]

$$r(t) = \frac{I_{||}(t) - GI_{\perp}(t)}{I_{||}(t) + 2GI_{\perp}(t)} \qquad 3.1$$

where G is an experimentally determined correction factor for the instrumental anisotropy, and $r(t)$ is a dimensionless quantity which is independent of the total

intensity emitted by the sample. For disordered chromophore dipole orientations, the anisotropy has a maximum value of 0.4 when the chromophores have collinear absorption and emission dipoles and when no rotational depolarization and/or energy migration take place. If the chromophore dipoles have a preferred orientation, a higher anisotropy value (> 0.4) is expected.[12a]

The fluorescence anisotropy decay of **MC-OPV2** gel in decane is shown in Figure 3.6a. The initial anisotropy value ($r_0$) is 0.29, which rapidly lose the anisotropy memory and reaches the plateau region ($r_\infty$) at 0.04 with a decay time $\tau_r$ = 169 ps. This extremely fast depolarization is an indication of the fast interchromophore singlet exciton migration leading to energy transfer to the acceptor in the gel state.[25] Under similar conditions, **BC-OPV2** showed slow depolarization (Figure 3.6b) indicating less efficient energy migration when compared to the former. In this case, the initial anisotropy ($r_0$) is 0.25 and the final

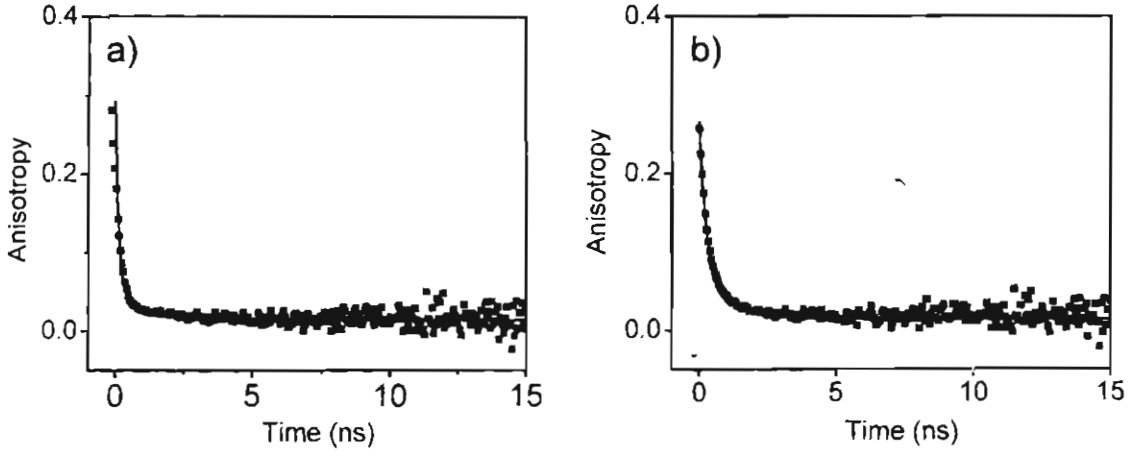


**Figure 3.6.** Anisotropy decay profiles of a) **MC-OPV2** and b) **BC-OPV2** gels in decane on excitation at 375 nm. ($c$ = 3 x $10^{-4}$ M, $l$ = 1 mm).

anisotropy value is 0.02 with a decay time of 880 ps. The mono- and bischolesterol derivatives with C16 alkyl side chains (**MC-OPV3** and **BC-OPV3**) exhibited similar properties as that of the corresponding C12 derivatives (**MC-OPV2** and **BC-OPV2**) in the gel state in decane.

### 3.3.3. The Selection Criteria of Donor-Acceptor Systems

The mono- and bischolesterol OPV derivatives (**MC-OPV2-3** and **BC-OPV2-3**) were selected as the donors and an oligomer phenylenevinylene-*co*-pyrrolylenevinylene (**PYPV**) with an average molecular weight (Mn) of ~ 4358 g/mol having a polydispersity index of 1.12 as the acceptor. This donor-acceptor system is selected in view of the formation of stable coassembly between them and due to the matching absorption and emission properties.

The emission of the self-assembled donors is significantly shifted towards the long wavelength side as a result of the excitation energy migration. Because of this red-shift, the donor emission in the gel state showed good spectral overlap with the acceptor (Figure 3.7). This is an important criterion for the selection of the donor-acceptor systems for energy transfer. The overlap integral expresses the degree of spectral overlap between the donor emission and the acceptor absorption. This overlap indicates that some of the energy levels of the donor match with that of the acceptor, i.e., the quantum mechanical coupling between donor and acceptor is possible and hence energy transfer will also be possible.[12a]

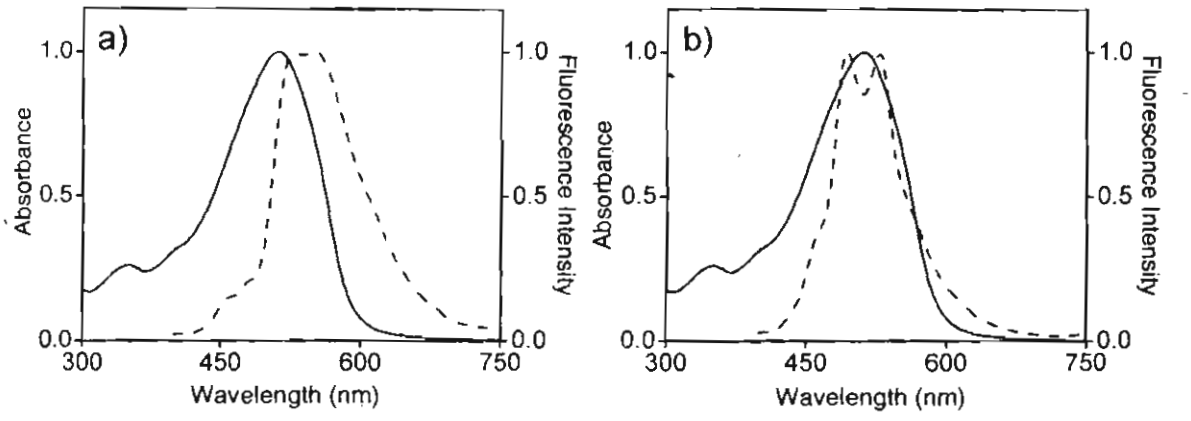


**Figure 3.7.** Spectral overlap between the absorption (——) of the acceptor (**PYPV**) and the emission (– –) of a) **MC-OPV2** and (b) **BC-OPV2** in decane at room temperature. ($c$ = 3 x $10^{-4}$ M, $l$ = 1 mm, $\lambda_{ex}$ = 380 nm).

The spectral overlap integral $J(\lambda)$ of the donor emission and the acceptor absorption was calculated from the above graph using eq 3.2.[12a]

$$J(\lambda) = \frac{\int_0^\infty F_D(\lambda)\varepsilon_A(\lambda)\lambda^4\, d\lambda}{\int_0^\infty F_D(\lambda)\, d\lambda} \qquad 3.2$$

where $F_D(\lambda)$ is the fluorescence intensity of the donor in the wavelength range $\lambda$ to $\lambda+\Delta\lambda$, $\varepsilon_A(\lambda)$ is the extinction coefficient of the acceptor at $\lambda$. The spectral overlap integral, $J(\lambda)$ for the donor-acceptor system **MC-OPV2/PYPV** and **BC-OPV2/PYPV** was found to be 3.61 × $10^{15}$ $M^{-1}cm^{-1}nm^4$ and 4.64 × $10^{15}$ $M^{-1}$ $cm^{-1}nm^4$ respectively.

The fluorescence quantum yield of **MC-OPV2** and **BC-OPV2** was found to be 0.32 and 0.55 respectively in the gel state in decane at room temperature.

The high quantum yield of the donor molecules makes them suitable for transferring their excitation energy to the acceptor molecules with high efficiency.

Another important criterion for an ideal energy transfer system is the less possibility for direct excitation of the acceptor on excitation of the donor in a donor-acceptor coassembly. In the present work, the energy transfer studies were carried out by exciting the donor at 375 or 380 nm. It was found that at these wavelengths, the acceptor has negligible absorption (Figure 3.8). Moreover, the maximum amount of acceptor used for energy transfer experiments was $\leq 2$ mol%. At this concentration, the relative absorption of the acceptor is minimum when compared to that of the donor. Because of these two reasons, the direct excitation of the acceptor will be negligible in this donor-acceptor system.

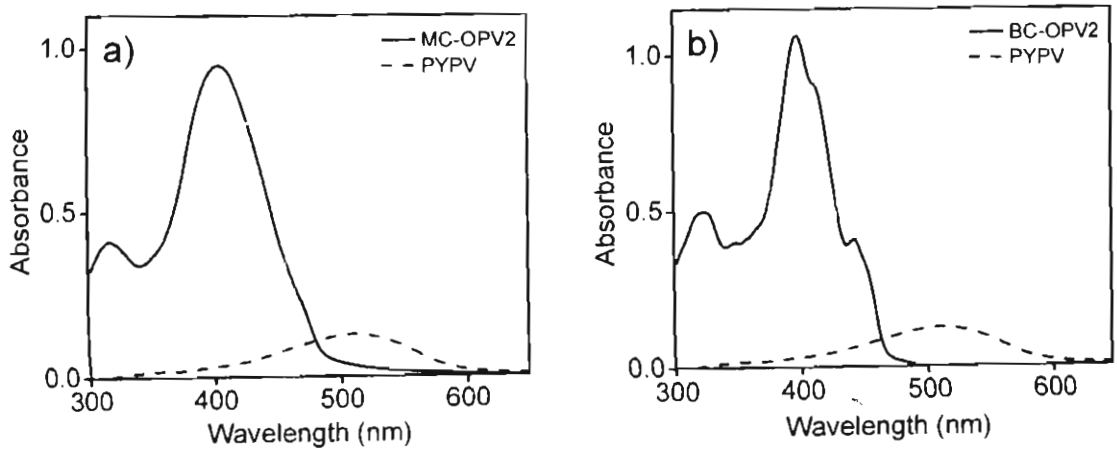


**Figure 3.8.** Comparison of the individual absorption spectra of the donor and the acceptor. a) **MC-OPV2** (—) and **PYPV** (– –). b) **BC-OPV2** (—) and **PYPV** (– –) in decane at room temperature (Conc. of donor = 3 x $10^{-4}$ M, Conc. of acceptor = 6 x $10^{-6}$ M, $l$ = 1 mm)

The coassembly between the donor and acceptor was studied using UV-vis absorption and circular dichroism spectroscopy. No absorption spectral changes were observed for the donor on addition of 2 mol% of the acceptor (Figure 3.9) indicating the absence of ground state interactions between the donor and the acceptor molecules. However, after the addition of the acceptor to the donor gel scaffold, absorption maximum of the former was red-shifted (23 nm in **MC-OPV2** and 17 nm in **BC-OPV2**) when compared to that of the acceptor alone. This could be due to the planarization of the **PYPV** in the constrained gel medium leading to an increase in the effective conjugation length. This red-shift in the absorption of the acceptor further reduces the possibility of its direct excitation.

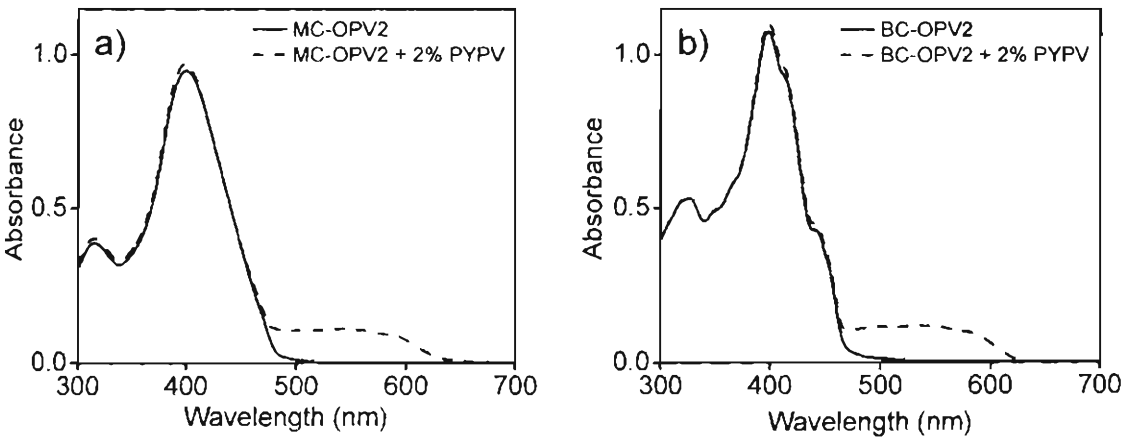


**Figure 3.9.** Absorption spectrum of a) **MC-OPV2** and b) **BC-OPV2** in the absence (——) and in the presence (– –) of 2 mol% of **PYPV**

Plots of the fraction of aggregated species (α) versus the temperature obtained from the temperature dependent UV-vis spectra showed a considerable decrease in the aggregate stability for the donor self-assembly in presence of the

acceptor. It is observed that the stability of the self-assembled species is decreased by 5 °C for **MC-OPV2** and 4 °C for **BC-OPV2** in presence of the acceptor (Figure 3.10). This observation is an indication of the coassembly of **PYPV** with the donor OPVs.

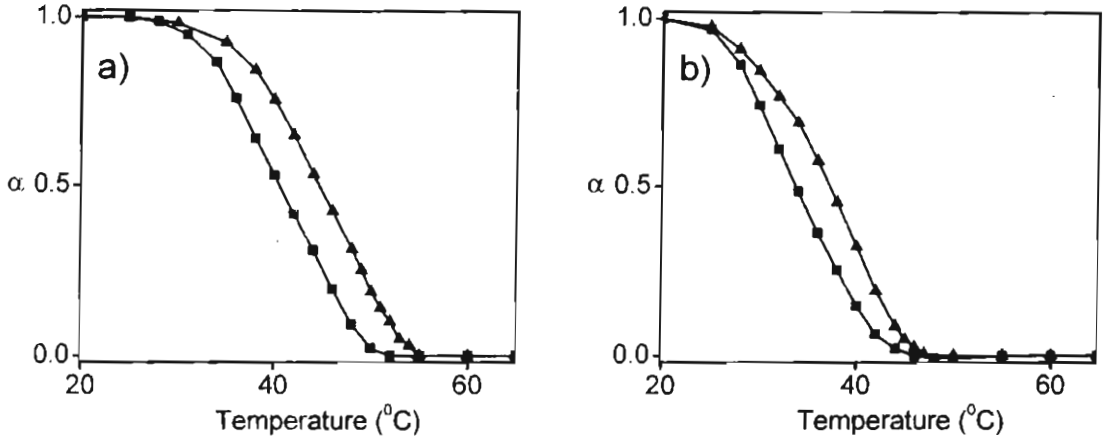


**Figure 3.10.** Plots of the fraction aggregate (α) versus temperature of a) **MC-OPV2** and b) **BC-OPV2** in the absence (▲) and in the presence (■) of 2 mol% of **PYPV** in decane.

The donor molecules show significant CD intensities during the self-assembly (see Chapter 2). CD spectra of the donors were monitored in presence of the acceptor to get an insight into the coassembly processes. Upon addition of the acceptor (0-2 mol%), the CD intensity of both donor molecules (**MC-OPV2** and **BC-OPV2**) gradually decreases indicating the encapsulation of the acceptor with the donor self-assembly (Figure 3.11).

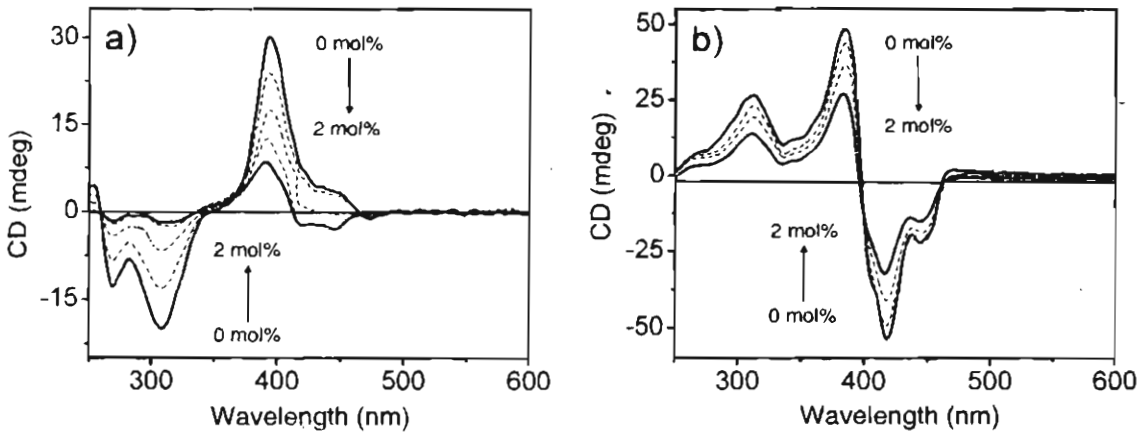


**Figure 3.11.** Circular dichroism spectral changes of a) **MC-OPV2** and b) **BC-OPV2** on addition of increasing amounts of the acceptor (0-2 mol%) in decane at room temperature. (conc. of donor = 3 x $10^{-4}$ M, *l* = 1 mm).

### 3.3.4. Energy Transfer Studies

The energy transfer studies were carried out in the gel state at room temperature using a quartz cuvette with 1 mm path length. Encapsulation of the acceptor within the self-assembly of the donor is achieved by dissolving small quantities of the former (0-2 mol%) in the decane solution of the latter keeping the donor concentration at $3 \times 10^{-4}$ M. The solution was then heated to 80 °C and kept under room temperature to form a coassembled self-supporting soft organogel. Excitation of **MC-OPV2** at 380 nm in the absence of **PYPV** gave a broad emission between 500 – 700 nm with a maximum around 560 nm. Addition of small amounts of **PYPV** to the donor gel followed by heating and cooling resulted in the quenching of the donor emission with a concomitant emission from the acceptor at 613 nm (Figure 3.12a). The quenching was found to be maximum

(90%) in presence of 2 mol% of the acceptor. No spectral changes were observed on addition of more than 2 mol% of the acceptor.

Upon excitation with 380 nm light in the absence of **PYPV**, the emission spectrum of **BC-OPV2** in the gel state exhibited two maxima at 492 nm and 528 nm with shoulders on either side (Figure 3.12b). The shoulder at 464 nm corresponds to the residual monomer emission of the donor. Addition of small amounts of the acceptor in decane, resulted in the quenching of the emission at 492 nm and 528 nm with the concomitant formation of a new peak at 607 nm which corresponds to the emission of the acceptor. Interestingly, only partial quenching (63%) was observed for the donor fluorescence in presence of 2 mol% of the acceptor. In this case also no spectral changes were observed on addition of more than 2 mol% of the acceptor.

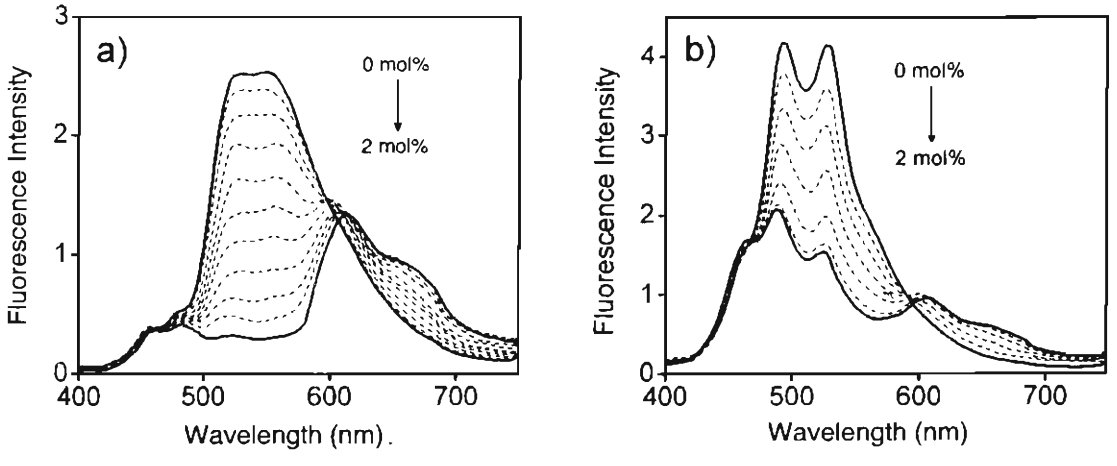


**Figure 3.12.** Fluorescence emission of the decane gels of a) **MC-OPV2** and b) **BC-OPV2** on addition of increasing amounts of **PYPV** (0-2 mol %) at room temperature. (Conc. of donor = 3 x $10^{-4}$ M, $l$ = 1 mm, $\lambda_{ex}$ = 380 nm).

Efficient energy transfer in the **MC-OPV2 – PYPV** system resulted in a bright red emission (Figure 3.13a). On the other hand, in the case of **BC-OPV2**, due to the partial quenching, a broad emission spectrum is obtained in the range of 400-750 nm which covers the red, green and blue regions leading to a white light emission with CIE co-ordinates of (0.28,0.34). Intense white light emission was observed on varying the donor ($3.2 \times 10^{-4}$ M) and acceptor (2.1 mol%) concentrations (Figure 3.13b). The white-light emission is a combination of the blue emission of the monomer species, green emission from the aggregated state and the red emission from the acceptor since all these species are simultaneously present. The chromaticity diagram (Figure 3.14) revealed that the CIE coordinates at this particular composition is (0.31,0.35) which are ideal for white light emission according to the 1931 CIE diagram.[30] Even though several strategies have been worked out for the realization of white light emission including polymer based systems,[31] transition metal complexes,[32] low molecular weight organic molecules[33] etc., this is the first report of white light emission using the concept of molecular self-assembly.

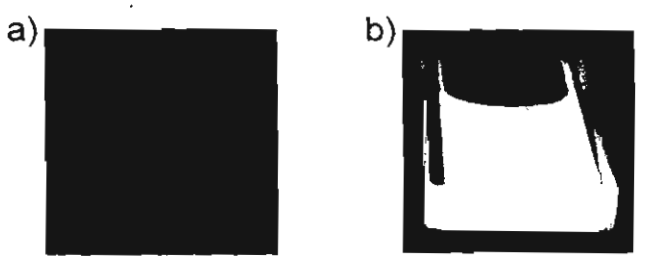


**Figure 3.13.** Photographs of the decane gels of a) **MC-OPV2** ($c = 3 \times 10^{-4}$ M) and b) **BC-OPV2** ($3.2 \times 10^{-4}$ M) in presence of **PYPV** on excitation with 365 nm light.

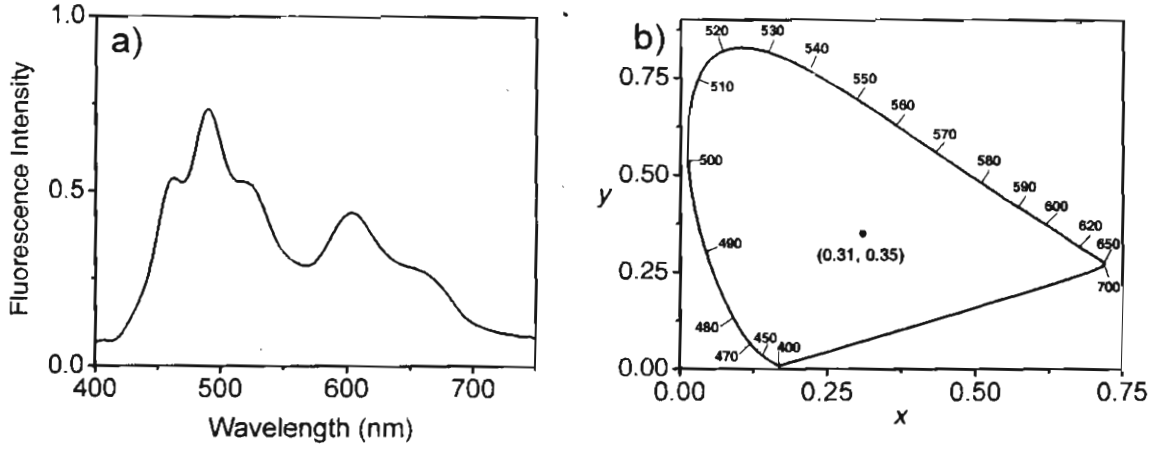


**Figure 3.14.** a) Fluorescence emission spectrum of **BC-OPV2** ($3.2 \times 10^{-4}$ M) in presence of 2.1 mol% of **PYPV** ($\lambda_{ex}$ = 380 nm, $l$ = 1 mm). b) CIE coordinate diagram of the resulting white light emission ($x$ = 0.31, $y$ = 0.35).

In order to confirm that the enhanced emission of **PYPV** in the presence of donor gels is due to energy transfer and not due to the restricted environment of the gel medium, we have carried out the following experiments. When the encapsulated **PYPV** is directly excited at 530 nm in the donor gel, the resultant emission spectrum ($\lambda_{em}$ = 613 nm for **MC-OPV2** and 607 for **BC-OPV2**) resembled that of the 380 nm excitation with less intensity (Figure 3.15). On the other hand, when **PYPV** alone in decane is excited at 530 nm, the resultant emission spectrum was blue-shifted ($\lambda_{em}$ = 587 nm) with almost same intensity as that of the spectrum obtained in the gel state upon 530 nm excitation (Figure 3b). These observations strongly support the fact that the enhanced emission of the encapsulated **PYPV** in the gel is due to energy transfer.[4b,6a] The red-shift (26 nm in **MC-OPV2** and 20 nm in **BC-OPV2**) in the emission of the encapsulated **PYPV**

when compared to that in the absence of donor gels in decane ($\lambda_{ex}$ = 530 nm), could be due to the planarization of the former in the constrained gel medium leading to an increase in the effective conjugation length which is also obvious from the shift in the absorption maximum (Figure 3.9).

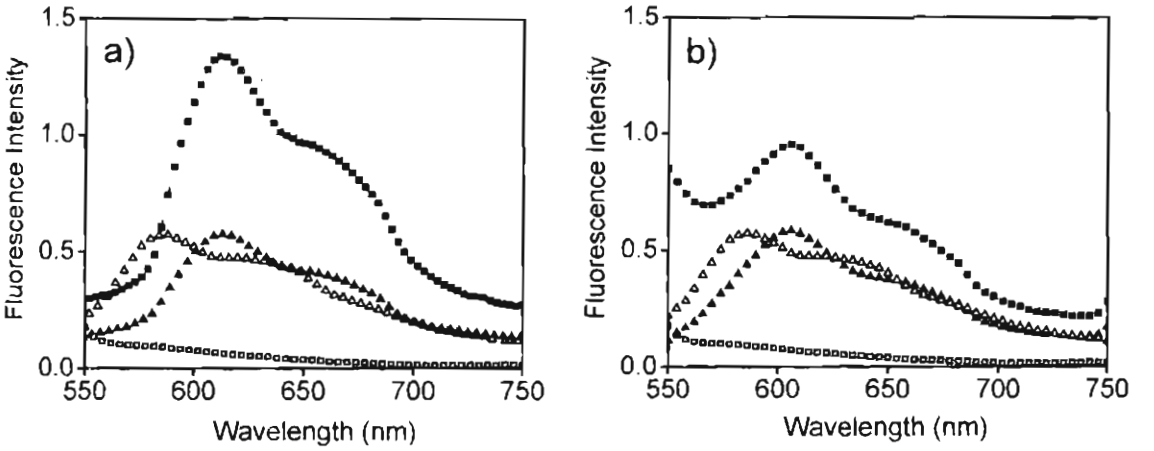


**Figure 3.15.** a) Comparison of the emission intensity of **PYPV** (2 mol%) in **MC-OPV2**-decane gel when excited at 380 nm (■) and at 530 nm (▲), **PYPV** in decane upon excitation at 530 nm (△) and **MC-OPV2**-decane gel upon excitation at 530 nm (□). b) Comparison of the emission intensity of **PYPV** (2 mol%) in **BC-OPV2**-decane gel when excited at 380 nm (■) and at 530 nm (▲), **PYPV** in decane upon excitation at 530 nm (△) and **BC-OPV2**-decane gel upon excitation at 530 nm (□).

Fluorescence spectra of **PYPV** excited at 380 nm in the presence and in the absence of the donors is also compared under identical conditions *(Figure 3.16).* Direct excitation of the acceptor in the absence of the donor at 380 nm shows extremely weak fluorescence. This weak fluorescence ruled out the possibility of the contribution of acceptor emission due to direct excitation in the emission intensity obtained on energy transfer.

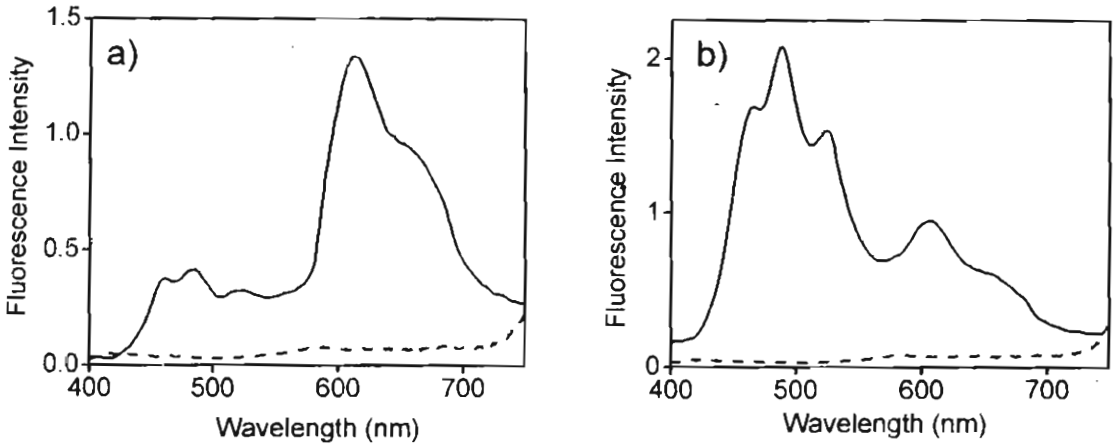


**Figure 3.16.** Comparison of emission intensity of **PYPV** in the presence (——) and in the absence (– –) of a) **MC-OPV2** and b) **BC-OPV2** in decane at room temperature. (conc. of donors = 3 × $10^{-4}$ M, conc. of acceptor = 6 × $10^{-6}$ M, $\lambda_{ex}$ = 380 nm)

Figure 3.17 shows the relative fluorescence intensities of the donor and the acceptor when plotted against their molar ratio. The relative fluorescence intensity value is a measure of the energy transfer efficiency,[34] and the values obtained for **MC-OPV2** is greater than that of the **BC-OPV2**. For **BC-OPV2**, the emission ratio exhibited a slow increase, whereas, in the case of **MC-OPV2**, the emission ratio showed remarkable increment with increase in the molar ratio. When the ratio reached to 2 × $10^{-2}$, the emission from **MC-OPV2** showed maximum quenching. The apparent efficiency of energy transfer estimated from the donor fluorescence quenching profile was 90% for **MC-OPV2** and 63% for **BC-OPV2** in the gel state at room temperature. These results indicate that the energy transfer process is highly efficient in **MC-OPV2**, whereas it is less efficient in **BC-OPV2**.

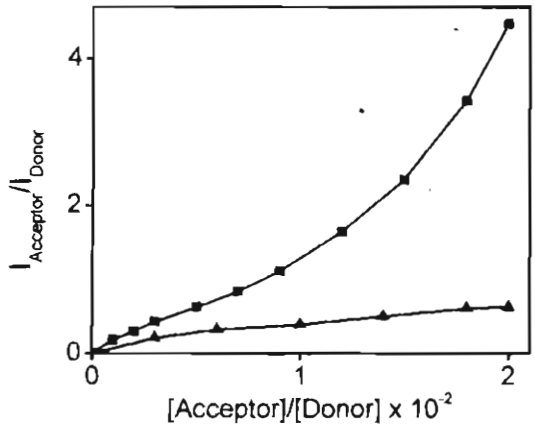


**Figure 3.17.** Plots of the relative fluorescence intensities against the molar ratio of **PYPV** and **MC-OPV2** (■)/**BC-OPV2** (▲) in decane.

### 3.3.5. Single Photon Counting Studies

Single photon counting has provided evidence for the nonradiative energy transfer processes between the donor and the acceptor molecules. Fluorescence lifetime decay profiles ($\lambda_{ex}$ = 375 nm) monitored at the aggregate emission maximum of **MC-OPV2** (Figure 3.18a) and **BC-OPV2** (Figure 3.18b) showed shortening of the decay profile on addition of increasing amounts (0-2 mol%) of **PYPV**. The accelerated decay of the donor fluorescence in presence of the acceptor rules out any trivial energy transfer pathway. Even though both systems showed a similar trend on addition of the acceptor, shortening of the decay profile is much more predominant in the case of **MC-OPV2** than that of **BC-OPV2**. This observation again proves that energy transfer efficiency is high for **MC-OPV2** than that of **BC-OPV2**.

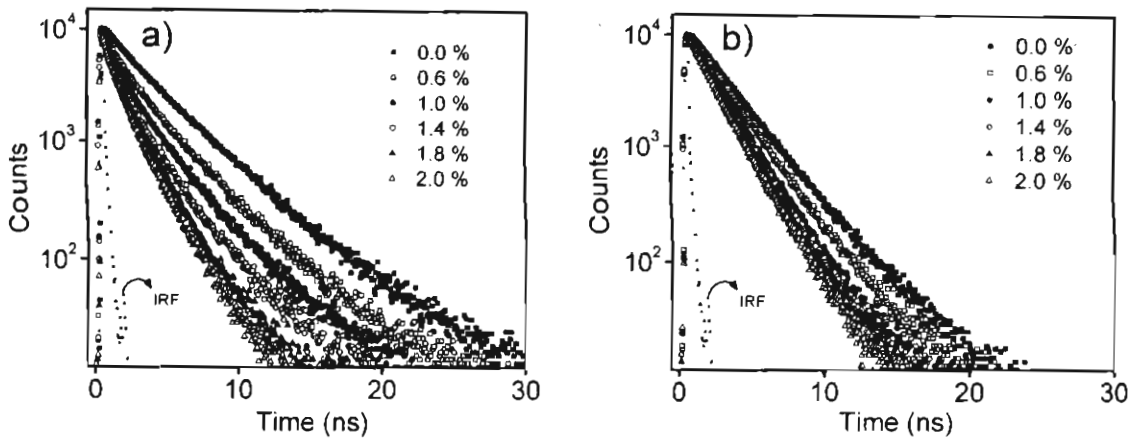


**Figure 3.18.** Lifetime decay profiles of a) **MC-OPV2** (monitored at 560 nm) and b) **BC-OPV2** (monitored at 528 nm) on addition of increasing amounts of **PYPV** in decane at room temperature. ($c$ = 3 x $10^{-4}$ M, $l$ = 1 mm, $\lambda_{ex}$ = 375 nm).

The fluorescence lifetime decay profiles of **MC-OPV2** gel ($\lambda_{ex}$ = 375 nm) exhibited biexponential decay with lifetimes 2.47 ns (54.4%) and 4.82 ns (45.6%) in the absence of the acceptor when monitored at the aggregate emission maximum (560 nm). Addition of increasing amounts of the acceptor increases the rate of the fluorescence decay of the donor. In presence of 2 mol% of the acceptor, donor exhibited fast biexponential decay with time constants 0.58 ns (73.3%) and 1.8 ns (26.7%). Similarly, the fluorescence lifetime decay profile of **BC-OPV2** gel ($\lambda_{ex}$ = 375 nm) in the absence of the acceptor monitored at the aggregate emission maximum (528 nm) exhibited biexponential decay with lifetimes 2.38 ns (79.6%) and 3.79 ns (20.4%). An acceleration of the fluorescence decay was observed with increase in the acceptor concentration. In the presence of 2 mol% of acceptor, **BC-**

**OPV2** exhibited fast biexponential decay with time constants of 1.85 ns and 0.57 ns with relative amplitudes of 93% and 7% respectively.

Further evidence for excitation energy transfer was obtained from the temporal rise in the decay profile of **PYPV** when excited at 375 nm after encapsulation within the donor gel (Figure 3.19). The growth observed for the coassembly at short time scales is associated with the initial population buildup of the excited states of **PYPV** upon energy transfer from the donor singlet which is followed by the decay.

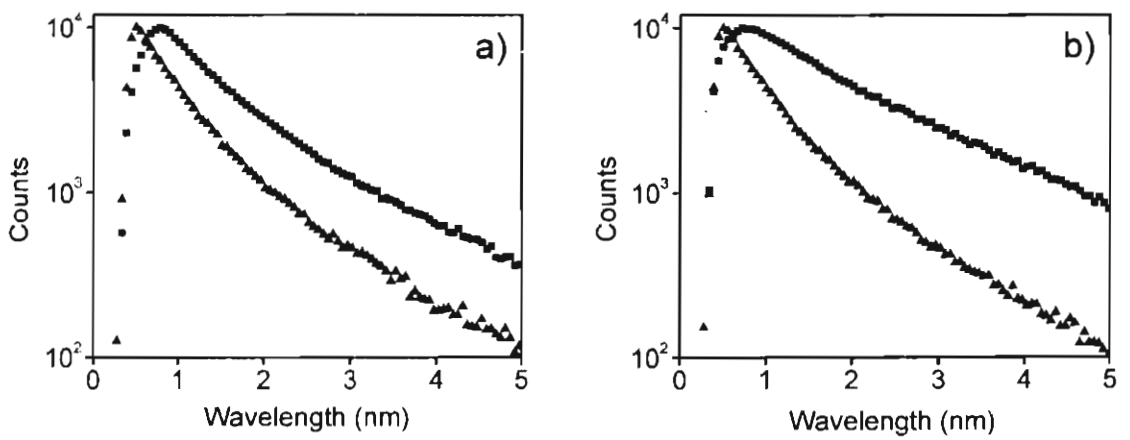


**Figure 3.19.** Fluorescence decay profiles of **PYPV** ($6 \times 10^{-6}$ M) alone (▲) and in the decane gel of a) **MC-OPV2** (■) and b) **BC-OPV2** (■) monitored at 660 nm. (conc. of donors = $3 \times 10^{-4}$ M, $\lambda_{ex}$ = 375 nm)

An estimate of the rate of energy transfer ($k_{ET}$) could be possible from the steady state fluorescence quenching studies and the excited state lifetimes of the donors ($\tau_D$) according to the eq 3.3, assuming that the observed quenching is due to energy transfer.[12a,10f,11g]

$$k_{ET} = \frac{Q_{max} - 1}{\tau_D} \qquad 3.3$$

$Q_{max} = I_D/I_{DA}$, is the maximum quenching observed in the fluorescence titration studies, $I_D$ and $I_{DA}$ are emission intensities of donor in the absence and in the presence of acceptor respectively. Since the lifetime of donors in the gel state shows biexponential decay, the average lifetime was calculated as per eq 3.4.[12a]

$$<\tau> = \frac{[\alpha_1 \tau_1^2 + \alpha_2 \tau_2^2]}{[\alpha_1 \tau_1 + \alpha_2 \tau_2]} \qquad 3.4$$

$\tau$ is the lifetime and $\alpha$ is the corresponding amplitude of the decay components. The average lifetime of **MC-OPV2** in decane in the gel state was found to be 3.93 ns and the rate of energy transfer ($k_{ET}$) was found to be 1.97 $ns^{-1}$ in the presence of 2 mol% of the acceptor. **BC-OPV2** also exhibited biexponential decay with average lifetime 2.81 ns and the value of $k_{ET}$ obtained was 0.62 $ns^{-1}$.

In order to study the importance of the self-organization of donor-acceptor chromophores on fluorescence resonance energy transfer, we extended the energy transfer studies of **MC-OPV2** and **BC-OPV2** in chloroform, in which both the derivatives exist as the monomeric species. Steady state emission studies showed that even though significant spectral overlap is observed between the emission of the cholesterol-OPV donors with the absorption of acceptor **PYPV**, energy transfer quenching of the donor emission is negligible. For example, the spectral

overlap of the **MC-OPV2** emission and the **PYPV** absorption (Figure 3.20a) and the fluorescence spectra of **MC-OPV2** in the presence and in the absence of **PYPV** (Figure 3.20b) are shown below. The emission of **MC-OPV2** remained nearly the same in the presence of **PYPV** which indicates practically no energy transfer between the two molecules in chloroform.

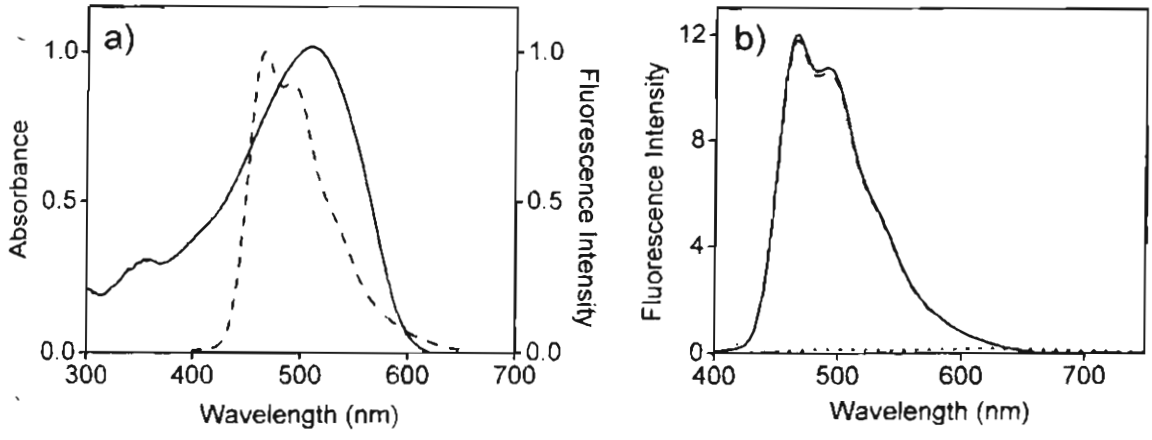


**Figure 3.20.** a) Spectral overlap of the emission of **MC-OPV2** (– –) and the absorption of **PYPV** (——) in chloroform. b) Fluorescence spectrum of **MC-OPV2** in the absence (——) and in the presence (– –) of **PYPV** (2 mol%) in chloroform. Fluorescence of **PYPV** alone in chloroform (····) is also shown for a comparison (conc. of donor = $3 \times 10^{-4}$ M, $l$ = 1 cm, $\lambda_{ex}$ = 380 nm).

In order to confirm the above observation, we have carried out detailed lifetime studies of the donors in the absence and in the presence of the acceptor in chloroform. Lifetime studies showed no shortening of the decay profiles of the donor fluorescence even in the presence of maximum loading of the acceptor (2 mol%) as shown in Figure 3.21. These observations indicate that mono- and bischolesterol OPV donors fail to bring about the energy transfer when they exist

as monomeric species. Moreover, these results substantiate the importance of the gelation of the donor-acceptor chromophores for efficient energy transfer process.

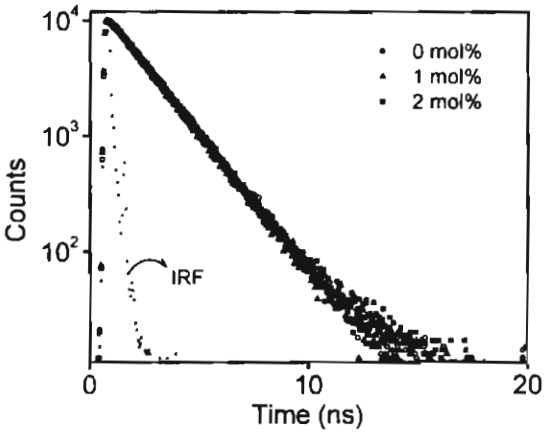


**Figure 3.21.** Lifetime decay profile of **MC-OPV2** (monitored at 468 nm) on addition of increasing amounts of **PYPV** in chloroform at room temperature. ($c$ = 3 x $10^{-4}$ M, $l$ = 1 mm, $\lambda_{ex}$ = 375 nm).

## 3.3.6. Thermoreversible Control of Energy Transfer

Since the donor-acceptor coassembly is a thermoreversible process, temperature plays a crucial role in the optical as well as the energy transfer properties. This is clear from the temperature dependent emission changes of **MC-OPV2** and **BC-OPV2** in presence of the acceptor (Figure 3.22). Energy transfer efficiency is high at low temperature and decreases on increasing the temperature. When the temperature reached above 55 °C, emission from the acceptor was completely disappeared and emission from the donor (monomer) was intensified. This phenomenon is the result of the thermoreversible breaking and making of the self-assembly which in turn thermally modulate the spectral overlap of the donor and the acceptor thereby controlling the energy transfer process.

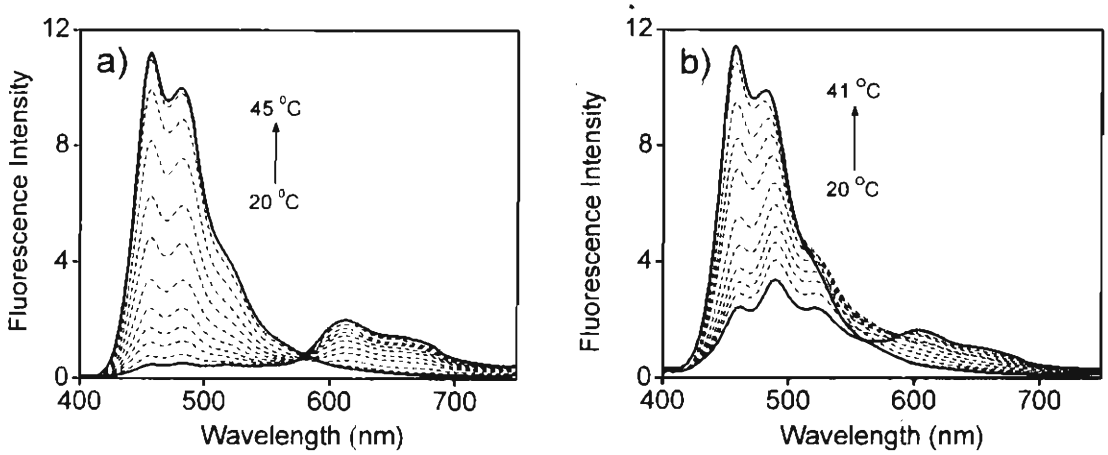


**Figure 3.22**. Temperature dependent fluorescence emission of a) **MC-OPV2** and (b) **BC-OPV2** in decane containing 2 mol % of **PYPV**. (conc. of donor = 3 × $10^{-4}$ M, *l* = 1 mm, $\lambda_{ex}$ = 380 nm)

## 3.4. Conclusions

The effect of chromophore packing on the efficiency of energy transfer in multichromophoric assemblies is established using mono- and bischolesterol OPV organogelators as the donors and a π-conjugated oligomer, phenylenevinylene-*co*-pyrrolylenevinylene, as the acceptor. Because of the difference in the chromophore packing, energy migration efficiency was different in these two donor assemblies. Fast exciton migration was observed in the coiled helical assembly of the monocholesterol derivatives which results in efficient energy transfer to the acceptor to yield bright red emission in the gel state. Energy migration was found to be slow in the twisted helical assembly of the bischolesterol derivatives which result in less efficient energy transfer to the acceptor. Consequently, an intense white emission with CIE coordinates of (0.31,0.35) in the gel state at room temperature was obtained. Thus, the difference

in the molecular arrangements achieved through a difference in the substitution pattern of gel forming OPVs has been utilized to the design of red and white light emitting organogels.

## 3.5. Experimental Section

### 3.5.1. Synthesis and Characterization

The details of the melting point, FT-IR, $^{1}H$ NMR and $^{13}C$ NMR and MALD-TOF instruments are described in the experimental section (section 2.5.1) of Chapter 2. Gel Permeation Chromatography (GPC) was carried out on a Shimadzu LC-8A GPC system equipped with a refractive index detector. Calibrations were done with standard polystyrene samples. Tetrahydrofuran (THF) was used as the eluent at a flow rate of 1 mL $min^{-1}$ at 25 °C.

**Preparation of PYPV:** A suspension of NaH (3.36 mmol) in THF (5 mL) was added carefully to a solution of the bisphosphonate **10b** (0.56 mmol) and the bisformyl derivative **12** (0.56 mmol) in THF (25 mL). After refluxing for 26 h the highly fluorescent reaction mixture was cooled and THF was removed under reduced pressure. The resultant residue was then extracted with dichloromethane and washed several times with saturated brine and water. The organic layer was dried over anhydrous $Na_2SO_4$ and the solvent was removed. The product thus obtained was purified by repeated precipitation by adding methanol to a dichloromethane solution which gave the pure oligomer **PYPV** as dark red solid.

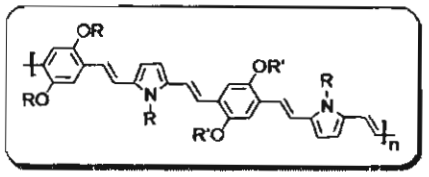

Yield: 53%. $^1$H NMR (300 MHz, $CDCl_3$, TMS): δ 0.87 (br, $-CH_3$), 1.24-1.88 (m, $-CH_2-$), 4.04 (br, $-NCH_2-$), 4.47 (br, $-OCH_2-$), 6.61 (br, pyrrole-*H*), 6.93-7.40 (m, phenyl-*H* and vinyl-*H*), 9.46 (s, trace, terminal –C*H*O) ppm; FT-IR (KBr): $\nu_{max}$ 863, 964, 1036, 1142, 1208, 1401, 1500, 1653, 2853, 2925 $cm^{-1}$. $M_n$ = 4358, $M_w / M_n$ = 1.12 by GPC.

### 3.5.2. General Procedure for Energy Transfer Studies

Energy transfer studies were carried out by mixing appropriate volumes of acceptor from a stock solution to the decane solution of the donor. The concentration of the donor was maintained at $3 \times 10^{-4}$ M while the amount of the acceptor varied from 0-2 mol %. The mixture was then heated to 80 °C and slowly cooled to room temperature to form the gel. The energy transfer was monitored by recording the emission of OPVs in the absence and in the presence of the acceptor after excitation of OPVs at 380 nm.

### 3.5.3. Description of Instrumental Techniques

The details of UV-vis absorption spectrophotometer, spectrofluorimeter and time-correlated picosecond single photon counting-(TCSPC) system are described in the section 2.5.2 of Chapter 2. Fluorescence lifetime, time resolved anisotropy and time resolved emission spectra were measured using IBH (FluoroCube)

TCSPC system. Solutions were excited with a pulsed diode laser (<100 ps pulse duration) at a wavelength of 375 nm (NanoLED-11) with a repetition rate of 1 MHz. For the TRES measurements, the decay curves were measured at multiple emission wavelengths (400 to 700 nm) to construct a 3D dataset of counts versus time versus wavelength. Using the Fluorescence Measurement and Analysis Studio (FMAS) software, this 3D dataset was then sliced orthogonally to the time axis to produce 2D spectra of counts versus wavelength to visualize how the emission spectrum evolves during the fluorescence lifetime. Fluorescence anisotropy was measured by setting peak count difference at 50,000 and the dwell time at 60 s.

## 3.6. References

1. a) W. Kühlbrandt, D. N. Wang, *Nature* **1991**, *350*, 130; b) W. Kühlbrandt, *Nature* **1995**, *374*, 497; c) G. McDermott, S. M. Prince, A. A. Freer, A. M. H.-Lawless, M. Z. Papiz, R. J. Cogdell, N. W. Isaacs, *Nature* **1995**, *374*, 517; d) X. Hu, K. Schulten, *Phys. Today* **1997**, *50*, 28; e) M. Yang, A. Damjanović, H. M. Vaswani, G. R. Fleming, *Biophys. J.* **2003**, *85*, 140.
2. Reviews on H-bonded donor-acceptor systems: a) M. D. Ward, *Chem. Soc. Rev.* **1997**, *26*, 365; b) C. A. Hunter, R. K. Hyde, *Angew. Chem. Int. Ed.* **1996**, *35*, 1936.
3. a) C. Devadoss, P. Bharathi, J. S. Moore, *J. Am. Chem. Soc.* **1996**, *118*, 9635; b) G. M. Stewart, M. A. Fox, *J. Am. Chem. Soc.* **1996**, *118*, 4354; c) D.-L. Jiang, T. Aida, *Nature* **1997**, *388*, 454; d) S. L. Gilat, A. Adronov, J. M. J. Fréchet, *Angew. Chem. Int. Ed.* **1999**, *38*, 1422; e) A. Adronov, J. M. J. Fréchet, *Chem. Commun.* **2000**,

1701; f) M.-S. Choi, T. Aida, T. Yamazaki, I. Yamazaki, *Angew. Chem. Int. Ed.* **2001**, *40*, 3194; g) T. S. Ahn, A. L. Thompson, P. Bharathi, A. Müller, C. J. Bardeen, *J. Phys. Chem. B* **2006**, *110*, 19810; h) M. Kozaki, K. Akita, S. Suzuki, K. Okada, *Org. Lett.* **2007**, *9*, 3315.

4. a) M. Nowakowska, V. P. Foyle, J. E. Guillet, *J. Am. Chem. Soc.* **1993**, *115*, 5975; b) D. M. Watkins, M. A. Fox, *J. Am. Chem. Soc.* **1994**, *116*, 6441; c) X. Schultze, J. Serin, A. Adronov, J. M. J. Fréchet, *Chem. Commun.* **2001**, 1160; d) K. Kuroda, T. M. Swager, *Macromolecules* **2004**, *37*, 716; e) C. Wu, H. Peng, Y. Jiang, J. McNeill, *J. Phys. Chem. B* **2006**, *110*, 14148.

5. a) P. J. Dutton, L. Conte, *Langmuir* **1999**, *15*, 613; b) H. Lahtivuori, H. Lemmetyinen, N. V. Tkachenko, *J. Am. Chem. Soc.* **2006**, *128*, 16036; c) T. Tang, A. Herrmann, K. Peneva, K. Müllen, S. E. Webber, *Langmuir* **2007**, *23*, 4623.

6. a) L. A. J. Chrisstoffels, A. Adronov, J. M. J. Fréchet, *Angew. Chem. Int. Ed.* **2000**, *39*, 2163; b) H. Yamada, H. Imahori, Y. Nishimura, I. Yamazaki, T. K. Ahn, S. K. Kim, D. Kim, S. Fukuzumi, *J. Am. Chem. Soc.* **2003**, *125*, 9129.

7. See the references 11-13 cited in Chapter 2 of the thesis.

8. For OPV based energy transfer systems, see: a) N. Armaroli, G. Accorsi, Y. Rio, J.-F. Nierengarten, J.-F. Eckert, M. J. Gómez-Escalonilla, F. Langa, *Synth. Met.* **2004**, *147*, 19; b) M. Wolffs, F. J. M. Hoeben, E. H. A. Beckers, A. P. H. J. Schenning, E. W. Meijer, *J. Am. Chem. Soc.* **2005**, *127*, 13484; c) G. de la Torre, F. Giacalone, J. L. Segura, N. Martín, D. M. Guldi, *Chem. Eur. J.* **2005**, *11*, 1267; d) F. Langa, M. J. Gomez-Escalonilla, J.-M. Rueff, T. M. F. Duarte, J.-F. Nierengarten, V. Palermo, P. Samorì, Y. Rio, G. Accorsi, N. Armaroli, *Chem. Eur. J.* **2005**, *11*, 4405; e) T. I. Hukka, T. Toivonen, E. Hennebicq, J.-L. Brédas, R. A. J. Janssen, D. Beljonne, *Adv. Mater.* **2006**, *18*, 1301; f) F. J. M. Hoeben, M. Wolffs, J. Zhang, S. D. Feyter,

P. Leclère, A. P. H. J. Schenning, E. W. Meijer, *J. Am. Chem. Soc.* **2007**, *129*, 9819; g) J. van Herrikhuyzen, R. A. J. Janssen, A. P. H. J. Schenning, S. C. J. Meskers, *Chem. Phys. Lett.* **2007**, *433*, 340.

9. a) A. P. H. J. Schenning, E. Peeters, E. W. Meijer, *J. Am. Chem. Soc.* **2000**, *122*, 4489; b) P. A. van Hal, R. A. J. Janssen, G. Lanzani, G. Cerullo, M. Zavelani-Rossi, S. De Silvestri, *Phys. Rev. B* **2001**, *64*, 075206/1; c) D. M. Guldi, A. Swartz, C. Luo, R. Gómez, J. L. Segura, N. Martín, *J. Am. Chem. Soc.* **2002**, *124*, 10875; d) A. M. Ramos, S. C. J. Meskers, P. A. van Hal, J. Knol, J. C. Hummelen, R. A. J. Janssen, *J. Phys. Chem. A* **2003**, *107*, 9269; e) M. Gutierrez-Nava, G. Accorsi, P. Masson, N. Armaroli, J.-F. Nierengarten, *Chem. Eur. J.* **2004**, *10*, 5076.

10. For OPV H-bonded energy transfer systems, see: a) E. H. A. Beckers, P. A. van Hal, A. P. H. J. Schenning, A. El-ghayoury, E. Peeters, M. T. Rispens, J. C. Hummelen, E. W. Meijer, R. A. J. Janssen, *J. Mater. Chem.* **2002**, *12*, 2054; b) E. H. A. Beckers, A. P. H. J. Schenning, P. A. van Hal, A. El-ghayoury, L. Sánchez, J. C. Hummelen, E. W. Meijer, R. A. J. Janssen, *Chem. Commun.* **2002**, 2888; c) F. J. M. Hoeben, L. M. Herz, C. Daniel, P. Jonkheijm, A. P. H. J. Schenning, C. Silva, S. C. J. Meskers, D. Beljonne, R. T. Phillips, R. H. Friend, E. W. Meijer, *Angew. Chem. Int. Ed.* **2004**, *43*, 1976; d) C. Daniel, L. M. Herz, D. Beljonne, F. J. M. Hoeben, P. Jonkheijm, A. P. H. J. Schenning, E. W. Meijer, R. T. Phillips, C. Silva, *Synth. Met.* **2004**, *147*, 29; e) D. Beljonne, E. Hennebicq, C. Daniel, L. M. Herz, C. Silva, G. D. Scholes, F. J. M. Hoeben, P. Jonkheijm, A. P. H. J. Schenning, S. C. J. Meskers, R. T. Phillips, R. H. Friend, E. W. Meijer *J. Phys. Chem. B* **2005**, *109*, 10594; f) F. J. M. Hoeben, A. P. H. J. Schenning, E. W. Meijer, *Chem. Phys. Chem.* **2005**, *6*, 2337.

11. For OPV-perylene bisimide systems, see: a) E. E. Neuteboom, E. H. A. Beckers, S. C. J. Meskers, E. W. Meijer, R. A. J. Janssen; *Org. Biomol. Chem.* **2003**, *1*, 198; b) E. E. Neuteboom, S. C. J. Meskers, P. A. van Hal, J. K. J. van Duren, E. W. Meijer, R. A. J. Janssen, H. Dupin, G. Pourtois, J. Cornil, R. Lazzaroni, J.-L. Brédas, D. Beljonne *J. Am. Chem. Soc.* **2003**, *125*, 8625; c) F. Würthner, *Chem. Commun.* **2004**, 1564; d) F. Würthner, Z. Chen, F. J. M. Hoeben, P. Osswald, C.-C. You, P. Jonkheijm, J. van Herrikhuyzen, A. P. H. J. Schenning, P. P. A. M. van der Schoot, E. W. Meijer, E. H. A. Beckers, S. C. J. Meskers, R. A. J. Janssen, *J. Am. Chem. Soc.* **2004**, *126*, 10611; e) E. E. Neuteboom, P. A. van Hal, R. A. J. Janssen, *Chem. Eur. J.* **2004**, *10*, 3907; f) A. M. Ramos, S. C. J. Meskers, E. H. A. Beckers, R. B. Prince, L. Brunsveld, R. A. J. Janssen, *J. Am. Chem. Soc.* **2004**, *126*, 9630; g) S. P. Dudek, M. Pouderoijen, R. Abbel, A. P. H. J. Schenning, E. W. Meijer, *J. Am. Chem. Soc.* **2005**, *127*, 11763;

12. a) N. J. Turro, *Modern Molecular Photochemistry*, University Science Books, Sausalito, **1991**; b) J. R. Lakowicz, *Principles of Fluorescence Spectroscopy* (2nd ed.), Kluwer Academic/Plenum Publishers, New York, **1999**.

13. a) T. Förster, in *Modern Quantum Chemistry*, Part III, (Ed. O. Sinanoglu), Academic, New York, **1965**; b) V.M. Agranovich, M. D. Galanin, *Electronic Excitation Energy Transfer in Condensed Matter*, North-Holland, Amsterdam, **1982**; c) *Resonance Energy Transfer*, (Eds. D. L. Andrews, A. A. Demidov), Wiley, Chichester, **1999**.

14. S. Jang, M. Newton, R. J. Silbey, *Phys. Rev. Lett.* **2004**, *92*, 218301/1.

15. M. H. Chang, F. J. M. Hoeben, P. Jonkheijm, A. P. H. J. Schenning, E. W. Meijer, C. Silva, L. M. Herz, *Chem. Phys. Lett.* **2006**, *418*, 196.

16. a) J. Eldo, E. Arunkumar, A. Ajayaghosh, *Tetrahedron Lett.* **2000**, *41*, 6241; b) J. Eldo, A. Ajayaghosh, *Chem. Mater.* **2002**, *14*, 410; b) M. Büschel, A. Ajayaghosh, J. Eldo, J. Daub, *Macromolecules* **2002**, *35*, 8405;

17. A. Ajayaghosh, V. K. Praveen, C. Vijayakumar, S. J. George, *Angew. Chem. Int. Ed.* **2007**, *46*, 6260.

18. R. M. Silverstein, F. X. Webster, *Spectroscopic Identification of Organic Compounds*, 6th ed., Wiley-VCH, Weinheim, **1997**.

19. a) M. Fujitsuka, A. Okada, S. Tojo, F. Takei, K. Onitsuka, S. Takahashi, T. Majima, *J. Phys. Chem. B* **2004**, *108*, 11935; b) E. Hennebicq, G. Pourtois, G. D. Scholes, L. M. Herz, D. M. Russell, C. Silva, S. Setayesh, A. C. Grimsdale, K. Müllen, J.-L. Brédas, D. Beljonne, *J. Am. Chem. Soc.* **2005**, *127*, 4744; c) E. E. Nesterov, Z. Zhu, T. M. Swagar, *J. Am. Chem. Soc.***2005**, *127*, 10083.

20. a) R. Kersting, U. Lemmer, R. F. Mahrt, K. Leo, H. Kurz, H. Bässler, E. O. Göbel, *Phys. Rev. Lett.* **1993**, *70*, 3820; b) M. Wohlgenannt, W. Graupner, F. P. Wenzl, S. Tasch, E. J. W. List, G. Leising, M. Graupner, A. Hermetter, U. Rohr, P. Schlichting, Y. Geerts, U. Scherf, K. Müllen, *Chem. Phys.* **1998**, *227*, 99.

21. E. J. W. List, C. Creely, G. Leising, N. Schulte, A. D. Schlüter, U. Scherf, K. Müllen, W. Graupner, *Chem. Phys. Lett.* **2000**, *325*, 132.

22. a) C. N. Fleming, P. Jang, T. J. Meyer, J. M. Papanikolas, *J. Phys. Chem. B* **2004**, *108*, 2205.

23. A. Damjanović, T. Ritz, K. Schulten, *Phys. Rev. E* **1999**, *59*, 3293.

24. A. Ruseckas, E. B. Namdas, T. Ganguly, M. Theander, M. Svensson, M. R. Andersson, O. Inganäs, V. Sundström, *J. Phys. Chem. B* **2001**, *105*, 7624.

25. a) H.-J. Egelhaaf, J. Gierschner, D. Oelkrug, *Synth.. Met.* **1996**, *83*, 221; b) J. Gierschner, H.-J. Egelhaaf, D. Oelkrug, *Synth. Met.* **1997**, *84*, 529.

26. M. I. Ranasinghe, M. W. Hager, C. B. Gorman, T. Goodson, III. *J. Phys. Chem. B* **2004**, *108*, 8543.

27. V. Pokorná, D. Výprachtický, J. Pecka, F. Mikeš, *Macromol. Chem. Phys.* **2001**, *202*, 155.

28. T. Ikeda, B. Lee, S. Kurihara, S. Tazuke, S. Ito, M. Yamamoto, *J. Am. Chem. Soc.* **1988**, *110*, 8299.

29. a) J. Baumann, M. D. Fayer, *J. Chem. Phys.* **1986**, *85*, 4087; b) M. N. Berberan-Santos, B. Valeur, *J. Chem. Phys.* **1991**, *95*, 8048.

30. a) http://hyperphysics.phy-astr.gsu.edu/hbase/vision/cie.html#c2; b) http://www.awitness.org/delphi_pascal_tutorial/intex.html.

31. a) X. Gong, W. Ma, J. C. Ostrowski, G. C. Bazan, D. Moses, A. J. Heeger, *Adv. Mater.* **2004**, *16*, 615; b) J. Liu, Q. Zhou, Y. Cheng, Y. Geng, L. Wang, D. Ma, X. Jing, F. Wang, *Adv. Mater.* **2005**, *17*, 2974; c) S. K. Lee, D.-H. Hwang, B.-J. Jung, N. S. Cho, J. Lee, H.-K. Shim, *Adv. Funct. Mater.* **2005**, *15*, 1647; d) G. Tu, C. Mei, Q. Zhou, Y. Cheng, Y. Geng, L. Wang, D. Ma, X. Jing, F. Wang, *Adv. Funct. Mater.* **2006**, *16*, 101; e) J. Liu, Q. Zhou, Y. Cheng, Y. Geng, L. Wang, D. Ma, X. Jing, F. Wang, *Adv. Funct. Mater.* **2006**, *16*, 957; f) Q. Niu, Y. Xu, J. Jiang, J. Peng, Y. Cao, *J. Lumin.* **2007**, *126*, 531; g) J. Liu, X. Guo, L. Bu, Z. Xie, Y. Cheng, Y. Geng, L. Wang, X. Jing, F. Wang, *Adv. Funct. Mater.* **2007**, *17*, 1917.

32. a) B. W. D'Andrade, M. E. Thompson, S. R. Forrest, *Adv. Mater.* **2002**, *14*, 147; b) B. W. D'Andrade, J. Brooks, V. Adamovich, M. E. Thompson, S. R. Forrest, *Adv. Mater.* **2002**, *14*, 1032; c) P. Coppo, M. Duati, V. N. Kozhevnikov, J. W. Hofstraat, L. D. Cola, *Angew. Chem. Int. Ed.* **2005**, *44*, 1806. d) T.-H. Kim, H. K. Lee, O O. Park, B. D. Chin, S.-H. Lee, J. K. Kim, *Adv. Funct. Mater.* **2006**, *16*, 611.

33. a) F. Steuber, J. Staudigel, M. Stössel, J. Simmerer, A. Winnacker, H. Spreitzer, F. Weissörtel, J. Salbeck, *Adv. Mater.* **2000**, *12*, 130; b) M. Mazzeo, V. Vitale, F. D. Sala, M. Anni, G. Barbarella, L. Favaretto, G. Sotgiu, R. Cingolani, G. Gigli, *Adv. Mater.* **2005**, *17*, 34; c) Y. Liu, M. Nishiura, Y. Wang, Z. Hou, *J. Am. Chem. Soc.* **2006**, *128*, 5592; d) T.-H. Kim, H. K. Lee, O O. Park, B. D. Chin, S.-H. Lee, J. K. Kim, *Adv. Funct. Mater.* **2006**, *16*, 611.

34. a) T. Nakashima, N. Kimizuka, *Adv. Mater.* **2002**, *14*, 1113; b) V. K. Praveen, S. J. George, R. Varghese, C. Vijayakumar, A. Ajayaghosh, *J. Am. Chem. Soc.* **2006**, *128*, 7542.

# Chapter 4

# Controlled Self-Assembly and Color Tunable Energy Transfer in Donor-Acceptor Organogels

## 4.1. Abstract

*Color tunable fluorescence resonance energy transfer (FRET) in donor-acceptor π-organogels through controlled self-assembly and energy migration is described. Picosecond time-resolved emission studies of a few oligo(p-phenylenevinylene) (OPV) derivatives in the gel state revealed that energy migration is slow or less efficient in OPV gelators with bulky end groups (**OPV1-2**) when compared to that of the gelators with small end groups (**OPV3-4**). FRET studies were carried out using **OPV1** and **OPV3** as donors and **OPV6** as the acceptor. Addition of small amounts of **OPV6** (0-2 mol%) results in the quenching of **OPV1** fluorescence at 509 nm with the formation of emission at 555 nm, corresponding to the monomer band of the acceptor. Upon further addition of **OPV6** (2-20 mol%), the emission was continuously red-shifted to 610 nm which corresponds to the aggregate emission of **OPV6**. Consequently, 98% quenching of the donor emission was observed at 509 nm. However, in the case of **OPV3**, maximum quenching (82%) occurred with 3-4 mol% of the acceptor due to fast energy migration. Further addition of the acceptor facilitated the disruption of the gel resulting in the monomer emission of the donor.*

## 4.2. Introduction

Tuning of the emission color over a range of wavelengths is important in the fields of biomedical labeling, light emitting diodes, full color displays, lasers and sensors.[1] Emission color of organic molecules can be modulated by functional group substitution,[2] controlling the effective conjugation length[3] or blending with fluorescent or phosphorescent materials.[4] Recently, doping techniques based on energy transfer have been proven to be an effective way to tune the emission color of photoluminescent and electroluminescent materials.[5] If two materials with different band gaps (and hence different emission colors) are mixed together, energy transfer from the higher to the lower band gap material may occur leading to emission solely or predominantly from the latter.

Tunable emission from self-assembled nanoparticles of 1,3,5-triphenyl-2-pyrazoline (TPP) **1** was achieved using energy transfer technique.[5a,c] TPP nanoparticles doped with 4-(dicyanomethylene)-2-methyl-6-(*p*-dimethyl-aminostyryl-4H-pyran (DCM) **2** were prepared by reprecipitation method. The absorption spectrum of DCM (acceptor) showed good spectral overlap with the emission spectrum of TPP (donor) as required for FRET. Aqueous dispersions of DCM doped TPP nanoparticles were found to show different emission colors depending upon the DCM content and efficiency of energy transfer. Fluorescence spectra and the photograph of the solutions clearly demonstrated the emission tuning from blue to red with increasing DCM content (Figure 4.1). A similar red

shift and decrease in the emission is also observed from solutions of acceptor alone with different concentrations. Therefore, the red shift, which directly contributes to the tunable emission, is ascribed to a change in the degree of aggregation of DCM molecules in nanoparticles and subsequent energy transfer to these aggregates.

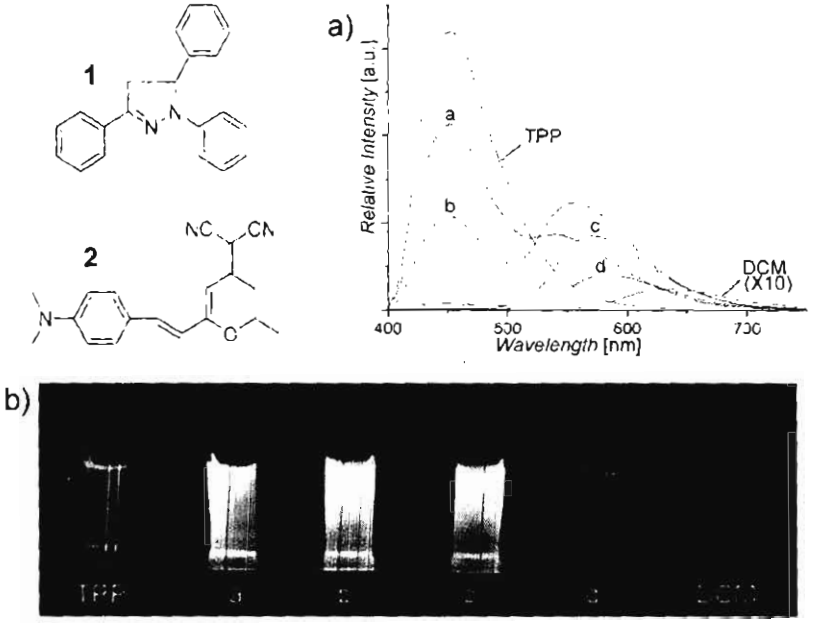


**Figure 4.1.** a) Fluorescence emission spectra and b) corresponding photographs of the suspensions of DCM (**2**) doped TPP (**1**) nanoparticles excited at 365 nm. The doping concentrations of DCM in the nanoparticles are 0, 0.1, 0.2, 2, 10 and 100% (molar) for containers labeled TPP, a, b, c, d and DCM respectively.

Dynamic π-π stacked molecular assembly of perylene derivatives (**3a-b**) in chloroform solution has been reported to show pure green, yellow, orange, and red photoluminescence on a single wavelength excitation as a consequence of self-assembly of these derivatives from single molecules to higher order assemblies.[6] As the concentration of **3a** or **3b** increases, rapid exchange of free monomers and

self-associated oligomers of **3** occurs on the NMR time scale. The self-organized oligomers of **3** emit green to red colors (Figure 4.2) depending upon the concentration of the solution. At a concentration of 31 mM, red photons (674 nm) are emitted, while at 7.7 mM, fluorescence has an orange color (643 nm). At 0.96 mM, mostly bright yellow emission occurs (577 nm), whereas light green color (535 nm) is emitted below 0.12 mM.

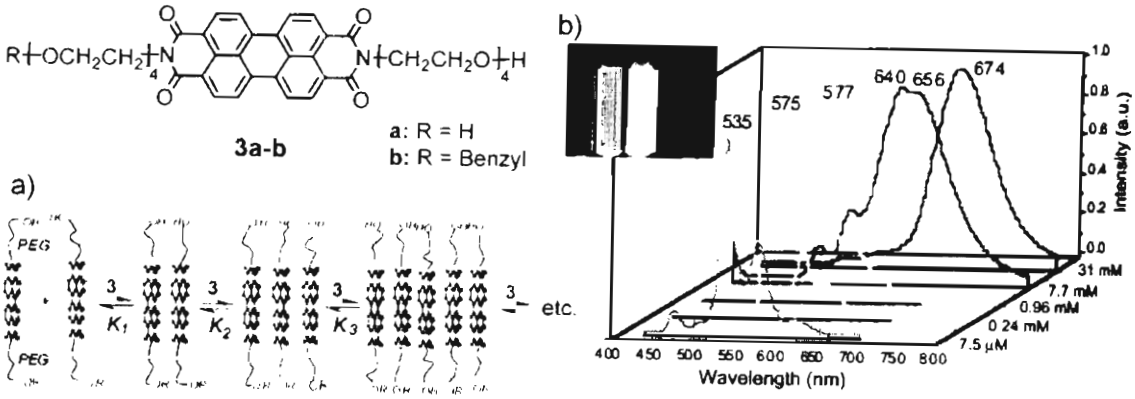


**Figure 4.2.** a) Dynamic self-assembly of perylene derivatives (**3a-b**) to higher order assemblies with increase in concentration. b) Fluorescence spectra of **3a** in chloroform at different concentrations. Inset shows the corresponding photographs of the solutions.

There are reports pertaining to systems where energy transfer occurs from aggregates to monomers[7] and aggregates to aggregates.[8] In many of such cases organogelators[9], dendrimers[10] and conjugated polymers[11] have been used as supramolecular scaffolds. However, control of energy transfer from self-assembled donors to monomers and aggregates of the same acceptor has not been successfully demonstrated so far except in a few cases.[5a] A combination of these two processes would provide a pathway for wavelength tunable emission upon a

single wavelength excitation. The success of such an objective lies in the control of energy migration (EM) and energy transfer (ET) through the judicious selection of the donor and acceptor molecules and the controlled placement of the acceptor within the donor self-assembly as 'isolated molecules' or 'stacked aggregates' of different dimensions. This chapter deals with the rational design of π-organogels that facilitate controlled EM and efficient ET, selectively from the self-assembled donors either to 'isolated' or to 'stacked' acceptors which are entrapped in a coassembly, thereby allowing a gradual tuning of the emission from green to red over a range of ca. 100 nm.

## 4.3. Results and Discussion

### 4.3.1. The Design Strategy

The motivation for this work stems from two seminal reports by Meijer and coworkers[7a] and Desvergne and coworkers[12] who *independently observed that* higher concentration of the acceptor in a supramolecular environment results in complex energy transfer processes. However a systematic investigation remains elusive mainly due to the problems associated with the conflict of the photophysical properties of the donor-acceptor system and the competing direct excitation of the acceptor. In order to overcome these limitations of supramolecular light harvesting assemblies, a rationale choice of the donor-acceptor motifs and their self-organization are extremely important. For this

purpose we have prepared a few oligo(*p*-phenylenevinyle) derivatives (**OPV1-6**) with different end functional groups. **OPV1-2** contains bulky tridodecyloxy benzene as the end groups connected to the OPV unit through ester and vinylic linkages respectively. **OPV3-4** contains small end groups such as methyl and ethyl respectively which is connected to the OPV through an ester linkage. The end functional groups could play a key role on the self-assembly and chromophore interactions in these gelators which in turn affect the efficiency of energy migration and hence FRET properties in the self-assembled state. **OPV5** is a chiral analogue of **OPV1** in which the alkyl chains in the central benzene ring is replaced with chiral alkyl chains. **OPV6** is incorporated with electron withdrawing groups such as cyano with the OPV backbone. Since the cyano group in this molecule is in conjugation with the OPV unit, the HOMO-LUMO energy gap of this molecule will be small when compared to the other derivatives. Hence this molecule can be used as an acceptor for the excitation energy from other OPV derivatives. This derivative might show more red-shifted absorption when compared to that of the other OPV derivatives under study which is necessary to minimize the self-excitation of the acceptor upon excitation of the donor in an energy transfer process. Furthermore, the structure of **OPV6** is designed in such a way that it can self-assemble to form higher order aggregates as well as coassemble with other OPVs.

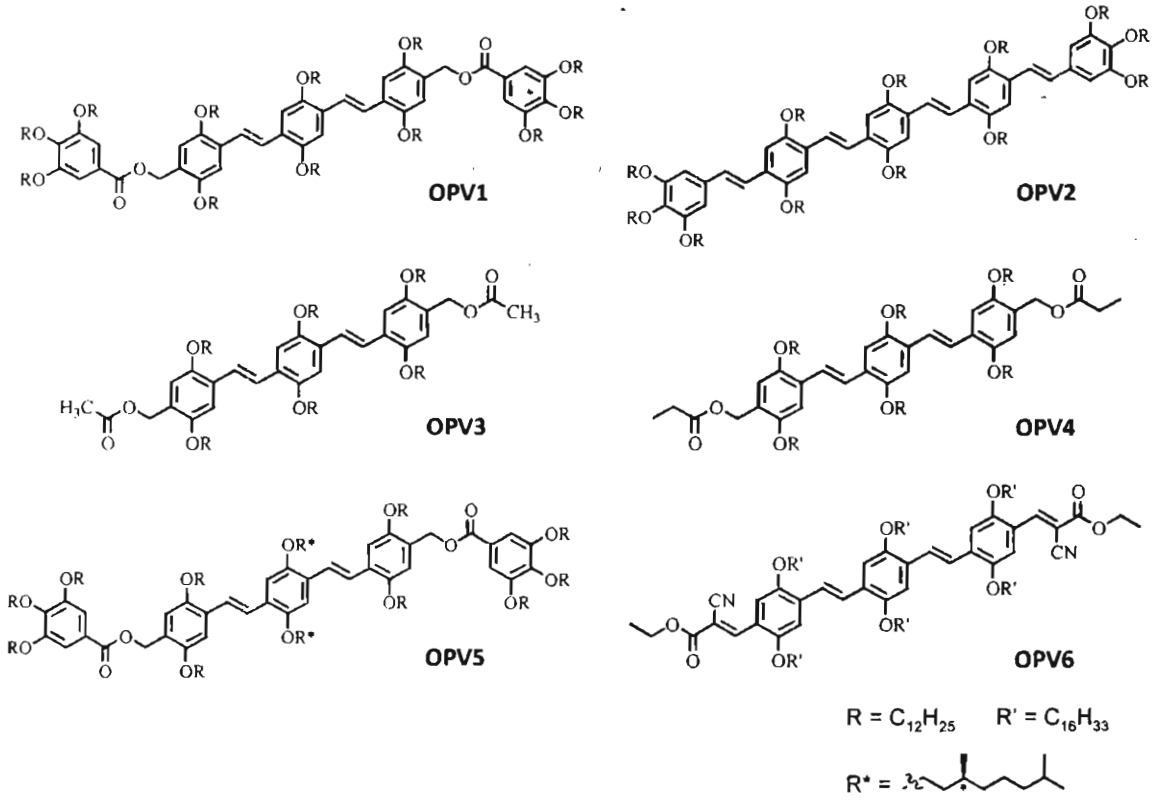


**Chart 4.1.** Structures of the OPV derivatives under study.

## 4.3.2. Synthesis of OPV Derivatives

**OPV1**, **OPV3**, **OPV4** and **OPV5** were synthesized from the corresponding OPV bisalcohol (**11a-b**), whereas, **OPV2** and **OPV6** were synthesized from OPV bisaldehyde (**12**) (Scheme 4.2). The OPV bisalcohols (**11a-b**) and the bisaldehayde (**12**) were prepared as reported earlier (see Chapter 2). The precursor, tridodecyloxy-benzene derivatives (**7** and **10**) were prepared according to Scheme 4.1. The 3,4,5-trihydroxy benzoic acid (gallic acid) **4** was esterified by refluxing in methanol in presence conc. $H_2SO_4$ to give **5** in 95% yield. This molecule on reaction with 1-bromo dodecane in DMF in presence of NaOH

readily afforded 3,4,5-tri(dodecyloxy)benzoate **6** in 86% yield. Subsequent hydrolysis using KOH and methanol resulted **7** in 94% yield. Upon reduction with $LiAlH_4$, the compound **6** gave the corresponding alcohol (**8**) in 72% yield. Bromination of **8** with $PBr_3$ in dry $CH_2Cl_2$ yielded the product **9** (82%). Phosphonation of **9** with triethyl phosphite yielded **10** in 98%.

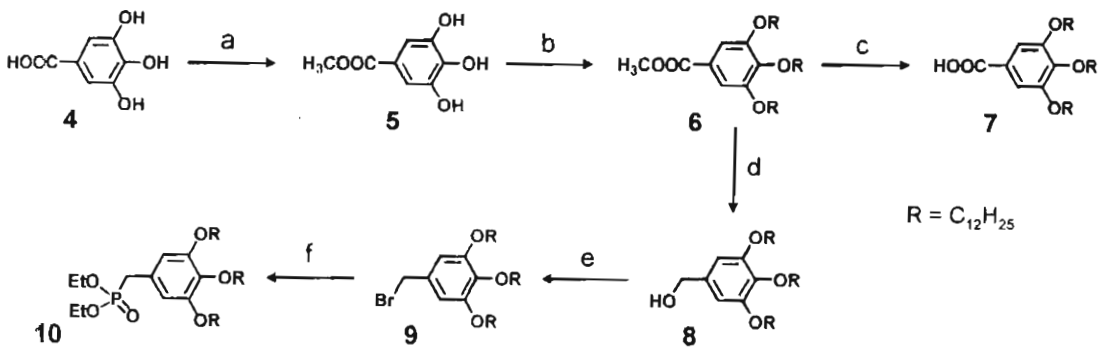


**Scheme 4.1.** Reagents and conditions: a) $H_2SO_4$, $CH_3OH$, reflux, 10 h, 95%; b) docecyl bromide, $K_2CO_3$, DMF, 60 °C, 8 h, 86%; c) KOH, ethanol, reflux, 2 h, 94%; d) $LiAlH_4$, THF (dry), 3 h, 72%; e) $PBr_3$, $CH_2Cl_2$ (dry), 0 °C – rt, 82%; f) triethyl phosphite, 120 °C, 8 h, 98%.

**OPV1** and its chiral analogue **OPV5** were prepared by treating OPV alcohols **11a** and **11b** respectively with **7** in dry dichloromethane in presence of DCC and DMAP. Reaction of **11a** with acetic acid or propionic acid under the same conditions yielded **OPV3** and **OPV4** respectively. Wittig reaction of OPV bisaldehyde (**12a**) with the phosphonate ester **10** in dry THF in presence of NaH yielded **OPV2**. Preparation of **OPV6** was accomplished by the condensation reaction of bisaldehyde **12b** with ethyl cyanoacetate in presence of ammonium acetate and acetic acid in toluene at 80 °C.

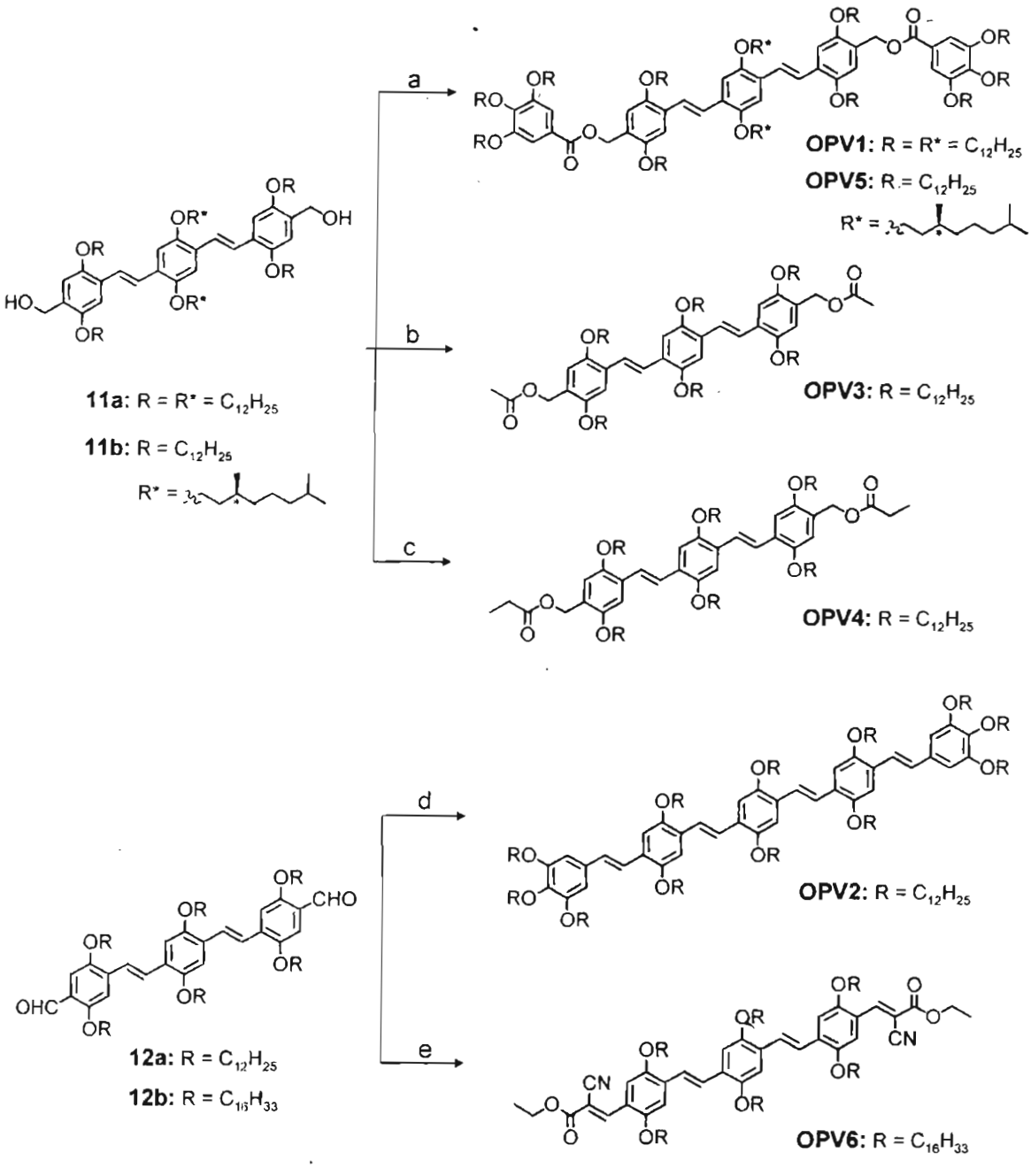


**Scheme 4.2.** Synthesis of **OPV1-6**. Reagents and conditions: a) compound **7**, DCC, DMAP, dichloromethane (dry), 0 °C - rt, 4 h, 96%; b) acetic acid, DCC, DMAP, dichloromethane (dry), 0 °C - rt, 4 h, 97%; c) propionic acid, DCC, DMAP, dichloromethane (dry), 0 °C - rt, 4 h, 96%; d) compound **10**, NaH, tetrahydrofuran (dry), 60 °C, 12 h, 70%; e) ethyl cyanoacetate, $NH_4OAc$, $CH_3COOH$, toluene, 80 °C, 4 h, 95%.

### 4.3.3. Gelation Studies

Gelation properties of the newly synthesized OPV derivatives were examined in a range of organic solvents. Dissolution of small amounts of the gelators in nonpolar hydrocarbon solvents such as decane, hexane, cyclohexane and methyl cyclohexane under heating followed by cooling resulted in stable transparent gels. The cooperative effects of several noncovalent forces such as π-stacking, van der Waals and dipole-dipole interactions could be the driving force for the gelation phenomena. However, they failed to form gels in polar solvents such as chloroform, dichloromethane, tetrahydrofuran etc. Critical gelator concentration (CGC) of all the derivatives in various nonpolar hydrocarbon solvents is summarized in Table 4.1. **OPV1-4** and **OPV6** were found to be excellent gelators, whereas, the chiral derivative (**OPV5**) was highly soluble in all the above solvents and hence failed to form gels. All the derivatives showed lowest CGC values (high gelation ability) in *n*-decane. It should be noted that **OPV1-2** showed better gelation ability when compared to the other three derivatives. This could be due to the presence of the 3,4,5-tridodecyloxybenzene moiety, which may assist the gelation by enhancing the van der Waals and π-stacking interactions between the neighboring molecules. **OPV2** is the better gelator when compared to **OPV1** probably due to the extended π-backbone of the former which enhances the π-stacking interactions.

**Table 4.1.** Critical gelator concentration (CGC) of the OPV derivatives.

| Solvent | **OPV1** mg/mL (mM) | **OPV2** mg/mL (mM) | **OPV3** mg/mL (mM) | **OPV4** mg/mL (mM) | **OPV6** mg/mL (mM) |
|---|---|---|---|---|---|
| *n*-Decane | 1.0 (0.36) | 0.8 (0.30) | 1.6 (1.04) | 1.6 (1.03) | 2.6 (1.59) |
| *n*-Hexane | 1.2 (0.43) | 1.0 (0.37) | 1.8 (1.17) | 1.7 (1.09) | 2.8 (1.71) |
| Cyclohexane | 1.5 (0.54) | 1.2 (0.45) | 2.0 (1.31) | 2.0 (1.28) | 4.3 (2.63) |
| Methyl cyclohexane | 2.6 (0.94) | 2.0 (0.74) | 2.9 (1.89) | 2.8 (1.79) | 4.5 (2.75) |

### 4.3.4. Absorption and Emission Studies

Intense absorption corresponding to the $\pi$-$\pi^*$ transition and strong emission with high quantum yields were observed for all the derivatives in various solvents. The photophysical properties of **OPV1-6** under investigation are summarized in Table 4.2.

All the derivatives under study exist as molecularly dissolved species in chloroform. **OPV1**, **OPV3**, **OPV4** and **OPV5** exhibited similar absorption and emission properties in chloroform. The absorption and emission spectra of **OPV1** and **OPV3** are shown in Figure 4.3a and 4.3c respectively. In these cases, the absorption maximum occurred at 409 nm and the emission maxima at 472 nm and 493 nm. When compared to these derivatives, the absorption and emission spectra of **OPV2** were shifted to red region due to its extended conjugation. The

absorption maximum was found at 448 nm and the emission maxima were at 525 and 552 nm (Figure 4.3b). **OPV6** showed maximum red-shifted absorption and emission spectra when compared to the other derivatives due to extended conjugation and the presence of electron withdrawing groups (Figure 4.3d). In this case, the absorption maximum was at 504 nm and the emission maximum was at 605 nm. Fluorescence quantum yields of these derivatives were found to be high in chloroform. Fluorescence lifetime analysis in chloroform exhibited monoexponential decay indicating only one emitting species.

**Table 4.2.** Photophysical properties of **OPV1-6**

| Compound | Solvent | Absorption | | Emission | | | |
|---|---|---|---|---|---|---|---|
| | | $\lambda_{max}$ (nm) | $\varepsilon \times 10^4$ ($M^{-1}cm^{-1}$) | $\lambda_{max}$ (nm) | $\Phi_f$ [a] | $\Phi_f$ [b] | $\tau$ (ns) |
| **OPV1** | Chloroform | 409 | 4.67 | 472, 493 | 0.71 | - | 1.73 |
| | Decane | 397, 470 | 3.83 | 509, 545 | - | 0.38 | 3.36 |
| **OPV2** | Chloroform | 448 | 6.15 | 525, 552 | 0.65 | - | 1.85 |
| | Decane | 434, 510 | 5.03 | 542, 585 | - | 0.26 | 3.78 |
| **OPV3** | Chloroform | 408 | 4.41 | 470, 495 | 0.72 | - | 1.75 |
| | Decane | 397, 460 | 3.78 | 507, 540 | - | 0.35 | 3.41 |
| **OPV4** | Chloroform | 408 | 4.32 | 468, 494 | 0.72 | - | 1.78 |
| | Decane | 398, 460 | 3.51 | 505, 536 | - | 0.32 | 3.25 |
| **OPV5** | Chloroform | 409 | 4.68 | 469, 497 | 0.74 | - | 1.79 |
| | Decane | 404 | 4.31 | 459, 485 | 0.72 | - | 1.82 |
| **OPV6** | Chloroform | 504 | 4.03 | 605, 639 | 0.61 | - | 2.04 |
| | Decane | 492 | 3.11 | 610, 635 | - | 0.12 | 4.25 |

[a] Fluorescence quantum yields of the monomeric species (in chloroform). [b] Fluorescence quantum yields of the self-assembled molecules (in decane). Quinine sulphate ($\Phi_f$ = 0.546 in 0.1 N $H_2SO_4$) and Rhodamine 6G ($\Phi_f$ = 0.9 in ethanol) were used as the standards, error limit ± 5%.

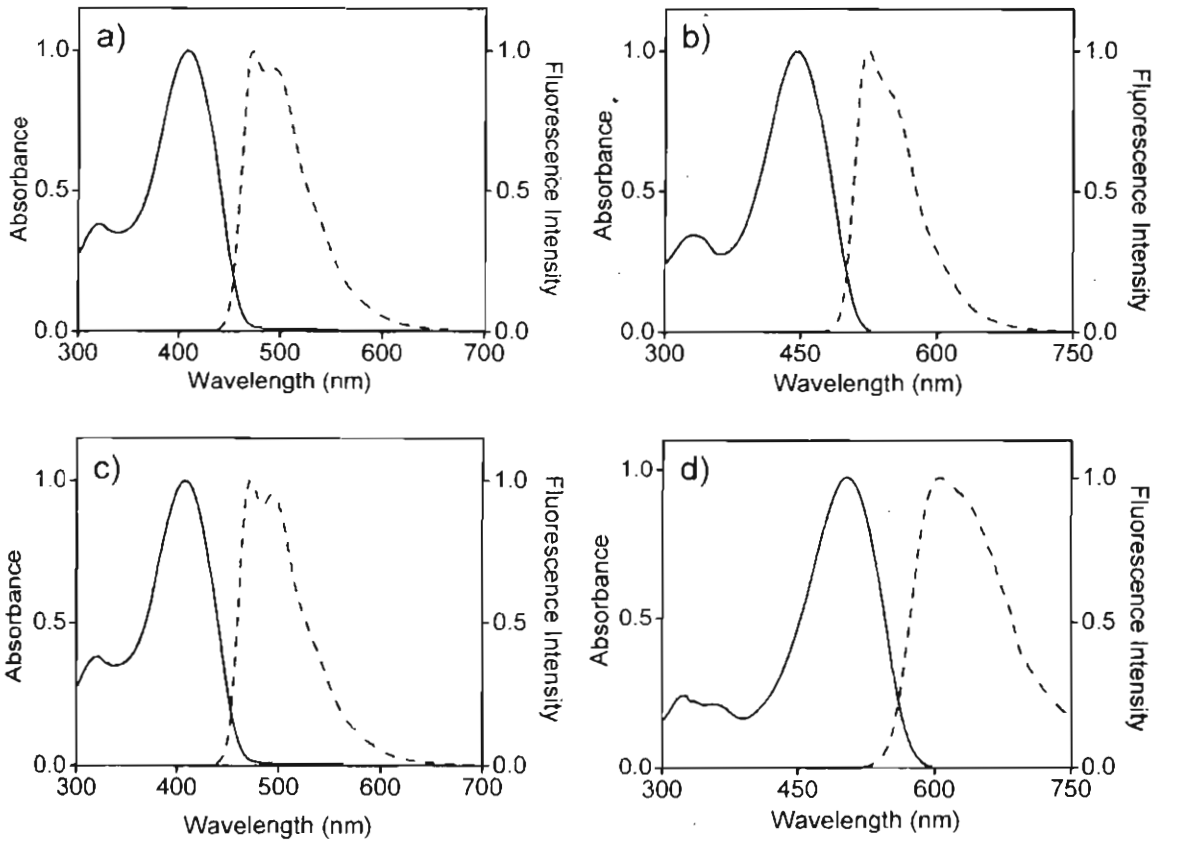


**Figure 4.3**. Absorption (——) and emission (– –) spectra of a) **OPV1** b) **OPV2** c) **OPV3** and d) **OPV6** in chloroform at room temperature. ($c$ = 3 × $10^{-4}$ M, $l$ = 1 mm, $\lambda_{ex}$ = 380 nm for **OPV1** and **OPV3**, 420 for **OPV2** and 480 nm for **OPV6**).

In decane at room temperature, **OPV1-4** and **OPV6** (3 × $10^{-4}$ M) exhibited characteristic absorption and emission properties of aggregated species. When compared to chloroform, a red-shifted shoulder was observed in the absorption spectra in decane which corresponds to the self-assembled species. Emission was quenched and red-shifted in decane at room temperature. For example, **OPV1** exhibited a broad absorption with a maximum at 397 nm and a shoulder around 470 nm at room temperature (Figure 4.4a). The emission maximum was found to

be at 509 and 545 nm (Figure 4.5a). **OPV3** and **OPV4** showed similar absorption and emission properties. However, they showed slight difference in the spectral features when compared to that of **OPV1** (Figure 4.4c and 4.5c). **OPV2** and **OPV6** showed more quenched emission in decane than the other derivatives. **OPV2** exhibited absorption maximum at 434 nm (Figure 4.4b) and emission maxima at 542 nm and 585 nm (Figure 4.5b). Absorption maximum of **OPV6** was found at 492 nm (Figure 4.4d), whereas, the emission maxima were at 610 nm and 635 nm at room temperature (Figure 4.5d). Low quantum yield and multiexponential decay with increased lifetime was observed for **OPV1-4** and **OPV6** in decane when compared to that of chloroform (Table 4.2) due to aggregation. Absorption and emission of **OPV5** in decane resembled the spectra obtained in chloroform because of its inability to form aggregates in decane.

Absorption and emission intensities of **OPV1-4** and **OPV6** in decane were changed with temperature due to the reversible formation of the self-assembly. On increasing temperature, the red-shifted shoulder in the absorption spectrum was decreased and finally disappeared with an enhancement in the intensity at the absorption maximum (Figure 4.4). Similarly, with increasing temperature, the intensity of the red-shifted emission of the self-assembled species was decreased with a concomitant increase in the emission corresponding to the monomer species (Figure 4.5).

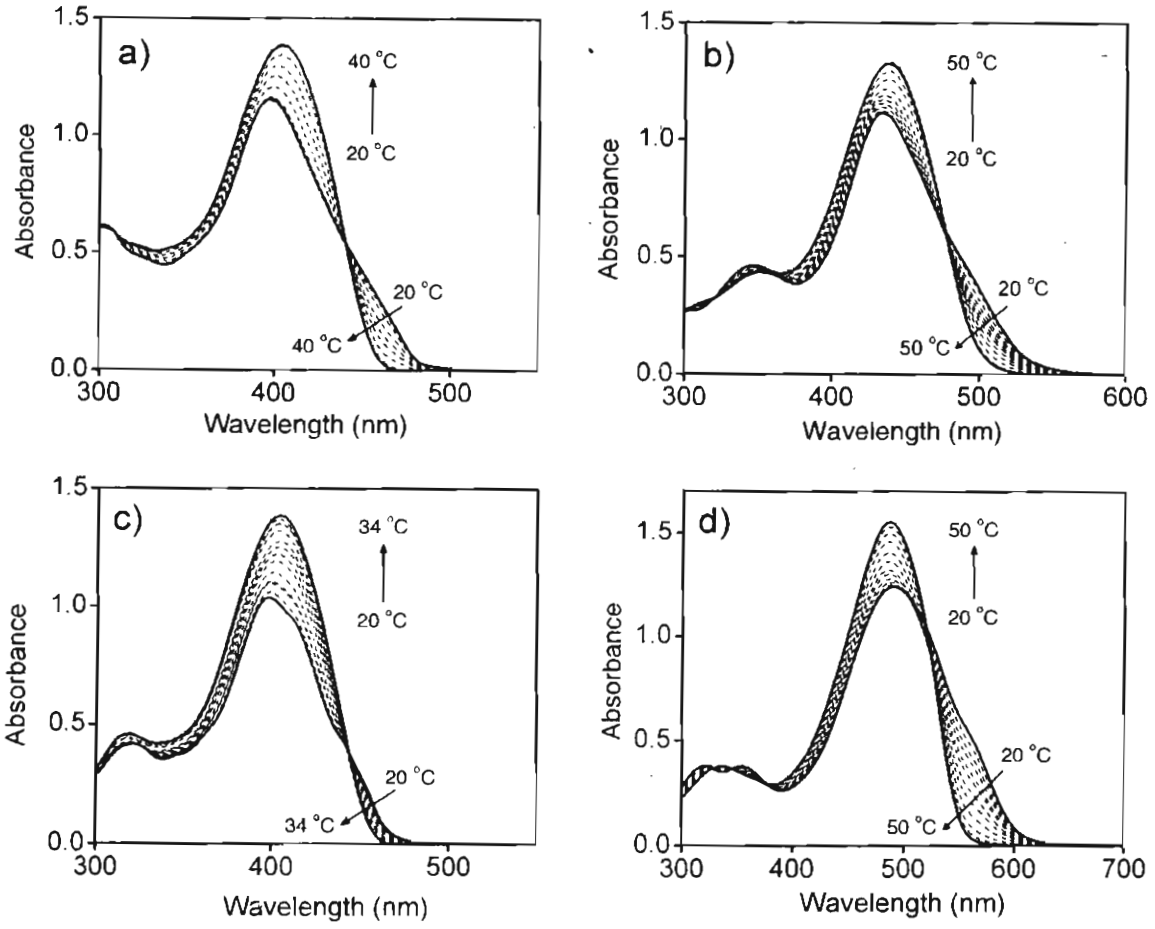


**Figure 4.4.** Temperature dependent absorption spectral changes of a) **OPV1** b) **OPV2** c) **OPV3** and d) **OPV6** in decane. ($c$ = 3 × $10^{-4}$ M, $l$ = 1 mm, **OPV4** showed similar absorption spectral changes as that of **OPV3**).

## 4.3.5. Energy Migration Studies

Our earlier studies revealed that energy migration within the donor scaffold plays an important role on the efficiency of excitation energy transfer from the donors to the acceptors.[13] In the present work, time resolved emission spectroscopic (TRES) studies of **OPV1-4** in the gel state at different time windows were carried out which revealed the decay of the shorter wavelength emission and

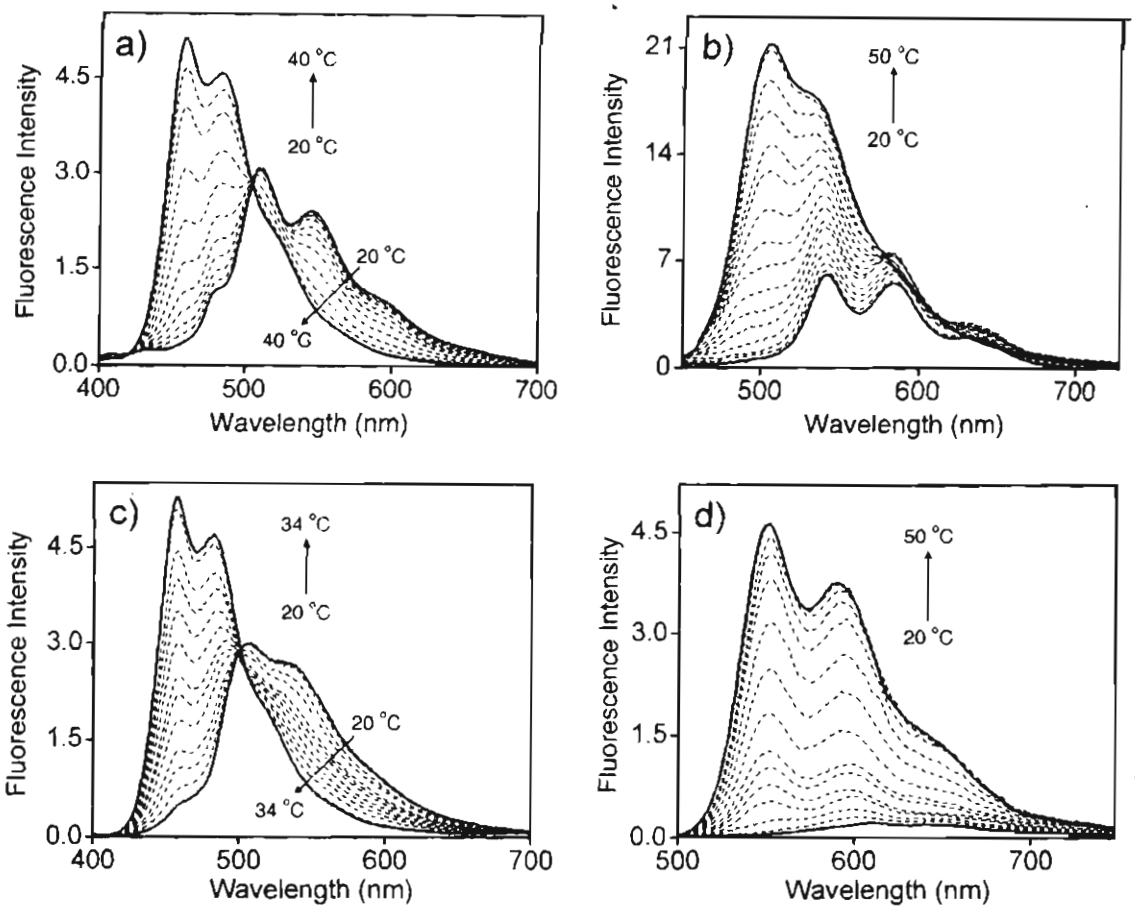


**Figure 4.5.** Temperature dependent emission spectral changes of a) **OPV1** b) **OPV2** c) **OPV3** and d) **OPV6** in decane. ($c = 3 \times 10^{-4}$ M, $l = 1$ mm, $\lambda_{ex} = 380$ nm for **OPV1** and **OPV3**, 420 for **OPV2** and 480 nm for **OPV6**, **OPV4** showed similar absorption spectral changes as that of **OPV3**).

enhancement of the longer wavelength emission with a red-shift in the emission maximum. The dynamic red-shift of the emission maximum with time is due to the population build up of the excited states of the higher order aggregates (lower HOMO-LUMO energy gap) through excitation energy migration from the lower order aggregates (higher HOMO-LUMO energy gap). However, under identical conditions, gelators with bulky end groups (**OPV1-2**) showed remarkable difference in the time resolved emission when compared to that of gelators with

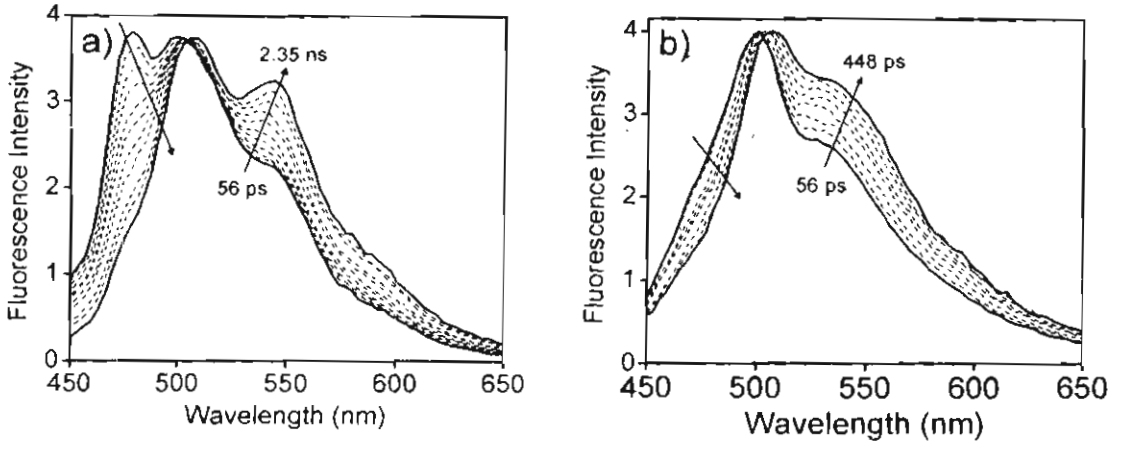


**Figure 4.6.** Time resolved emission spectra of a) **OPV1** and b) **OPV3** in the gel state in decane at room temperature. ($c = 5.6 \times 10^{-4}$ M, $l = 1$ mm, $\lambda_{ex} = 375$ nm).

small end groups (**OPV3-4**). For example, the time resolved emission spectra of the decane gel of **OPV1** and **OPV3** ($5.6 \times 10^{-4}$ M) at different time settings at room temperature is shown in Figure 4.6. On excitation of **OPV1** with 375 nm laser, structured emission with maxima at 478 nm and 499 nm was observed at 56 ps. With time, it gradually shifted towards red and finally resembled the steady state emission with maxima at 509 and 544 nm after 2.35 ns. Interestingly, in the case of **OPV3**, only 448 ps were needed to get the emission spectrum equivalent to the steady state, i.e., energy migration is fast in this case compared to that of **OPV1**. The emission maximum of the initial spectrum was at 501 nm and finally it reached to 509 nm. **OPV2** showed similar property as that of **OPV1**, whereas, **OPV4** showed similar properties of **OPV3**. Time span of 2.02 ns and 448 ps were required to get the emission equivalent to the steady state emission of **OPV2** and

**OPV4** respectively. This observation indicates that energy migration is less efficient in organogelators with bulky end groups (**OPV1-2**), whereas, it is more efficient in gelators with small end groups (**OPV3-4**).

The wavelength dependence of the emission decay of **OPV1** and **OPV3** in the gel state is depicted in Figure 4.7, which gives further evidence for the difference in the energy migration efficiencies in these two self-assemblies. The fluorescence decay collected at 430 nm is biexponential and decays faster than the higher wavelength emissions. With increasing emission wavelength, the decay becomes slower and triexponential with the formation of a rising component in the initial time scale (Figure 4.7c and 4.7d), indicating the possible energy migration from lower order aggregates to higher order aggregates. In the case of **OPV1**, time scale of the growth component was found to be 473 ps, whereas, that of **OPV3** was 224 ps indicating that the former needs more time for energy migration when compared to that of the latter. Similarly, the growth time observed in **OPV2** and **OPV4** was 416 and 226 ns respectively. These observations again prove that energy migration is fast in OPV gelators with small end groups, whereas, it is slow in gelators with bulky end groups.

Fluorescence anisotropy studies were conducted in these molecular assemblies to get more insight into the difference in the energy migration efficiencies. Figure 4.8a shows the fluorescence anisotropy decay of **OPV1** gel in decane monitored at 509 nm. The initial anisotropy value ($r_0$) was 0.24, which

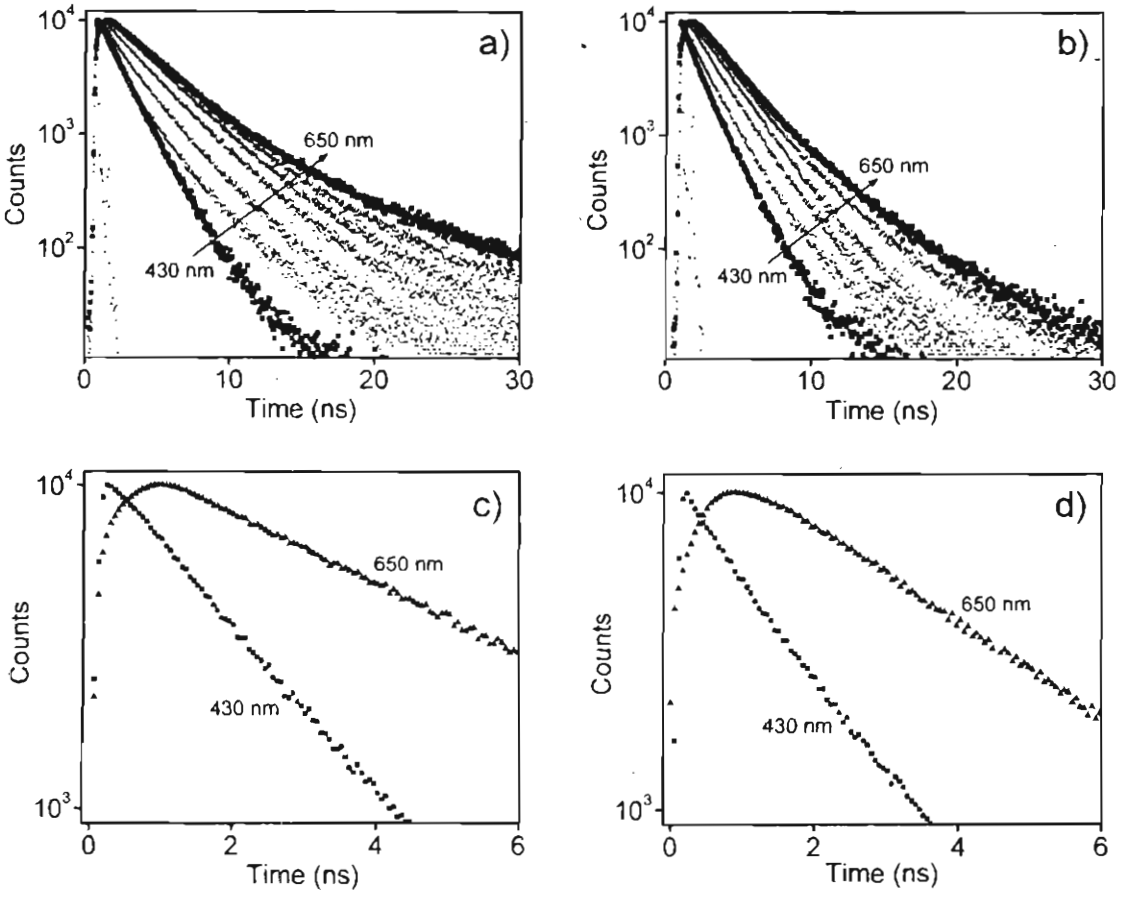


**Figure 4.7.** Wavelength dependent fluorescence decay profiles of a) **OPV1** and b) **OPV3** gels in decane at room temperature. c) and d) shows the corresponding zoomed portion of the decay at the initial time scales monitored at 430 nm (■) and 650 nm (▲). ($c$ = 5.6 × $10^{-4}$ M, $l$ = 1 mm, $\lambda_{ex}$ = 375 nm).

lose the anisotropy memory and reaches the plateau region ($r_\infty$) at 0.09 with a decay time of 550 ps. Figure 4.8b shows the fluorescence anisotropy decay of **OPV3** gel in decane. In this case, $r_0$ (0.23) reached to $r_\infty$ (0.09) with a fast decay time of 245 ps. Similar studies on **OPV2** and **OPV4** were conducted at identical conditions. Fast depolarization was observed in **OPV4** as in the case of **OPV3**,

whereas, slow depolarization is observed in **OPV2** similar to **OPV1**. The difference in the emission depolarization confirmed that energy migration is slow in **OPV1-2**, whereas, it is fast in **OPV3-4**.

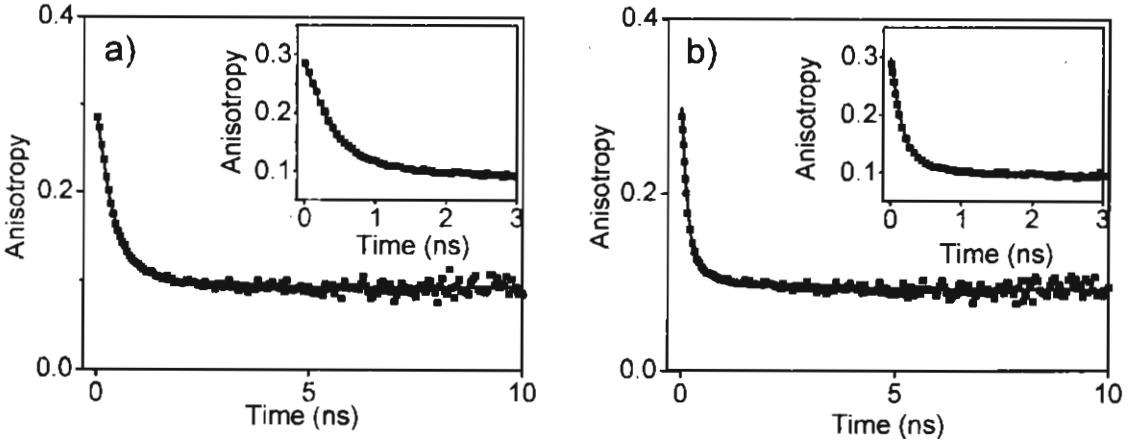


**Figure 4.8.** Time resolved fluorescence depolarization of a) **OPV1** and b) **OPV3** in the gel state in decane at room temperature. ($c$ = 5.6 × $10^{-4}$ M, $l$ = 1 mm, $\lambda_{ex}$ = 375 nm). Inset shows the corresponding zoomed portion of the anisotropy decay at the initial time scales.

The above experiments indicate that the bulkiness of the end group plays a crucial role on the energy migration efficiencies of **OPV1-4**. The bulky tridodecyloxybenzene might reduce the chromophore interaction in the gel state and hence slow down energy migration within the self-assembled scaffolds of **OPV1-2**. Such a hindering due to the bulkiness of the end group is absent in **OPV3-4**.

Studies with the non-gelling chiral derivative **OPV5** under similar conditions revealed that no energy migration occurs in this case. No change was observed in the emission spectrum with time (Figure 4.9a). Lifetime decay profiles

monitored at different wavelengths (450-650 nm) when excited at 375 nm was found to be same (Figure 4.9b). Moreover, the fluorescence depolarization showed slow decay which gave further evidence for the absence of energy migration (Figure 4.9c). The slow decay might be due to the rotational diffusion of the molecularly dissolved chromophores in solution. These observations indicate that self-assembly of the molecules is necessary for energy migration.

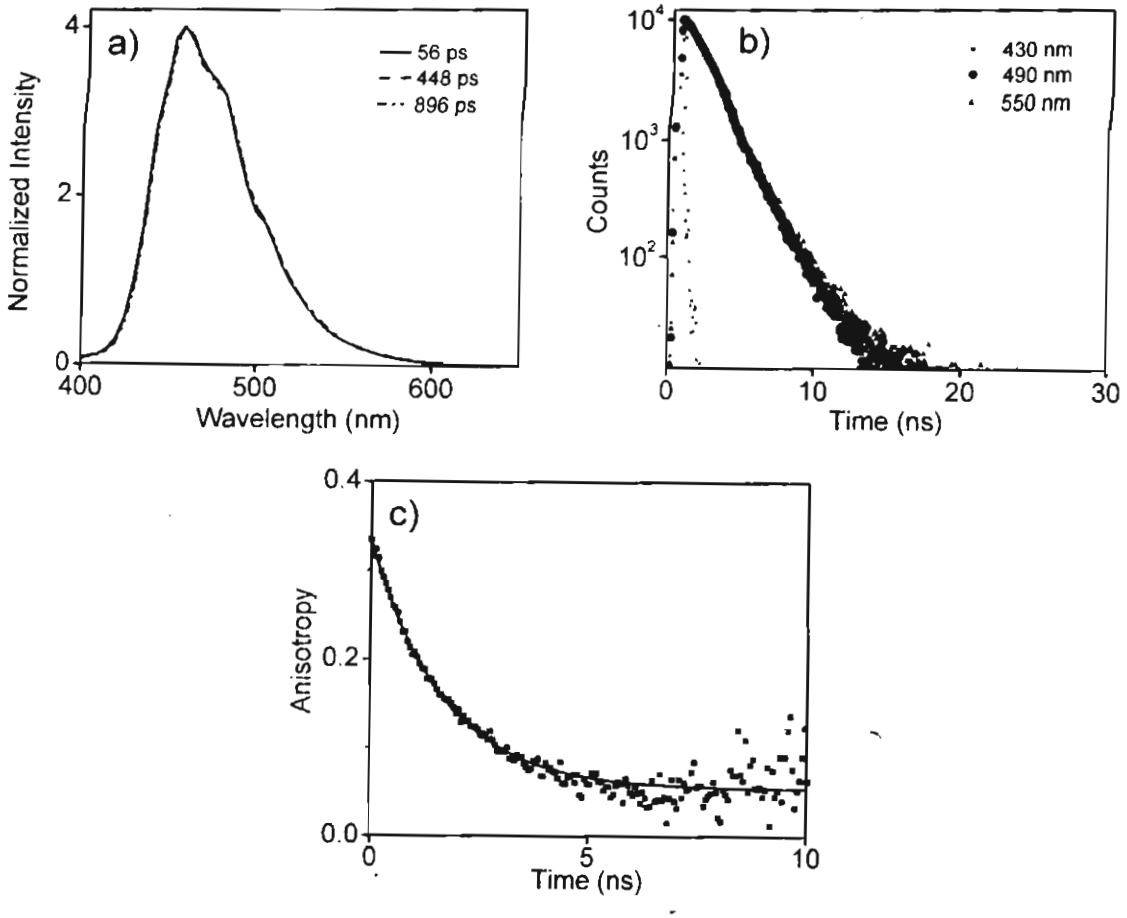


**Figure 4.9.** a) Time-resolved emission spectra, b) wavelength dependent fluorescence decay and c) fluorescence anisotropy decay of **OPV5** in decane at room temperature. ($c$ = 5.6 × $10^{-4}$ M, $l$ = 1 mm, $\lambda_{ex}$ = 375 nm).

### 4.3.6. FRET Properties of OPV1

The emission of the donor (**OPV1**) and the absorption of the acceptor (**OPV6**) showed significant spectral overlap which is necessary for efficient energy transfer (Figure 4.10a). The overlap integral was found to be $1.78 \times 10^{15}$ $M^{-1}cm^{-1}nm^4$. It should be noted that the acceptor has minimum absorption at the $\lambda_{max}$ of the donor (Figure 4.10b) which allow the excitation of the donor without the acceptor being get excited directly. These properties of **OPV1** and **OPV6** are ideal for the fluorescence resonance energy transfer between these molecules.

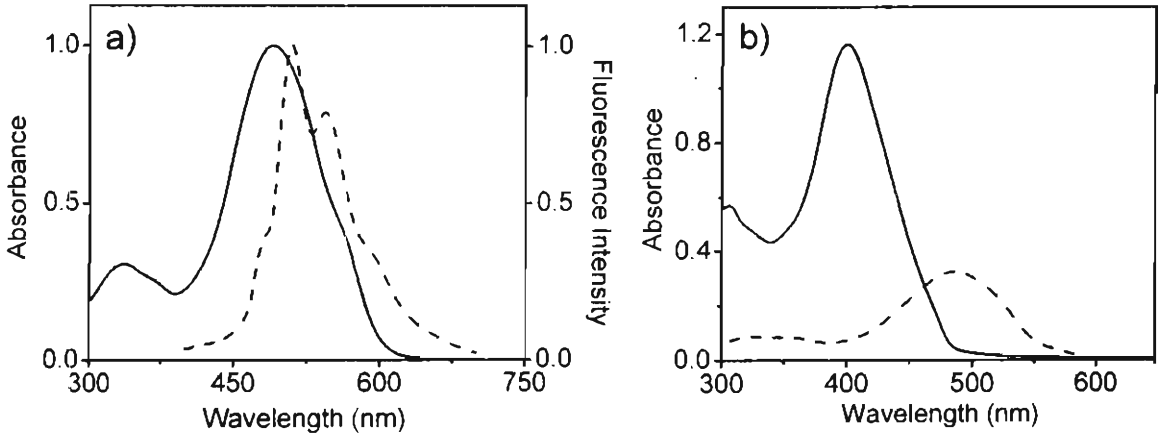


**Figure 4.10.** a) Spectral overlap of the emission of **OPV1** (– –) and the absorption of **OPV6** (——); b) Comparison of the absorption of **OPV1** (——) and **OPV6** (– –) in decane at room temperature. (conc. of donor = $3 \times 10^{-4}$ M, conc. of acceptor = $6 \times 10^{-5}$ M, $l$ = 1 mm, $\lambda_{ex}$ = 380 nm)

Prior to the FRET studies, coassembly of the donor and acceptor is confirmed by UV-vis, X-ray diffraction (XRD) and atomic force microscopic (AFM) studies. Temperature dependent UV-vis absorption studies showed two transitions upon heating a decane solution of the coassembly (donor conc. = 3 ×

$10^{-4}$ M) containing 20 mol% of **OPV6** (Figure 4.11). The increase in the intensity of the absorption around 400 nm and the decrease of the shoulder band at 470 nm at 20-40 °C, correspond to the disruption of the donor scaffold. The second transition observed at 40-50 °C with an increase in the absorption around 491 nm corresponds to the melting of the acceptor aggregates. This observation is a clear indication of the aggregation of the acceptor molecules within the donor scaffold.

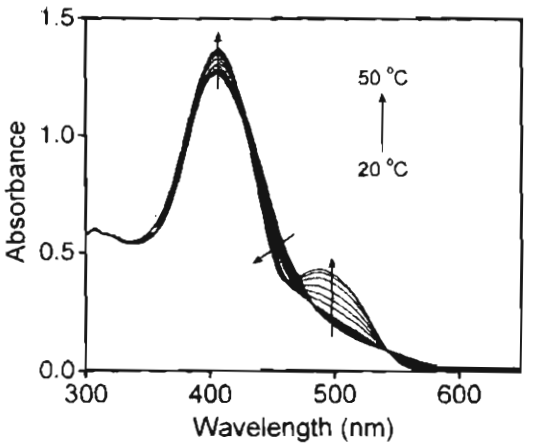


**Figure 4.11.** Temperature dependent absorption changes of **OPV1** ($3 \times 10^{-4}$ M) in presence of 20 mol% **OPV6** in decane. Red lines indicate the spectral changes from 20-40 °C which corresponds to the melting of the donor aggregates. Blue lines indicate the spectral changes from 40-50 °C which corresponds to the melting of the acceptor aggregates formed within the self-assembly of the donor molecules.

The X-ray diffraction patterns of **OPV1** in the xerogel state prepared from decane solution showed sharp reflections corresponding to the *d*-spacing of 30.15, 25.30, 9.93, 4.70, 4.29 and 3.78 Å which are indications of $\pi$-stacked lamellar packing of the molecules (Figure 4.12a). Absence of the sharp reflections, particularly at 9.93 Å, the broadening of the peaks at the short and the wide angle

regions and the shift in the π-stacking distance from 3.78 to 4.07 Å with 20 mol% of the acceptor indicates the disruption of the continuous lamellar packing of **OPV1** as a result of the coassembly of **OPV6** (Figure 4.12b and 4.12c).

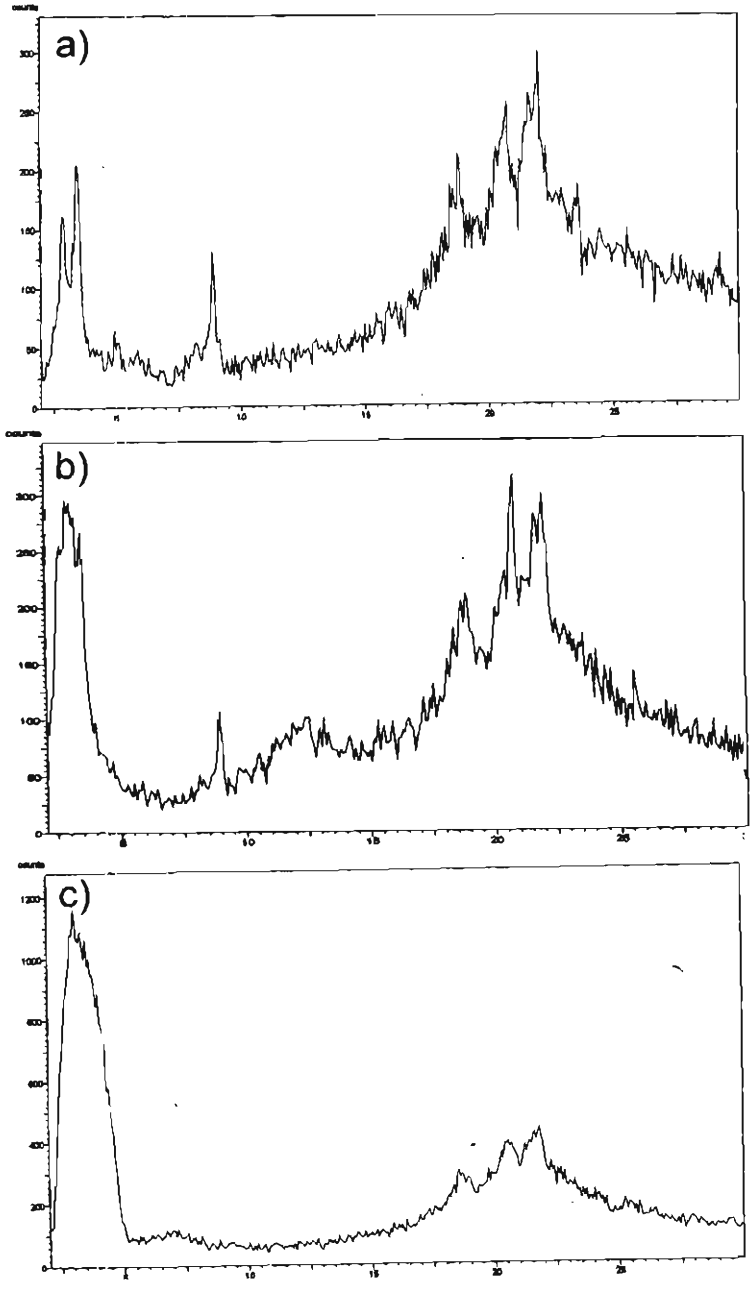


**Figure 4.12.** X-ray diffraction pattern of **OPV1** containing a) 0 mol%, b) 10 mol% and 20 mol% of **OPV6** in the xerogel state.

AFM images of **OPV1**, **OPV6** and the coassemblies drop-cast from decane solution ($1 \times 10^{-5}$ M) on freshly cleaved mica surface revealed the formation of micrometer sized extended structures with distinct morphological features. For example, the morphology of **OPV1** exhibits short fibrous texture, several of which are aligned together to form bundles (Figure 4.13a). The individual strands are a few micrometers in length, 100-160 nm in width and 8-20 nm in height which are not entangled. On the other hand, **OPV6** forms entangled structures of infinite length having 40-200 nm width and 5-50 nm height (Figure 4.13b). Interestingly, the coassembly of **OPV1** with 20 mol% of **OPV6** showed morphological features of both compounds (100-300 nm width and 5-50 nm height, Figure 4.13c). These observations confirmed the coassembly of the acceptor within the donor gel scaffold in decane.

The FRET studies were conducted in the gel state in decane. Upon excitation of the aggregates of **OPV1** at 380 nm in the presence of 0-2 mol% of **OPV6**, gradual decrease in the emission of the former with the concomitant formation of the monomer emission of the latter was observed. However, coassemblies with 2-20 mol% of **OPV6** showed continuous shift of the emission towards long wavelength, eventually resulting in the aggregate emission of **OPV6** (Figure 4.14a). Thus, a continuous red-shift of the emission from 509-610 nm ($\Delta\lambda$ = 101 nm) could be possible by varying the concentration of the acceptor resulting in ca. 98 % quenching of the monomer emission with a rate of $1.78 \times 10^{10}$ $s^{-1}$. This

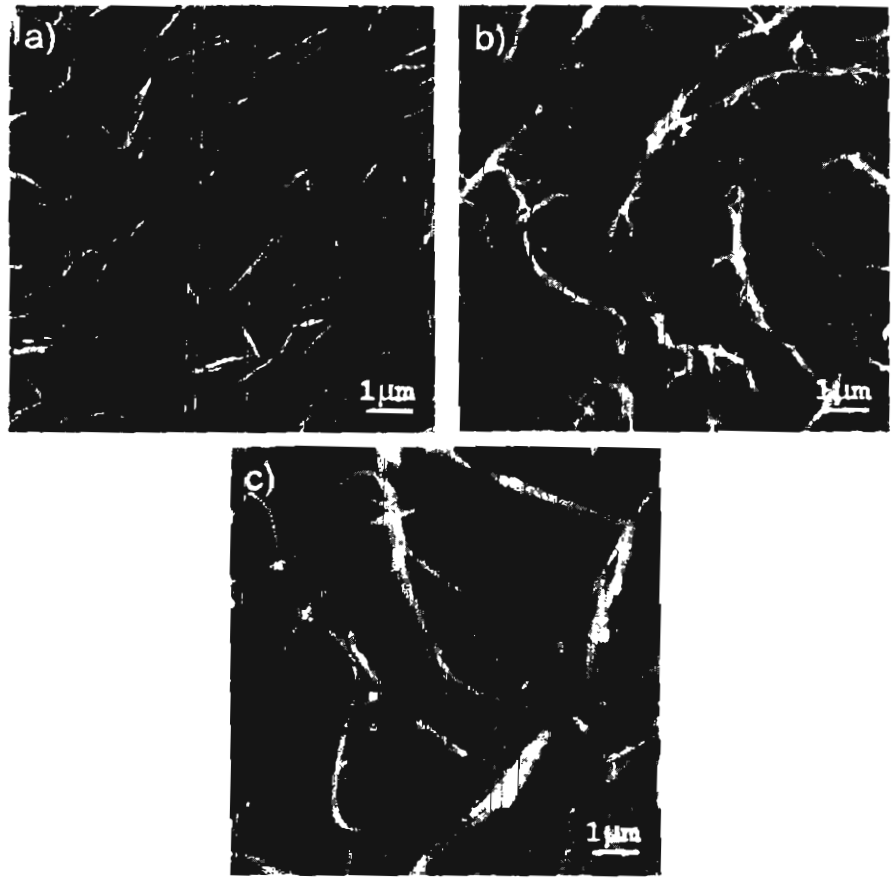


**Figure 4.13.** Tapping mode AFM height images of (a) **OPV1** alone (b) **OPV6** alone (c) coassembly of **OPV1** with 20 mol% of **OPV6** (donor conc. = 1 x $10^{-5}$ M), recorded at same magnification.

rate is comparable with that reported for other supramolecular systems.[14] Not much change was observed in the UV-vis absorption spectum of the donor on addition of increasing amounts (0-20 mol%) of the acceptor (Figure 4.14b).

Fluorescence lifetime decay profiles of **OPV1** ($\lambda_{ex}$ = 375 nm) monitored at the aggregate emission maximum of the donor (509 nm) showed decrease in the lifetime with increasing concentration of the acceptor (Figure 4.15). The accelerated decay of the donor fluorescence in the presence of acceptor ruled out

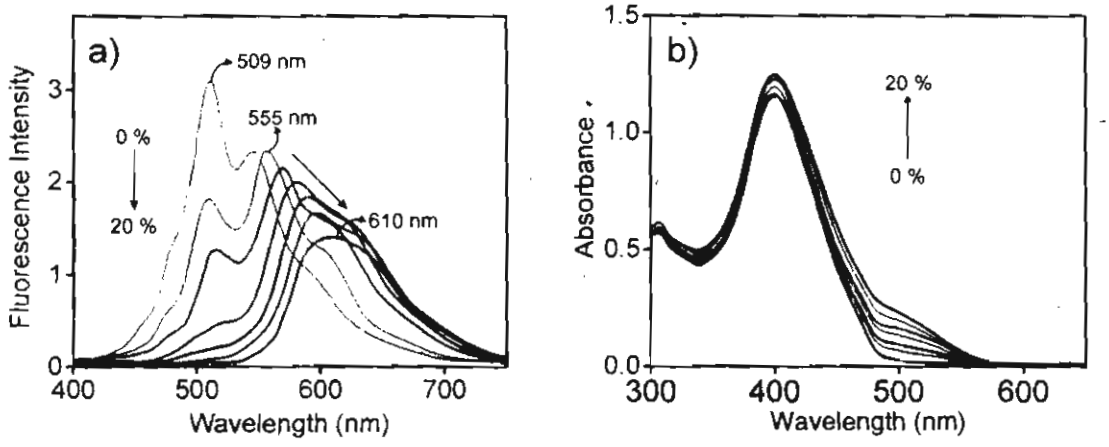


**Figure 4.14.** a) Fluorescence spectra and b) the corresponding absorption spectra of **OPV1** ($c$ = 3 x $10^{-4}$ M, $l$ = 1 mm, $\lambda_{ex}$ = 380 nm) on addition of increasing amounts of **OPV6** (0-20 mol%).

any trivial energy transfer pathways. The excited donor scaffold efficiently transfers the energy to the acceptors which populate the excited states of the latter before it decays by radiative mechanism.[7a,15] This is clear from Figure 4.16a, which depicts the fluorescence decay of **OPV6** (probed at 610 nm) alone in decane and in the coassembly (20 mol% of **OPV6**). The growth observed at short timescale is associated with the population increase of the excited states of the acceptor upon energy transfer from the donor singlet which is followed by the decay.[15a,16] Comparison of the fluorescence spectra of **OPV6** in the presence ($\lambda_{ex}$ = 380 nm) and in the absence of **OPV1** ($\lambda_{ex}$ = 490 nm) under identical experimental conditions reveals 2-fold increase in the intensity of the FRET emission (Figure 4.16b). Due to the low extinction coefficient of **OPV6** at 380 nm, direct excitation of the acceptor during energy transfer is negligible as evidenced by the extremely weak emission.

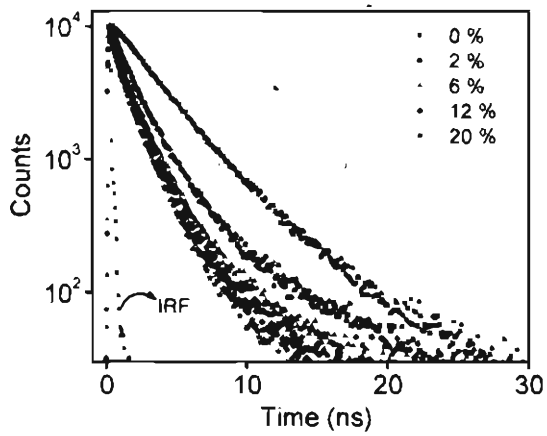


**Figure 4.15.** Fluorescence lifetime decay profiles of **OPV1** ($c$ = 3 × $10^{-4}$ M, $l$ = 1 mm, $\lambda_{ex}$ = 375 nm) monitored at 509 nm on addition of different amounts of **OPV6** (0-20 mol%).

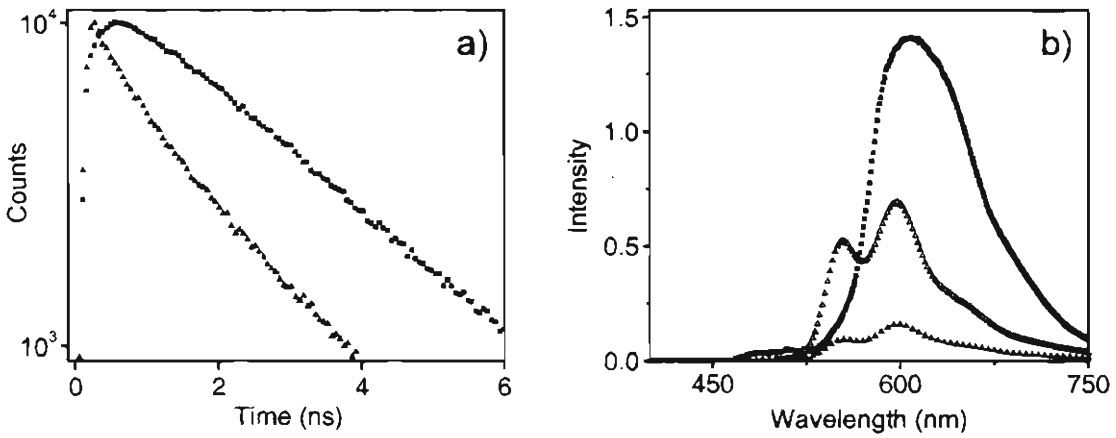


**Figure 4.16.** a) Fluorescence lifetime decay profiles of **OPV6** alone (▲) and in **OPV1** gel (■) in decane (monitored at 610 nm, $\lambda_{ex}$ = 375 nm). b) Comparison of the FRET emission with 20 mol% (6 × $10^{-5}$ M) of **OPV6** in presence of **OPV1** excited at 380 nm (■), upon direct excitation of **OPV6** in the absence of **OPV1** excited at 380 nm (▲) and 490 nm (△).

Fluorescence microscopic images of **OPV1** and **OPV6** under different compositions provide visual evidence for the color tunable FRET process. In the absence of **OPV6**, the donor exhibits bright green emission (Figure 4.17a). On adding 2 mol% of **OPV6**, emission color changes to yellow due to the energy

transfer from the donor aggregates to the monomers of the acceptor (Figure 4.17b). In presence of 20 mol% of the acceptor, red emission was observed which is of the acceptor aggregates through energy transfer from the donor aggregates (Figure 4.17c).

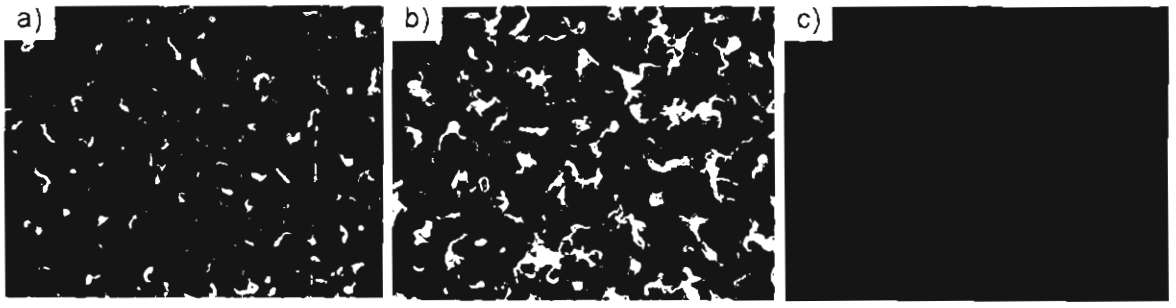


**Figure 4.17.** Fluoresecence microscopy images of **OPV1** containing a) 0 mol%, b) 2 mol% and c) 20 mol% of **OPV6**. Samples prepared by drop-casting the freshly prepared decane solution containing various compositions of donor and acceptor.

Photographs of **OPV1** gel in decane containing different concentrations of **OPV6** are shown in Figure 4.18. On addition of increasing amounts of acceptor to the donor followed by heating and cooling yielded stable gels, whose emission color ($\lambda_{ex}$ = 365 nm) change from green to red through yellow and orange.


**Figure 4.18.** Photographs of the decane gels of **OPV1** containing different compositions of **OPV6** i) 0 mol%, ii) 1 mol%, iii) 2 mol%, iv) 6 mol%, v) 12 mol% and vi) 20 mol% under illumination with 365 nm light.

The reason for the observed shift in the emission of **OPV1** in the presence of varying amounts of **OPV6** is depicted in Figure 4.19. Coassembly of **OPV1** and **OPV6** facilitates the encapsulation of the latter within the self-assembly of the former. Under low mol%, **OPV6** exists as isolated monomers within the coassembly. At this point, partial transfer of the excitation energy occurs to the monomer of **OPV6** resulting in yellow emission ($\lambda_{max}$ = 555 nm). In contrast, under higher mol% of **OPV6**, a statistical distribution of the aggregates with different HOMO-LUMO gap is possible providing an energy gradient. In these cases, the eventual FRET emission occurs from the higher order aggregates[16] available at each compositions of **OPV6** resulting in a gradual red-shift of the emission to 610 nm with a complete quenching of the donor emission.

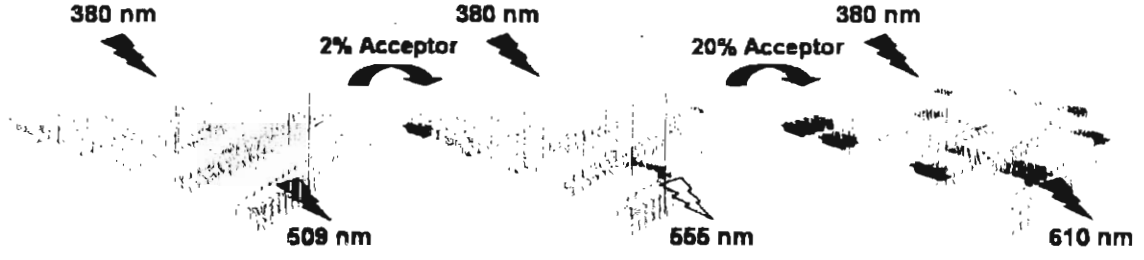


**Figure 4.19.** Schematic representation of the color tunable fluorescence resonance energy transfer process within the coassemblies having different amounts of the acceptor.

It is important to remember that this phenomenon is not possible if the acceptor does not aggregate in a controlled way within the coassembly, or in the case of ultrafast energy transfer with very low mol% of the acceptor resulting in complete quenching of the donor emission. The success of the present approach is

the control of the subtle balance between these two processes. This was proved from the FRET properties of **OPV3** using the same acceptor. Studies have shown that the gelation ability of **OPV3** was less, whereas, energy migration is more efficient when compared to that of **OPV1**.

### 4.3.7. FRET Properties of OPV3

Similar to **OPV1**, the emission spectrum of **OPV3** showed good spectral overlap with the absorption spectrum of **OPV6** (Figure 4.20). The overlap integral was found to be $1.81 \times 10^{15}\ M^{-1}cm^{-1}nm^4$.

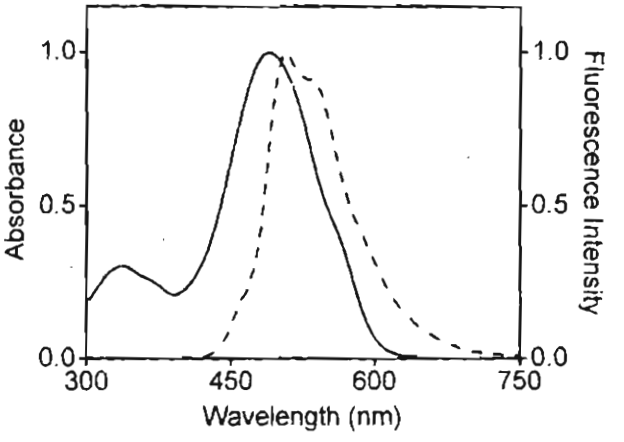


**Figure 4.20.** Spectral overlap of the emission of **OPV3** (– –) and absorption of **OPV6** (——) in decane at room temperature. (conc. of donor = $5.6 \times 10^{-4}$ M, conc. of acceptor = $1.12 \times 10^{-4}$ M, $l$ = 1 mm, $\lambda_{ex}$ = 380 nm)

As expected, the energy transfer efficiency was found to be better in **OPV3** because of the high energy migration efficiency. Maximum quenching was observed for **OPV3** emission on addition of 3.1 mol% of the acceptor. At this particular condition, 82% quenching was observed. Addition of further amount of

the acceptor into **OPV3** gel results gradual breaking of the coassembly and hence the monomer emission of the donor becomes predominant. This could be due to the less stability of the gel formed by **OPV3**, which undergo destruction in the presence of the acceptor (**OPV6**). Figure 4.21 shows the change in fluorescence emission and lifetime decay profile of **OPV3** on addition of varying amounts of **OPV6**. Due to the efficient energy transfer even with small amount (3.1 mol%) of the acceptor, subsequent addition does not make any change in the FRET emission. In fact, addition of the acceptor above 3.1 mol% exhibited increase in the emission intensity corresponding to the donor monomer emission indicating the disruption of the coassembly.

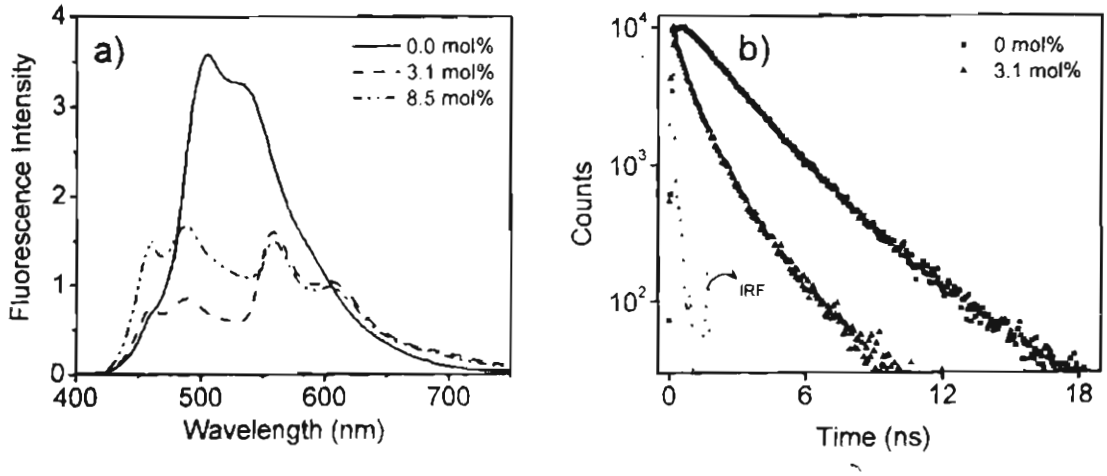


**Figure 4.21.** a) Fluorescence emission spectrum and b) fluorescence decay profiles of **OPV3** in the presence of different amounts of **OPV6** in decane at room temperature. (conc. of donor = $5.6 \times 10^{-4}$ M, $l$ = 1 mm, $\lambda$ = 375 nm).

## 4.4. Conclusions

Remarkable control on energy migration could be achieved by the structural modifications of the OPV gelators. Picosecond time resolved emission studies revealed less efficient energy migration in gelators with bulky end groups when compared to that of the gelators with small end groups. Slow energy migration allows tuning of the emission by the self-location of an acceptor as 'isolated' or 'aggregated' energy trap within the self-assembled donor gel in a controlled manner. The supramolecular approach described here allows the continuous shift of the emission from green to red upon a single wavelength excitation.

## 4.5. Experimental Section

### 4.5.1. Synthesis and characterization

The details of melting point, FT-IR, $^{1}H$ NMR and $^{13}C$ NMR and MALDI-TOF instruments are described in the experimental section of Chapter 2 of this thesis (section 2.5.1).

#### 4.5.1.1. General Procedure for the Preparation of OPV1, OPV3, OPV4 and OPV5

The OPV bisalcohol (**11a** or **11b**, 1 mmol) was dissolved in dry $CH_2Cl_2$ (40 mL) by stirring under argon atmosphere. The required acid (2.1 mmol) and catalytic amount of DMAP was added to this solution and the reaction mixture

was cooled to 0 °C by keeping in an ice-salt bath. DCC (2.5 mmol) was added to the reaction mixture and stirring was continued for 4 h at room temperature. The reaction mixture was filtered and the product was precipitated by the addition of methanol. The crude product was then purified by eluting through a silica column (100-200 mesh) using 1:3 $CHCl_3$-hexane mixture.

#### 4.5.1.2. General Procedure for the Preparation of OPV2

The OPV aldehyde (**12a**, 1 mmol) was dissolved in dry THF (15 mL) under argon atmosphere. Suspension of NaH (4.5 mmol) and the phosphonate ester (2.1 mmol) dissolved in dry THF (15 mL) was added drop-wise to this from a pressure equalizer. The reaction mixture was heated at 60 °C for 12 h. The solution was concentrated, extracted with chloroform and evaporated to dryness. It was then purified by eluting through a silica column (100-200 mesh) using 1:3 $CHCl_3$-hexane mixture.

#### 4.5.1.3. General Procedure for the Preparation of OPV6

A mixture of the OPV aldehyde (**12b**, 0.5 mmol), ethyl cyanoacetate (1.2 mmol), $NH_4OAc$ (20 mg), and acetic acid (5 mL) in toluene (30 mL) were stirred at 80 °C for 4 h. The solvent was removed under reduced pressure. The residue was extracted with chloroform and washed several times with water. The organic layer was dried over anhydrous $Na_2SO_4$ and concentrated to give the

corresponding OPV derivatives. Further purification was done by repeated precipitation from chloroform by adding methanol.

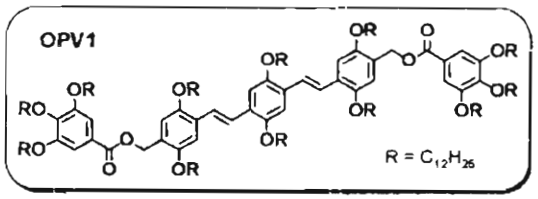


Yield 96%. mp 80-82 °C. $^1$H NMR (300 MHz, $CDCl_3$, TMS): δ 0.78-0.82 (m, 36H), 1.19 (s, 192H), 1.35-1.44 (m, 24H), 1.62-1.81 (m, 24H), 3.90-4.00 (m, 24H), 5.31 (s, 4H), 6.91 (s, 2H), 7.07 (s, 4H), 7.22 (s, 8H), 7.40 (s, 4H) ppm. $^{13}$C NMR (75 MHz, $CDCl_3$): δ 14.11, 22.68, 26.07, 26.13, 26.22, 29.37, 29.43, 29.49, 29.59, 29.70, 31.93, 62.27, 67.77, 69.00, 69.16, 69.59, 73.50, 108.06, 109.51, 110.41, 114.76, 116.24, 123.18, 123.74, 124.76, 124.96, 127.28, 127.91, 150.46, 151.00, 151.39, 152.79, 166.38 ppm. FT-IR (KBr): $\nu_{max}$ 690, 723, 758, 804, 855, 899, 932, 966, 1024, 1068, 1120, 1209, 1250, 1333, 1383, 1427, 1464, 1508, 1591, 1717, 2850, 2920 $cm^{-1}$. MALDI-TOF MS (MW = 2760.41): m/z = 2760.40 [$M^+$].

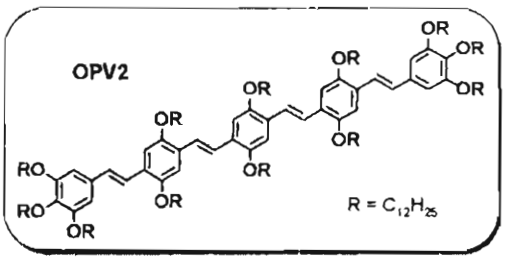


Yield: 70%. mp 103-105 $^0$C. $^1$H NMR (300 MHz, $CDCl_3$, TMS): δ 0.82 (s, 36H), 0.91-2.38 (m, 192H), 3.90-4.05 (m, 24H), 6.88 (s, 2H), 7.07 (s, 4H), 7.22 (s, 8H), 7.53 (s, 4H), 7.68 (s, 4H) ppm. $^{13}$C NMR (75 MHz, $CDCl_3$): δ 12.34, 13.98, 19.56, 20.95, 22.64, 22.90, 24.28, 25.58, 27.62, 28.20, 28.78, 28.95, 29.32, 29.52, 29.61, 29.61, 29.72, 31.71, 32.11, 32.23, 36.19, 36.72, 37.31, 37.42, 37.99, 39.88, 40.14, 42.62, 49.72, 56.64, 56.88, 63.72, 68.27, 69.51, 76.46, 108.73, 114.34, 116.18, 124.41,

126.86, 127.56, 128.21, 133.21, 138.93, 142.73, 154.63, 155.84, 155.95 ppm. FT-IR (KBr): $\nu_{max}$ 698, 725, 791, 857, 949, 969, 1002, 1032, 1077, 1208, 1261, 1352, 1379, 1423, 1462, 1503, 2850, 2922 $cm^{-1}$. MALDI-TOF MS (MW = 2696.43): m/z = 2696.46 [$M^+$].

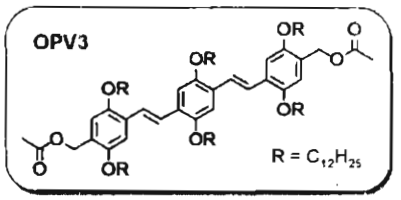


Yield: 97%. mp 88-90 °C. $^1$H NMR (300 MHz, $CDCl_3$, TMS): δ 0.79-0.81 (m, 18H), 1.18-1.26 (m, 96H), 1.34-1.42 (m, 12H), 1.66-1.79 (m, 12H), 2.11 (s, 6H), 3.89-4.00 (m, 12H), 5.15 (s, 4H), 6.90 (s, 2H), 7.13 (s, 4H), 7.46 (s, 4H) ppm. $^{13}$C NMR (75 MHz, $CDCl_3$): δ 14.42, 21.34, 22.98, 26.50, 26.54, 26.63, 29.67, 29.78, 29.86, 29.97, 30.00, 32.22, 62.06, 69.10, 69.66, 69.89, 96.43, 109.85, 110.89, 115.40, 123.59, 124.23, 124.59, 127.64, 128.53, 150.76, 151.36, 151.65, 170.98 ppm. FT-IR (KBr): $\nu_{max}$ 688, 721, 759, 803, 856, 898, 932, 967, 1025, 1066, 1122, 1208, 1252, 1335, 1382, 1426, 1465, 1506, 1591, 1718, 2852, 2921 $cm^{-1}$. MALDI-TOF MS (MW = 1531.28): m/z = 1531.23 [$M^+$].

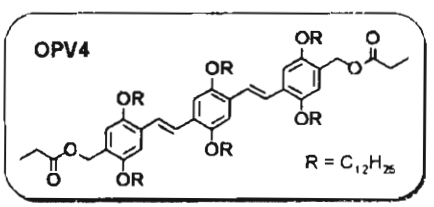


Yield: 96%. mp 87-89 °C. $^1$H NMR (300 MHz, $CDCl_3$, TMS): δ 0.78-0.82 (m, 18H), 0.96 (s, 6H) 1.14-1.25 (m, 96H), 1.33-1.40 (m, 12H), 1.64-1.78 (m, 12H), 2.10 (s, 4H), 3.90-4.00 (m, 12H), 5.14 (s, 4H), 6.88 (s, 2H), 7.11 (s, 4H), 7.44 (s, 4H) ppm. $^{13}$C NMR (75 MHz, $CDCl_3$): δ 14.33, 21.32, 22.92, 26.39, 26.50, 26.55, 26.62, 29.61, 29.70, 29.86, 29.79, 30.57, 32.15, 62.12, 69.33, 69.68,

69.77, 96.45, 109.16, 110.79, 117.46, 122.87, 123.47, 123.63 126.95, 127.65, 150.72, 151.28, 151.55, 171.02 ppm FT-IR (KBr): $\nu_{max}$ 689, 722, 763, 802, 858, 900, 931, 969, 1024, 1068, 1124, 1210, 1252, 1333, 1381, 1427, 1463, 1504, 1592, 1719, 2853, 2922 $cm^{-1}$; MALDI-TOF MS (MW = 1559.31): m/z = 1559.36 $[M^+]$.

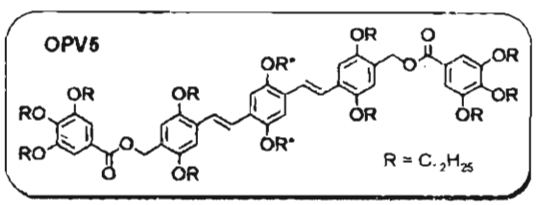


Yield: 97%: mp 74-75 °C. $^1$H NMR (300 MHz, $CDCl_3$, TMS): δ 0.82-0.88 (m, 36H), 1.25 (m, 192H), 1.38-1.45 (m, 24H), 1.72-1.89 (m, 24H), 3.98-4.01 (m, 20H), 4.09-4.11 (t, 4H), 5.38 (s, 4H), 6.98 (s, 2H), 7.15 (s, 4H), 7.30 (s, 8H), 7.61 (s, 4H) ppm. $^{13}$C NMR (75 MHz, $CDCl_3$): δ 14.11, 19.845, 22.56, 22.69, 24.74, 26.07, 26.13, 26.22, 27.94, 29.37, 29.44, 29.50, 29.59, 29.70, 30.19, 30.34, 31.92, 36.52, 37.39, 39.27, 62.27, 67.77, 69.00, 69.16, 69.59, 73.50, 108.06, 109.52, 110.41, 114.76, 116.24, 123.18, 123.74, 124.77, 124.96, 127.28, 127.92, 150.46, 151.01, 151.39, 152.78, 166.39 ppm. FT-IR (KBr): $\nu_{max}$ 691, 723, 760, 804, 854, 899, 933, 967, 1024, 1069, 1121, 1209, 1251, 1332, 1384, 1428, 1464, 1508, 1592, 1717, 2852, 2922 $cm^{-1}$; MALDI-TOF MS (MW = 2704.24): m/z = 2704.32 $[M^+]$.

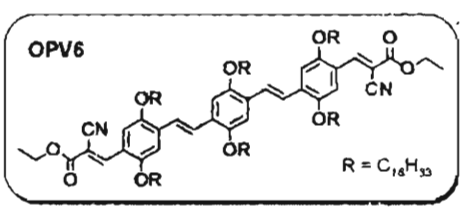


Yield: 95%. mp 107-109 °C. $^1$H NMR (300 MHz, $CDCl_3$, TMS): δ 0.85-0.88 (m, 18H), 1.24 (s, 96H), 1.42-1.52 (m, 18H), 1.84-1.89

(m, 12H), 4.07-4.09 (m, 12H), 4.34-4.41 (q, 4H), 7.16. (s, 4H), 7.49-7.54 (d, 2H), 7.60-7.66 (d, 2H), 7.98 (s, 2H), 8.78 (s, 2H) ppm. $^{13}C$ NMR (75 MHz $CDCl_3$,): δ 4.32, 14.43, 22.90, 26.34, 26.46, 26.53, 29.46, 29.59, 29.69, 29.74, 29.95, 32.15, 62.49, 69.38, 69.59, 100.14, 109.78, 110.93, 111.88, 116.95, 120.37, 123.34, 127.12, 127.73, 134.74, 148.82, 150.74, 151.63, 154.08, 163.46 ppm. FT-IR (KBr): $\nu_{max}$ 719, 763, 802, 854, 961, 1024, 1049, 1091, 1165, 1213, 1240, 1294, 1346, 1365, 1394, 1429, 1467, 1506, 1571, 1726, 2214, 2848, 2916, 2956 $cm^{-1}$; MALDI-TOF MS (MW = 1969.68): m/z = 1969.73 [$M^+$].

### 4.5.2. General Procedure for Energy Transfer Studies

The energy transfer experiments were carried out in the gel state in decane at room temperature. Gels for the FRET studies were prepared by adding appropriate concentration of the acceptor (0-20 mol%) to 250 $\mu$L of the donor in decane. Subsequent heating and cooling results stable coassembled gels at room temperature. These samples were subjected to fluorescence measurements which provided information on the FRET properties.

### 4.5.3. Description of Instrumental Techniques

#### 4.5.3.1. Electronic Spectral Measurements

The details of UV-vis absorption spectrophotometer, spectrofluorimeter and time correlated picosecond *single photon counting* (TCSPC) system are described in the section 2.5.2 of Chapter 2.

### 4.5.3.2. X-Ray Diffraction Studies

Concentrated solutions of the samples were prepared by dissolving it in decane by heating. The hot solution was poured on to a glass plate and allowed to evaporate slowly to get good xerogel films. X-ray diffractograms of the dried xerogel films were recorded on a Phillips Diffractometer using Ni filtered Cu Kα radiation.

### 4.5.3.3. Fluorescent Microscopic Studies

Fluorescent microscopic images were recorded on a Nikon EpiFluorescent Microscope TE300 using UV light (330-380 nm) as the excitation source. Samples were prepared by drop casting decane solution (concentration of the donor was kept at $3 \times 10^{-4}$ M and concentration of the acceptor varied from 0-20 mol%) on a glass slide followed by slow evaporation.

## 4.6. Reference

1. a) M. P. Bruchez, M. Moronne, P. Gin, S. Weiss, A. P. Alivisatos, *Science* **1998**, *281*, 2013; b) T. Virgili, D. G. Lidzey, D. D. C. Bradley, *Adv. Mater.* **2000**, *12*, 58; c) J. Chen, P. R. Selvin *J. Am. Chem. Soc.* **2000**, *122*, 657; d) A. Mokhir, A. Kiel, D.-P. Herten, R. Kraemer, *Inorg. Chem.* **2005**, *44*, 5661; e) N. Ananthakrishnan, G. Padmanaban, S. Ramakrishnan, J. R. Reynolds, *Macromolecules* **2005**, *38*, 7660.
2. a) F. Würthner, S. Ahmed, C. Thalacker, T. Debaerdemaeker, *Chem. Eur. J.* **2002**, *8*, 4742; b) S.-H. Jin, S.-Y. Kang, I.-S. Yeom, J. Y. Kim, S. H. Park, K. Lee, Y.-S. Gal, H.-N. Cho, *Chem. Mater.* **2002**, *14*, 5090; c) Q. Liu, M. S. Mudadu, H. Schmider, R. Thummel, Y. Tao, S. Wang, *Organometallics* **2002**, *21*, 4743; d) Y.

Wu, P. V. Lawson, M. M. Henary, K. Schmidt, J.-L. Brédas, C. J. Fahrni, *J. Phys. Chem. A* **2007**, *111*, 4584; e) H.-C. Li, Y.-P. Lin, P.-T. Chou, Y.-M. Cheng, R.-S. Liu, *Adv. Func. Mater.* **2007**, *17*, 520; f) T. Jiu, Y. Li, H. Liu, J. Ye, X. Liu, L. Jiang, M. Yuan, J. Li, C. Li, S. Wang, D. Zhu, *Tetrahedron* **2007**, *63*, 3168.

3. a) R. Gowri, D. Mandal, B. Shivkumar, S. Ramakrishnan, *Macromolecules* **1998**, *31*, 1819; b) K. Y. Musick, Q.-S. Hu, L. Pu, *Macromolecules* **1998**, *31*, 2933; c) Y. Dienes, S. Durben, T. Kárpáti, T. Neumann, U. Englert, L. Nyulászi, T. Baumgartner, *Chem. Eur. J.* **2007**, *13*, 7487; d) F. Bureš, W. B. Schweizer, J. C. May, C. Boudon, J.-P. Gisselbrecht, M. Gross, I. Biaggio, F. Diederich, *Chem. Eur. J.* **2007**, *13*, 5378.

4. a) C. Ego, D. Marsitzky, S. Becker, J. Zhang, A. C. Grimsdale, K. Müllen, J. D. MacKenzie, C. Silva, R. H. Friend, *J. Am. Chem. Soc.* **2003**, *125*, 437; b) E. B. Namdas, T. D. Anthopoulos, I. D. W. Samuel, M. J. Frampton, S.-C. Lo, P. L. Burn, *Appl. Phys. Lett.* **2005**, *86*, 1.

5. a) A. D. Peng, D. B. Xiao, Y. Ma, W. S. Yang, J. N. Yao, *Adv. Mater.* **2005**, *17*, 2070; b) Y. You, S. Y. Park, *J. Am. Chem. Soc.* **2005**, *127*, 12438; c) M. Sun, T. Pullerits, P. Kjellberg, W. J. D. Beenken, K. Han, *J. Phys. Chem. A* **2006**, *110*, 6324; c) P. P. Pompa, R. Chiuri, L.Manna, T. Pellegrino, L. L. del Mercato, W. J. Parak, F. Calabi, R. Cingolani, R. Rinaldi, *Chem. Phys. Lett.* **2006**, *417*, 351; d) C. Mei, G. Tu, Q. Zhou, Y. Cheng, Z. Xie, D. Ma, Y. Geng, L. Wang, *Polymer* **2006**, *47*, 4976; e) N. You, K. S. Kim, T. K. Ahn, D. Kim, S. Y. Park, *J. Phys. Chem. C* **2007**, *111*, 4052.

6. W. Wang, J. J. Han, L.-Q. Wang, L.-S. Li, W. J. Shaw, A. D. Q. Li, *Nano Lett.* **2003**, *3*, 455.

7. a) F. J. M. Hoeben, L. M. Herz, C. Daniel, P. Jonkheijm, A. P. H. J. Schenning, C. Silva, S. C. J. Meskers, D. Beljonne, R. T. Phillips, R. H. Friend, E. W. Meijer, *Angew. Chem., Int. Ed.* **2004**, *43*, 1976; b) F. J. M. Hoeben, I. O. Shklyarevskiy, M. J. Pouderoijen, H. Enjelkamp, A. P. H. J. Schenning, P. C. M. Christianen, J. C. Maan, E. W. Meijer, *Angew. Chem. Int. Ed.* **2006**, *45*, 1232.

8. a) T. Miyatake, H. Tamiaki, A. Holzwarth, K. Schaffner, *Photochem. Photobiol.* **1999**, *69*, 448; b) X. Li, L. E. Sinks, B. Rybtchinski, M. R. Wasielewski, *J. Am. Chem. Soc.* **2004**, *126*, 10810.

9. See the references 27-34 cited in Chapter 1 of the thesis.

10. a) D.-L. Jiang, T. Aida, *J. Am. Chem. Soc.* **1998**, *120*, 10895; b) C. Devadoss, P. Bharathi, J. S. Moore, *J. Am. Chem. Soc.* **1996**, *118*, 9635; c) A. P. H. J. Schenning, E. Peeters, E. W. Meijer, *J. Am. Chem. Soc.* **2000**, *122*, 4489; d) P. Furuta, J. Brooks, M. E. Thompson, J. M. J. Fréchet, *J. Am. Chem. Soc.* **2003**, *125*, 13165; e) K. R. J. Thomas, A. L. Thompson, A. V. Sivakumar, C. J. Bardeen, S. Thayumanavan, *J. Am. Chem. Soc.* **2005**, *127*, 373; f) A. Adronov, J. M. J. Fréchet, *Chem. Commun.* **2005**, 1701.

11. a) I. A. Levitsky, J. Kim, T. M. Swager, *J. Am. Chem. Soc.* **1999**, *121*, 1466; b) D. T. McQuade, A. H. Hegedus, T. M. Swager, *J. Am. Chem. Soc.* **2000**, *122*, 12389; c) B. Liu, B. S. Gaylord, S. Wang, G. C. Bazan, *J. Am. Chem. Soc.* **2003**, *125*, 6705; d) C. Tan, E. Atas, J. G. Müller, M. R. Pinto, V. D. Kleiman, K. S. Schanze, *J. Am. Chem. Soc.* **2004**, *126*, 13685; e) S. Wang, B. S. Gaylord, G. C. Bazan, *J. Am. Chem. Soc.* **2004**, *126*, 5446; f) J. G. Müller, E. Atas, C. Tan, K. S. Schanze, V. D. Klieman, *J. Am. Chem. Soc.* **2006**, *128*, 4007; g) N. Tian, Q.-H. Xu, *Adv. Mater.* **2007**, *19*, 1988.

12. A. D. Guerzo, A. G. L. Olive, J. Reichwagen, H. Hopf, J.-P. Desvergne, *J. Am. Chem. Soc.* **2005**, *127*, 17984.

13. A. Ajayaghosh, V. K. Praveen, C. Vijayakumar, S. J. George, *Angew. Chem. Int. Ed.* **2007**, *46*, 6260.

14. a) E. H. A. Beckers, P. A. van Hal, A. P. H. J. Schenning, A. El-ghayoury, E. Peeters, M. T. Rispens, J. C. Hummelen, E. W. Meijer, R. A. J. Janssen, *J. Mater. Chem.* **2002**, *12*, 2054; b) E. E. Neuteboom, E. H. A. Beckers, S. C. J. Meskers, E. W. Meijer, R. A. J. Janssen, *Org. Biomol. Chem.* **2003**, *1*, 198.

15. a) U. Lemmer, A. Oche, M. Deussen, R. F. Mahrt, E. O. Göbel, H. Bässler, P. H. Bolivar, G. Wegmann, H. Kürz, *Synth. Met.* **1996**, *78*, 289; b) L. C. Palilis, J. S. Melinger, M. A. Wolak, Z. H. Kafafi, *J. Phys. Chem. B* **2005**, *109*, 5456.

16. a) P. H. Bolivar, G. Wegmann, R. Kersting, M. Deussen, U. Lemmer, R. F. Mahrt, H. Bässler, E. O. Göbel, H. Kürz, *Chem. Phys. Lett.* **1995**, *245*, 534; b) B. K. Kaletaş, R. Dobrawa, A. Sautter, F. Würthner, M. Zimmine, L. De Cola, R. M. Williams, *J. Phys. Chem. A* **2004**, *108*, 1900.

## List of Publications

1. Cholesterol-Aided Supramolecular Control over Chromophore Packing: Twisted and Coiled Helices with Distinct Optical, Chiroptical and Morphological Features
   A. Ajayaghosh, **C. Vijayakumar**, R. Varghese, S. J. George
   *Angew. Chem. Int. Ed.* **2006**, *45*, 456. (*VIP article*)

2. Transcription and Amplification of Molecular Chirality to Oppositely Biased Supramolecular π-Helices
   A. Ajayaghosh, R. Varghese, S. J. George, **C. Vijayakumar**
   *Angew. Chem. Int. Ed.* **2006**, *45*, 1141. (*VIP article with front cover page*)

3. Self-Location of Acceptors as "Isolated" or "Stacked" Energy Traps in a Supramolecular Donor Self-Assembly: A Strategy to Wavelength Tunable FRET Emission
   A. Ajayaghosh, **C. Vijayakumar**, V. K. Praveen, S. S. Babu, R. Varghese
   *J. Am. Chem. Soc.* **2006**, *128*, 7174.

4. Self-Assembled π-Nanotapes as Donor Scaffolds for Selective and Thermally Gated Fluorescence Resonance Energy Transfer (FRET)
   V. K. Praveen, S. J. George, R. Varghese, **C. Vijayakumar**, A. Ajayaghosh
   *J. Am. Chem. Soc.* **2006**, *128*, 7542.

5. Molecular Wire Encapsulated into π-Organogels: Efficient Supramolecular Light Harvesting Antennae with Color-Tunable Emission
   A. Ajayaghosh, V. K. Praveen, **C. Vijayakumar**, S. J. Goerge
   *Angew. Chem. Int. Ed.* **2007**, *46*, 6260. (*With inside cover page*)

6. Organogels as scaffolds for Excitation Energy Transfer and Light Harvesting
   A. Ajayaghosh, V. K. Praveen, **C. Vijayakumar**
   *Chem. Soc. Rev.* **2008** (DOI: 10.1039/b704456a)

## Patent

1. White Light Emitting Organogel and Process thereof. *(Submitted)*
   A. Ajayaghosh, **C. Vijayakumar**, V. K. Praveen

## Posters Presented at Conferences

1. Organogels Derived from Helical Self-Assembly of Cholesterol Appended Oligo(*p*-phenylenethynylene)s
   **C. Vijayakumar**, S. J. George, A. Ajayaghosh
   3rdTrivandrun International Symposium on Recent Trends in Photochemical Sciences, Trivandrum, India, January 5-7, 2004, p41.

2. Self-Assembled Helical Nanostructures of Gel Forming π-Conjugated Molecules: A Novel Approach to Optoelectronic Modulation and Light Harvesting.
   S. J. George, V. K. Praveen, R. Varghese, **C. Vijayakumar** and A. Ajayaghosh
   Indo-US Frontiers of Science Symposium, Bangalore, India, January 9-11, 2005, p6.

3. Supramolecular Control of Chromophore Orientation in Optical and Chiroptical Properties Cholesterol Appended Oligo(*p*-phenylenevinylene)s
   **C. Vijayakumar**, A. Ajayaghosh
   7th National Symposium in Chemistry, IACS, Kolkatha, India, February 4-6, 2005, p166.

4. Supramolecular Control over Chromophore Packing in Cholesterol Appended OPVs.
   **C. Vijayakumar**, R. Varghese, A. Ajayaghosh
   International Symposium on Advances in Organic Chemistry (INSOC 2006), Kottayam, India, January 9-12, 2006, p142.

5. The "Sergeant and Soldiers" Approach in Chirality Induction and Amplification in Coassembled π-Gels: Helicity Inversion and Stereomutation.
   R. Varghese, **C. Vijayakumar**, V. K. Praveen, A. Ajayaghosh
   8th CRSI National Symposium in Chemistry, IIT-Bombay, India, February 3-5, 2006, p89.

6. Molecular Self-Assemblies as Energy Donor Scaffolds for Light Harvesting: A Rational Approach to Wavelength Tunable FRET Emission.
   **C. Vijayakumar**, V. K. Praveen, S. S. Babu, A. Ajayaghosh
   Second JNC Research Conference on Chemistry of Materials, Kollam, India, October 29-31, 2006, p18.

7. Supramolecular Control over Helical Packing of Chromophores: Molecular Functionalization Approach to Twisted and Coiled Helices. (*Selected for oral presentation*)
   **C. Vijayakumar**, A. Ajayaghosh
   Asia Academic Seminar on Molecular and Supramolecular Materials with Designed Functions, NCL Pune, India, February 23-28, 2007.